A groundwater flow model for the Little Plover River Basin in Wisconsin's Central Sands. Bulletin 111 2017

Bradbury, K. R.; Fienen, Michael N.; Kniffin, Maribeth L.
Madison, Wis.: University of Wisconsin--Extension, Wisconsin Geological and Natural History Survey, 2017

WISCONSIN GEOLOGICAL AND NATURAL HISTORY SURVEY

A Groundwater Flow Model for the Little Plover River Basin in Wisconsin's Central Sands

Bulletin 111 • 2017

Kenneth R. Bradbury
Michael N. Fienen
Maribeth L. Kniffin
Jacob J. Krause
Stephen M. Westenbroek
Andrew T. Leaf
Paul M. Barlow

UW Extension
University of Wisconsin-Extension

Wisconsin Geological and Natural History Survey

Kenneth R. Bradbury, *Director and State Geologist*

WGNHS staff

William G. Batten, *geologist*
Eric C. Carson, *geologist*
Peter M. Chase, *geotechnician*
Linda G. Deith, *editor*
Anna C. Fehling, *hydrogeologist*
Madeline B. Gotkowitz, *hydrogeologist*
Brad T. Gottschalk, *archivist*
Grace E. Graham, *hydrogeologist*
David J. Hart, *hydrogeologist*
Irene D. Lippelt, *water resources specialist*
Sushmita S. Lotlikar, *administrative manager*
Stephen M. Mauel, *GIS specialist*
M. Carol McCartney, *outreach manager*
Michael J. Parsen, *hydrogeologist*
Jill E. Pongetti, *office manager*
J. Elmo Rawling III, *geologist*
Caroline M.R. Rose, *GIS specialist*
Kathy Campbell Roushar, *GIS specialist*
Peter R. Schoephoester, *assistant director*
Aaron N. Smetana, *system administrator*
Val L. Stanley, *geologist*
Esther K. Stewart, *geologist*
Carolyn M. Streiff, *geophysicist*
Jay Zambito, *geologist*
and approximately 15 graduate and undergraduate student workers

Emeritus staff

John W. Attig, *geologist*
Bruce A. Brown, *geologist*
Thomas J. Evans, *geologist*
Ronald G. Hennings, *hydrogeologist*
Frederick W. Madison, *soil scientist*
Stanley A. Nichols, *biologist*
Deborah L. Patterson, *GIS specialist*
Roger M. Peters, *subsurface geologist*
James M. Robertson, *geologist*

Research associates

Jean M. Bahr, *University of Wisconsin–Madison*
Mark A. Borchardt, *USDA–Agricultural Research Station*
Philip E. Brown, *University of Wisconsin–Madison*
Charles W. Byers, *University of Wisconsin–Madison (emeritus)*
William F. Cannon, *U.S. Geological Survey*
Michael Cardiff, *University of Wisconsin–Madison*
William S. Cordua, *University of Wisconsin–River Falls*
Robert H. Dott, Jr., *University of Wisconsin–Madison (emeritus)*
Charles P. Dunning, *U.S. Geological Survey*
Daniel T. Feinstein, *U.S. Geological Survey*
Michael N. Fienen, *U.S. Geological Survey*
Timothy J. Grundl, *University of Wisconsin–Milwaukee*
Nelson R. Ham, *St. Norbert College*
Paul R. Hanson, *University of Nebraska–Lincoln*
Karen G. Havholm, *University of Wisconsin–Eau Claire*
Randy J. Hunt, *U.S. Geological Survey*
John L. Isbell, *University of Wisconsin–Milwaukee*
Mark D. Johnson, *University of Gothenburg*
Joanne L. Kluessendorf, *Weis Earth Science Museum*
George J. Kraft, *Central Wisconsin Groundwater Center*
Evan R. Larson, *University of Wisconsin–Platteville*
John A. Luczaj, *University of Wisconsin–Green Bay*
J. Brian Mahoney, *University of Wisconsin–Eau Claire*
Shaun Marcott, *University of Wisconsin–Madison*
Joseph A. Mason, *University of Wisconsin–Madison*
Daniel J. Masterpole, *Chippewa Co. Land Conservation Dept.*
David M. Mickelson, *University of Wisconsin–Madison (emeritus)*
Donald G. Mikulic, *Illinois State Geological Survey*
William N. Mode, *University of Wisconsin–Oshkosh*
Maureen A. Muldoon, *University of Wisconsin–Oshkosh*
Beth L. Parker, *University of Guelph*
Robert E. Pearson, *Wisconsin Dept. of Transportation*
Kenneth W. Potter, *University of Wisconsin–Madison*
Todd W. Rayne, *Hamilton College*
Daniel D. Reid, *Wisconsin Dept. of Transportation*
Randall J. Schaetzl, *Michigan State University*
Allan F. Schneider, *University of Wisconsin–Parkside (emeritus)*
Madeline E. Schreiber, *Virginia Tech*
Susan K. Swanson, *Beloit College*
Kent M. Syverson, *University of Wisconsin–Eau Claire*
Lucas Zoet, *University of Wisconsin–Madison*

The Wisconsin Geological and Natural History Survey also maintains collaborative relationships with a number of local, state, regional, and federal agencies and organizations regarding educational outreach and a broad range of natural resource issues.

Bulletin 111 • 2017

A Groundwater Flow Model for the Little Plover River Basin in Wisconsin's Central Sands

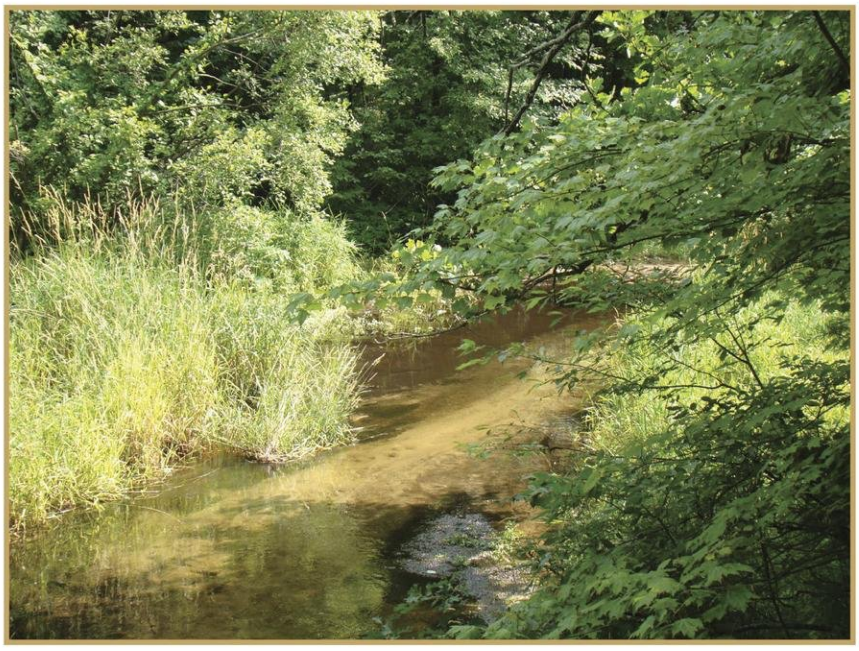

Kenneth R. Bradbury
WISCONSIN GEOLOGICAL AND NATURAL HISTORY SURVEY

Michael N. Fienen
U.S. GEOLOGICAL SURVEY, WISCONSIN WATER SCIENCE CENTER

Maribeth L. Kniffin
WISCONSIN GEOLOGICAL AND NATURAL HISTORY SURVEY

Jacob J. Krause
WISCONSIN GEOLOGICAL AND NATURAL HISTORY SURVEY

Stephen M. Westenbroek
U.S. GEOLOGICAL SURVEY, WISCONSIN WATER SCIENCE CENTER

Andrew T. Leaf
U.S. GEOLOGICAL SURVEY, WISCONSIN WATER SCIENCE CENTER

Paul M. Barlow
U.S. GEOLOGICAL SURVEY, OFFICE OF GROUNDWATER

UW Extension
University of Wisconsin-Extension

Suggested citation:

Bradbury, K.R., Fienen, M.N., Kniffin, M.L., Krause, J.J., Westenbroek, S.M., Leaf, A.T., and Barlow, P.M., 2017, Groundwater flow model for the Little Plover River basin in Wisconsin's Central Sands: Wisconsin Geological and Natural History Survey Bulletin 111, 82 p.

The use of company names in this document does not imply endorsement by the Wisconsin Geological and Natural History Survey or by the U.S. Geological Survey.

"Groundwater fundamentals" sidebars were adapted from Groundwater Quantity Fundamentals in Wisconsin's Central Sands Region *(Bradbury and others, 2017).*

Published by and available from:

Wisconsin Geological and Natural History Survey

3817 Mineral Point Road ■ Madison, Wisconsin 53705-5100
608.263.7389 ■ www.WisconsinGeologicalSurvey.org
Kenneth R. Bradbury, Director and State Geologist

ISSN: 0375-8265
ISBN: 978-0-88169-986-9

Contributors

Editors: Linda Deith, Cindy Foss
Graphics: Caroline Rose (maps), Kristen Rost (graphs, illustrations)
Photographs: Ken Bradbury, Maribeth Kniffin
Layout: Kristen Rost, Linda Deith

Contents

The model files, user's manual, and this report are available online.
Visit http://wgnhs.org/little-plover-river-groundwater-model.

Figures

Tables

Appendices

(Available at http://wgnhs.org/pubs/b111)

Executive summary

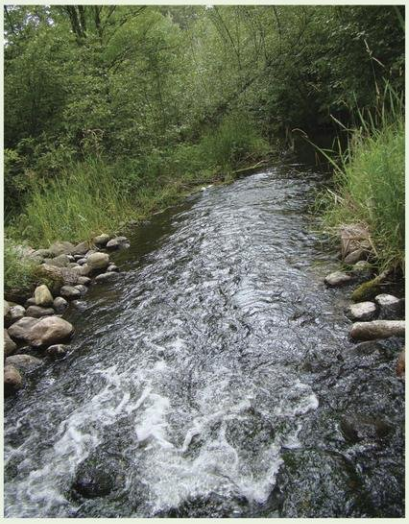

The Little Plover River is a groundwater-fed stream in the Central Sands region of Wisconsin. In this region, sandy sediment deposited during or soon after the last glaciation forms an important unconfined sand and gravel aquifer. This aquifer supplies water for numerous high-capacity irrigation, municipal, and industrial wells that support a thriving agricultural industry. In recent years, the addition of many new wells, combined with observed diminished flows in the Little Plover and other nearby rivers, has raised concerns about the impacts of the wells on groundwater levels, and on water levels and flows in nearby lakes, streams, and wetlands. Diverse stakeholder groups, including well operators, growers, environmentalists, local landowners, and regulatory and government officials have sought a better understanding of the local groundwater–surface water system and have a shared desire to balance the water needs of the agricultural, industrial, and urban users with the maintenance and protection of groundwater-dependent natural resources. To help address these issues, the Wisconsin Department of Natural Resources requested that the Wisconsin Geological and Natural History Survey and U.S. Geological Survey cooperatively develop a groundwater flow model that could be used to demonstrate the relationships among groundwater, surface water, and well withdrawals and also to be a tool for testing and evaluating alternative water-management strategies for the Central Sands region. Because of an abundance of previous studies, data availability, local interest, and existing regulatory constraints, the model focuses on the Little Plover River watershed, but the modeling methodology developed during this study can apply to much of the larger Central Sands region of Wisconsin.

The Little Plover River groundwater flow model simulates three-dimensional groundwater movement in and around the Little Plover River basin under steady-state and transient conditions. This model explicitly includes all high-capacity wells in the model domain and simulates seasonal variations in recharge and well pumping. The model represents the Little Plover River, and other significant streams and drainage ditches in the model domain, as fully connected to the groundwater system, computes stream baseflow resulting from groundwater discharge, and routes the flow along the stream channels. A separate soil-water-balance (SWB) model was used to develop groundwater recharge arrays as input for the groundwater flow model. The SWB model uses topography, soils, land use, and climatic data to estimate recharge as deep drainage from the

soil zone. The SWB model explicitly includes recharge originating as irrigation water and computes irrigation using techniques similar to those used by local irrigation operators.

The groundwater flow model uses the U.S. Geological Survey's MODFLOW modeling code, which is freely available, widely accepted, and commonly used by the groundwater community. The groundwater flow model and the SWB model use identical high-resolution numerical grids that have model cells 100 feet on a side, with physical properties assigned to each grid cell. This grid allows accurate geographic placement of wells, streams, and other model features. The three-dimensional grid has three layers: layers 1 and 2 represent the sand and gravel aquifer, and layer 3 represents the underlying sandstone. The distribution of material properties in the model (hydraulic conductivity, aquifer thickness, etc.) comes from previously published geologic studies of the region, updated by calibration to recent streamflow and groundwater-level data. The SWB model operates on a daily time step. The groundwater flow model was calibrated to monthly stress periods, with time steps ranging from 1 to 16 days. More detailed time discretization is possible.

The groundwater model was calibrated to water-level and streamflow data collected during 2013 and 2014 by adjusting model parameters (primarily hydraulic conductivity, storage, and recharge) until the model produced a conditionally optimal fit between field observations and model output, subject to consistency with previously published geologic studies. Calibration was performed under both steady and transient conditions, and used a sophisticated parameter-estimation procedure (PEST) for the calibration process and to identify important model parameters. For the Little Plover River, the two most important parameters are the global recharge multiplier and the hydraulic conductivity of the stream bed. The calibrated model produces water-level and mass-balance results that are consistent with field observations and previous studies of the area.

The completed model is a powerful tool for testing and demonstrating alternative water-management scenarios. Example model applications described in this report include simulating how the cumulative impacts of pumping and land-use change have affected average baseflow in the Little Plover River. Depletion-potential mapping represents a method for predicting which wells and well locations have the greatest impact on nearby surface-water resources.

The completed model is publicly available, along with a companion user's guide to assist with its operation, at http://wgnhs.org/little-plover-river-groundwater-model.

Introduction

Background

The region generally known as Wisconsin's Central Sands spans parts of several counties in central Wisconsin (fig. 1). This report defines the Central Sands as the contiguous area east of the Wisconsin River with sand and gravel surficial deposits greater than 50 feet thick, which is the definition used by the Wisconsin Department of Natural Resources (R. Smail, DNR, personal communication, 2/2/2017). Much of this region consists of sandy outwash and lake sediment deposited in a large glacial lake basin at the close of the Pleistocene Epoch, around 11,700 years ago in Wisconsin. These sands and gravels form an important shallow aquifer that supplies water for major row crops, vegetable packaging industries, cranberry production, and domestic supply for several communities. The aquifer is approximately 100 feet thick and lies on less-permeable bedrock. The region includes more than 80 lakes and more than 600 miles of headwater streams (Kraft and others, 2012) that comprise important recreational and ecological resources. Irrigated land, which increased dramatically in the years after 1950, currently covers about 183,000 acres. Irrigation supports production of potatoes, sweet corn, snap beans, and other vegetables. The main source of the irrigation water is groundwater pumped from relatively shallow high-capacity wells in the sandy aquifer. The number of wells has increased every year for the past several decades.

Groundwater and surface water are well-connected in the Central Sands region, and concerns over the possible impacts of irrigated agriculture on surface-water resources and groundwater levels first appeared in the mid-1960s and early 1970s (Holt, 1965; Weeks, 1969; Weeks and Stangland, 1971). These concerns became more acute during the 2000s, with the occurrence of extremely low water levels in several area lakes and extraordinarily low flows and associated fish kills in some local streams. From 2005 to 2009, the Little Plover River—a class 1 trout stream deriving 80 to 90 percent of its flow from groundwater discharge (based on calculations herein)—completely dried up each year in at least one stretch. Kraft and others (2012) simulated the region's groundwater using a regional flow model and concluded that irrigation has reduced recharge in some parts of the region by up to 5.6 inches per year (in/yr) and caused average groundwater levels to decline by more than 3 feet in some areas. The Wisconsin Geological and Natural History Survey (WGNHS) carried out several hydrogeological studies in the Central Sands during the 1980s (Bradbury and others, 1992; Faustini, 1985). Kniffin and others (2014) developed an extensive summary and overview of hydrologic conditions in the region and summarized the results of numerous previous studies.

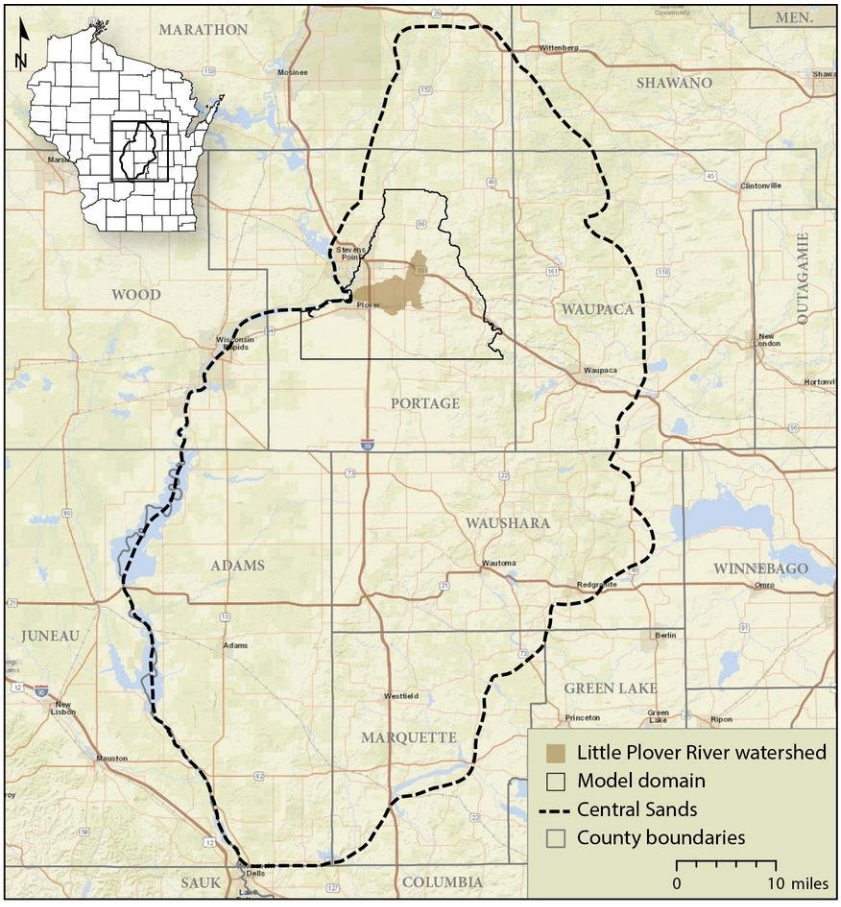

Figure 1. Location of the Central Sands with the model domain and Little Plover River watershed.

GROUNDWATER FUNDAMENTALS

A single groundwater flow system underlies the Central Sands

DETAILS: The Central Sands groundwater flow system occurs mainly in a single, interconnected sand-and-gravel aquifer that underlies virtually all of the region. It is highly permeable and ranges from very thin to nearly 200 feet thick. In places the sand and gravel aquifer is underlain by a sandstone aquifer, and in other places the sand and gravel is interrupted by a clayey layer called the New Rome Formation. With the exception of some very small isolated locations, groundwater in the Central Sands flows through a connected large system that receives recharge from local precipitation. Groundwater naturally flows to streams where it discharges and leaves the watershed.

WHY IT MATTERS: The groundwater flow system is well connected, wide-ranging, and the aquifer stores and transmits water to surface water and to wells.

Irrigation is often cited as being essential to the economy of central Wisconsin and for food production (for example, search for "Irrigated vegetable production key to central Wisconsin economy" at http://agriview.com), but in recent years, there has been disagreement over the interrelations among irrigation, climate, groundwater pumping, lake levels, and stream flows (see http://grow.cals.wisc.edu/agriculture/vanishing-waters). Although the general hydrogeology over most of the Central Sands is relatively simple and well understood (Bradbury and others, 1992), uncertainty about quantification of groundwater recharge and evapotranspiration remains an important scientific issue.

Although most water users, regulatory officials, and citizens in central Wisconsin recognize the links among groundwater pumping, groundwater levels, lake levels, and streamflows, there has been public disagreement over cause-and-effect relationships and over potential management actions performed to mitigate low flows and lake levels. There has been no broadly accepted method for regulators and other interested parties to assess the complex interactions of land use, climate, irrigation, and groundwater withdrawals in the context of maintaining stream flows or lake levels. Among some groups, there also has been uncertainty about how well the groundwater system has been characterized or understood.

Groundwater flow models are scientific tools for quantitatively integrating the complexities of geology, groundwater recharge and discharge, surface-water flow, well development and use, and water balance into a single conceptual package. Such models can simulate the complex temporal and spatial interactions among streamflow, pumping, and climate; models can also provide users "what-if" evaluations of possible decisions involving management or land-use changes. In this way, models provide a fundamental scientific basis for decision support. Modern graphical interfaces (for example, Model Viewer, (Hsieh and others, 2002)) allow the model structure and model results to be viewed and illustrated in non-technical, three-dimensional diagrams. With visualization and an appropriate level of presentation, such models also can be extremely useful as educational tools to help people better understand groundwater systems.

In 2013, the Wisconsin Department of Natural Resources (DNR) requested that the Wisconsin Geological and Natural History Survey (WGNHS) and U.S. Geological Survey (USGS) cooperatively develop a groundwater flow model for a portion of the Central Sands. Following proposal development and review by stakeholders and a technical oversight committee, the DNR provided funding for the development of a groundwater flow and optimization model focused on the Little Plover River watershed in Portage County, Wisconsin. The Wisconsin Potato and Vegetable Growers Association (WPVGA) contributed additional funding to support model development. The project was undertaken jointly by the WGNHS and USGS and formally began in November 2013.

Purpose and scope

Overall goals

The overall goal of the project was to develop a state-of-the-art groundwater flow and optimization model for the Little Plover River (LPR) basin, and to provide a defensible scientific basis for water optimization and other decision-support simulations and a starting point for wider groundwater modeling in Wisconsin's Central Sands. The goal of the model development was to develop a tool that can be widely accepted by citizens, user groups, and regulators as a way to predict how both natural changes (seasonal and climate variations) and management options (locations, design, and operation

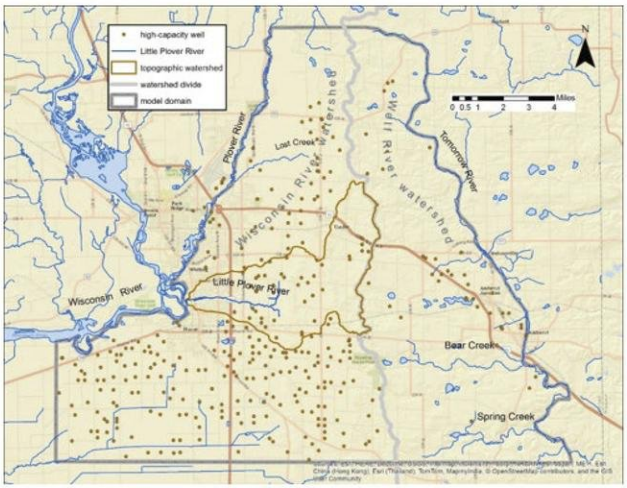

Figure 2. Study area.

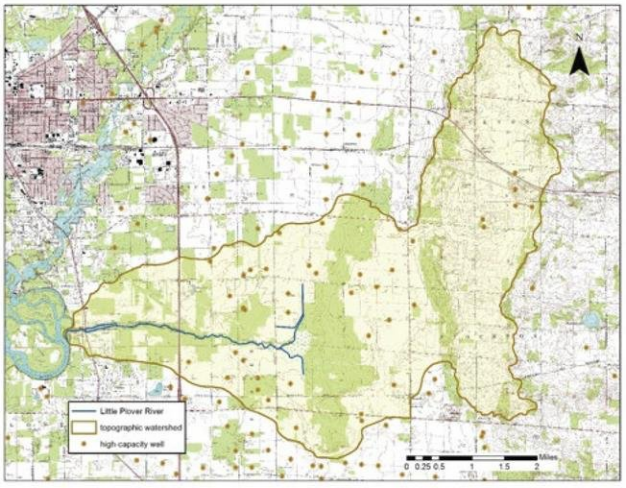

Figure 3. Little Plover River basin.

of irrigation wells; and changes in land use) affect groundwater and surface-water resources in the basin. Such a tool is critical for undertaking cost-benefit analyses and formalizing the trade-offs inherent to water-use decisions under competing demands.

This work is intended as a demonstration of the type of 21st-century hydrogeologic analysis and optimization that can inform decision-making over wider areas of the Central Sands and other areas of Wisconsin where water-resources conflicts arise. Although the main purpose of this work is decision support, the completed model also will be valuable as an educational tool to help regulators, water users, and citizens visualize and thus understand the dynamics of groundwater flow and the connections among groundwater, surface water, and water use. The model will also serve as an example and prototype of the type of hydrogeologic predictive analysis that can help inform public and private decision-making for groundwater issues in other parts of the Central Sands and other regions of Wisconsin.

Choice of the Little Plover River

The Little Plover River (LPR) basin was chosen as the focus of this effort because there has been ongoing controversy about the possible impact of nearby high-capacity wells on flows in the river. The river and its surrounding drainage basin (figs. 2 and 3) have been previously studied in detail by the USGS and WGNHS (Weeks and others, 1965), and the geology and hydrogeology of the basin are well understood. In addition, the DNR has established public rights minimum flow/stage requirements for the river, which help articulate and formalize societal constraints needed to assess management trade-offs (see the "Little Plover River Rights Flow Order" report at http://dnr.wi.gov/water/basin/cwrb). Researchers in central Wisconsin (Clancy and others, 2009; Kraft and others, 2012; Kraft and Mechenich, 2010) have documented recent conditions in and around the river.

Objectives

Objectives of this project were to develop the following:

- A groundwater flow and optimization model as a science-based expert system for decision support of water management in the Little Plover River basin and as a pilot study to evaluate techniques that can later be expanded to the entire Central Sands.
- A platform to demonstrate fundamental scientific constraints inherent to the hydrologic system and context for the costs and benefits for differing scenarios.
- An educational tool for fostering science-based discussion for both the public and the technical community.

Approach

This project developed a three-dimensional, transient groundwater flow model of the Little Plover River basin using the U.S. Geological Survey's MODFLOW code (Harbaugh, 2005), and a related USGS groundwater optimization code, GWM-2005 (Ahlfeld and others, 2005). Recharge for the model was estimated using a soil-water-balance (SWB) technique (Dripps and Bradbury, 2007; Westenbroek and others, 2010) developed by WGNHS and USGS scientists in Wisconsin and now in routine use for regional modeling studies.

Setting and study extent

The Little Plover River is located in Portage County, Wisconsin, south and east of the city of Stevens Point and the Village of Plover (fig. 2). The focus of this study is the Little Plover River and its topographic drainage basin (fig. 3), but the area investigated and simulated in this work extends westward to the Wisconsin and Plover Rivers and east to the Tomorrow River (fig. 2). This larger study area represents the extent of the active groundwater model and will be referred to as the model domain in the remainder of this document. Most of this area is rural or semi-rural, and the climate is humid and temperate, with average (1971–2000) precipitation of 32.7 inches and average temperature of 44.2°F (http://aos.wisc.edu/~sco/clim-history/division/4705-climo.html). Winters are typically cold and snowy, with many days below freezing; summers can be hot and humid.

The Little Plover River flows westward and drains into the Wisconsin River. The river's surface water basin covers 21.4 square miles (Henrich and Daniel, 1983) and extends from the Wisconsin River to a regional divide between the Wisconsin and Wolf River basins. East of this watershed divide, surface water flows eastward, discharging into the Tomorrow River and eventually into the Wolf River. USGS discharge measurements at the Little Plover River Hoover Avenue gage (USGS site 05400650) for the period 1959–1987 record average, minimum, and maximum daily discharges of 10.6, 3.9, and 81 cubic feet per second (cfs), with a $Q_{7,10}$ of 4.75 cfs. "The 7-day, 10-year low flow ($Q_{7,10}$) is a statistical estimate of the lowest average flow that would be experienced during a consecutive 7-day period with an average recurrence interval of 10 years. Because it is estimated to recur on average only once in 10 years, it is usually an indicator of low flow conditions during drought" (Illinois State Water Survey, 2015). Clancy and others (2009) report Q_{10} and Q_{50} of 6.6 and 9.4 cfs respectively for the 1959–1987 period. Their Q_{10} and Q_{50} statistics are analogous to the more commonly used USGS flow duration statistics, reported by the USGS as 90 percent flow duration = 6.5 cfs and 50 percent flow duration = 9.4 cfs (http://streamstatsags.cr.usgs.gov/gagepages/html/05400650.htm#31). Kraft and others (2014) updated these statistics using baseflow separation and reported Q_{10} and Q_{50} of 6.4 and 9.0 cfs respectively for baseflow at the USGS gage at Hoover Avenue.

Legally established public rights flows exist for the Little Plover River and are discussed in the model streamflow measurement section of this report. The public rights flow is the flow "of sufficient volume and depth to protect fish and wildlife (including aquatic life), and their respective habitats" (see the "Little Plover River Rights Flow Order" report at http://dnr.wi.gov/water/basin/cwrb). These minimum flows were established by DNR order in March 2009.

Funding sources and acknowledgments

The Wisconsin Department of Natural Resources (DNR) provided the majority of funding for this project. The Wisconsin Potato and Vegetable Growers Association (WPVGA) contributed funding to purchase geophysical equipment used in the project, and the U.S. Geological Survey (USGS) contributed federal matching funds. DNR staff (Daniel Helsel, Larry Lynch, Eric Ebersberger, and Shaili Pfeiffer) provided administrative oversight and helped facilitate public meetings. Members of the WPVGA Water Task Force, including Louis Wysocki, Nick Somers, Randy Cherney, and Alvin Bussan, were extremely helpful in providing access to land, helping the research team understand current irrigation and cropping practices, verifying land-use data, and developing the land-use and irrigation tables for the soil-water-balance model. The Village of Plover (Dan Mahoney) provided streamflow and water-level data, and Del Monte Foods Inc. shared data on groundwater monitoring and infiltration. Personnel from Roberts Irrigation Company Inc. (Paul Roberts and Marvin Hopp) were invaluable in answering questions about local groundwater conditions and irrigation practices. WGNHS personnel who assisted with the project include Pete Chase, Linda Deith, Anna Fehling, Steve Mauel, Mike Parsen, Caroline Rose, Pete Schoephoester, and Carolyn Streiff.

A technical advisory committee established for the project met with the project team several times and provided invaluable advice. Members of the committee included Charles Andrews, Douglas Cherkauer, George Kraft, John Panuska, and Ken Wade.

This report underwent an extensive peer review process following WGNHS and USGS protocols. David Hart (WGNHS) and Howard Reeves (USGS) provided formal peer reviews. Adam Freihoefer (DNR) compiled additional reviews from the DNR staff and members of the technical advisory committee. Jim Butler (Kansas Geological Survey) and James Drought (GZA GeoEnvironmental Inc.) submitted additional informal comments. The authors thank these individuals for their very thorough and helpful comments and suggestions. Madeline Gotkowitz (WGNHS) served as the review coordinator and significantly improved the final document.

Geology, hydrostratigraphy, and hydrology of the Little Plover River region

Geology and hydrostratigraphy

Geological materials in the Little Plover River study area consist of sandy or gravelly stream or lake sediment and till over Cambrian sandstone and Precambrian crystalline rock. Previous investigators (Clayton, 1986; Holt, 1965; Weeks and others, 1965) describe most of the material in the basin as undifferentiated Pleistocene-age sand and gravel deposited as stream and offshore lake sediment in front of glaciers advancing from the northeast. The most recent glacial advances, occurring between 10,000 and 20,000 years ago, deposited a series of moraines just east of the headwaters of the Little Plover River. These moraines are composed of sandy till that contains boulders and cobbles. Clayton (1986) reports that the sandy till is difficult to distinguish from the underlying stream sediment in subsurface samples, and the boundary between the moraines and the underlying sediment is uncertain. Behind (east of) the moraines, the landscape is hummocky due to the presence of ice-contact features such as kettle lakes. In front (west) of the moraines, the landscape is generally flat, with a regional slope toward the Wisconsin River of about 10 feet per mile.

The thickness of Pleistocene sediment ranges from more than 150 feet in and east of the moraines, to absent where bedrock outcrops at the surface in the western and northern parts of the study area. Over most of the study area, the underlying bedrock is Precambrian crystalline rock (usually gneiss, schist, or coarse-grained granite) (Weeks and others, 1965). However, isolated patches of Cambrian sandstone form the uppermost bedrock in places in the western half of the Little Plover River basin (fig. 4). These sandstone knobs occasionally outcrop at the surface. The buried bedrock surface often consists of a clayey or silty weathered residuum. Windblown sand forms thin patchy dunes at the surface in the western and southern parts of the basin. Peat deposits occur in low-lying areas, notably in the headwaters of the Little Plover and in a larger area in the northwest in the model domain.

The Precambrian surface, which forms a lower boundary to the groundwater system, slopes generally from northwest to southeast across the project area (fig. 5). The elevation of this surface ranges between 1,000 and 1,100 feet above mean sea level (msl) along the Wisconsin and Plover Rivers and slopes to about 900 feet above msl in the southeast. The discontinuous Cambrian sandstone occurs in mounds up to 57 feet high in the western part of the Little Plover River basin, where a few outcrops of sandstone occur at the land surface (fig. 6).

The sand and gravel in the study area forms an important and prolific unconfined aquifer. The top of this aquifer is the water table, assumed to be the top of the saturated zone. The capillary fringe, where the aquifer pores are saturated, but under negative pressure, extends above the water table, but is presumably less than a few inches thick in the sandy material and is not considered in the remainder of this report. The bottom of the aquifer is the Precambrian surface. Where present, the Cambrian sandstone is generally much less permeable than the overlying sand and gravel. Over most of the study area, Precambrian crystalline rock makes up the uppermost bedrock. This crystalline rock has low hydraulic conductivity and forms the lower boundary of the groundwater system.

The aquifer system in the project area is thin, with the combined sand and gravel and sandstone ranging in thickness from more than 100 feet

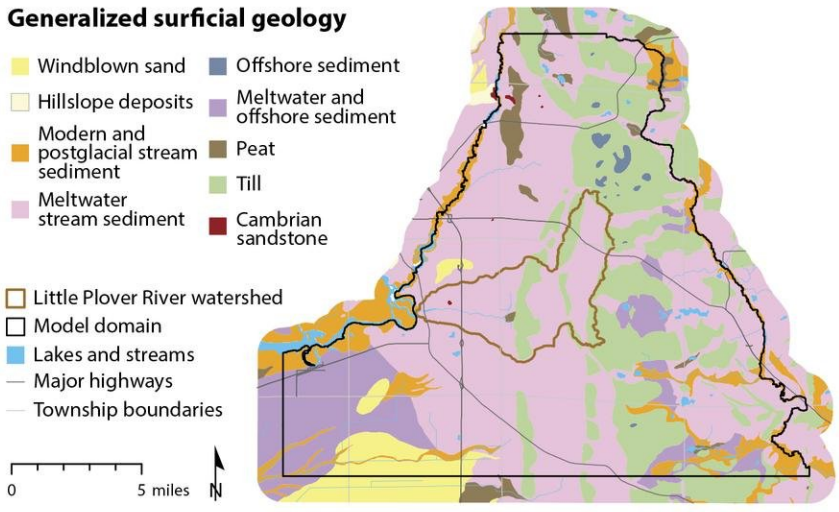

Figure 4. Generalized surficial geology. Modified from Clayton (1986).

to less than 10 feet across the model domain (fig. 7). A nearly identical range applies to aquifer thickness in the Little Plover River basin.

Although a regional aquitard (the New Rome silt) is probably present in the sand and gravel south of the study area (Clayton, 1986), we found no evidence of a continuous aquitard in several cores collected in the LPR basin. Some of the cores contained non-continuous silty or clayey intervals that likely contribute to horizontal to vertical hydraulic anisotropy in the aquifer.

Surface-water features

Rivers and streams

The study area is well drained, with few unaltered streams. The Little Plover River begins in a series of drainage ditches just west of the Village of Arnott and flows to the west, discharging to the Wisconsin River between the Villages of Plover and Whiting (figs. 2 and 3). Just upstream of the discharge point, the Little Plover is artificially impounded by a dam, forming Springville Pond. About 6 miles north of the Little Plover, Lost Creek also flows west, discharging to the Plover River. Lost Creek drains a large wetland complex called the Jordan Swamp. About 4 miles south of the Little Plover, a series of drainage ditches conducts water westward into Buena Vista Creek and finally to the Wisconsin River. These ditches are more than 100 years old, and range from 5 to 10 feet deep and 5 to 15 feet wide. They are maintained by occasional dredging and generally flow year-round. Faustini (1985) studied the ditches in the Buena Vista basin and concluded that they have major influence on

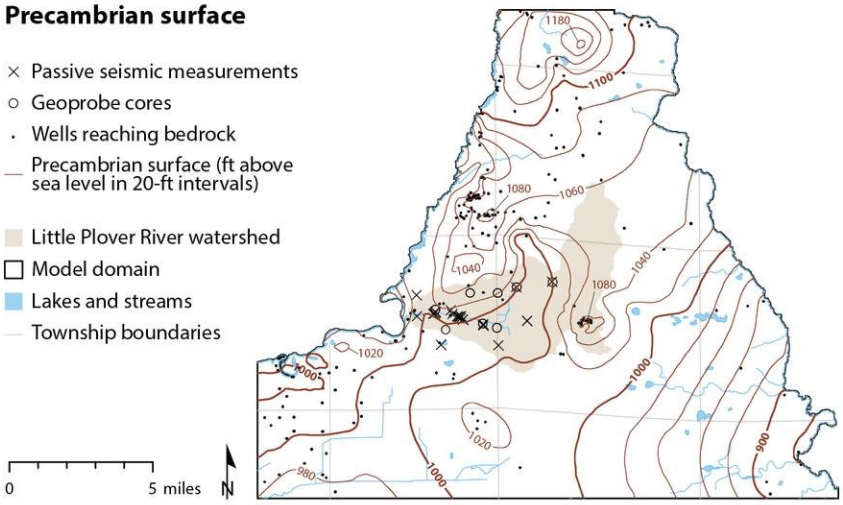

Figure 5. Precambrian surface of the study area.

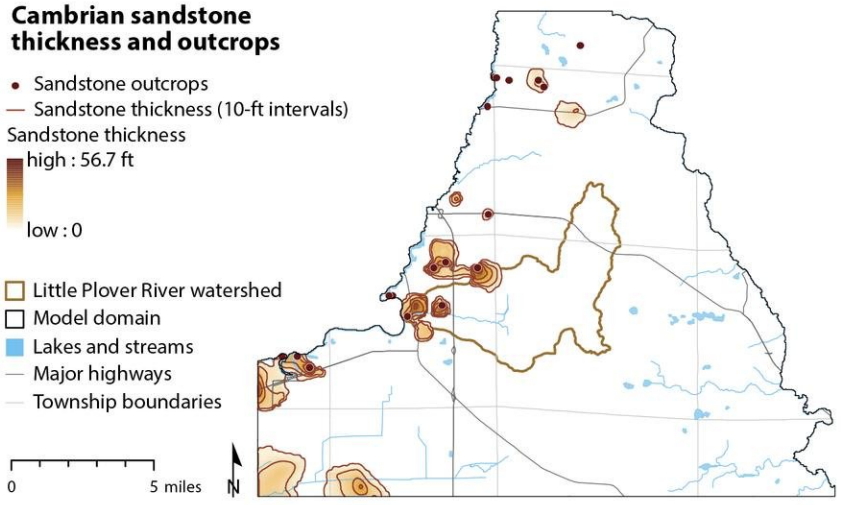

Figure 6. Cambrian sandstone thickness and outcrops.

regional groundwater flow paths and can be hydraulically fully penetrating, in some cases allowing no groundwater to pass beneath them.

East of the regional topographic divide, several small streams have their headwaters in the hummocky moraine near the divide and flow eastward to discharge to the Tomorrow River. From south to north these streams are (fig. 2) Spring Creek, Bear Creek, and an unnamed creek near Nelsonville commonly referred to as Stoltenberg Creek. Stoltenberg Creek is not named on the USGS 7.5-minute topographic map, but is listed in the DNR register of waterbodies. These streams range in length from 3 to 5 miles and generally flow year-round.

Lakes and wetlands

The few natural lakes in the model domain all occur in the hummocky terrain east of the regional topographic divide (fig. 2). Major lakes (from south to north), include Spring Lake (on Spring Creek), Lake Lime, Bear Lake and Adams Lake (in the headwaters of Bear Creek), Thomas Lake, and Lake Emily. Small lakes west of the regional topographic divide were artificially created by dredging to the water table, often as part of construction projects. These lakes include Bluebird Lake, Lake Clar-Re, and an unnamed lake just southwest of the Hwy 51/Hwy 54 intersection. With the exception of Bluebird Lake, none of these lakes are in the Little Plover River topographic basin.

The Jordan Swamp is the largest wetland in the model domain and lies between the terminal moraine and the Little Plover River about 6 miles north of the Little Plover. A small wetland occurs at the head of the Little Plover just west of the moraine.

GROUNDWATER FUNDAMENTALS

Groundwater and surface water—a single resource

DETAILS: Surface waters (lakes, streams, wetlands) in the region occur at places where the water table intersects the land surface. Streams in central Wisconsin are supplied by groundwater discharge. Lakes and wetlands, depending on their location in the landscape, can be groundwater discharge points or flow-through features.

WHY IT MATTERS: Groundwater and surface water are well connected and should be thought of as a single resource. Groundwater discharge is the source of baseflow in streams. Groundwater controls lake levels. Changes to the groundwater system affect surface water and changes to surface water affect groundwater.

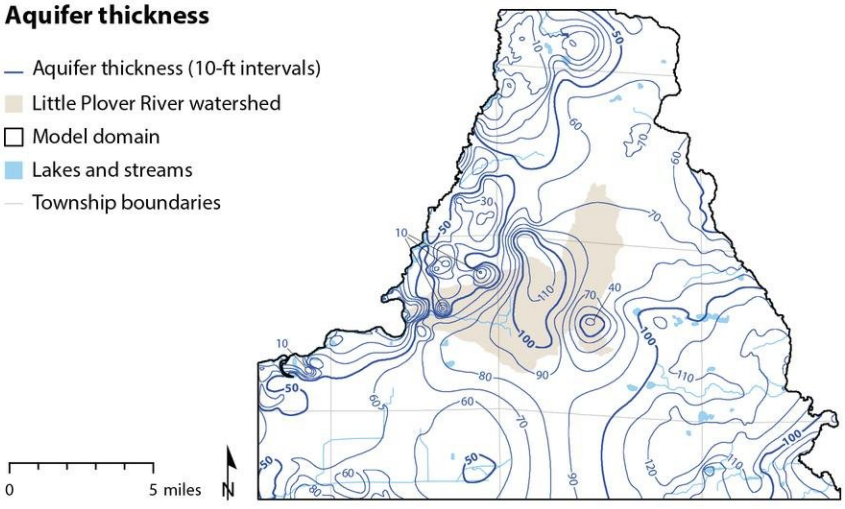

Figure 7. Aquifer thickness in the study area.

Study methods

Water use

The location and pumping rates of both public and private high-capacity wells—those wells capable of withdrawals greater than 100,000 gallons per day (gpd) or roughly 70 gallons per minute (gpm)—were obtained from databases maintained by the Wisconsin Department of Natural Resources (R. Smail, personal communication, 2015). Since 2007, Wisconsin high-capacity well owners have been required to report monthly total water use to the DNR, but complete records only go back to about 2011.

High-capacity wells

High-capacity wells in the study area fall into three main categories: agricultural irrigation wells, industrial wells, and municipal wells. Irrigation wells generally operate only during the growing season (June through September) and during that time are used sporadically, depending on weather, crop type, and stage of plant growth to deliver appropriate crop irrigation. Most local growers use some form of irrigation scheduling (an approach that uses relationships among weather patterns, crop needs, and soil conditions to predict the best times to irrigate) to optimize use of irrigation water. Industrial wells in the area include wells used for vegetable processing and for sand and gravel washing at several gravel pits located along the moraines. These wells operate somewhat seasonally. In contrast, municipal wells in the area operate year-round and are generally used every day. Other high-capacity wells in the area serve non-irrigation agricultural uses, including fire protection, public businesses, and commercial supply. During 2013, there were 498 high-capacity wells located in the model domain, of which 424 were reported to be in use. Table 1 shows the breakdown of these wells by major water-use categories.

Groundwater use in the model domain varies throughout the year and from year to year. Figure 8 illustrates the distribution of water use during 2013 and 2014. In 2013, a typical year, municipal water use is relatively constant through the year at about 2 million gallons per day (mgd), and industrial use increases from about 3 mgd in the winter to 4 mgd during the summer. Irrigation pumping does not occur in the winter, but rises to over 110 mgd during the summer growing season. Water use in 2014, a wetter year, follows a similar pattern, but has a slightly lower magnitude of irrigation pumping during the summer months.

Low-capacity wells

Numerous low-capacity wells—those that produce less than 70 gpm—occur in the model domain and primarily serve single-family homes and farms. Some of these wells were professionally drilled and have an accompanying well-construction report; others are driven sand points lacking any construction information. The DNR does not collect water-use information from private low-capacity wells. Moreover, many of these wells are on properties with onsite septic systems, and the water pumped is largely recycled on the same property. Based on Village of Plover and Portage County records (C. Mechenich, Central Wisconsin Groundwater Center, personal communication, 2015) there are 95 residences, 4 multi-family dwellings, and 9 commercial facilities in the Village of Plover served by low-capacity

Table 1. Distribution of water use by high-capacity wells in the model domain during 2013. See figure 8 for distribution of pumping over the year.

Water-use category	Number of wells	Total annual use (Mgal)	Daily average (mgd)	Percent of total	Use rank
Irrigation	346	9,215.69	25.25	81.36	1
Industrial	19	1,381.64	3.79	12.20	2
Public supply (municipal)	8	650.07	1.78	5.74	3
Non-irrigation agricultural use	23	75.94	0.21	0.67	4
Fire protection	4	1.71	0.00	0.02	5
Public other than municipal	11	1.23	0.00	0.01	6
Domestic supply	11	0.97	0.00	0.01	7
Commercial	2	0.36	0.00	0.00	8
Totals	**424**	**11,327.61**	**31.03**		

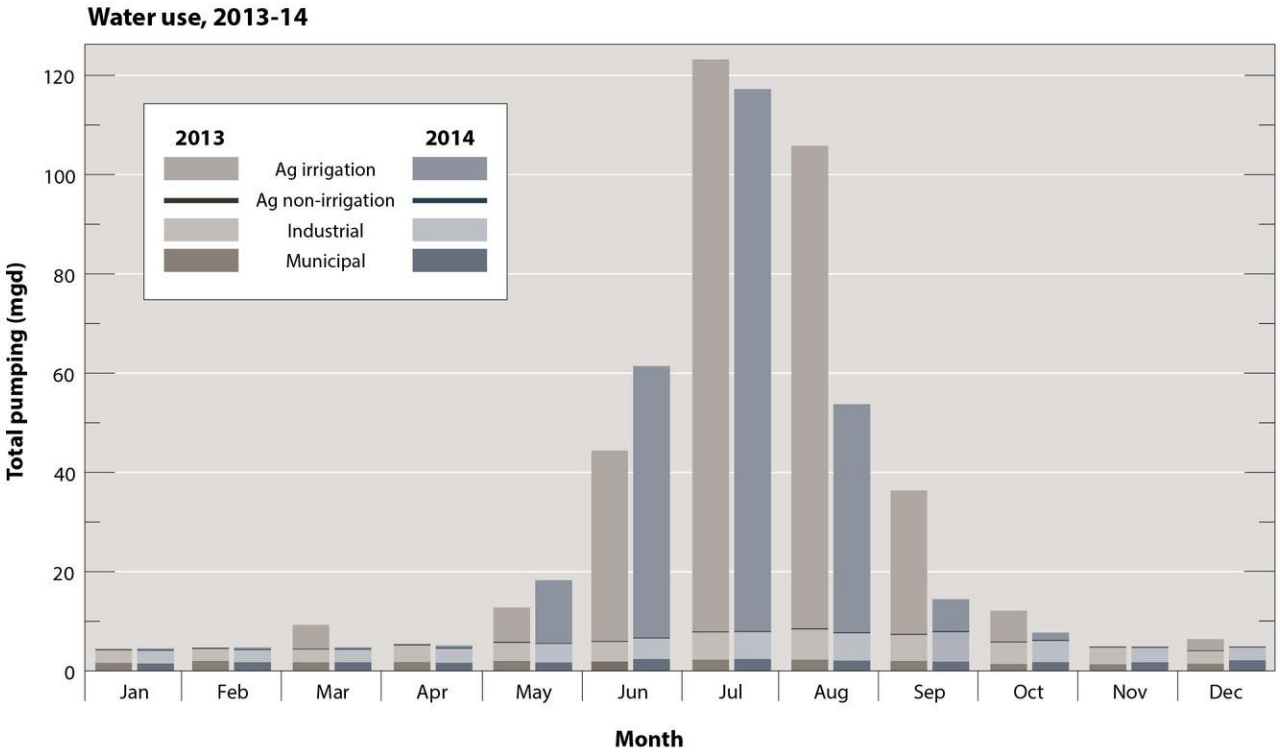

Figure 8. Groundwater use, by type, in the model domain, 2013–2014.

wells, and these are the majority of low-capacity wells in the entire model domain. The estimated combined water use from these wells ranges from 0.01 to 0.06 mgd. This range is an order of magnitude smaller than the major water uses shown in table 1, and the use is distributed over a wide area. These wells are not considered a substantial portion of the water balance for the purposes of this project and were not included in the groundwater flow model.

Streamflow measurements

Discharge records for the Little Plover River

Records of the discharge history of the Little Plover River are important for determining how river discharges have varied historically, for determining the low-flow and public rights flows of the river, and for establishing flow targets for model calibration. The

Table 2. Flow data availability along the Little Plover River.

Location name	Drainage basin area (mi^2)	Collection agency	Type of measurement	Period of record	Comments
Kennedy Avenue	2.24	USGS (site #: 05400600, name: LPR near Arnott)	continuous	7/1/59–7/9/76	discontinued 1976
		Village of Plover	continuous	11/1/09–7/1/14	stage only, many gaps in record
		UWSP	periodic baseflow	5/11/05–present	stage and discharge
Eisenhower Avenue	16.6	USGS (site #: 05400625, name: LPR near Plover)	continuous	11/14/13–present	new gage installed 11/13
		Village of Plover	continuous	11/1/09–10/28/14	stage only, many gaps in record
		UWSP	periodic baseflow	11/7/07–present	stage and discharge
Highway 51/I-39	n/a	UWSP	periodic baseflow	7/11/05–present	stage and discharge
Hoover Avenue	19.0	USGS (site #: 05400650, name: LPR at Plover)	continuous	7/1/59–9/30/87	discontinued 1987
		UWSP	periodic baseflow	5/4/05–present	stage and discharge

history of discharge measurements on the Little Plover River is summarized up to 2009 in Clancy and others (2009). Since 2009, researchers at the University of Wisconsin-Stevens Point (UWSP) have continued to measure "discharge during baseflow conditions" at specific locations (G. Kraft, personal communication, 2014).

Locations of flow measurements

Several agencies and research groups have collected measurements of flow in the Little Plover River. Most of these measurements come from four locations (fig. 9). Table 2 summarizes these records. Clancy and others (2009) and Weeks and others (1965) document incidental measurements at other locations along the river, and a citizen group, the Friends of the Little Plover River, also collects flow data (see http://www.friendsofthelittleplover-river.org/science/flow-rates/).

Developing a record of recent flows in the Little Plover River required a synthesis of the stage and discharge data collected at the various sites along the river. The three sites having the most abundant flow measurements are the river crossings at

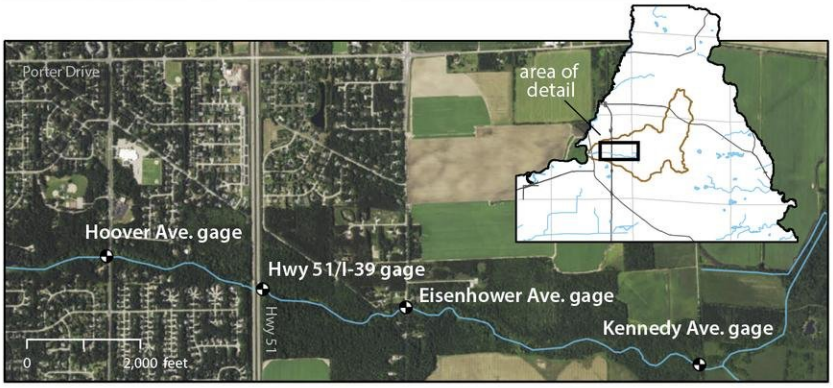

Figure 9. Streamflow measurement sites along the Little Plover River. *(Basemap source: Esri)*

Hoover Avenue, Eisenhower Avenue, and Kennedy Avenue. Hoover Avenue is the location of the longest-term gaging station on the river. It was operated by the USGS beginning in 1959, but discontinued in 1987. Eisenhower Avenue is the site of a concrete flow-measurement weir installed by the USGS during detailed studies of the river in the 1960s (Weeks and others, 1965). The Village of Plover monitored river stage at this weir from 2009 to 2015, but did not collect any corresponding discharge data. The weir itself is damaged and cannot be used alone to develop a stage-discharge curve. In November 2013, the USGS installed a new gaging station directly adjacent to the old weir and began continuous-stage monitoring combined with periodic flow measurements that allow the construction of a rating curve. Kennedy Avenue was the site of a USGS gage discontinued in 1976. The Village of Plover has monitored river stage at this site continuously since 2009, but winter freeze-ups and equipment problems have resulted in a very sporadic record at this site, and no rating curve was constructed.

Development of new rating curves

Eisenhower Avenue site

The purpose of developing new stage-discharge rating curves at the gaging sites is to establish a relationship between the near-continuous stage measurements and the periodic river-discharge measurements. This relationship allows calculation of river discharge at any measured stage level. Since 2013 at the Eisenhower site, there are a number of USGS-measured discharges that correspond to Village of Plover stage measurements. Using nine USGS discharge measurements collected between November 2013 and October 2014, the best-fit regression at the Eisenhower site yields a 2nd-degree polynomial:

(EQUATION 1)

$$Y = 0.321 + 0.146 * X + 0.047 * X^2,$$ with $R^2 = 0.968$

where Y = discharge (cfs), and X = stage (feet above datum). Adding additional measurements collected by UWSP researchers gives a total of 17 data points and changes the regression only slightly, to

(EQUATION 2)

$$Y = 0.456 + 0.153 * X + 0.046 * X^2,$$ with $R^2 = 0.965$

Figure 10 shows the resulting rating curves for the Eisenhower site. The curves with and without the UWSP data are virtually identical. The UWSP data focus on baseflow conditions and it is appropriate to include these data in the overall rating curve. The 95-percent confidence envelope for the regression line gives a measure of the expected error in this relationship and shows that both the USGS and UWSP measurements agree equally well.

Kennedy Avenue site

A stage-discharge curve is more difficult to develop at the Kennedy Avenue gaging site because no USGS discharge measurements exist, the Village of Plover stage measurements are sporadic, and the channel geometry is apparently somewhat unstable. Plotting the UWSP discharge measurements made at this site through late 2014 gives the relationship in figure 11. The best-fit linear rating curve, using 50 data points is:

(EQUATION 3)

$$Y = 0.495 * X - 3.81,$$ with $R^2 = 0.57$

As shown on the figure, this rating is very uncertain, with a broad envelope on the 95-percent confidence level around the regression line.

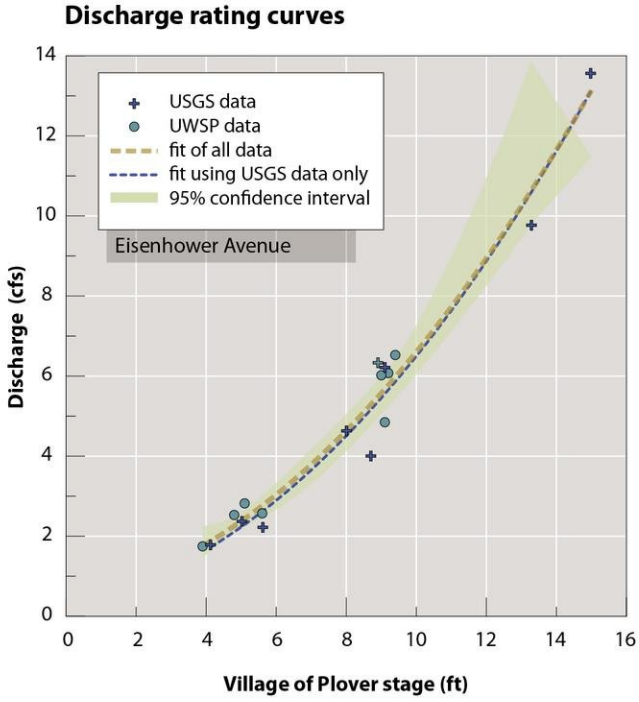

Figure 10. Discharge rating curve, Eisenhower Avenue gage.

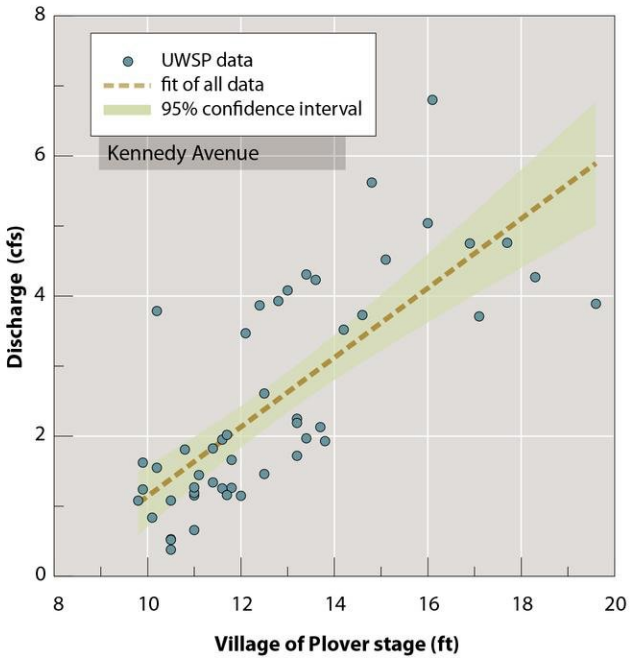

Figure 11. Discharge rating curve, Kennedy Avenue gage.

Reconstructed flow records

Development of new rating curves for the Kennedy and Eisenhower sites has two purposes. First, the rating equations, using the river stage data collected by the Village of Plover, allow the construction of flow hydrographs for these two sites over the periods when the village recorder was operational. Second, reconstruction of these records, which (for the Eisenhower site) are independent of the flow data collected by UWSP scientists, allows comparisons between the UWSP and Village of Plover data.

Beginning at the most upstream site, the hydrograph for Kennedy Avenue (fig. 12) shows that the flows measured by the Village of Plover gage varied between about 0.7 and 8.0 cfs between January 2010 and December 2014. During parts of this time, the river was below the public rights minimum flow of 1.9 cfs. The UWSP data generally agree with this record during the time when both records are available. The UWSP-measured discharges are sometimes lower, and sometimes higher, than the village-measured data, and this variation is largely attributable to the uncertainty in the rating equation (fig. 11). During 2009, prior to installation of the village gage, the UWSP data show that the river discharge was consistently below the public rights minimum and was as low as 0.2 cfs during late summer that year.

Stream discharge calculated from the Village of Plover stage monitoring at Eisenhower Avenue (fig. 13) varied between 1 cfs and about

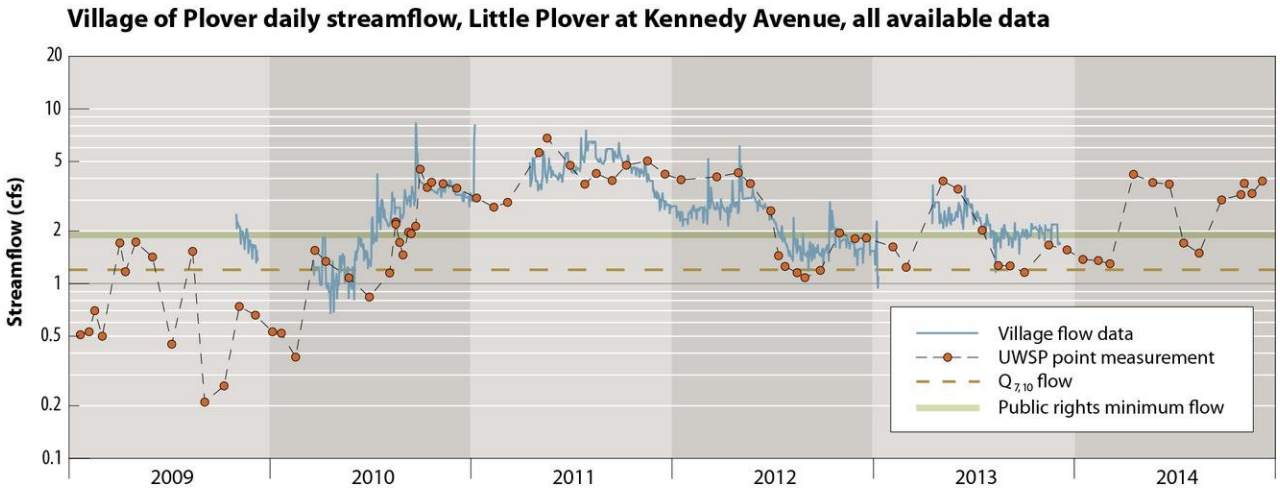

Figure 12. Reconstructed flow at Kennedy Avenue.

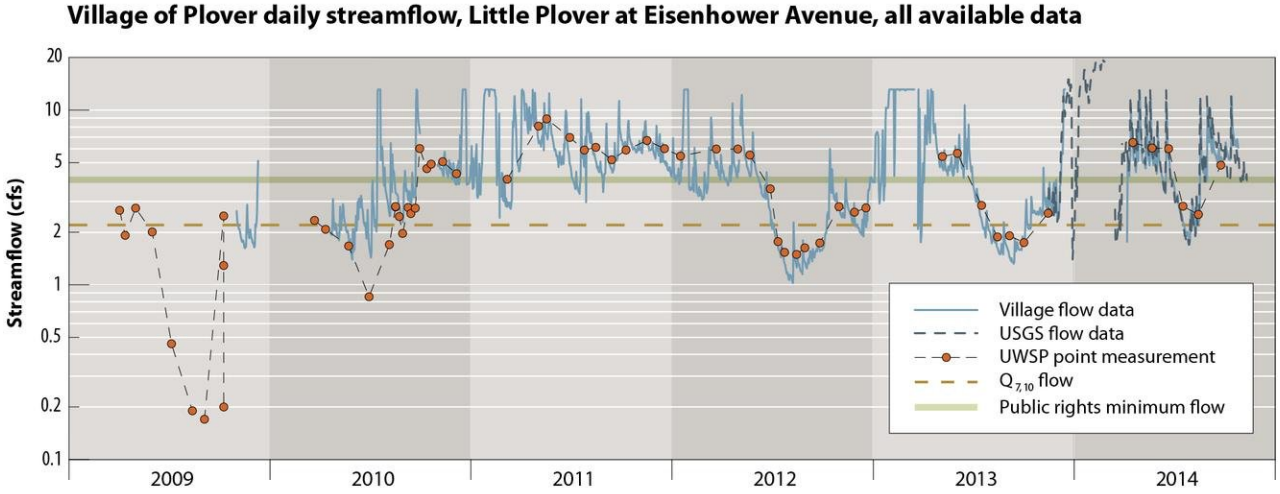

Figure 13. Reconstructed flow at Eisenhower Avenue.

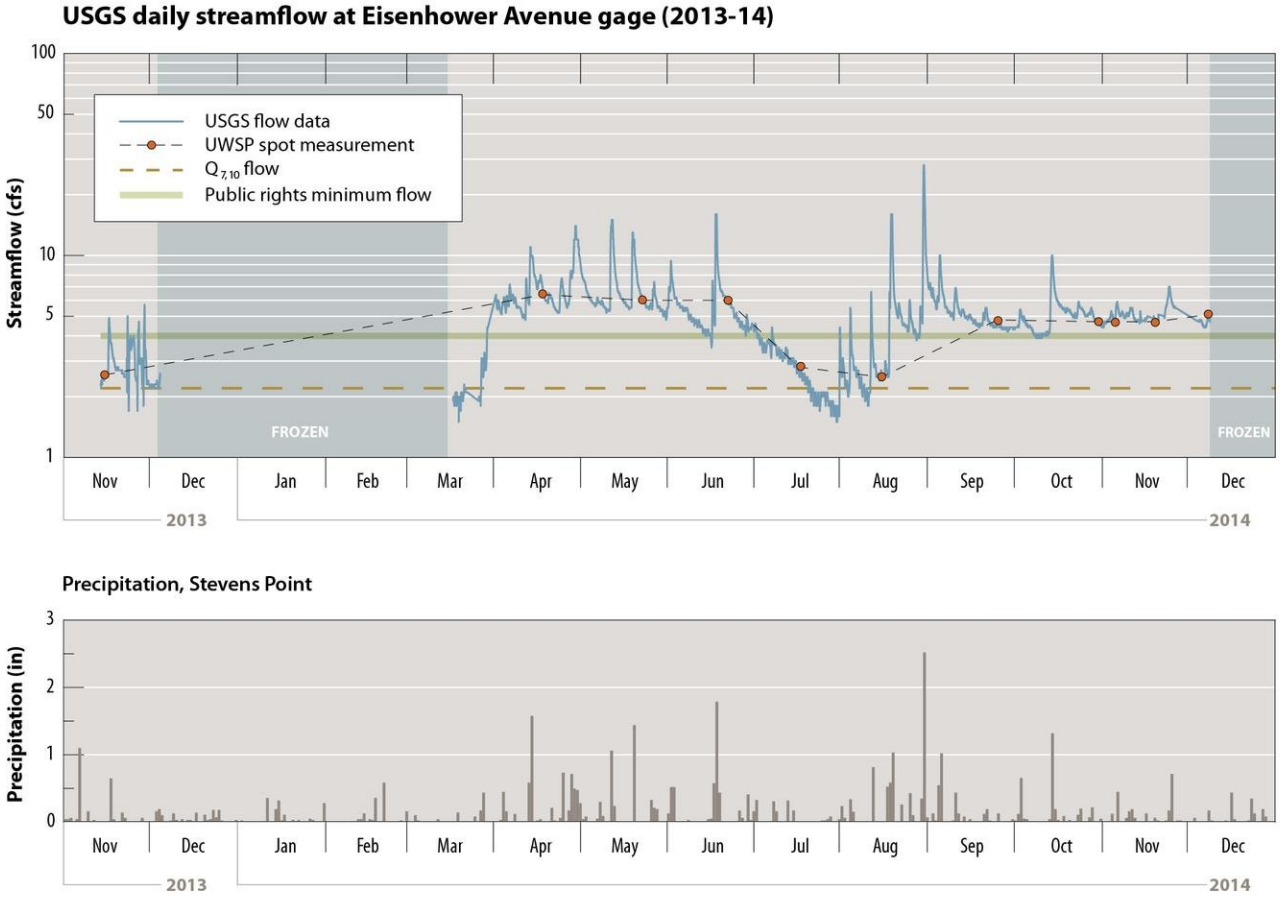

Figure 14. USGS daily streamflow at Eisenhower Avenue and precipitation at Stevens Point, 2013–2014.

12 cfs between January 2010 and December 2014. The village's stage record for this period is more complete than the record at Eisenhower Avenue. During parts of this time, the river was below the public rights minimum flow at Eisenhower of 4 cfs. Based on visual inspection, UWSP flow data from the same period generally agree well with the village data. USGS measurements at this site, which began in November 2013, also appear to agree well with both the village and UWSP data. As with the Eisenhower gage, the UWSP data extend back to 2005, and show that the river flow was exceptionally low for most of that year, reaching a low of about 0.2 cfs during late summer.

Flow monitoring by the USGS, which began in November 2013 and continues to the present day, probably represents the most reliable recent flow record at the Eisenhower Avenue site. The USGS has a long history and reputation for reliable streamflow measurements (Water Science and Technology Board, 2004). Figure 14 is a hydrograph generated by the USGS for late 2013 through 2014. For much of 2014, the flow at Eisenhower Avenue exceeded the public rights stage, but fell below the public rights stage during parts of March, July, and August. Spot measurements taken by UWSP personnel during this period agree very closely with the USGS data.

Analyses of these hydrographs suggest that going forward (after November 2013), the USGS gage is probably giving the most reliable flow data for the Eisenhower site. Prior to installation of the USGS gage the UWSP data set represents a reliable measure of flow at both the Eisenhower and Kennedy sites.

Other streamflow measurements

A round of streamflow measurements was made on December 5, 2013 by USGS personnel. These measurements make up the synoptic measurements discussed in the steady-state observations section. The date was chosen

based on a period interpreted as baseflow conditions due to relatively flat flow conditions at nearby gages and the time of year. The intent was to cover a large portion of surface-water discharge that leaves the model domain to help constrain the overall water balance of the groundwater model. The streamflow measurements were made following standard protocols (Mueller and others, 2013; Turnipseed and Sauer, 2010) with a FlowTracker acoustic flow measurement device. Appendix 1 contains these miscellaneous measurements.

Collection of geologic information

The geology and stratigraphy of the model area reported here is largely based on the work of Clayton (1986). Additional information was obtained from well-construction reports completed by well drillers and stored in a database at the WGNHS. More than 2,000 of these construction reports were examined and geolocated during the data collection phase. A series of Geoprobe cores (appendix 1) collected at 8 sites in the LPR basin during summer 2014 provided additional data on depth to bedrock and samples of the geologic materials present. WGNHS installed piezometers and water-level recorders in these Geoprobe holes. A seismic survey using a Tromino passive seismic instrument performed by WGNHS provided additional estimates of depth to bedrock at 21 sites (see appendix 1). Figures 5 and 15 show the locations of these data sources.

Collection of water-level information

We obtained water-level information for locations throughout the project area from a variety of sources. These sources include:

- Monitoring wells operated by the USGS as part of the statewide groundwater monitoring network
- Monitoring wells operated by the Village of Plover
- Monitoring wells operated by the Del Monte Foods Inc.
- Monitoring wells installed by the Wisconsin Institute for Sustainable Agriculture (WISA)
- Measurements of static water levels in production wells provided by Plover River Farms
- Measurements of static water levels in miscellaneous production wells provided by Roberts Irrigation Company Inc.
- Measurements in piezometers installed by the WGNHS as part of this project. Nested piezometers provided hydraulic heads at two different depths to allow calculation of vertical hydraulic gradients.

For the USGS, Village of Plover, and Del Monte wells, the measuring agency provided measuring-point elevations. For the remaining wells, the project team determined measuring-point elevations in the field using a real-time kinetic (RTK) global positioning system (GPS). Figure 15 shows locations of these data points.

Delineation of bedrock surfaces

Understanding the configuration of the Precambrian and Cambrian bedrock surfaces was important because these formations form the lower boundary to the groundwater system and were used in the Little Plover River model to define model-layer geometry. We used a subset of the geologic data described above to produce contour maps of the bedrock surfaces. This data set included 161 well-construction reports, 33 WGNHS geologic logs, 26 passive seismic soundings at 21 sites, and 17 mapped bedrock outcrops. The surfaces were initially generated using interpolation tools (kriging, inverse weighted distance) in ArcGIS. We manually edited the resulting surface contours

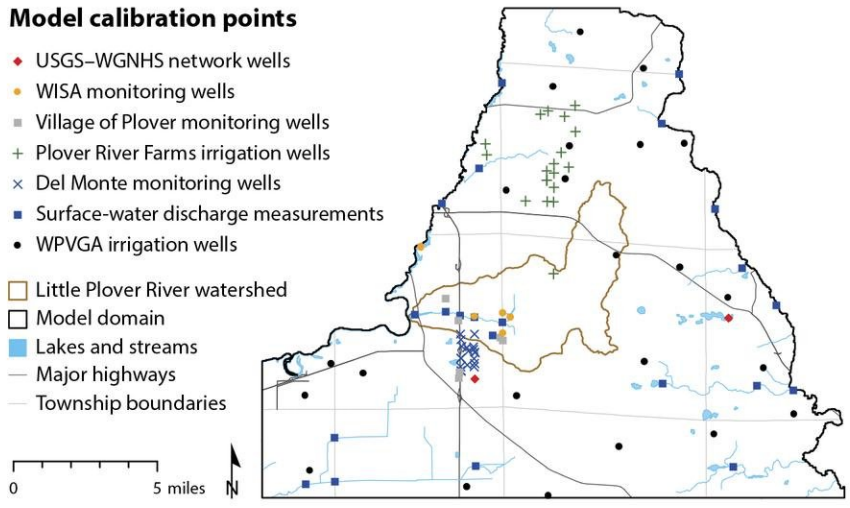

Figure 15. Model calibration points.

to reflect geologic interpretation. We used records from wells that were relatively deep, but did not encounter bedrock, to further refine the bedrock surface contours.

Compilation of hydraulic conductivity data

A wealth of transmissivity and hydraulic conductivity data exist from previous studies in and around the project area. These data include single-well slug tests in wells and piezometers, specific-capacity information recorded by well drillers, and multi-well pumping tests conducted by prior researchers. The quantity and availability of these data eliminated the need for additional testing for the current project. Results from multi-well pumping tests, in which drawdown at nearby observation wells due to pumping a well at a known rate for a known time is measured, are available from reports from USGS studies (Holt, 1965; Weeks, 1969; Weeks and others, 1965; Weeks and Stangland, 1971), as well as a graduate student thesis (Karnauskas, 1977). Bradbury and others (1992) reported values from numerous single-well slug tests in the region. Additional estimates of hydraulic conductivity were obtained from specific-capacity data reported from well-completion tests using the method of Bradbury and Rothschild (1985).

The data compilation included results from 44 slug tests, 305 specific-capacity tests, and 15 multi-well pumping tests (table 3). As expected in heterogeneous materials (Bradbury and Muldoon, 1990), hydraulic conductivity estimates increase with test scale, with the multi-well pumping test values (130 to 500 ft/day) being most appropriate for the regional modeling described in this report. Figure 16 shows that the distribution of hydraulic conductivity is generally log-normal for the pumping tests and specific-capacity data, and skewed for the slug-test data, so that the geometric mean values given in table 3 are valid descriptors of the means of the specific-capacity and pumping-test data. As expected, the mean value for the slug-test data is less robust due to the small volume of material tested (see Bradbury and Muldoon, 1990). Information about vertical hydraulic conductivity is limited. Weeks (1969) used pumping tests to estimate horizontal to vertical hydraulic anisotropy in the Central Sands region and reported values ranging from 2 to 25.

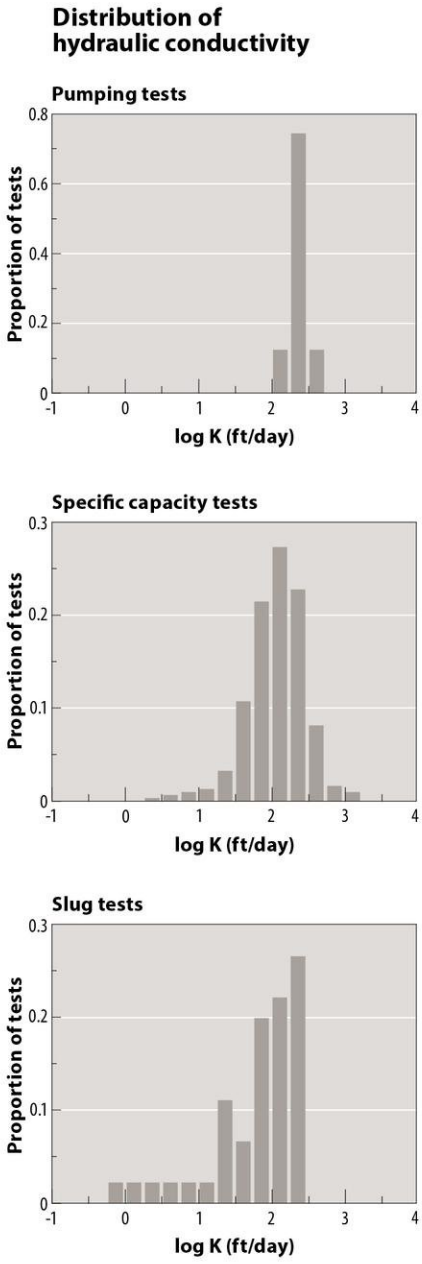

Figure 16. Distribution of hydraulic conductivity using three different methods.

Table 3. Summary of hydraulic conductivity measurements in and around the study area.

	Piezometer-slug tests	Specific-capacity tests	Multi-well pumping tests
Number of tests	44	305	15
Min (ft/day)	0.7	3	130
Max (ft/day)	270	1280	500
Mean (ft/day)	107	172	241
Geometric mean (ft/day)	61	120	228

Groundwater recharge estimation

Understanding the spatial and temporal distributions of groundwater recharge in the study area is critical to building a reliable and useful groundwater flow model. Recharge is a function of precipitation, soils, topography, evapotranspiration, land use, and applied irrigation, and is difficult or impossible to measure directly over large areas. For this project, we initially estimated recharge using a soil-water-balance (SWB) approach; we refined this estimate during model calibration, described in the next section of this report.

Numerical simulation methods

The groundwater flow model uses the USGS MODFLOW-NWT finite-difference code (Harbaugh, 2005; Hunt and Feinstein, 2012) with a Newton solver to improve the handling of unconfined conditions. The model is transient and three-dimensional. It explicitly simulates groundwater–surface water interaction with streamflow routing. We used the Groundwater Vistas graphical user interface (Environmental Simulations Inc., 2011) to facilitate model input and visualize model output. Model calibration used the parameter estimation code PEST (Doherty and others, 2010). Calibration targets used for history matching included heads, streamflows, and lake stages. Steady-state calibration focused on the year 2013; transient calibration focused on spring and summer 2014.

Stakeholder engagement

Relevance

Stakeholder engagement was an important aspect of the Little Plover River model development process. The team aimed to engage stakeholders early and often throughout the project in an effort to improve the ability of the soil-water-balance and groundwater flow models to aid decision-making processes by (1) ensuring model relevancy through the incorporation of structural components necessary for simulating stakeholder-identified questions or concerns, (2) reducing model uncertainty by including datasets collected by numerous institutions, stakeholder groups, and individuals, and (3) increasing stakeholder trust and confidence in the model by validating local and experiential knowledge through inclusion of stakeholder-collected data (stream-stage records and pumping data), testing stakeholder questions, and soliciting stakeholder feedback on intermediary model results.

Methods

Stakeholder engagement took the form of synthesis and verification of stakeholder-collected data; presentations to and discussions with interest groups; public presentations; presentations at local conferences; informal meetings with stakeholders; and tours of farm property, ditches, and irrigation systems. The project team also engaged in periodic update meetings with a technical advisory committee. The Department of Natural Resources, as the project funder, identified committee members. Members represented groups from a variety of interests, including UW-Madison, UW-Stevens Point, DNR, and private consultants.

Recharge estimation

Overview

Groundwater recharge is an important input to the Little Plover River groundwater model, and is defined as water that infiltrates from the land surface, crosses the water table, and becomes part of the groundwater system (Anderson and others, 2015). This project developed a spatially and temporally variable recharge array for the Little Plover River basin model using a modified version of a soil-water-balance (SWB) model (Dripps and Bradbury, 2007; Westenbroek and others, 2010). The SWB model treats groundwater recharge as deep drainage from the soil zone and does not simulate redistribution, storage, or time lag in the unsaturated zone above the water table. Recharge results from the SWB model were used as initial values for the recharge array in the Little Plover River groundwater flow model. This recharge array was subsequently modified using model-wide adjustment factors during groundwater model calibration.

The approach to estimating recharge used in this study involves using two different models—the SWB model and the groundwater flow model (MODFLOW)—sequentially. This approach lacks a direct link between groundwater pumping, which is derived from monthly grower water-use reports, and the fate of that water applied as irrigation, which varies daily in SWB, depending on crop type, growing season, antecedent moisture, temperature, and irrigation amount. While it is theoretically possible to develop a direct link between water use and actual irrigation applications, the collection of sufficient data to do so was beyond the scope of the current project. Instead, the models are linked indirectly; output from SWB is used to develop the steady-state and transient recharge arrays for MODFLOW.

Use of the SWB model allows additional analyses related to the hydrologic cycle in the project area. Of particular interest are differences in the fate of applied water (irrigation) and precipitation and snowmelt under various land uses and crop types. This is accomplished by running the SWB with and without the irrigation module and subsequently evaluating differences in the estimated amounts of evapotranspiration, irrigation return water, and recharge to the groundwater system.

Soil-water-balance method

We used the SWB model [version compiled on February 13, 2015] (Dripps and Bradbury, 2007; Westenbroek and others, 2010) to estimate spatially and temporally variable recharge and evapotranspiration for the model domain. SWB is a deterministic, physically based model that applies a modified Thornthwaite-Mather approach to conduct soil-water accounting (Thornthwaite and Mather, 1957). The model divides the project area into 100-foot grid cells and computes deep drainage based on hydrologic parameters for each grid cell. The SWB grid is coincident with the numerical groundwater model grid.

Water-budget equation

The SWB model operates on a daily time step using climatic, soil, and land-use/land-cover data for a simulated time period. SWB calculates daily deep drainage for each grid cell using a modified Thornthwaite and Mather (1957) soil-water accounting method as the difference between the change in soil moisture and sources and sinks of water within each grid cell (fig. 17). The water-budget equation is:

(EQUATION 4)

$$Recharge = (precipitation + snowmelt + inflow + irrigation) - (interception + outflow + actual\ ET) - change\ in\ soil\ moisture$$

Each water-budget term is defined as follows:

- **Recharge:** The total amount of water (inches per day) that infiltrates into the soil column, reaches the water table, and enters the saturated zone; assumed equivalent to deep drainage. In the soil-water accounting approach to recharge estimation, once the soil column is filled to saturation, recharge occurs. Vadose zone dynamics, such as capillary action, are ignored.
- **Precipitation:** The total amount of precipitation (inches per day) that falls as rain, sleet, hail, or snow; precipitation input into SWB is partitioned into rain or snow.
- **Snowmelt:** The total amount of water (inches per day) that melts from previously accumulated snow; snowmelt is calculated in SWB based on a temperature-index method.
- **Inflow** (entering surface runoff): The total amount of water (inches per day) entering a grid cell via water flowing over the land surface; often called runoff; this overland flow is calculated using a digital-elevation, model-based flow-direction grid.
- **Irrigation:** The amount of pumped groundwater (inches per day) applied directly to the land (grid) surface for agricultural crops; applied irrigation in SWB is dependent on soil moisture and is triggered when soil moisture reaches the maximum allowable depletion.
- **Interception:** The total amount of water (inches per day) that is intercepted by foliage; a maximum quantity of interception is specified.
- **Outflow** (exiting surface runoff): The total amount of water (inches per day) exiting a grid cell via surface runoff; SWB outflow is calculated by use of a digital-elevation, model-based flow-direction grid.
- **Potential ET** (used for calculating actual ET): The total amount of water (inches per day) that could evaporate or transpire from a reference crop if soils are at or close to field capacity.
- **Actual ET** (or AET): The total amount of water (inches per day) that can evapotranspire from a soil layer at a given soil-moisture deficit; actual ET is a scaled portion of potential ET dependent on the available soil moisture. The ratio between actual ET and potential ET is assumed to scale from 1, when a soil is at field capacity, to 0, when a soil reaches the permanent wilting point.

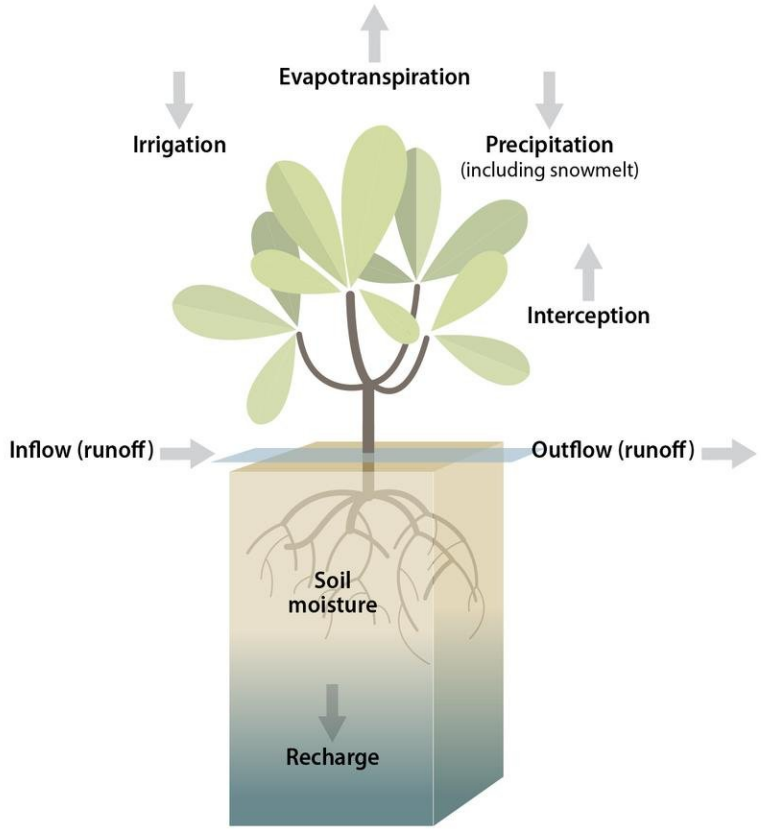

Figure 17. Elements of the soil-water-balance (SWB) model.

- **Change in soil moisture:** Soil moisture on the current day of simulation minus the soil moisture on the previous day; a negative value is obtained when moisture is being removed from the soil layer. The change in soil moisture is limited by a soil's field capacity.

Recharge is generated with equation 4 when inputs minus outputs result in completely saturated soils and some amount of surplus moisture. For a more detailed description of the methodology used for calculating water-budget terms, see Westenbroek and others (2010), Dripps and Bradbury (2007), and Hargreaves and Samani (1985).

Land use

Land use is a critical component of the SWB approach because many of the parameters used in SWB depend on land use. The 2013 USDA National Agricultural Statistics Service (NASS) land-use database identifies 23 land-use categories representing 96 percent of land use in the model domain. Land-use types were separated into irrigated and nonirrigated land use. The seven most prevalent land uses in the model domain are deciduous forest, field corn, alfalfa, grass/pasture, sweet corn, potatoes, and developed open space. Figure 18 shows the spatial distribution and relative percentages of all land uses. In 2013, 26 percent of the land in the model domain was irrigated with high-capacity wells (fig. 19).

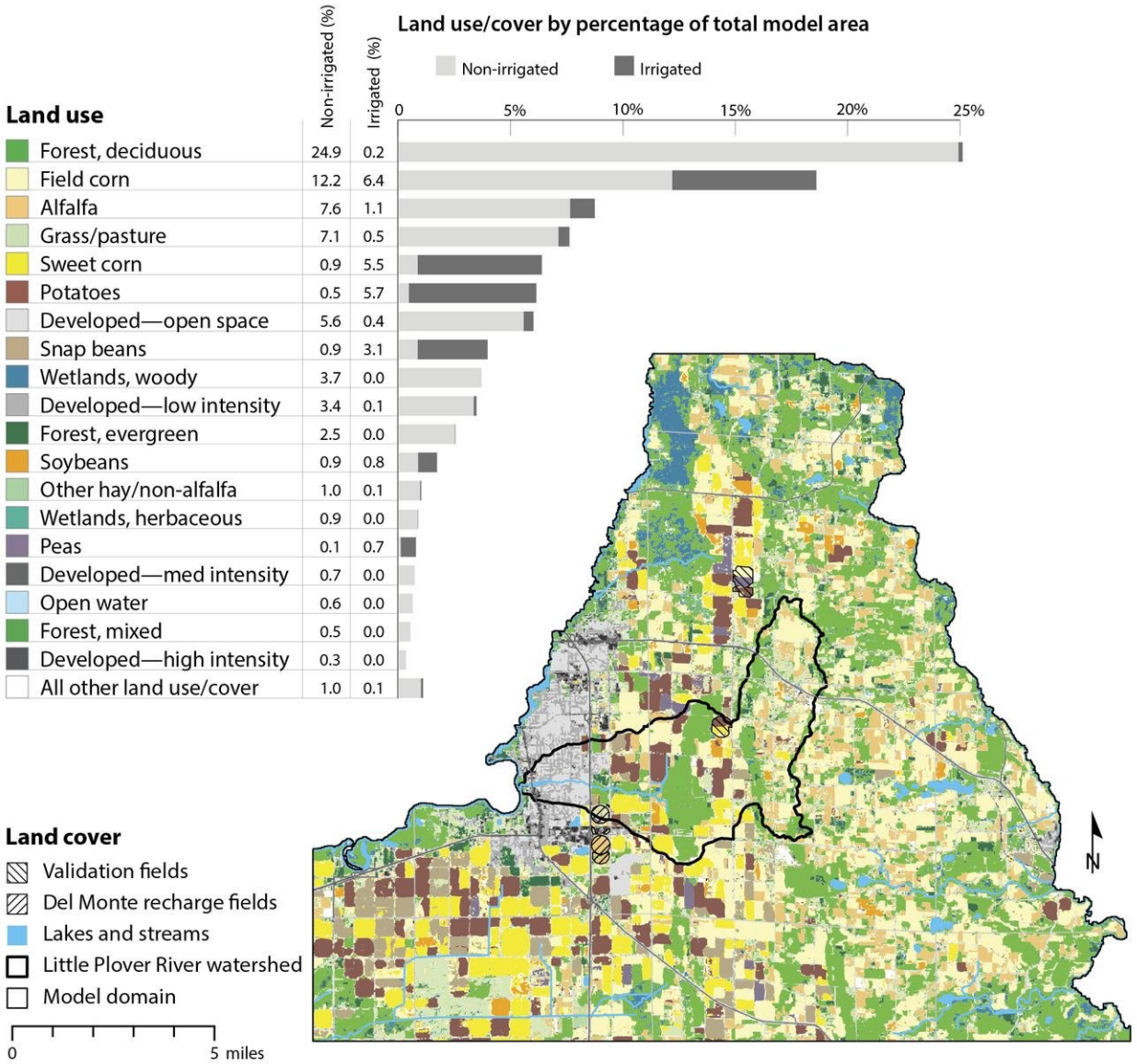

Figure 18. Land use and land cover within the model domain.

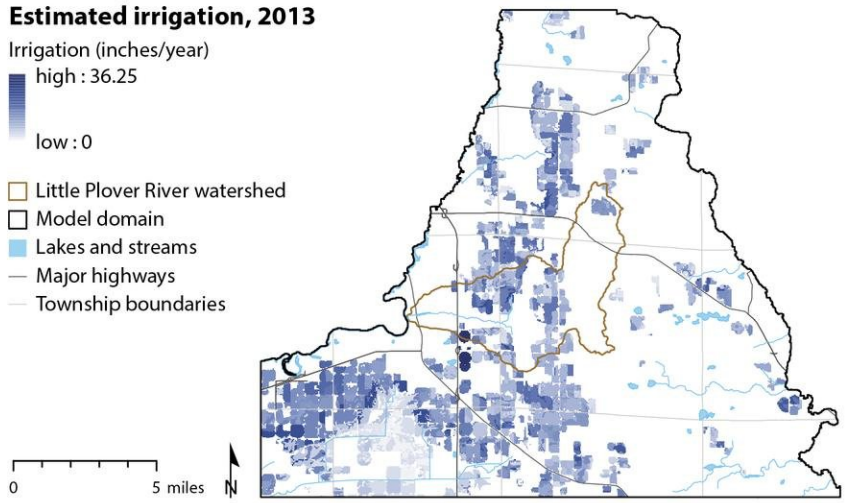

Figure 19. Irrigated land within the model domain, showing model-estimated irrigation rates in 2013.

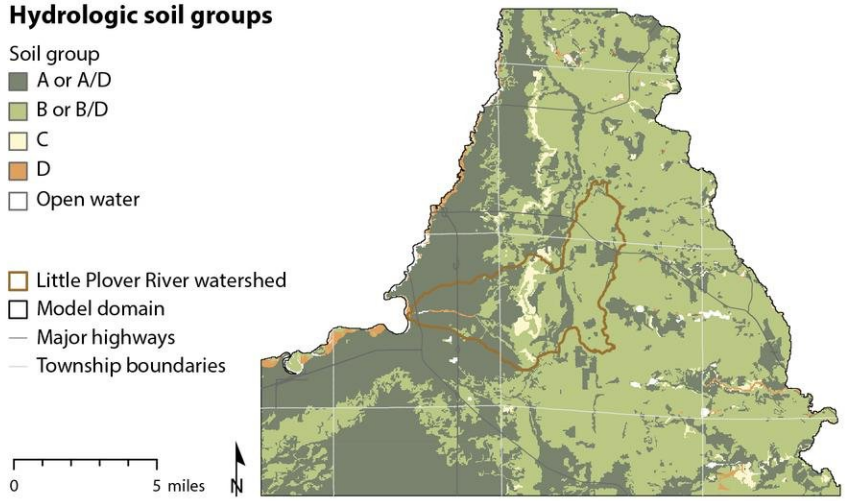

Figure 20. Hydrologic soil groups in the SWB model domain.

Calculation of potential evapotranspiration

The SWB model calculates potential ET in one of five ways chosen by the user. For this project, we calculated potential ET using the Hargreaves and Samani (1985) method, which estimates potential ET using daily maximum and minimum air temperatures and solar radiation (equation 5).

(EQUATION 5)

$$ET_o = 0.0135 K_T (T + 17.78)(T_{max} - T_{min})^{0.5} R_a$$

where:

K_T is an empirical coefficient (0.162 for "interior" regions, 0.19 for coastal regions),

T is the average daily temperature,

T_{max} and T_{min} are the maximum and minimum daily temperatures, and

R_a is the extraterrestrial solar radiation. Air temperatures are expressed in degrees Celsius; solar radiation is expressed as equivalent evaporation, in millimeters per day. The Hargreaves and Samani (1985) method was chosen for its simplicity because it requires only maximum and minimum daily temperatures to estimate potential ET.

Calculation of actual evapotranspiration

To calculate actual ET for the water budget, we used the dual crop coefficient and irrigation module available in SWB to calculate spatially and temporally variable actual ET. This dual crop coefficient methodology calculates actual ET for specific vegetation types by scaling daily potential ET by two coefficients that account for plant transpiration and base soil evaporation, respectively:

(EQUATION 6)

$$ET_c = ET_o * (K_{cb} + K_e)$$

where:

ET_c is crop-specific ET,

ET_o is potential ET,

K_{cb} is the plant transpiration coefficient that reduces potential ET when limited water availability (dry soils) inhibits potential ET rate due to plant stress, and

K_e is the soil evaporation coefficient that increases ET to the potential ET rate when transpiration is not at the potential ET rate and additional energy (in this case, in the form of temperature) is available to evaporate water in the topsoil following a rain or irrigation event.

For additional information regarding K_{cb} and K_e, see Allen and others (1998).

Irrigation simulation

The irrigation module in SWB simulates irrigation by adding water to specific fields using criteria similar to the irrigation scheduling calculations used by many local growers. The irrigation module operates only on specific fields that receive irrigation from high-capacity wells. These irrigated areas were identified using aerial photos, high-capacity pumping locations specified in the DNR high-capacity well database (2013), and discussions with local growers or industry personnel. The irrigation season for most crops was assumed to begin on June 15 and cease September 9. Between these two dates, for most crops an irrigation amount of 0.5 inches was simulated every time the predicted soil-moisture depletion exceeded a vegetation-specific maximum allowable depletion. The 0.5-inch application amount was based on irrigation application amounts reported by growers to the project team. For simplicity, irrigation efficiency, defined as the amount of irrigation water that reaches the crop (not lost to leaks, evaporation in the air, falling on impermeable surfaces, etc.) was assumed to be 100 percent. Irrigation return is defined as the amount of irrigation water that is not used by the crop and is available to recharge groundwater.

Assumptions

The soil-water-balance (SWB) model assumes the following:

- Annual and monthly SWB applied irrigation as computed by SWB and pumping reported by growers to the DNR are similar in magnitude.
- Water that surpasses the plant root zone is considered to be recharge.
- Irrigation parameters for individual crop types are identical.
- No recharge occurs in grid cells specified as "open water" because they drain surface water features.

In addition, the analyses did not include double cropping or cover crops.

Data sources

Using the modified Thornthwaite and Mather soil-water accounting and the FAO 56 dual-crop coefficient (Allen and others, 1998) and irrigation methods, the SWB codes require parameters for climate (daily temperature, daily precipitation), land use/land cover (percent assumed impervious area), soil classification (hydrologic soil group), soil characteristics (NRCS-based curve numbers for runoff, infiltration rates, interception storage, and depth of root-zone parameters), topographic gradients (flow direction for runoff routing), and irrigation (where appropriate) into the simulations (see appendices 2a and 2b). We obtained daily precipitation and temperature data from the National Climatic Data Center's (NCDC) precipitation and maximum and minimum temperature dataset at the Stevens Point airport (http://www.ncdc.noaa.gov/cdo-web/). Daily precipitation and temperature values were assumed to be uniform across the domain. Spatial land-use/land-cover classification over the

GROUNDWATER FUNDAMENTALS

Evapotranspiration from land cover influences water levels and streamflows

DETAILS: Evapotranspiration refers to evaporation off plants, open water, bare ground and transpiration from plants. In the Central Sands transpiration is larger than evaporation. Plants remove water from the soil using their roots and pass it as vapor through stomata into the atmosphere; this flux can be appreciable on the basin scale. The amount of water transpired by plants is a function of the type, density, and size of the vegetation as well as amount of water available in the root zone and time of year. Native plants and trees typically transpire for more of the season than shallow rooted plants and irrigated crops. Evapotranspiration rates are related to plant type, where some wetland plants have appreciably higher rates than upland plants. Regardless of plant type, the highest rates of evapotranspiration occur during the summer months. Peer-reviewed research as well as empirical observations in the Central Sands region indicate that evapotranspiration is most often greatest under irrigated land cover, with differences among the various irrigated crops, followed by forest, nonirrigated agriculture, and grassland. In general, groundwater recharge follows an opposite continuum. Understanding the relative transpiration of native vegetation and irrigated crops is an active area of interest to stakeholders and thus merits greater study.

WHY IT MATTERS: All landscapes lose water to evapotranspiration. The effect of adding irrigation to a landscape increases evapotranspiration relative to the pre-existing land cover.

model domain was defined using the 2013 National Agricultural Statistics Service (NASS) Crop Data Layer (CDL) database (https://www.nass.usda.gov/Research_and_Science/Cropland/metadata/meta.php). Spatial classification of soils follows the U.S. Department of Agriculture's National Resources Conservation Service (NRCS) hydrologic soil groups. Seven hydrologic soil types were modeled in SWB: A, B, C, D, A/D, B/D, and null (open water) (fig. 20). Dual hydrologic soil groups A/D and B/D are used for wet soils that could be adequately drained. The A/D soil was classified as A because the area is adequately drained by ditches. We used a 10-meter-resolution, digital-elevation model (DEM) to determine the topographic gradient and flow direction for each grid cell.

We selected soil, land-use and irrigation parameters in two stages. First, we identified irrigated and nonirrigated land uses/land covers with >1 percent aerial extent of the model domain. For agricultural areas and forested/wetland areas, we adjusted land-use/land-cover type parameters to match those specific to the region. For other land use/land covers and those with <1 percent of the land use, we used default values that have been verified with previous projects using SWB. Regional land-use/land-cover type and irrigation parameters were determined using a combination of published literature, local conference presentations, and personal communication with UW-Extension specialists and growers (appendices 2a, 2b, and 2c).

Selection of test years

We selected 2013 as an appropriate year for developing and testing the SWB approach in the LPR model because it is the most recent year having complete reports of irrigation pumping available. (The 2014 data were not yet available as of April 2015.) More importantly, 2013 is near the 30-year average for annual precipitation. The most recent 30-year average (1984–2014) is 32.6 in/yr (fig. 21). Precipitation for 2013 was 31.5 inches. The wettest months during 2013 were April, May, June, and October, while December was the driest month (fig. 22). The heaviest single precipitation event occurred in early April. During July and August, there were several very dry periods punctuated with one-day rain events.

After establishing reasonable SWB land- and water-use parameters using 2013 data, we ran SWB with climate data from 2012 (a dry year) and 2014 (a wet year) to investigate how recharge varied from year to year and from place to place. Precipitation for 2012 and 2014 was 29.9 and 36.5 inches, respectively. As discussed in the groundwater model calibration section of this report, we used 2014

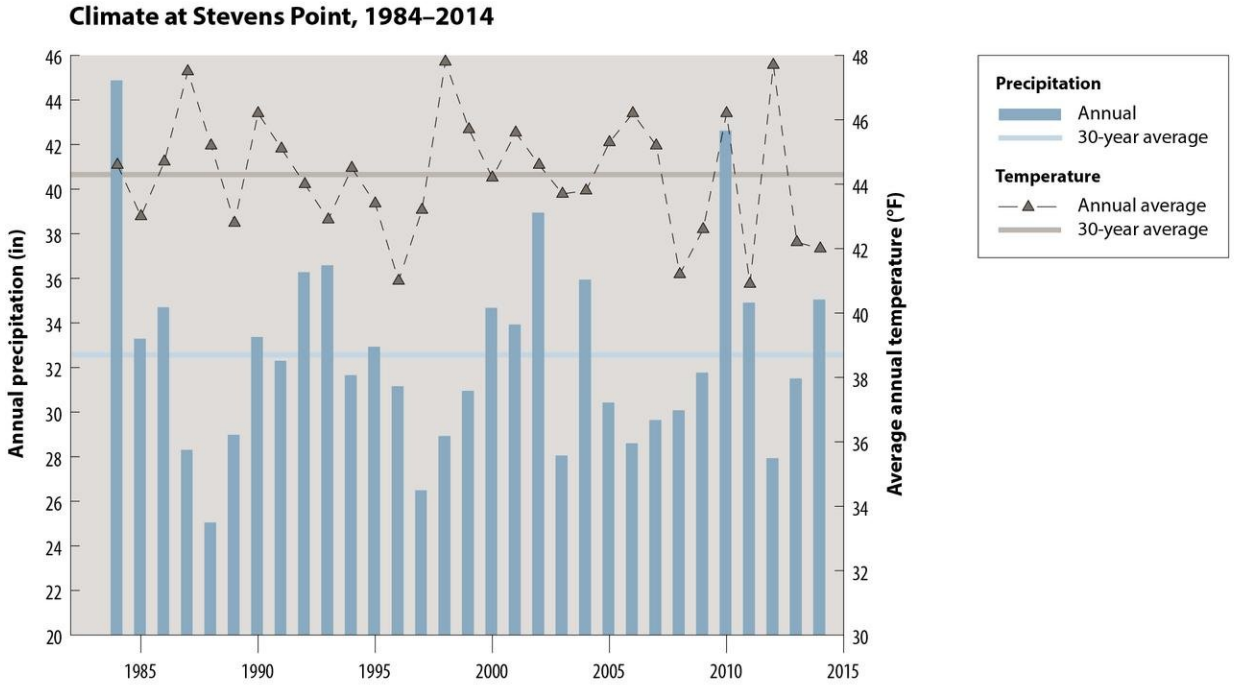

Figure 21. Climate record at Stevens Point, 1984–2014.

SWB-estimated monthly recharge in the groundwater flow model for transient calibration. SWB output from 2012 was not used directly in the groundwater flow model, but serves as a check to better understand the variability in SWB recharge output during dry climate conditions.

Del Monte wastewater application

Del Monte Foods Inc. applies wastewater from their industrial processes to fields in six locations south of the Little Plover River (figs. 18 and 19). The application fields vary in size and contain a variety of crops and land uses. Monthly application records are available from Del Monte for each location for 2013 and 2014. A portion of this applied water reaches the groundwater flow system, while some evapotranspires or runs off. To be consistent with the recharge estimation approach used over rest of the model area, we used the SWB model to partition evapotranspiration and recharge at the Del Monte application sites. Parameters in the SWB model were modified until simulated seasonal total applied irrigation amounts matched reported seasonal total Del Monte applications (+/- 0.5 inches). Del Monte field irrigation and recharge was treated separately and was not used to validate SWB results for the rest of the model.

Model review and validation

Technical advisory committee

As part of the evaluation of the Little Plover project, a technical advisory committee met with the project team two times during the course of model development and analysis. Committee members also were given a mid-project status report focused on recharge and provided written feedback to the model development team. Discussions and report comments revolved around finding acceptable ranges for water-budget terms based on expert knowledge, particularly actual evapotranspiration for specific crop types; land use and irrigation tables; conducting water-budget component comparisons; refining soil hydrologic group parameters; clarifying report summary statistics; stating assumptions and limitations of model runs; and clarifying the method of irrigation application in SWB. Discussions and suggestions from this committee were extremely helpful and were incorporated into this study to the extent possible within the project scope.

Validation methods

Direct field measurements of groundwater recharge are very difficult to obtain and rarely available to hydrogeologists, and this is the case in central Wisconsin. The lack of direct measurements means that SWB recharge estimates are best validated by making comparisons with esti-

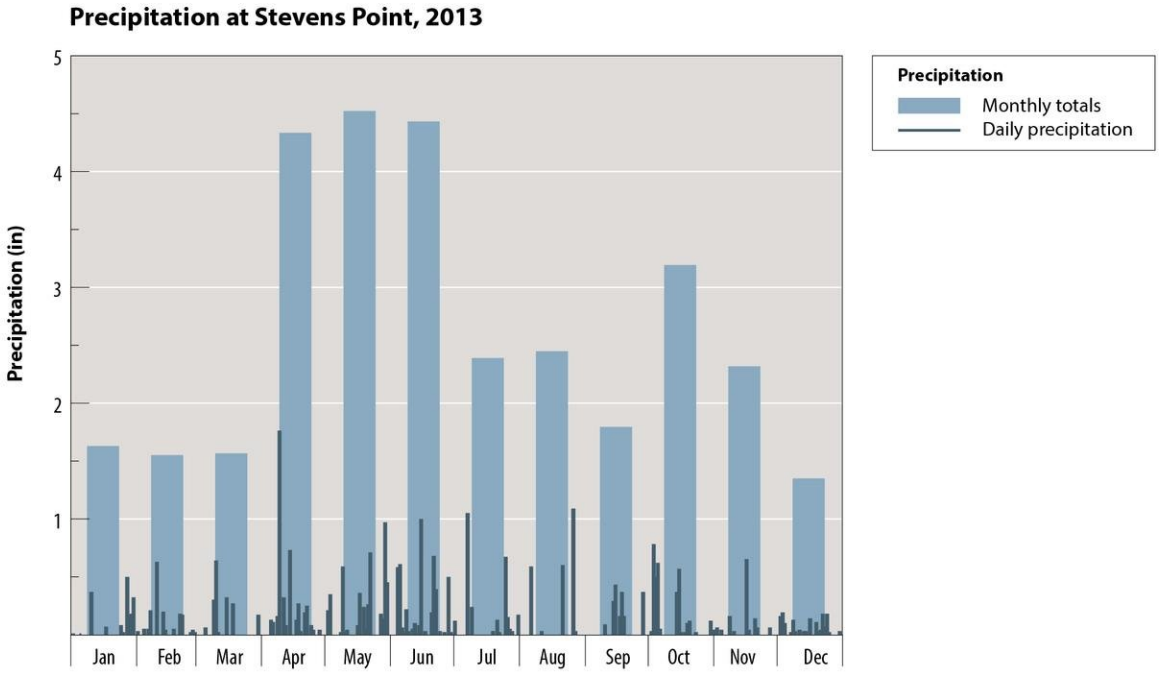

Figure 22. Precipitation at Stevens Point, 2013.

mates of water-budget components, a central topic during meetings with the technical advisory committee. Key recommendations from the meetings were to conduct the following comparisons:

1. **Compare remotely sensed land-use data obtained from the NASS data layer with information from individual growers.** We compared 2013 NASS CDL cropland-use data within the LPR surface watershed with grower records from a survey distributed at a meeting of the Wisconsin Potato and Vegetable Grower Association. Growers and agronomists who owned or worked on cropland within the LPR surface watershed filled out the surveys.

2. **Compare SWB-based estimates of potential ET and coincident estimates from the University of Wisconsin-Extension Agriculture Weather group.** We compared estimated 2013 daily potential ET for a hypothetical field of irrigated corn under identical soil and climate conditions from SWB with estimates from the UW-Extension Agriculture Weather group, which produces the Wisconsin Irrigation Scheduling Program (WISP) (http://agwx.soils.wisc.edu/uwex_agwx/sun_water/et_wimn). Many growers in the Central Sands use WISP or similar software as tools to determine daily irrigation application amounts to maintain maximum water efficiency. Thus, agreement between these two methods for estimating potential ET is important. The UW-Extension Agriculture Weather group uses the Priestly-Taylor method for estimating potential ET in WISP. SWB uses the Hargreaves-Samani (1985) method for estimating potential ET.

3. **Compare SWB-based estimates of applied irrigation and high-capacity irrigation-water use reported to the DNR.** We compared 2013 SWB-modeled estimates of annual applied irrigation and the annual pumping reported to the DNR by growers. We assigned specific high-capacity pumping wells to individual fields based on interpretation of aerial photos and information provided by local growers and conducted field-scale comparisons. At the model-domain scale, we compared 2013 annual applied irrigation estimated using SWB with 2013 annual applied irrigation reported to the DNR.

4. **Compare SWB estimates and satellite-based (MODIS) estimates of actual ET available from NASA.** At the model-domain scale, we compared 2013 actual ET estimated using SWB and NASA's Moderate Resolution Imaging Spectroradiometer (MODIS) (http://modis.gsfc.nasa.gov/data). MODIS data is gridded at a 3,280 x 3,280-foot resolution, while SWB is gridded at a 100 x 100-foot resolution.

Results

Recharge estimates from the SWB model

Output values from the SWB model vary spatially from grid cell to grid cell across the model domain according to differences in soils, topography, crop type, and land use. In this section, we report results as spatial averages over (1) the entire model domain, (2) the Little Plover River watershed, or (3) irrigated fields, as appropriate and as indicated in the text. Unless stated otherwise, these averages include irrigation application to the Del Monte infiltration fields.

A well-known characteristic of the SWB code is the generation of anomalously high recharge values at individual nodes located in closed depressions in the digital-elevation model. To correct this problem, we removed the anomalous values by replacing the recharge value at all nodes exceeding the highest 0.1 percent of recharge values across the entire model domain with the value of the 99.9^{th} percentile for the spatially averaged recharge over the model domain. This correction removed "bulls-eye" anomalies, but had a negligible effect on the recharge distribution or averages.

The results report significant figures to 0.1 inch in order to compare different model runs, but, given known parameter uncertainty, the absolute results are only accurate to about 1 inch. Recharge reported in this section refers to results from the SWB model; the recharge values were

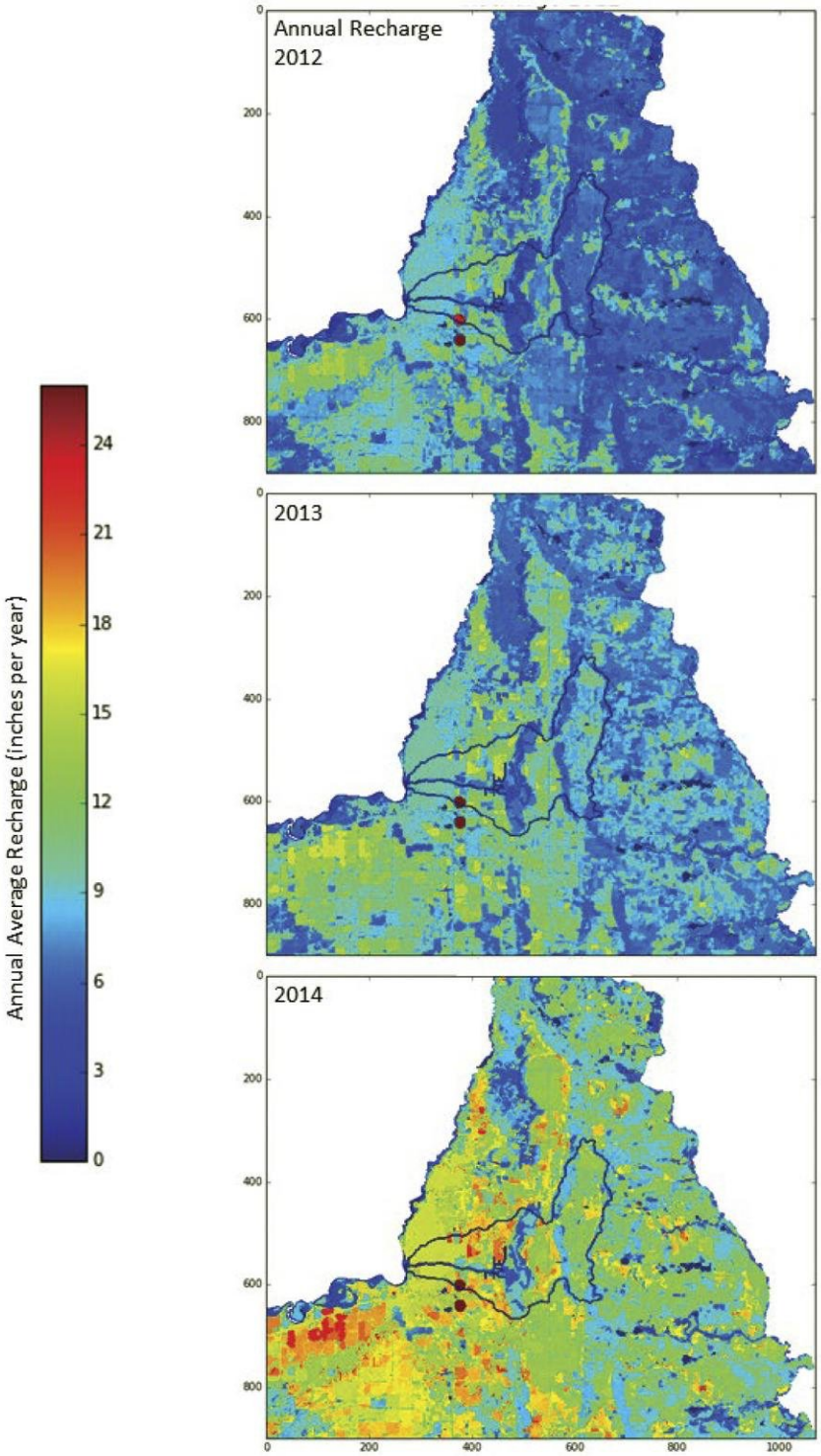

Figure 23. SWB-estimated annual recharge (uncalibrated), 2012–2014. Red circles indicate the Del Monte infiltration fields.

subsequently adjusted using global multipliers during calibration of the steady-state and transient groundwater flow model as described in the section on model calibration.

Recharge varied between dry, average, and wet precipitation years. Measured annual precipitation for 2012, 2013, and 2014 was 27.9, 31.5, and 36.5 in/yr, respectively. SWB-estimated annual mean recharge over the model domain was 7.0, 9.2, and 12.5 in/yr for 2012, 2013, and 2014, respectively (fig. 23, appendix 2d); annual mean recharge over the Little Plover River topographic basin was 7.4, 9.6, and 13.1 in/yr for 2012, 2013, and 2014, respectively.

In general, annual mean recharge was greatest in the western portion of the model domain, which contains flatter topography, coarser soils, and irrigated lands. Spatially averaged recharge over irrigated areas was 9.6, 12.5, and 16.4 inches, respectively, and over nonirrigated areas was 6.1, 8.1, and 11.2 inches, respectively (appendix 2e). [For vegetation-specific estimates of annual recharge for 2012, 2013, and 2014, see appendix 2g.]

The SWB code estimates daily recharge values, but for this project, the results were summed into monthly and annual totals. Spatially averaged recharge over the model domain varied seasonally during each of the three years modeled. The greatest amounts of recharge occurred in the spring; smaller recharge events occurred in the fall (fig. 24, appendices 2h and 2i). April contained the greatest monthly total recharge (>4 inches) in 2013 and 2014, while May contained the greatest monthly

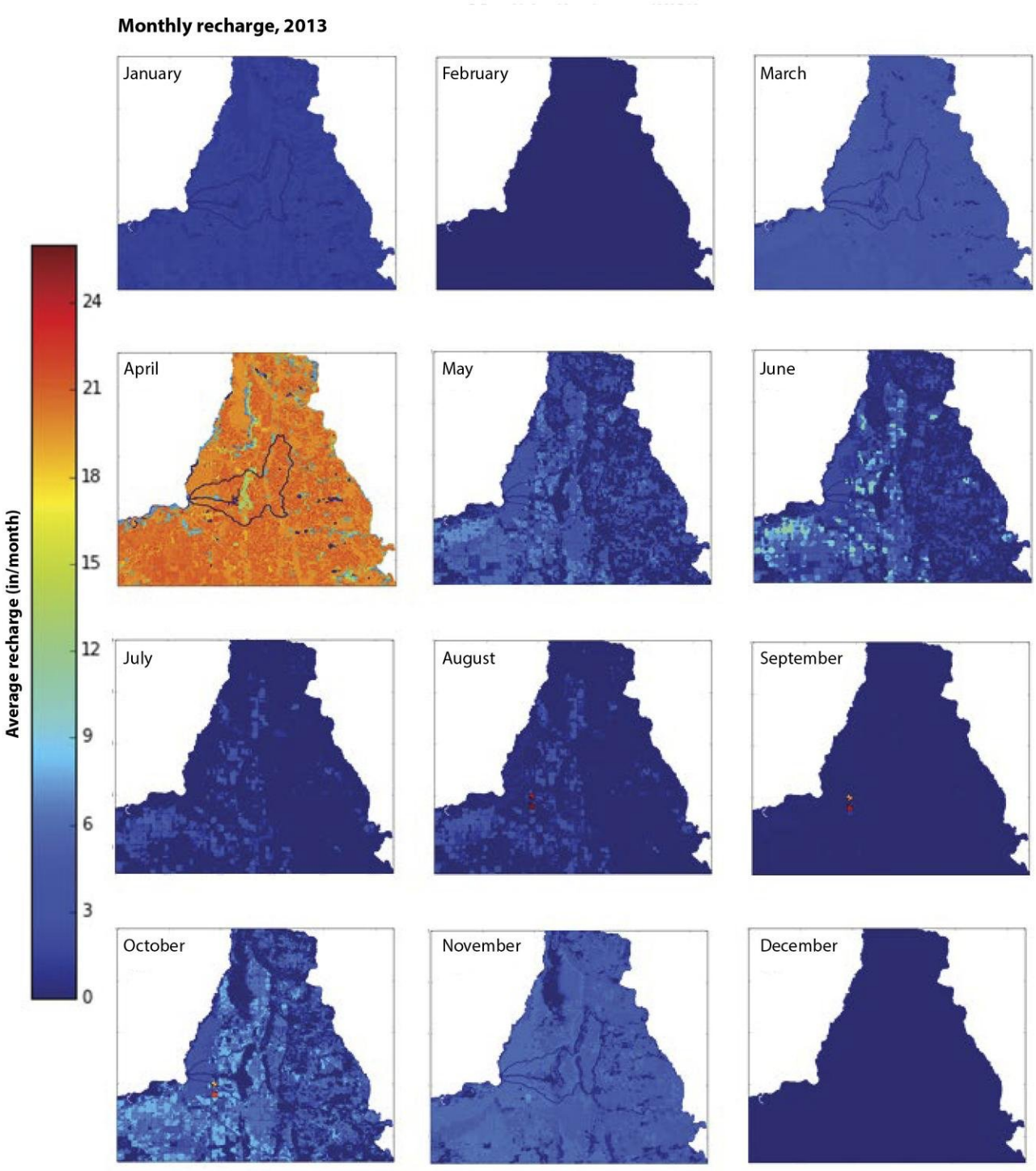

Figure 24. Estimated recharge (uncalibrated) by month, 2013.

total recharge (1.6 inches) in 2012. Very little cumulative recharge (<0.7 inches) occurred during June, July, August, and September during 2012 and 2013, while 2.6 inches occurred during the same months in 2014. For 2012 and 2013, approximately 1 inch of cumulative recharge occurred during December, January, and February, respectively, while 2013 contained 2 inches of cumulative recharge. For all years, October and November contained at least 1.2 inches of recharge. [For mean monthly recharge estimates in 2012, 2013, and 2014, see appendix 2i.]

To evaluate the influence of irrigation on recharge for 2012, 2013, and 2014, we ran the SWB model with identical parameters, but applied no irrigation (by turning off the irrigation module) and compared the results to the previous model runs. Irrigation increased simulated annual recharge by approximately 0.3 in/yr averaged over the model domain during each year. The increase in recharge was 1.1, 1.3, and 1.5 in/yr (between 9 and 12 percent of annual recharge) on irrigated lands for 2012, 2013, and 2014, respectively (appendix 2f). Differences in recharge between irrigated and nonirrigated SWB runs were negligible on nonirrigated lands. These results indicate that if irrigation had not been applied, recharge would have been 1.1 to 1.5 inches less in irrigated areas (8.5, 11.2, and 14.9 in/yr for 2012, 2013, and 2014, respectively) and 0.3 in/yr less averaged throughout the model domain. Comparing these values to the amount of irrigation applied in the model, simulated irrigation return rates ranged from 10 to 21 percent of the annual water recharged (increase in recharge due to irrigation/total applied irrigation x 100). [For vegetation-specific estimates of annual irrigation for the most prevalent land uses, see appendix 2g.]

To evaluate water applied in SWB due to irrigation demand, we summed the amount of simulated annual irrigation. This amount, spatially averaged over the model domain (including both irrigated and nonirrigated lands), was 2.8, 2.2, and 1.8 in/yr for 2012, 2013, and 2014, respectively (appendix 2d). Simulated annual irrigation spatially averaged over irrigated fields was 10.8, 8.5, and 7.0 in/yr for 2012, 2013, and 2014, respectively (appendix 2e). [For 2012-2014 SWB-modeled monthly irrigation spatially averaged over the model domain, see appendix 2i.]

Simulated annual actual evapotranspiration (including interception) spatially averaged over the model domain (including both irrigated and nonirrigated lands) was 21.8, 23.7, and 25.2 in/yr for 2012, 2013, and 2014, respectively (appendix 2d). SWB-modeled annual actual evapotranspiration spatially averaged over irrigated fields was 27.3, 26.8, and 26.7 in/yr for 2012, 2013, and 2014, respectively (appendix 2e). [For 2012-2014 SWB-modeled vegetation-specific estimates of annual actual evapotranspiration for most prevalent land uses or monthly actual evapotranspiration spatially averaged over the model domain, see appendices 2g and 2i, respectively.]

To determine the influence of irrigation on actual ET for 2012, 2013, and 2014, similar to the analysis conducted for recharge, we compared statistics from the SWB models conducted with identical parameters, but without the application of irrigation. Results showed that irrigation increased annual actual ET approximately 2.5, 1.9, and 1.5 inches throughout the model domain in 2012, 2013, and 2014, respectively. When averaged over irrigated lands, actual ET increased approximately 9.6, 7.1, and 5.6 inches for 2012, 2013, and 2014, respectively. Differences in actual ET between model runs with and without irrigation were negligible on nonirrigated lands. These results indicate that approximately 89 percent, 84 percent, and 79 percent in 2012, 2013, and 2014, respectively, of applied irrigated water evapotranspired over irrigated lands (increase in actual ET due to irrigation/total applied irrigation x 100; appendix 2f).

SWB output validation

Land-use comparison

The widely available NASS cropland-data layer is an appropriate measure of land use for the SWB model. Results from the land-use survey distributed to growers and agronomists owning or working on agricultural land within the Little Plover River surface watershed showed that the categorization of 80 percent of the NASS cropland-data layer pertaining to agricultural crops within the watershed matched grower records.

Potential evapotranspiration: point comparison

The potential evapotranspiration (PET) calculation used in the SWB code compares favorably with PET estimates from other sources. For identical soil and climate condi-

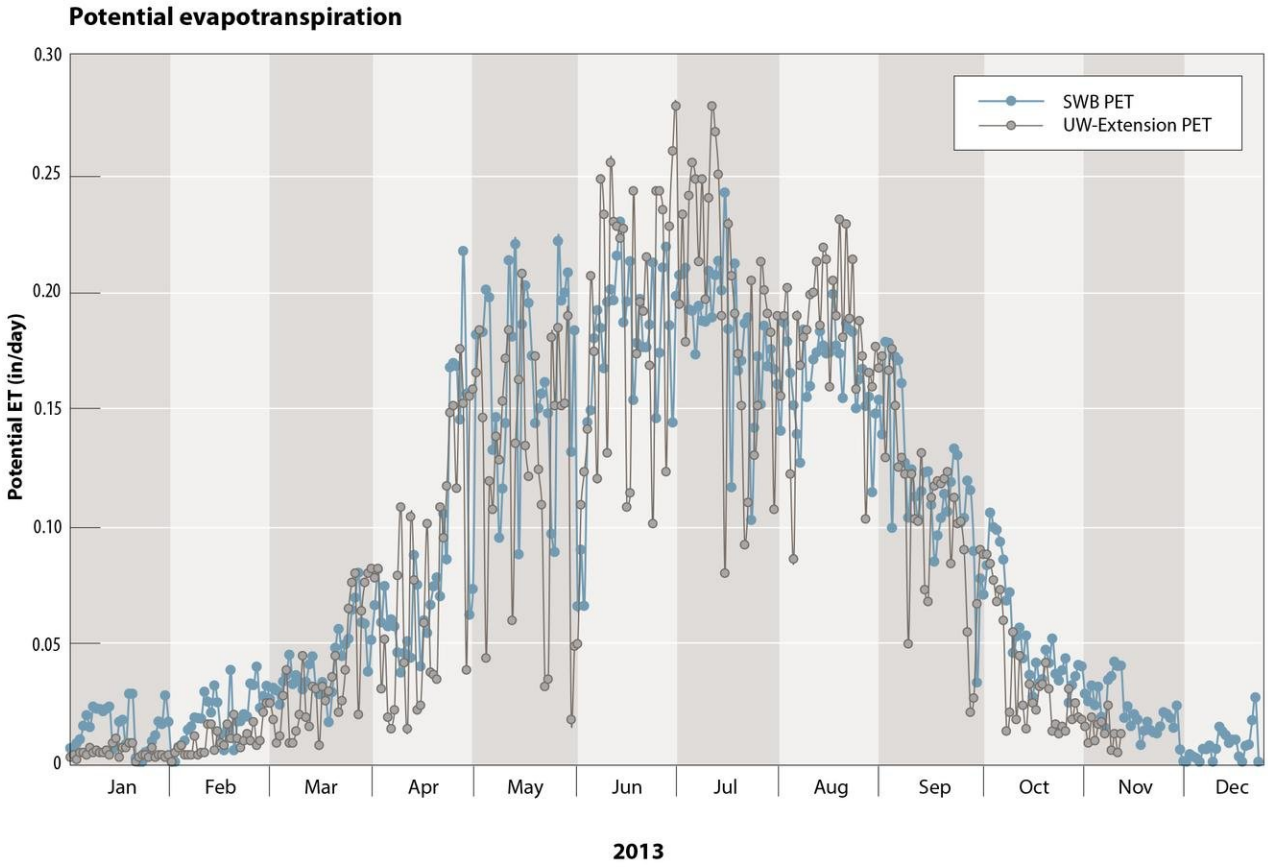

Figure 25. Comparison between 2013 estimates of potential evapotranspiration (PET) from the soil-water-balance model and from the UW-Extension Ag Weather Group for irrigated corn.

tions, we compared daily irrigated corn potential ET for 2013 calculated by SWB (Hargreaves-Samani, temperature-based method) and the UW-Extension Ag Weather Group (Priestly-Taylor, radiation-based method). The comparison was conducted for a hypothetical field of irrigated corn under identical soil and climate conditions at a specific point in the model domain (fig. 25). For 2013, potential ET records for 2013 from the UW-Extension Ag Weather Group ended on November 18. Total potential ET from January 1 to November 18, 2013 estimated via SWB and UW-Extension was 31.9 and 29.8 in/yr, respectively. On a daily time step, SWB-estimated potential ET was often higher in cool-weather months (January, February, November, and December) and lower in warm weather months (June, July, and August) than UW-Extension Ag Weather Group-estimated potential ET.

Comparison of irrigation estimates to water-use records

Although there are inherent uncertainties in both reported water use and in model-derived irrigation estimates, we found reasonable agreement between the two. Simulated annual irrigation for 2013 was 2.2 in/yr spatially averaged over the model domain (including both irrigated and nonirrigated lands) and 8.5 in/yr spatially averaged only over irrigated fields. The DNR annual reported applied groundwater pumped irrigation of 2.5 in/yr spatially averaged over the model domain and 9.6 in/yr averaged only over irrigated fields. For potatoes, field corn, sweet corn, and snap beans, 2013 SWB estimated average annual irrigation rates per crop type ranged between 7.2 and 10.3 in/yr, while the DNR average annual pumping rates per crop type ranged between 7.4 and 9.0 in/yr (DNR, personal communication, April 2015) (table 4).

Actual evapotranspiration comparison

For 2013, SWB-estimated actual ET spatially averaged over the model domain was 23.7 in/yr. In comparison, MODIS-estimated actual ET for 2013 over the model domain was 22.1 in/

yr. SWB-estimated actual ET averaged over the two most prevalent agricultural crops (field corn at 25 in/yr and potatoes at 26 in/yr) was greater than that estimated by MODIS (field corn at 21 in/yr and potatoes at 21 in/yr). SWB-estimated actual ET was slightly less than MODIS-estimated actual ET for the most prevalent land-use type: deciduous forest (22 versus 23 in/yr, respectively). These actual ET values average over specific vegetation types across the model domain and do not distinguish between irrigated and nonirrigated areas. Interestingly, when averaging over irrigated (approximately 6 percent of the model domain) and nonirrigated areas for field corn (approximately 12 percent of the model domain), SWB-estimated actual ET for irrigated field corn was approximately 9 inches greater than that for nonirrigated field corn, while MODIS-estimated AET did not show significant differences (<1 inch) for irrigated and nonirrigated field corn.

Table 4. Comparisons between soil-water-balance (SWB) estimates and pumping-based estimates of irrigation for specific crops, averaged over the irrigated area of the model for 2013.

Crop type	Reported pumping (in/yr)	SWB estimate (in/yr)
Potatoes	9.0	10.3
Corn	8.6	7.5
Sweet corn	7.6	7.2
Snap beans	7.4	8.5

Application of recharge results to the model

Methodology

Soil-water-balance (SWB) output served as initial (pre-calibration) values for recharge rates in both steady-state and transient versions of the groundwater flow model. Daily recharge arrays calculated in SWB were aggregated into gridded annual and monthly recharge arrays for input into the MODFLOW recharge package (described in the model construction section of this report). The SWB-calculated recharge array is one of several parameters adjusted during groundwater model calibration. The calibration process determined multipliers, which applied an equal fractional increase or decrease in the initial recharge rates to each node in the groundwater flow model to improve model calibration. The process for the transient groundwater flow model was similar, with the exception that daily recharge arrays calculated in SWB were for 2014 and were summed by month, providing an array of monthly recharge for model calibration.

Recharge calibration

Steady-state groundwater flow model calibration was conducted with the 2013 SWB-estimated annual recharge array. As discussed in the groundwater flow model calibration section of this report, the best-calibrated steady-state model used a recharge multiplier of 1.08, indicating that an 8 percent increase in the SWB-estimated recharge throughout the model domain was required to obtain a reasonable fit to groundwater head and surface water flow observations. The SWB-estimated mean recharge over the model domain was 9.2 in/yr; after parameter estimation, the optimum mean recharge used in the flow model was 9.9 in/yr.

Transient groundwater flow model calibration was conducted using the 2014 SWB-estimated monthly recharge values as starting points for the calibration. The best-calibrated transient model used recharge multipliers that varied by month and that totaled an annual multiplier of 1.16. Transient groundwater flow model calibration coefficients are discussed in the model calibration section, along with the SWB-estimated recharge.

Discussion

The purpose of the SWB analyses was to develop arrays of spatially and temporally variable recharge over the domain of interest as input for both steady-state and transient groundwater flow models. Annual SWB-estimated recharge results spatially averaged over the Little Plover River basin varied within ranges similar to previous studies reported in the basin. SWB estimates of annual basin recharge in this study were approximately 7.4 inches in 2012 (below-average precipitation), 9.6 inches in 2013 (near-average precipitation), and 13.1 inches in 2014 (above-average precipitation). Weeks and others (1965) estimated recharge rates over the LPR basin of 9.5 and 8.9 in/yr for 1960 and 1961 (note that recharge is equated to estimated discharge), two years with slightly above the 30-year (1984–2014) average precipitation. Gebert and others (2011), using long-term baseflow analysis (1960–1987), estimated average annual recharge of 6.9 in/yr for the LPR basin. Clancy and others (2009) estimated recharge between 10.5 and 13.7 in/yr for a groundwater flow model with calibration targets collected between 1963 and 2007.

For this study, calibration of the steady-state groundwater flow model for 2013 required an 8 percent increase in the SWB recharge estimates in order to reasonably match calibration targets. Several factors probably contribute to this necessary adjustment in recharge. One factor could be the application of a single station precipitation record (Stevens Point Municipal Airport) to the entire model domain. Using spatially variable precipitation would allow for an improved understanding of spatial variability in the groundwater flow model, particularly because the western and eastern portions of the model domain have differing long-term precipitation trends (Kucharik and others, 2010). Other factors that might contribute to the need for adjusting SWB-estimated recharge during the groundwater flow model calibration process include overestimating actual ET and/or underestimating the amount of applied irrigation water. Many parameters determine actual evapotranspiration, including the crop/vegetation coefficients.

For the purposes of this model, the NASS data layer was an effective characterization of the different land-use types and corresponded well with what growers reported. Additional land-use characterization could help to further elucidate trends in water use over the course of several years to decades. Future analyses could include crop rotations and additional delineation of non-irrigated lands, such as types of forests, so that characteristics such as vegetation age, density, and species compositions are considered.

The method selected for computing evapotranspiration affects model results. Comparing SWB-estimated potential ET (Hargreaves-Samani) and the potential ET estimated by the UW-Extension Agriculture Weather group (Priestly-Taylor), showed that SWB-estimated potential ET was often higher in cool-weather months (January, February, November, and December) and lower in warm weather months (June, July, and August) than the potential ET estimated by the UW-Extension Agriculture Weather group. This difference is likely due to the assumptions in the empirical equations of the Hargreaves-Samani temperature-based method versus the Priestly-Taylor solar-radiation-based method for calculating potential ET. Future SWB modeling efforts could consider adjusting the Hargreaves-Samani equation to better match local conditions (Allen and others, 1998).

Uncertainty in actual water use and irrigation rates contributes to model uncertainty. Results reported here indicate that SWB-estimated irrigation over the model domain is similar to, but slightly lower than, water-use records reported to the DNR by Central Sands growers. For 2013, SWB estimated 0.3 inches less irrigation than irrigation pumping records reported to the DNR when averaged over the domain (SWB: 2.2 in/yr; DNR: 2.5 in/yr) and 1.1 inches less irrigation when averaged over irrigated lands (SWB: 8.5 in/yr; DNR: 9.6 in/yr). Such differences in estimated and reported irrigation probably result from both the method and accuracy of modeling and uncertainty in reporting. SWB applies water when soil moisture reaches a maximum allowable depletion. For this study, the maximum allowable depletion ranged between 0.35 and 0.6, depending on the crop. When this maximum allowable depletion occurs, the model applies a user-defined amount of water. For this study, 0.5 inches of water was applied to all crops except alfalfa, which received 0.2 inches of water. Irrigation water is not applied when the soil moisture is above the maximum allowable depletion, allowing rainfall to meet vegetation ET demands. SWB's method of irrigation application captures irrigation trends, but, in reality, the method of irrigation application and its efficiency greatly varies between growers (WPVGA Water Task Force meetings, 2014–2015, personal communication).

Comparisons of SWB-modeling annual actual ET estimates to MODIS-estimated actual ET show that the two estimates are similar when averaged at the domain scale. Averages on a vegetation-specific basis show differences between outputs from the two estimates, which are likely due to differences in estimate scale (the SWB estimates have a much finer resolution) and methods of calculating actual ET. Improving accuracy of these estimates would require field-based observations of evapotranspiration for model calibration. For additional discussion about actual ET in the region, see Weeks and Stangland (1971), Weeks and others (1965), Kraft and others (2012), Motew and Kucharik (2013), and Naber (2011).

Groundwater flow model construction

Overview

The Little Plover River groundwater flow model is a numerical finite-difference model for steady-state and transient three-dimensional groundwater flow. Finite-difference models simulate groundwater flow by dividing the model domain into a geometric grid of rows, columns, and layers—a process called discretization. As a result, the model domain is made up of numerous grid cells, each of which takes on hydraulic or boundary properties appropriate to its position in the groundwater system. Standard groundwater flow equations, which include flow, recharge, discharge, boundary conditions, pumping, and changes in storage, are solved approximately in the finite-difference scheme, and the resulting solution includes hydraulic heads and flow rates. The model uses the USGS MODFLOW-2005 code (Harbaugh, 2005) with the Newton solver, which provides a more numerically stable numerical solution for thin or dewatered model cells (Hunt and Feinstein, 2012; Niswonger and others, 2011). A recent textbook (Anderson and others, 2015) provides a state-of-the-art description of these modeling techniques.

Conceptual model of the groundwater system

A conceptual model of the groundwater system is a synthesis and interpretation of what is known about the study area, and/or a collection of hypotheses about how the groundwater system works, which is subsequently tested and refined in the modeling process (Anderson and others, 2015). Figure 26 illustrates the conceptual understanding of groundwater flow in the project area. The figure is a block diagram that is oriented approximately west to east along the axis of the Little Plover River. The water table forms the upper boundary of the groundwater system, and crystalline rock forms the lower boundary. Most of the unconfined aquifer material is sand and gravel; Cambrian sandstone occurs above the crystalline bedrock in the western part of the model. Lateral hydrogeologic boundaries include the Wisconsin River on the west and the Tomorrow River on the east; these function as regional groundwater discharge points and have approximately constant heads. Recharge from precipitation varies spatially and temporally and occurs almost everywhere in the landscape. Additional recharge occurs under irrigated fields compared to nonirrigated

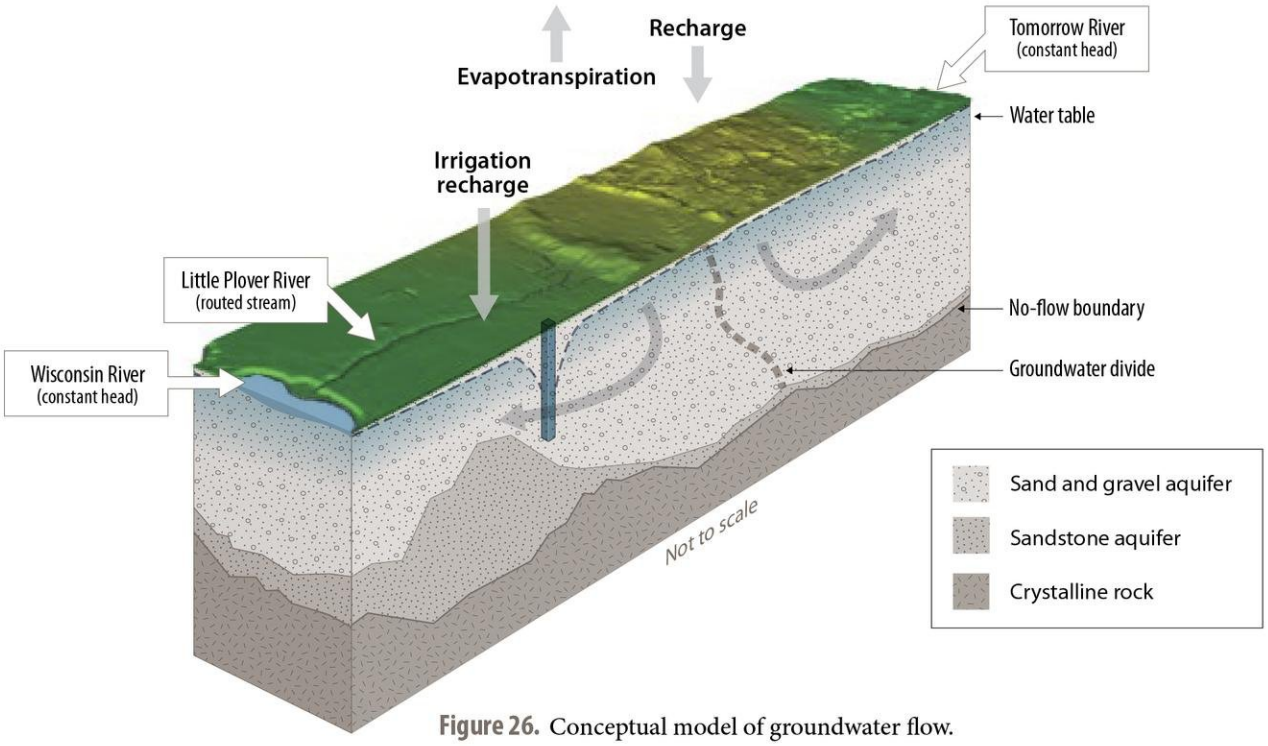

Figure 26. Conceptual model of groundwater flow.

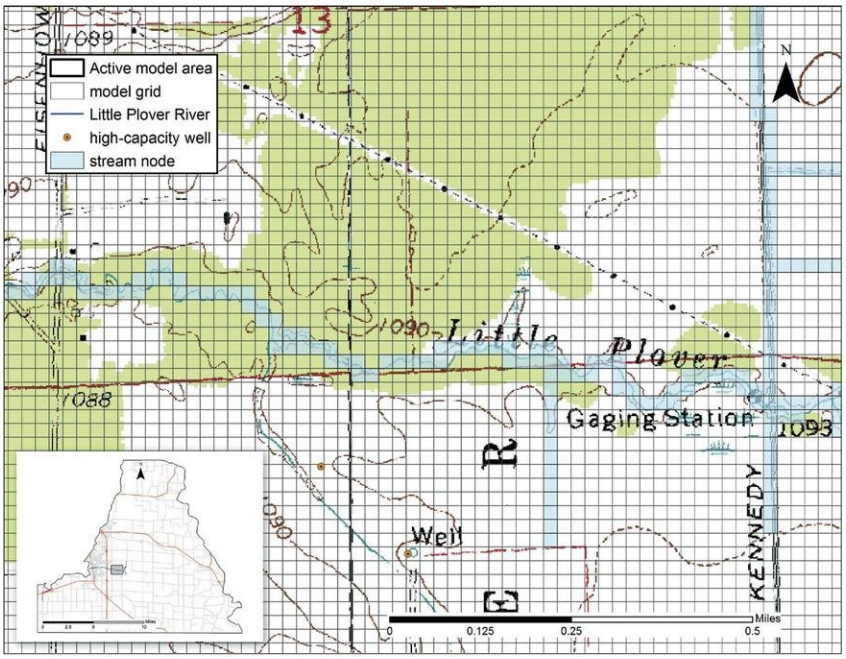

Figure 27. Model grid spacing.

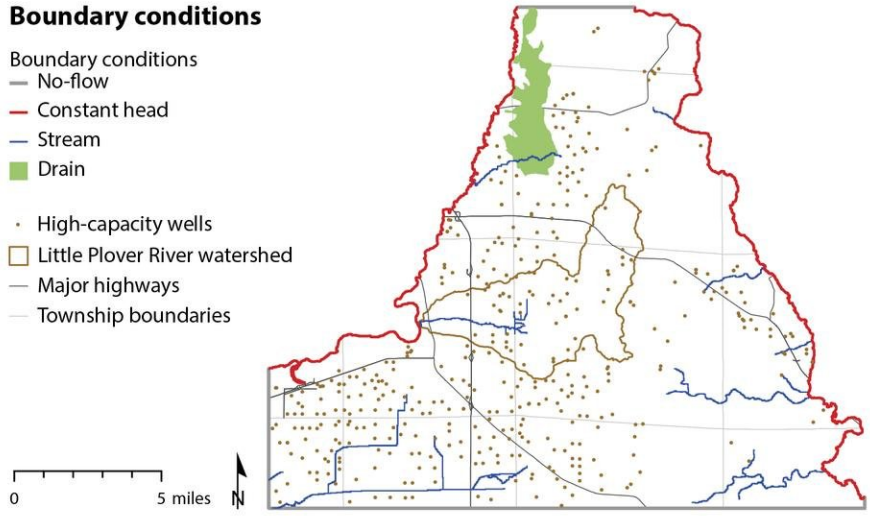

Figure 28. Model domain and boundary conditions.

fields due to return of irrigation water. Evapotranspiration is also spatially and temporally variable and removes water from the system.

Groundwater flows vertically and laterally from the water table until it reaches a discharge point. A regional groundwater divide extends from the water table to bedrock in the middle of the section; groundwater west of this divide flows toward the Wisconsin River and its tributaries while groundwater east of this divide flows toward the Tomorrow River and its tributaries. The Little Plover River is a location of groundwater discharge, and conducts surface water toward the west. Groundwater also discharges to tributary streams, drainage ditches, and high-capacity wells in the region. There is no evidence of a discrete aquitard in the Little Plover River watershed. Measurements of head in nested piezometers were used to calculate vertical hydraulic gradients at six locations (appendix 1). The hydraulic gradients—calculated as the difference in hydraulic head between the shallow and deep piezometers, divided by the vertical separation between the open intervals of the two piezometers—were generally very small, ranging from 0.01 upward to 0.004 downward, with one outlier of 0.08 upward and with several measured gradients less than 0.000. These small gradients, combined with the lack of discrete clay or silt layers in the Geoprobe cores, are consistent with a conceptual model of uniform, though hydraulically anisotropic, aquifer.

Model grid and layering

The Little Plover River model grid covers 345 square miles and consists of three layers, with a uniform cell spacing of 100 feet on a side. Figure 27 shows part of the model domain with the model grid overlaid on a topographic map. Each layer contains 900 rows (east-west direction) and 1,070 columns (north-south direction) for a total of 2,889,000 model cells, of which 1,746,329 are active, covering an area of 209 square miles. Nodes outside the model boundaries are removed from the model solution and termed inactive. These inactive nodes occur because the overall model grid is necessarily rectangular, but the model domain of interest has an irregular shape (fig. 28).

The three-layer conceptualization of the model is a compromise designed to minimize model complexity while preserving the capability to simulate

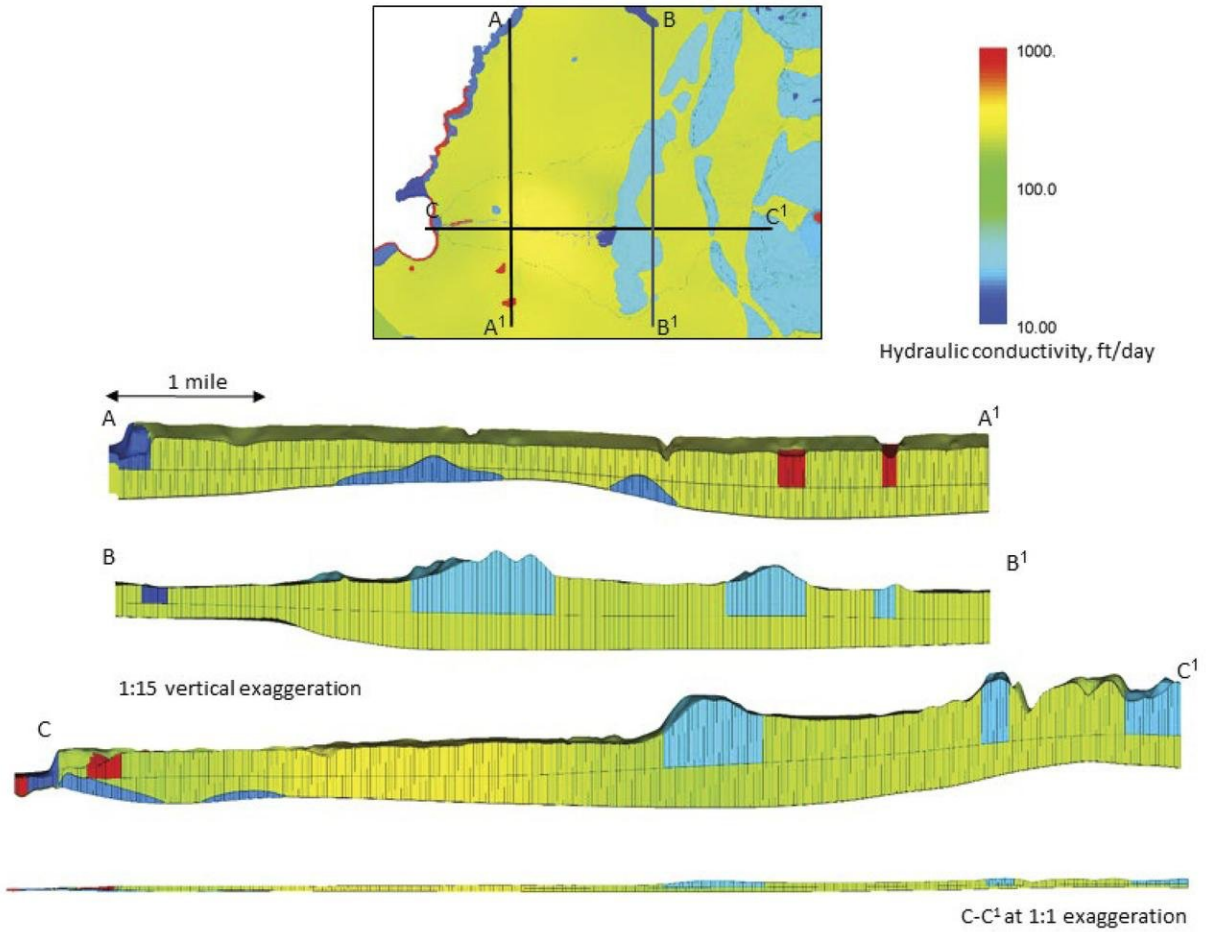

Figure 29. Cross sections through the model grid near the Little Plover River.

vertical groundwater flow, simulate flow beneath surface-water features, and allow hydraulic properties to vary vertically. Model layers are continuous across the entire grid, have irregular thicknesses, and are numbered 1 (top layer), 2 (middle layer), and 3 (bottom layer). The top of layer 1 is the land surface. Elevations for the layer top were imported from the existing 30-meter digital-elevation model for Portage County. The bottom of layer 2 is the top the Cambrian sandstone where it is present or one foot above the Precambrian surface where the sandstone is absent. One-foot thickness is assigned to a layer where it is absent in reality because MODFLOW requires that each layer be continuous across the model domain. Sandstone thicknesses are based on the map shown in figure 6. Due to a lack of any clear or mappable stratigraphic marker within the sand aquifer, the boundary between layers 1 and 2 was arbitrarily placed at one half the distance between the long-term water-table elevation and the bottom of layer 2. This boundary was adjusted in places during model calibration where mathematical convergence problems occurred due to layer 2 being very thin. The bottom of layer 3 is the Precambrian surface (fig. 5). Layers 1 and 2 represent the sand and gravel in the region, and are simulated as unconfined, meaning that the water table is the effective top boundary of the groundwater system in these layers. These layers can go completely dry if the simulated water table falls below their base. Layer 3 represents the Cambrian sandstone and is simulated as a convertible layer, meaning that it becomes unconfined if the water table falls below the top of this layer.

Cross sections through a portion of the model grid near the Little Plover River (fig. 29) show how the layer thicknesses vary across the basin. These sections also illustrate how thin the sand-and-gravel aquifer is relative to its lateral extent.

GROUNDWATER FUNDAMENTALS

Pumping affects groundwater levels

DETAILS: A basic principle of well hydraulics is that removing water from a well always reduces total hydraulic pressure, or head, in the aquifer near the well. This pressure change results in a lowering of groundwater levels near the well, known as drawdown. The amount of drawdown is directly related to the pumping rate, aquifer transmissivity, aquifer storativity, and distance from the well and can be predicted by well-established equations. The three-dimensional extent of drawdown is generally cone-shaped and is called the "cone of depression." This cone grows larger the longer a well is pumped. A typical cone of depression for a high-capacity well in the Central Sands is measurable for a half a mile or more around a well. While a distinct cone of depression comes and goes as a well cycles on and off, it is important to realize there is always less water in the aquifer, and thus lower water levels, for a short period after a well is pumped. The complete recovery of the water table can take months or longer.

WHY IT MATTERS: The effect of each well pumping is a reduction in groundwater levels. The distance, timing, and magnitude of the reduction depends on the properties of the aquifer and the amount, duration, and location of pumping.

Boundary conditions

Specified head and no-flow boundaries

Specified (constant) head boundaries occur along the east and west sides of the model, corresponding to the Wisconsin and Plover Rivers on the west and the Tomorrow River on the east (fig. 28). Each of these rivers flows continually and constitutes a regional discharge location for groundwater. In addition, each of these boundaries was judged to be distant enough from the area of interest (Little Plover River basin) so that any boundary errors would not significantly impact model results. The specified head at each boundary node was interpolated from the topographic elevation of the relevant water body, based on contours on the USGS 7.5-minute quadrangle maps. The heads were set identically in all three model layers.

No-flow boundaries are located along the northern and southern ends of the model. The northern no-flow boundary is near a regional groundwater divide and in an area where the sand and gravel aquifer is very thin. The southern no-flow boundary is generally parallel to regional groundwater flow paths in that area. Both boundaries are far from the area of interest. In addition, all model nodes west of the western specified head boundary and east of the eastern specified head boundary were also set to no-flow. This designation removes the cells from the numerical solution and improves model performance.

Drains

The model simulates the large wetland complex known as the Jordan Swamp using the MODFLOW drain package (Harbaugh, 2005). Drains in MODFLOW are head-dependent flow boundaries that remove groundwater from the system when the head at the boundary exceeds a specified elevation corresponding to the base of the hydrologic feature. However, when the head falls below the base of the drain, no additional water is supplied to the groundwater system. Boundaries of the wetland complex were taken from statewide wetland delineation coverage, and elevations of the wetland were interpolated from the USGS 7.5-minute topographic map. These drain nodes (fig. 28) are more than 4 miles away from the Little Plover River and are located in an area where the aquifer is very thin and few wells are located. The presence of the wetland has little impact on the rest of the model, but was included for completeness.

Lakes

The model represents several lakes in the model domain as high-hydraulic conductivity features ($1x10^6$ feet per day) in model layer 1. When represented in this manner, the lakes are not boundary conditions, but instead represent outcrops of the water table and were used as water-level targets during the calibration process. Recharge is set to zero over lakes.

Streams

Internal streams (Little Plover River, Spring Creek, Bear Creek, Lost Creek, Stoltenberg Creek, and several drainage ditches, see figs. 2 and 3) are represented in the model as head-dependent flow boundary conditions with the Streamflow Routing (SFR2) package. This approach accounts for baseflow accumulated from stream leakage (Niswonger and Prudic, 2005; Prudic and others, 2004). Input for the SFR2 package was developed from existing GIS coverages in the National Hydrography Dataset NHDPlus (McKay and others, 2012) and hand-digitized linework. The hand-digitizing removed a tributary in the headwaters of the Little Plover River that is no longer present

(except during large precipitation events), due to leveling of the land and added drainage ditches directly connected to the river that were not present in NHDPlus. The procedure for developing the SFR2 package input is summarized below.

1. Preliminary SFR2 reaches were created by intersecting the stream linework with the model grid cells and subdividing the linework at the grid cell boundaries. Attribute information associated with the linework was joined to the intersecting grid cells.
2. The preliminary reaches were grouped into segments based on confluences (so that segments would start at headwater reaches or confluences, and end at confluences or outlets to the stream network). Routing connections between segments were developed based on proximity between segment start and end locations.
3. Preliminary streambed elevations for each reach were set to the minimum elevation from the 10-meter DEM in each grid cell containing SFR2. Where available, field measurements of streambed elevation were used instead of the minimum DEM values. In SFR2 cells with multiple field measurements, the minimum value was used.
4. The segment end elevations were made to be consistent with the minimum and maximum preliminary elevation values in each segment, and with adjacent upstream segments so that the starting elevation of each segment was less than or equal to the ending elevation of the adjacent upstream segment.
5. Many headwater drainage ditches in the study area are incised to a depth of 5 or more feet relative to the surrounding land surface, but are too narrow to be captured in the 10-meter DEM. Where field measurements of streambed elevations were unavailable, these incisions were represented in the model by manually setting the starting elevation of the stream segment representing the ditch to maintain a small gradient along the ditch (approximately 0.0001 to 0.001 feet per foot), and an incision at the segment start of approximately 5 to 10 feet.
6. The streambed elevations of the interior reaches in each segment were then smoothed to maintain a flat or decreasing streambed elevation in the downstream direction.
7. Stream widths were estimated from total upstream drainage length (called the arbolate sum) using a regression relationship (Feinstein and others, 2010).
8. Intersection of the stream linework with the finite difference grid results in many instances where multiple line fragments (preliminary reaches) are collocated in a single model cell, due to stream meandering and confluences. To avoid undesirable circular routing between collocated stream reaches, the total streambed conductance was computed for each cell with collocated reaches, and assigned to the collocated reach with the largest upstream drainage. Conductances for the remaining collocated reaches were set to be effectively zero by assigning small values for streambed hydraulic conductivity.
9. The model layering was adjusted so that all SFR2 streambed top and streambed bottom elevations were in layer 1. Tops and bottoms of subsequent layers were adjusted downward to maintain a minimum layer thickness of 1 foot.

Recharge

Recharge is added to the uppermost active cell at each grid location, and varies cell by cell across the model domain. Recharge values were developed using the soil-water-balance (SWB) methodology described earlier. Aggregated recharge rates are inputs for the MODFLOW groundwater flow model as a spatially variable recharge array, either on an annual basis (for steady-state simulations) or on a monthly basis (for transient simulations). Steady-state runs used a single recharge array corresponding to the year simulated. Transient runs used a different recharge array for each month (stress period) simulated (fig. 24). As described earlier, evapotranspiration and applied irrigation rates are explicitly calculated in SWB, but are not input directly into MODFLOW. Instead, they are incorporated in the gridded average annual and monthly recharge rate inputs. SWB, strictly speaking, estimates deep drainage, while MODFLOW accepts recharge as input. This disconnect means that the vadose zone is ignored in MODFLOW and all water draining from the root zone (output from SWB) is applied at the water table without modification or delay. This assumption is a common practice in groundwater models, and is appropriate in the Central Sands region, which has a relatively thin vadose zone composed of permeable sand and gravel.

The SWB recharge estimates were adjusted during model calibration using multipliers applied to the SWB results. Multipliers allow a fractional increase or decrease in the SWB values to help match MODFLOW calibration targets. A single multiplier can be applied to the entire SWB-calculated recharge array, or several multipliers can be applied to various regions (for example, land-use or soil types) throughout the domain.

The use of an adjustment multiplier enables the leverage of head and flow information that is available for calibrating other aspects of the MODFLOW model (for example, hydraulic conductivity) to inform the overall SWB water balance. Due to correlation of parameters within SWB, long run times, and lack of available recharge data, direct calibration of SWB parameters is often impractical.

Wells

The fine grid spacing (100 feet) in the Little Plover River model allows wells to be located accurately within the model domain. The model simulates high-capacity wells using the standard well package in MODFLOW (Harbaugh, 2005). Well locations were obtained from the DNR and, where necessary, corrected through consultation with well owners and study of aerial photographs. The elevations of the top and bottom of the screened interval of each well were calculated using information from well-construction reports and attached to the well database. Well data were imported to the model using the Groundwater Vistas interface, which placed each well in the appropriate model node and specified the model layers open to the well. The numerical simulation assumes that each well is located at the geographic center of a model node, but the fine grid spacing assures that the spatial error associated with this approximation can be no more than about 70 feet.

Both the steady-state and transient versions of the model include all high-capacity wells within the model domain, with nonzero reported pumping for the time period simulated. The model does not simulate low-capacity domestic and commercial wells; review of available water-use estimates showed low-capacity groundwater use to be an insignificant part of the overall water budget in the model area. The DNR maintains a database of high-capacity well locations and reported monthly and annual pumping volumes. Groundwater Vistas uses open interval elevations to determine which layer a well should pump from and partitions the pumping between multiple layers based on transmissivity. For wells without casing information, the well was assumed to draw water from layer 2 because that layer is the most extensive. In the steady-state model, pumping rates were calculated using the reported annual pumping volume for each well, converted to cubic feet per day. Transient modeling uses monthly stress periods, and the pumping rates were determined by converting the reported monthly volume into cubic feet per day for each well.

Time discretization

The steady-state model was based on stresses from 2013, which are considered average conditions in recent time. The transient model represented stresses from 2014, which was a wetter year than average, with proportionally less irrigation water use over the model domain. (Water use in 2013 was 11.3 mgd; 2014 water use was 9.5 mgd). The MODFLOW code discretizes time (for transient runs) into stress periods and time steps. Stress periods represent intervals during which time-dependent model parameters and stresses (such as recharge or pumping) remain constant. Stress periods are, in turn, divided into time steps, and the model solves the transient groundwater flow equation for each time step in sequence. For most problems, the solution needs fewer time steps during periods of small changes in stresses (such as winter) than during periods of larger changes in stress (such as the summer pumping season). In general, time steps follow a geometric progression, being shortest at the beginning of each stress period and longest at the end of each period. Steady-state runs require only a single stress period with one time step.

The transient Little Plover River model as described and calibrated in this report uses stress periods corresponding to the months of the year, so that

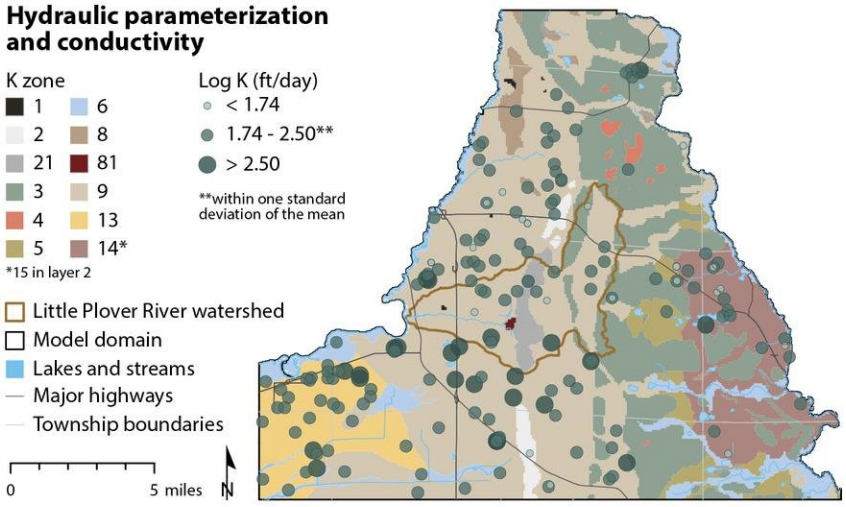

Figure 30. Parameterization of hydraulic conductivity in model layer 1 using TGUESS hydraulic conductivity results.

each simulated year contains 12 stress periods. The head solution from the steady-state calibrated model was used as the starting condition for the transient model. The length of each stress period corresponds to the number of days in the month (January has 31 days, February has 28 days, etc.) so that the entire model year contains 365 days. The number of time steps per stress period ranged from 2 in January, when there is little stress on the system, to 5 in July and August, when most stresses occur, with 1.2 as the time-step multiplier. The length of the stress periods and the number of time steps can easily be changed for specific simulation requirements.

Initial conditions

Initial conditions for the transient runs were taken from converged-model output from the steady-state calibration run. Fixed boundary conditions (constant heads, no-flow boundaries) for the transient runs were identical to those used in the steady-state runs.

Model parameterization

Parameterization refers to the assignment of hydraulic properties to spatially variable geologic materials or regions, and is a key part of model development (Anderson and others, 2015).

Hydraulic conductivity

Existing maps of Quaternary materials (Clayton, 1986) guided zonation of hydraulic conductivity for the Little Plover River model. Assigning areas into zones was an iterative process during model calibration, with the goal of keeping the zones as simple as possible while accounting for spatial variability in geologic materials. Figure 30 shows the hydraulic conductivity zonation for model layer 1. (Compare to the geologic map in fig. 4.) Table 5 summarizes the hydraulic conductivity zones. The glacial till units are limited to layer 1. There are 13 zones in all, numbered non-consecutively because some zones were added or deleted during model development and calibration. Most zones were treated as spatially uniform in both horizontal (Kx) and vertical (Kv) hydraulic conductivity, meaning that a single hydraulic conductivity value was assigned over the entire zone. Zone 9, the largest and most important zone, was assigned spatially variable hydraulic conductivity. Hydraulic conductivity is assumed to be isotropic in the X and Y directions.

Storage

The transient Little Plover River model requires storage parameters: specific storage and specific yield. Specific yield (Sy) represents the amount of water lost or gained from storage for a given water-level change in an unconfined aquifer, and is dimensionless (such as feet of water released per feet of water-table change). Specific storage (Ss) is the analogous parameter for confined aquifers, but is orders of magnitude smaller because the change in storage relates to compression of the aquifer and fluid, rather than to physical dewatering of pores. Ss has units of 1/foot. A number of investigators have previously measured or estimated these parameters in the Little Plover River area. Review of work by Holt (1965), Weeks and others (1965), and Weeks and Stangland (1971) suggests that a reasonable range of Sy in the LPR basin is 0.14 to 0.24, with a median value of 0.15. Reported values of Ss range from 0.001 to 0.003, with a median value of 0.0019. The optimal estimated values from calibration were 0.12 and 0.001 for Sy and Ss, respectively.

The sand and gravel materials in model layers 1 and 2 are treated as unconfined and assigned a single value of Sy across the entire model domain. Layer 3, representing Cambrian sandstone, is treated as confined, and assigned a single value of Ss across the entire model domain, but converts to unconfined if the simulated water table drops below the top of the layer.

Table 5. Hydraulic conductivity zonation. Refer to figure 30 for zone locations. "Clayton unit" refers to map units in Clayton (1986). "Model layers" indicates the layers where the zone is active.

Zone	Clayton unit(s)	Description	Model layers
1	c	Cambrian sandstone	1,2,3
2	gk	till of Keene member	1
21	gk	till of Keene member in LPR headwaters	1
3	gd	till of Mapleview member	1
4	od	offshore sediment over till	1
5	ou, oc	meltwater stream and offshore sediment	1,2
6	sp	postglacial stream sediment	1
8	p	peat	1
81	p	peat in LPR headwaters	1
9	su	streams and offshore lakes	1,2
13	ou, oc	meltwater stream and offshore sediment	1,2
14	ou, oc	meltwater stream and offshore sediment	1
15	ou, oc	meltwater stream and offshore sediment	2

GROUNDWATER FUNDAMENTALS

Pumping diverts water from streams

DETAILS: Streams in the Central Sands are natural areas of groundwater discharge, and this groundwater discharge sustains streamflow throughout the year. By removing groundwater from the aquifer, well pumping modifies and interrupts natural groundwater flow and thus reduces the volume of groundwater discharge to streams. This reduction is called diversion, because water that would have discharged to a stream under natural conditions is diverted away from the stream. If a well is close enough to a stream or lake, it can also induce water directly from that surface-water feature. The amount of diversion caused by a well depends on the pumping rate, pumping period, distance from a stream, and local geology.

WHY IT MATTERS: Each pumping well in the Central Sands impacts streams by diverting groundwater discharge and reducing streamflows. Even wells outside the surface-water basin of a particular stream can divert water away from the stream.

Streambed properties

The vertical hydraulic conductivity of streambed sediments helps govern the exchange of groundwater with surface-water features. Weeks and others (1965) estimated the Kv of Little Plover River sediments using nearby pumping tests and reported a range of 1.3 to 5.4 feet per day. Faustini (1985) measured Kv of sediments at six sites in drainage ditches just south of the Little Plover River basin in the Buena Vista basin and reported a range of 0.7 to 23.8 feet per day with a mean value of 7.9 feet per day. The relatively large values and narrow range of these field measurements, combined with the field observations that most stream and ditch sediments in the study area are loose and sandy, suggests that treating the streambed properties as uniform for all streams and ditches simulated in the model is reasonable. This uniform streambed Kv was varied during the calibration step described below; the final calibrated value was 2.5 feet per day, well within the range of field measurements reported in the literature.

Parameter estimation and model calibration

Model calibration is the process of adjusting model parameters so that both model inputs and model outputs produce acceptable fits to "hard" knowledge (observations of water levels and flows) as well as "soft" knowledge (professional experience and judgment) about the model domain. Calibration of the Little Plover River model involved adjustment of uncertain model parameters (parameter estimation) and comparison of results to an array of model targets, a process called "history matching." This term refers to the specific aspect of calibration that was used in this work, and it is used interchangeably with "calibration" in this report.

Parameter estimation

The parameter estimation process used for the LPR flow model was performed in multiple steps. These steps, outlined broadly, were (1) assembling available data, (2) assigning weights to data, (3) defining hydraulic parameterization (discretization and zoning), (4) conducting manual "trial-and-error" history matching to determine initial parameter values, (5) conducting sensitivity analysis, (6) iteratively exchanging parameter values between parameter estimation steps, and (7) revising the conceptual model and observation weights. These steps do not necessarily follow in sequence from one to the other because feedback throughout the process identifies shortcomings and indicates changes that cascade throughout the process. The final model is based on the results at each step, as described in this section. Appendix 3 describes the parameter estimation algorithm and provides context for the steps outlined.

History matching was first performed using a steady-state version of the model. The steady-state model is much faster to run and provides important information about hydraulic conductivity, streambed conductance, and a general adjustment to the SWB recharge array. Using the steady-state results as a starting point, history matching was then performed on the transient model. For the transient model, the same hydraulic conductivity estimated in the steady-state history matching effort was retained, but recharge multipliers, streambed conductance, and storage parameters were estimated. The streambed conductance estimated in the transient model was then reapplied to the steady-state to ensure that changes were minimal.

MODFLOW simulates surface-water flows as the baseflow component of flow in streams. As a result, calibration targets for streamflow are approximations of the baseflow component, rather than full streamflow. MODFLOW simulates baseflow entering streams and routes the flow to downstream stream cells, so calibration targets represent cumulative baseflow.

Data sources: heads and flows

Calibration data were made up of water levels in wells and lakes, and baseflow estimates derived from flow measurements in streams and ditches. Processing was necessary for both sets of data to obtain representative values for both steady-state and transient calibration. In the following sections, we describe the processing for head and flow data for the steady-state and transient datasets, respectively.

Steady-state calibration

The steady-state model is designed to represent average conditions given a recent time period. The stresses for the steady-state model (such as water use and recharge) were derived from 2013 conditions.

Steady-state head observations

For head observations, values were selected from time series spanning 2010–2014, with the exception of 2012, which was anomalously dry. Mean water-level values were selected from the 2010–2011 and 2013–2014 periods. The values were then divided into groups based on the data source. Groups were named "wisa_h" for WISA (Wisconsin Institute for Sustainable Agriculture), "dm_h" for Del Monte, "prf_h" for Plover River Farms, "ri_h" for Roberts Irrigation, "usgs_h" for water levels from the National Water Information System of USGS, "wgnhs_h" for WGNHS piezometers, and "lake_h" for lake elevations measured for December 2013. Adjusted head target values are in the "heads" page of accompanying digital data files available in appendix 4. The naming scheme indicates the group and a well number; for example, measurement DM_10 represents a well from group dm_h (Del Monte), with well number 10. These short names are necessary for the PEST software, which limits the length of observation names.

The initial weights were assigned for PEST as the reciprocal of the assumed standard deviation (see table 6) as outlined in Doherty (2014). Such error-based weight assignment is consistent with overdetermined regression theory (Hill and Tiedeman, 2007). These error-based weights do not, however, fully account for all aspects contributing to the objective function, which is the total sum of model error and usually calculated as the sum of squared weighted residuals (Anderson and others, 2015). For example, the number of observations in each group can overemphasize or underemphasize the importance of matching targets in the group. As a result, an adjustment was made such that each group would account for a desired percentage of the objective function (PHI) based on the initial parameter values (Doherty (2014). These percentage values reported in table 6 as are the resulting weights and the adjusted standard deviation indicated by each weight. The group "wisa_h" was assigned a weight of 0.0 because measurement errors, while not quantifiable, were clearly too high. The remaining head groups, in aggregate, were targeted to make up 20 percent of the steady-state objective function.

Steady-state flow observations

Flow observations were derived from continuous readings at the Eisenhower gage and a series of syn-

Table 6. Head target groups and weighting scheme for steady state.

Head group	Initial standard deviation (ft)	Weight (1/ft)		Adjusted standard deviation (ft)	Target PHI (%)	
		Initial	Adjusted		Steady state	Transient
wisa_h	1.00	1.00	0	0	n/a	0.0
dm_h	0.50	2.00	0.65	1.55	4.0	12.3
prf_h	2.00	0.50	0.30	3.32	2.0	7.7
ri_h	3.00	0.33	0.25	4.04	2.0	n/a
usgs_h	0.25	4.00	1.37	0.73	2.0	7.7
vp_h	1.00	1.00	0.72	1.39	4.0	12.3
wgnhs_h	0.25	4.00	0.65	1.54	4.0	6.2
lake_h	2.00	0.50	0.35	2.88	2.0	n/a

Abbreviations: PHI = objective function (sum of squared errors between the model and observations); n/a = not applicable.

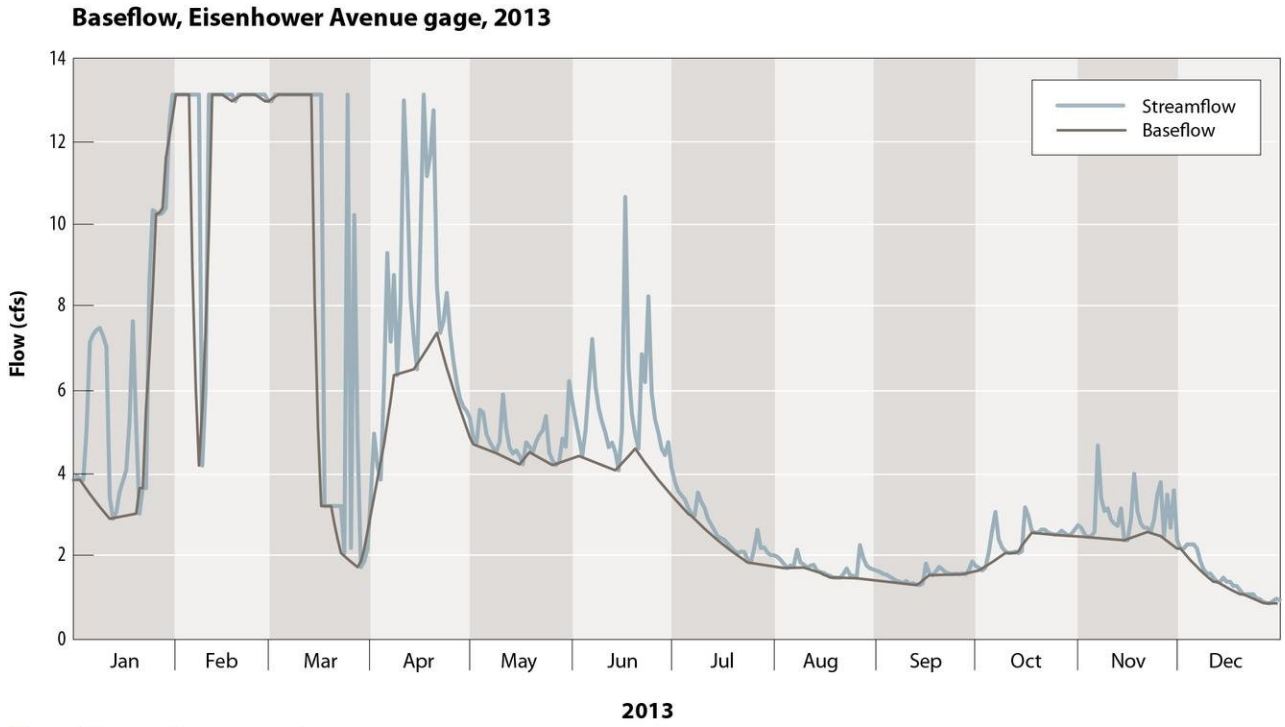

Figure 31. Baseflow at Eisenhower Avenue, 2013.

optic measurements made at various locations throughout the model area in December 2013, as discussed earlier in the report.

The continuous readings include all flow past the gage—baseflow and stormflow. The groundwater model only simulates the baseflow component of the total flow (such as the amount of flow emanating from the groundwater system) so baseflow separation is necessary to separate the two components of flow. This was accomplished using the HYSEP algorithm in TSPROC (Westenbroek and others, 2012). A window of 5 days was applied to daily streamflow values at Eisenhower. A comparison of the baseflow to total flow record for 2013 is shown in figure 31. Baseflow makes up approximately 86 percent of the total flow.

High values at the beginning of the year are apparently due to ice forming on the gaging equipment; these values were disregarded for calculating a median baseflow target value at Eisenhower. The median baseflow at the Eisenhower gage was thus calculated assuming that the 2013 winter baseflow value (from December 2013) was also representative of January 1, 2013–March 15, 2013. With these values replaced, a median baseflow value was calculated for the year 2013 at Eisenhower. The synoptic measurements at other locations were assumed to be biased higher than the representative baseflow for the year. This assumption was backed up by noting that the median annual baseflow at the Eisenhower gage was 83 percent of the flow measured in the synoptic measurement at the same location. As a result, all synoptic baseflow measurements were subjected to this same ratio (83 percent) to reduce their volumes consistent with the observations at Eisenhower. All the synoptic measurements were made under the same flow conditions (within a 2-day window in December 2013) so the bias observed in the synoptic measurement collocated with the annual median value at the Eisenhower gage was assumed to apply to all synoptic measurements throughout the model area. The resulting values are presented in table 7.

The flow observations were divided into two groups: "flux_lpr" and "flux." The "flux_lpr" group contains the four baseflow estimates made along the length of the Little Plover River. All other baseflow observations are in the "flux" group. A similar weighting strategy was adopted for baseflow observations as for head. Initially, a 10 percent coefficient of variation was assumed to characterize the error in each observation. Coefficient of variation is defined as

(EQUATION 7)

$$cv = \frac{\sigma}{\bar{x}}$$

where: σ is the standard deviation, and $\bar{x}$ is the mean observation value.

Given a cv value of 10 percent, this equation can be rearranged as

(EQUATION 8)

$$cv = 0.1 = \frac{\sigma}{\bar{x}}$$

then

(EQUATION 9)

$$\sigma = \frac{\bar{x}}{10}$$

To assign the weight for PEST as $1/\sigma$, the weight for each observation is

(EQUATION 10)

$$weight = \frac{1}{\frac{\bar{x}}{10}} = \frac{10}{\bar{x}}$$

Once again, this error-based strategy provides a starting point based on aleatory, or intrinsic, uncertainty, but does not account for other sources of epistemic uncertainty (uncertainty related to incomplete knowledge), including model quality, number of observations per group, units of measure, and others. As a result, a multiplier was applied to all weights within each group to achieve portions of the initial objective function of 20 percent and 60 percent for the groups "flux" and "flux_lpr," respectively. This left 20 percent of the objective function to be made up of the head groups, as indicated above. These target proportions of the objective function are subjective and based on professional judgment. The high proportion assigned to the flow groups highlights the importance of streamflow to the model results. Table 7 shows both the initial and adjusted weights for flow observations.

Transient calibration

The transient observations represent measurements made in 2014, an anomalously wet year. These correspond with the stresses of the same year. Processing is more straightforward for the transient observations, as they represent a mean condition in the month they were measured, rather than needing adjustment to represent a longer-term average condition.

Transient-head observations

Transient-head targets were based on the average value calculated for each month in 2014. The spatial arrangement of observation locations differs from the steady state because they represent only values observed in 2014. The groups were assigned similar names as for the steady state, although neither lake observations nor Roberts Irrigation measurements were part of the 2014 dataset. The table "head_groups" in appendix 4 shows the same group names as used for the steady state and the breakdown of objective function contribution used to adjust the weights. Also in appendix 4, the "heads_transient" table lists the transient-head targets and values. The naming scheme for each measurement is similar to the steady state, but with the stress period (month) appended on the end: so measurement DM_10_12 represents a well from group dm_h (Del Monte), with well number 10 and the average water level from month 12 (December).

Transient-flow observations

In 2014, continuous-flow measurements were available for the Little Plover River at Eisenhower. The record was available from April–December 2014. A similar approach to baseflow separation was performed to separate baseflow from total (including storm) flow. The HYSEP technique was used as in the steady-state case, although

Table 7. Flow targets and weights for steady state.

Name	Description	Flow (cfd)	Flow (cfs)	Group[a]	Initial weight	Adjusted weight
lprken	LPR at Kennedy	78,519.13	1.47	flux_lpr	11.00	27.74
lpri39	LPR at Hwy 51/I-39	345,770.06	4.00	flux_lpr	2.50	6.30
lprhoov	LPR at Hoover	450,914.10	5.22	flux_lpr	1.92	4.83
lpreis	LPR at Eisenhower	168,245.23	1.95	flux_lpr	5.14	12.95
bearq	Bear Creek at Q	738,365.37	8.55	flux	1.17	1.66
springq	Spring Creek	316,717.77	3.67	flux	2.73	3.88
ditch2	Isherwood Ditch	417,935.93	4.84	flux	2.07	2.94
noname	Stoltenberg Creek	105,001.14	1.22	flux	8.23	11.69
swcan3	Southwest Canal 3	1,375,512.43	15.92	flux	0.63	0.89
swcan2	Southwest Canal 2	1,059,151.72	12.26	flux	0.82	1.16
swcan1	Southwest Canal 1	649,281.48	7.51	flux	1.33	1.89

[a] The "flux_lpr" group contains the four baseflow estimates made along the length of the Little Plover River; the "flux" group contains all other baseflow observations.

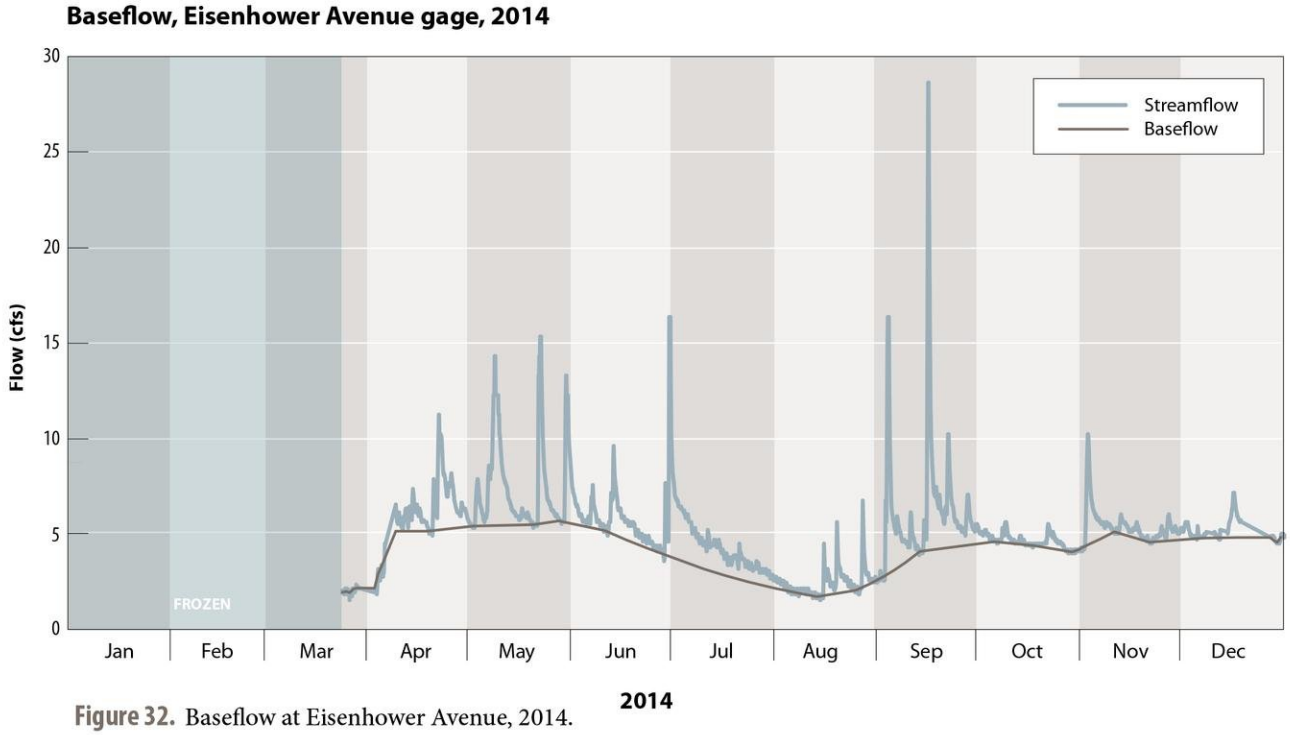

Figure 32. Baseflow at Eisenhower Avenue, 2014.

the window was widened to 11 days to accommodate a slower return to baseflow conditions after a closer (in time) grouping of high storm-flow events in 2014 relative to 2013. Figure 32 shows both the baseflow and total flow during 2014. Baseflow makes up approximately 78 percent of the total flow for 2014.

Following baseflow separation, the monthly mean baseflow was calculated for each month for Eisenhower. These values were used as targets for flow for 2014. Synoptic measurements were available at other locations, both on the Little Plover River and in other streams. Synoptic measurements were adjusted to more closely represent conditions at the continuous Eisenhower location. For each synoptic measurement, the ratio of the flow measured on that day at Eisenhower, compared to the monthly mean for Eisenhower for the given month, was calculated. Then the synoptic-flow measurement was adjusted by applying the ratio to determine the calibration target.

Transient-flow targets consisted of a series of observations at each gaging point through time (see appendix 4e). Initial weights were assigned using a coefficient of variation of 10 percent, the same way used for the steady-state observations. Weights were then adjusted to assign weight of 0.0 to all flow observations other than the Little Plover River and 54 percent of the objective function to the flow observations for the Little Plover River. This emphasis on the Little Plover highlights the management interest in the river as the main driver for this work. Flows in other streams and the head observations, while still of interest, are emphasized less to ensure that the Little Plover River baseflow values are met as nearly as possible.

Parameterization

Model calibration consisted of adjusting model parameters during the history-matching process, with the goal of obtaining an optimum match between model output and model targets. For the steady-state calibration, the adjusted parameters were hydraulic conductivity, streambed conductance, recharge, and specific storage. For the transient calibration, the adjusted parameters were recharge and specific yield.

Hydraulic conductivity values were assigned in two ways: through homogeneous zones and using pilot points in zones where hydraulic conductivity varies spatially. As discussed above, hydraulic conductivity zones were first assigned based on lithology, and uniform values throughout each zone were assumed. In zone 9, which represents stream and offshore lake deposits, a single homogeneous value would not be sufficient to represent the variability

of hydraulic conductivity. In this case, pilot points were employed following the guidelines in Doherty and others (2010). Pilot points are used not only where variability is important, but also where observation data can inform parameter values through history matching (Doherty and others, 2010). Interpolation for the pilot point values to fill in the entire zone of model cells is accomplished through kriging using an exponential variogram. Following Doherty and others (2010), a long range was used so that the exponential variogram behaves as a linear interpolator between pilot points. The roughness or smoothness of the fields is then controlled more through regularization than through interpolation. At each pilot point location, a separate value was estimated for vertical and horizontal hydraulic conductivity, and those values were interpolated to all model cells using the same variogram parameters.

Recharge was initially estimated for the model using the SWB code, as discussed earlier. In the steady-state model, a single multiplier was assigned to the recharge array to allow a minor adjustment to overcome uncertainty in the SWB process and account for uncertainty in the baseflow targets. This single multiplier allows for minor adjustment of the overall water balance, without deviating from the spatial pattern determined in SWB as a function of land use, soil type, and other characteristics. In the transient calibration phase, a single multiplier for each stress period was applied to the entire recharge array. One challenge with summarizing recharge by months is that in MODFLOW, all stresses (such as pumping and recharge) are assigned at the start of the stress period and assumed constant during that timeframe (in this case, one month). However, on August 30, 2014, a major precipitation event resulted in nearly 1 inch of recharge at the end of the August stress period. This stress should really be introduced to the model at the beginning of the following month (September). As a result, for the purpose of recharge only, the August recharge was made up of the sum of all SWB daily estimates from August 1 through 29, 2014, and the September recharge was the sum of SWB daily estimates from August 30 through September 30, 2014. This transposition of the storm does not change the overall mass balance of recharge, but shifts the timing to be more consistent with conditions at the site. The recharge multipliers for stress periods 8 and 9, therefore, were applied to the storm-transposed recharge rather than the original SWB results. All other stress period recharge multipliers were applied to the sum of the calendar month SWB results.

Parameter-estimation results

Evaluating parameter-estimation results requires analysis of model fit, parameter values, and parameter identifiability. Model fit is the agreement between modeled values and their associated measured observations. The calibration process also must ensure that the estimated parameters fall within realistic ranges. There is a tradeoff between model fit and parameters. Excellent fit values can often be obtained with parameters that are inconsistent with knowledge of the geology of an area. Care must be taken to properly strike the balance between fit and realistic parameter values. Finally, identifiability—a highly parameterized adjunct to sensitivity—can provide information about which parameters are important to observations. The following three subsections are dedicated to observed fit, parameter values, and identifiability.

Fit to observed values

The history-matching results show generally good agreement between modeled values and their associated measured observations (see appendix 5a for head results). Table 8 shows the measured and modeled equivalent values for steady-state flows, and

Table 8. Steady-state flow results.

Name	Description	Baseflow value (cfs)		Difference (cfs)	Difference (%)
		Observed	Modeled		
lprken	LPR at Kennedy	1.47	0.96	0.51	–34.7
lpri39	LPR at Hwy 51/I-39	4.00	3.69	0.31	–7.8
lprhoov	LPR at Hoover	5.22	5.24	0.02	0.4
lpreis	LPR at Eisenhower	1.95	2.11	–0.16	8.2
bearq	Bear Creek at Q	8.55	7.70	0.85	–9.9
springq	Spring Creek	3.67	5.29	–1.62	44.1
ditch2	Isherwood Ditch	4.84	4.74	0.10	–2.1
noname	Stoltenberg Creek	1.22	1.38	–0.16	13.1
swcan3	Southwest Canal 3	15.92	18.40	–2.48	15.6
swcan2	Southwest Canal 2	12.26	13.62	–1.36	11.1
swcan1	Southwest Canal 1	7.51	3.18	4.33	57.7

figures 33 and 34 show the fit graphically on one-to-one graphs[1]. Error bars correspond to the initial standard deviation values that were part of assigning weights at the beginning of the process. Note that the fit for flow measurements on the Little Plover River (group flux_lpr) is particularly good, reflecting the chief goal of the model being matching those values. Table 9 summarizes the statistics of model fit for each group in the steady-state model. Figures 35 and 36 show weighted and unweighted residuals for steady-state heads and flows, respectively. The main impact of assigning weights corrects for the difference in units between heads and flows. This normalizes the impact of both groups on the objective function.

Appendix tables 5c and 5d contain the measured and modeled equivalent values for transient heads and flows, respectively. Figures 37 and 38 show the fit graphically on one-to-one graphs. As in the steady-state case, error bars correspond to the initial standard deviation values that were part of assigning weights at the beginning of the process. In figure 38, the poor fit to the q_other group (flow targets outside the LPR) is expected, as they were assigned zero

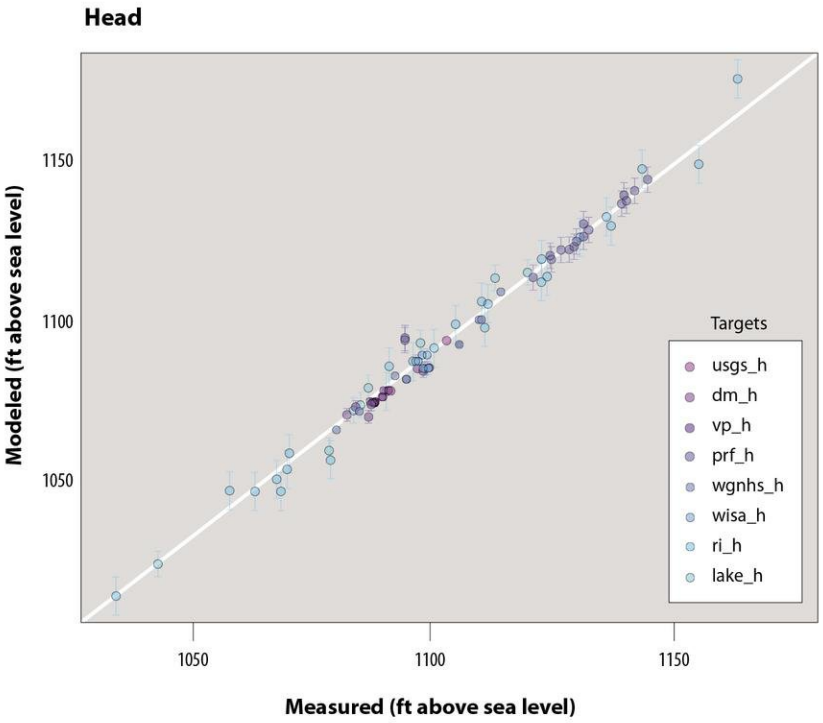

Figure 33. Steady-state head calibration.

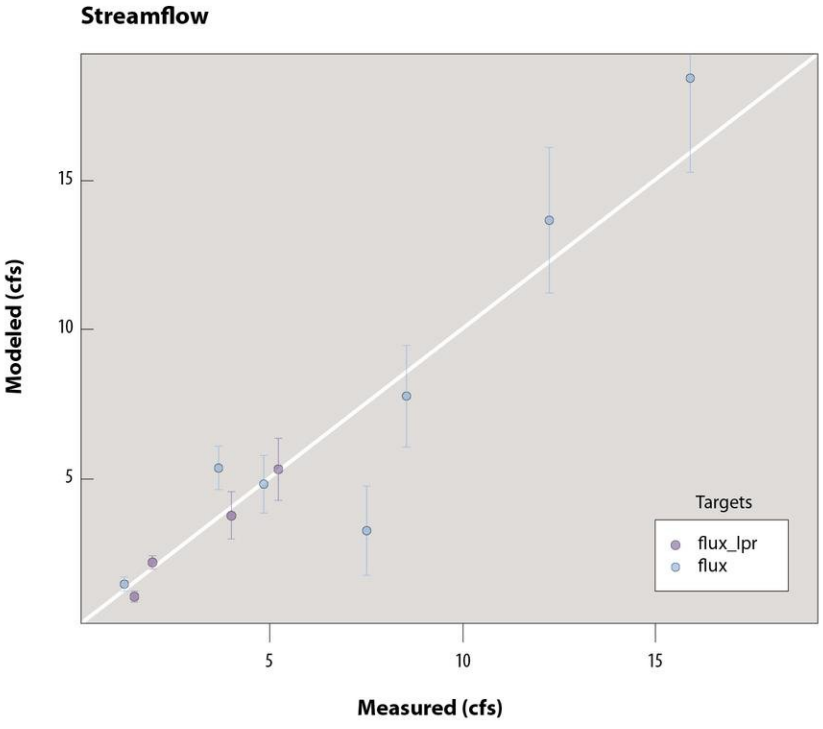

Figure 34. Steady-state flow calibration.

[1] *In the review process of this work, a typographical error in the parameter estimation files was found in which the value 0.91 cfs for the steady-state adjusted flow at the Kennedy gage should actually be 1.47 cfs. Tables 7 and 8 and figures 34 and 36 have been corrected. This discrepancy only impacts flow entering the Little Plover River from the headwaters to the Eisenhower gage; about 0.56 cfs of the total streamflow should enter the stream higher in the watershed than simulated. This error does not impact the overall parameter estimation results.*

weight for the transient calibration. This is attributed to insufficient information on stream elevations, streambed conductance, and fewer nearby head targets in the streams other than the Little Plover River. Table 10 summarizes the statistics of model fit for each group in the transient model. Figures 39 and 40 show unweighted and weighted residuals for heads and flows, respectively, for the transient calibration. The main impact of weighting is observed in the flows where the effect of zero-weighting observations outside the Little Plover River resulted in fewer outliers and a less biased spread of residuals for the Little Plover River observations.

For the transient data, it is also important to evaluate the fit during the course of time series values. Hydrographs of flow and head are presented in figures 41 and 42, respectively. In these figures, the stress period on the x axis indicates the month of simulation for 2014. Head measurements were somewhat scattered through time, with most

Table 9. Steady-state calibration metrics. All values refer to differences between measured and modeled values.

						Absolute		Mean absolute		
Group	n	Range	Max	Min	Mean	Max	Min	error	RMSE	RMSE/range
Head (feet)										
dm_h	12	1.77	2.55	0.78	1.91	2.55	0.78	1.91	1.99	1.12
lake_h	8	14.01	6.36	−7.65	−1.47	7.65	0.26	3.19	4.23	0.30
prf_h	17	12.27	1.74	−10.53	−1.38	10.53	0.04	2.15	3.73	0.30
ri_h	25	20.69	9.70	−10.99	0.40	10.99	0.24	3.71	4.67	0.23
usgs_h	3	2.30	2.36	0.06	1.41	2.36	0.06	1.41	1.72	0.75
vp_h	6	6.19	5.35	−0.84	2.38	5.35	0.52	2.84	3.36	0.54
wgnhs_h	12	6.56	4.50	−2.06	2.15	4.50	1.19	2.70	3.00	0.46
wisa_h	6	5.63	4.59	−1.05	1.04	4.59	0.06	1.64	2.37	0.42
Flow (cfs)										
flux	7	6.82	4.34	−2.48	−0.05	4.34	0.10	1.56	2.08	0.30
flux_lpr	4	0.47	0.31	−0.16	0.02	0.31	0.02	0.14	0.18	0.38

Abbreviations: n = number of values in a group; RMSE = root mean squared error.

Table 10. Transient calibration statistics. All values are in feet and refer to differences between measured and modeled values.

						Absolute		Mean absolute		
Group	n	Range	Max	Min	Mean	Max	Min	error	RMSE	RMSE/range
dm_h	24	3.03	0.57	−2.46	−0.60	2.46	0.03	0.74	0.96	0.32
prf_h	17	13.28	1.70	−11.58	−1.51	11.58	0.03	2.32	4.04	0.30
q_lpr	33	4.30	2.28	−2.02	0.07	2.28	0.11	0.78	1.01	0.23
q_other	24	13.45	13.08	−0.37	4.07	13.08	0.06	4.14	5.84	0.43
usgs_h	11	3.43	2.40	−1.04	0.51	2.40	0.02	1.31	1.52	0.44
vp_h	28	6.22	3.58	−2.64	0.48	3.58	0.21	1.77	2.00	0.32
wgnhs_h	40	8.50	4.37	−4.13	1.19	4.37	0.06	2.03	2.40	0.28
wisa_h	49	6.50	4.45	−2.04	−0.04	4.45	0.03	1.17	1.57	0.24

Abbreviations: n = number of values in a group; RMSE = root mean squared error.

sites only being measured in either the spring or the fall, but not both. The data provide a valuable signal about the temporal dynamics of the system, but they are not necessarily informative about the entire year. This poses a challenge for the PEST algorithm, which considers each measurement to be similarly informative as enforced by the assigned weights. In general, the patterns and magnitudes of head values show the correct trends. Misfit between measured and modeled values can be an artifact of the need to average stresses over a month, even though, in many cases, head observations are instantaneous. In other words, a head observation, collected at a certain time during a month, is the result of stresses (for example, recharge and pumping) that vary on a timescale smaller than a month. However, as discussed elsewhere in the report, we must apply stresses averaged over each month. As a result, it is not expected that head observations will perfectly agree with their modeled equivalents in all cases.

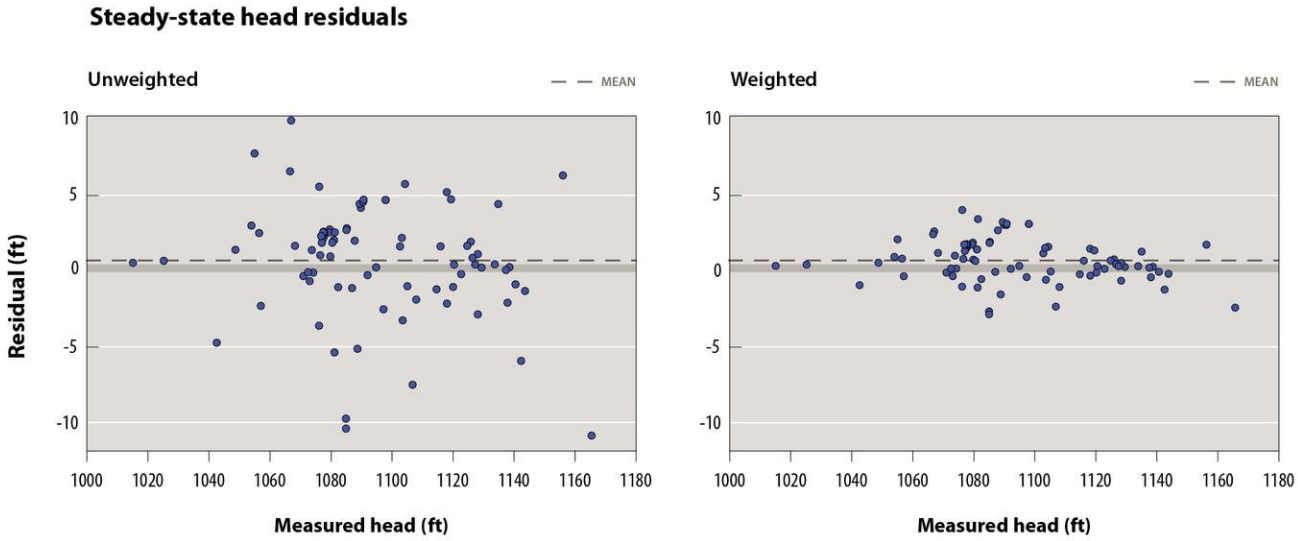

Figure 35. Steady-state head residuals, showing unweighted (left) and weighted (right) targets.

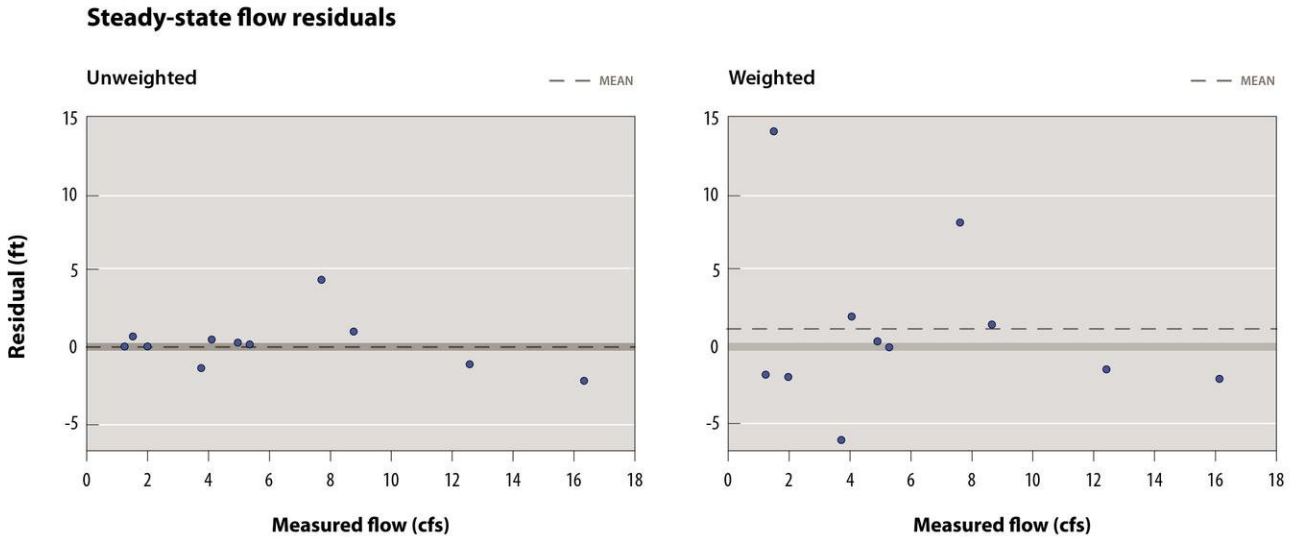

Figure 36. Steady-state flow residuals, showing unweighted (left) and weighted (right) targets.

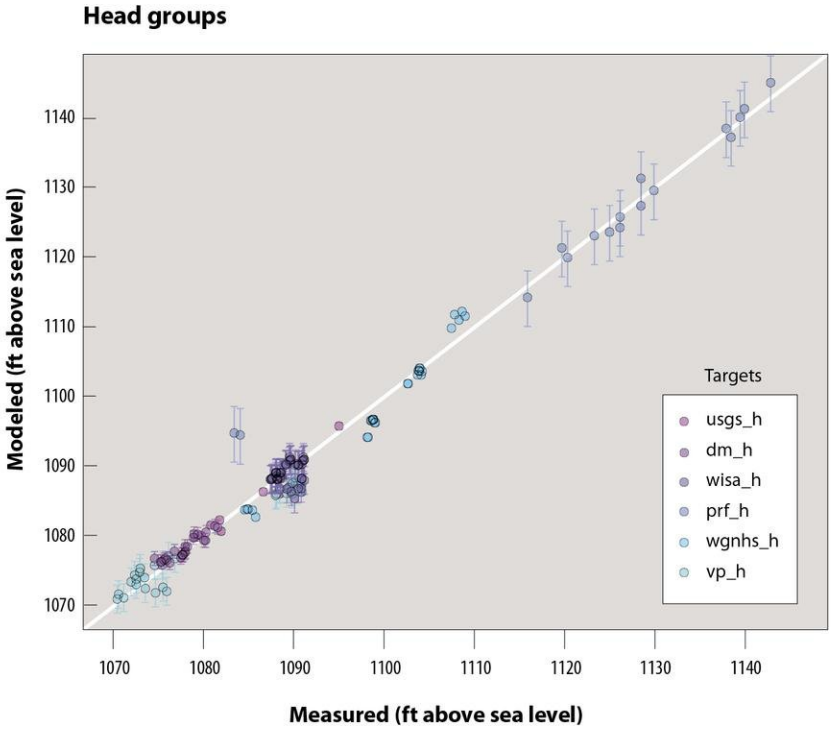

Figure 37. Transient head calibration.

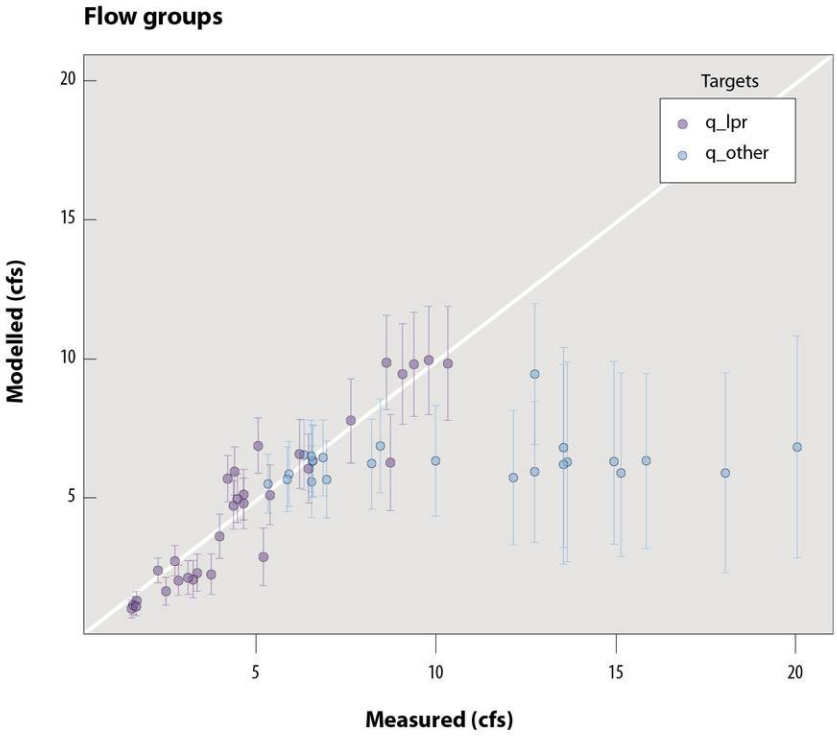

Figure 38. Transient flow calibration.

Flow values on the Little Plover River (at Kennedy, Eisenhower, and Hoover gage locations) were available for most months of 2014. Figure 41 shows that the Kennedy gage was slightly underestimated throughout the 2014 simulation, but both Eisenhower and Hoover were closely reproduced—especially for the important summer months. As with the steady-state calibration, adjustment of parameters is made by the PEST algorithm to minimize the squared differences with little overall bias in the results. Accordingly, within a gage and among them, some targets are simulated too high and others too low. The transient response also depends on some phenomena that are not explicitly simulated, such as the vadose zone and the actual changes in recharge and pumping within each monthly time step. The close agreement between measured and modeled values at the low-flow conditions during summer in the Little Plover River was a primary goal of model development, and the calibration meets that objective.

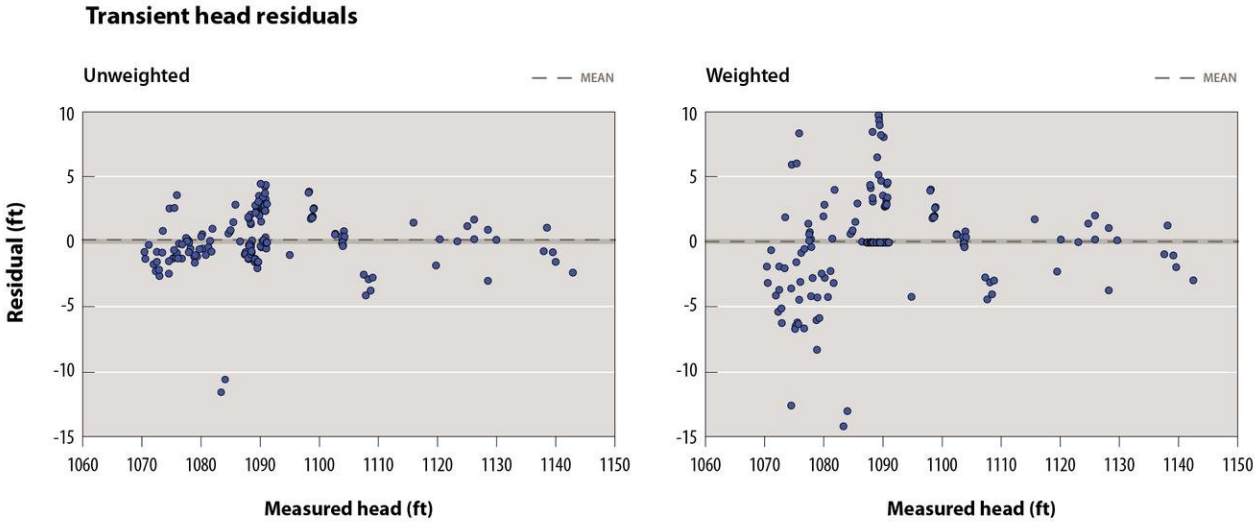

Figure 39. Transient head residuals, showing unweighted (left) and weighted (right) targets.

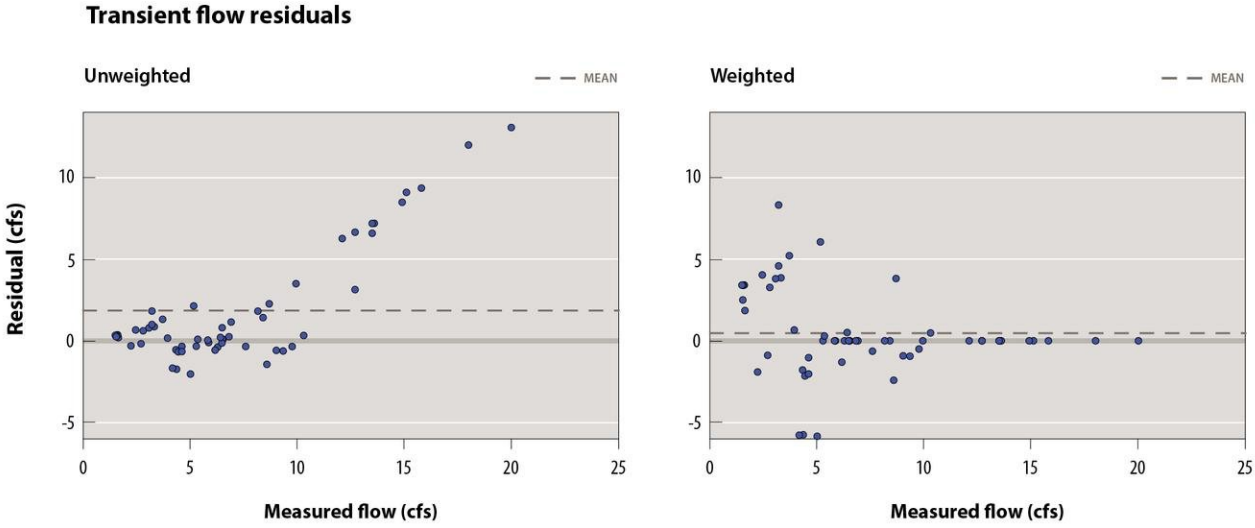

Figure 40. Transient flow residuals, showing unweighted (left) and weighted (right) targets.

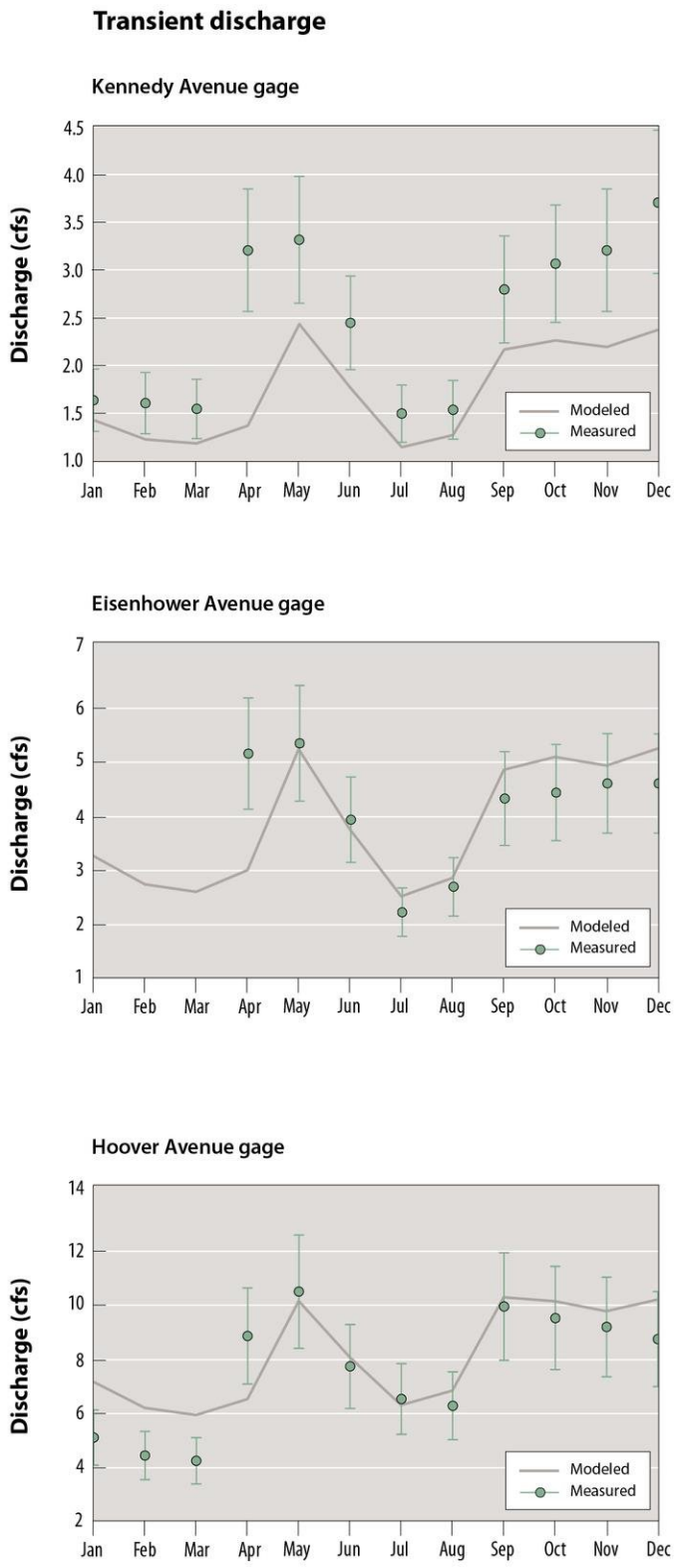

Figure 41. Transient results for Little Plover River gaging sites.

Estimated parameters

As indicated earlier, the fit-to-observed values is only part of the criteria in determining that parameter estimation has been carried out successfully. It is also critical that the parameters estimated are reasonable, given professional judgment and the extensive knowledge about Central Sands hydrogeology from earlier studies. Estimated parameters include a recharge multiplier, streambed hydraulic conductivity, and both vertical and horizontal hydraulic conductivity throughout the model domain.

The steady-state hydraulic conductivity calibration produced the zones listed in table 11. Preliminary calibration of zone 5 resulted in an estimate of Kv>Kx, which is physically unrealistic. Rather than enforcing that Kx>Kv a priori, we left the flexibility to the algorithm to estimate parameters with the intention of overriding unreasonable parameters after estimation, if necessary. Only zone 5 required such intervention.

Zone 9 is the most important hydraulic conductivity zone in the model. The sands that underlie much of the agricultural activity, and to which the Little Plover River is connected, are in this zone. Previous observations indicated heterogeneity in these stream and offshore lake sediments and specific homogeneous zones have not been mapped. The thickness of the aquifer in this zone is also variable. A distributed field of pilot points each for horizontal and vertical hydraulic conductivity for the three model layers provides the flexibility of the information contained in observa-

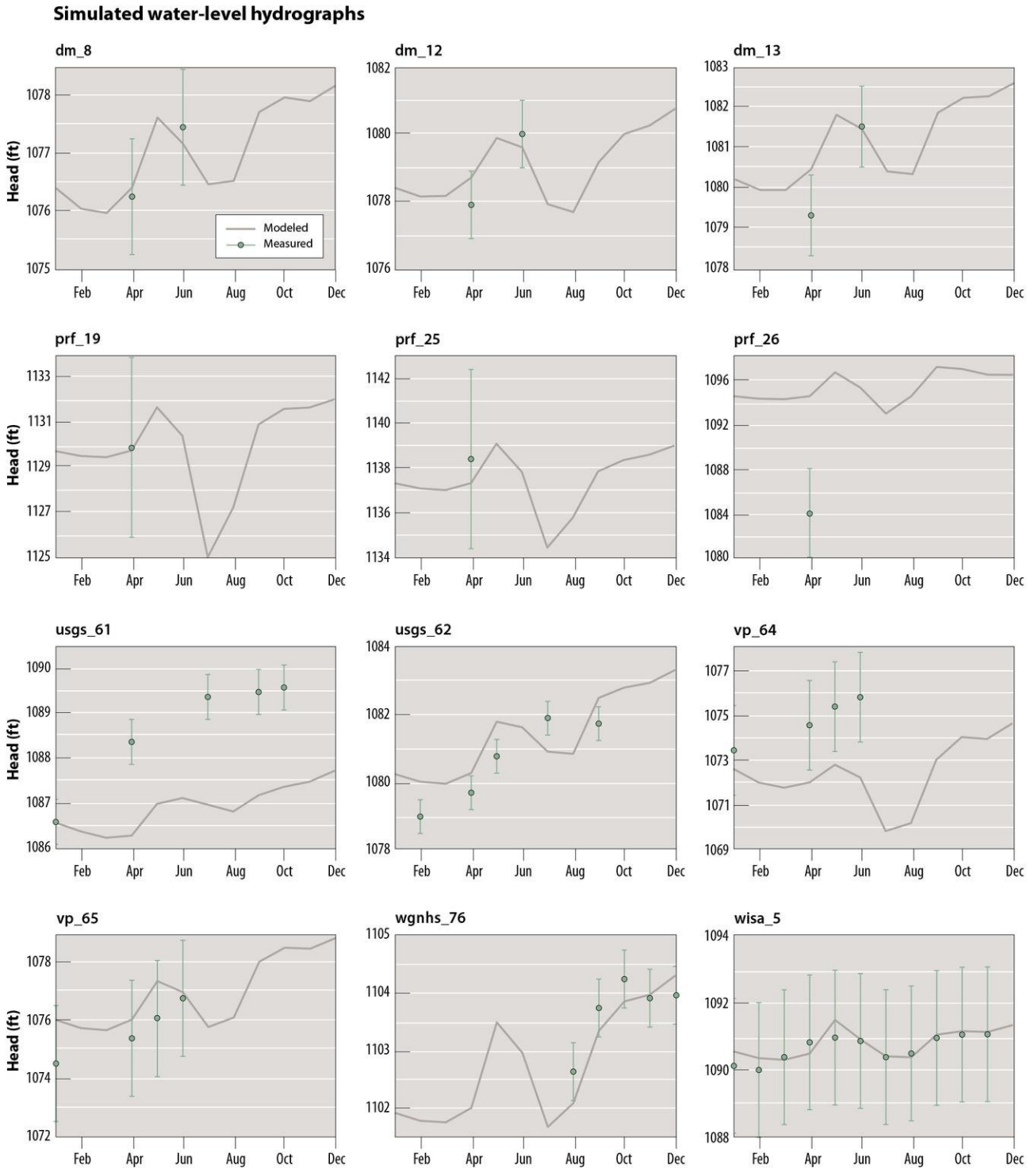

Figure 42. Selected simulated water-level hydrographs for transient calibration. See appendix 5 for additional results.

Table 11. Calibrated hydraulic conductivity zonation. Refer to figure 30 for zone locations. "Clayton unit" refers to map units in Clayton (1986). "Model layers" indicates the layers where the zone is active.

Zone	Clayton unit(s)	Description	Model layers	Initial estimates		Final calibration values	
				Kx (ft/d)	Kv (ft/d)	Kx (ft/d)	Kv (ft/d)
1	c	Cambrian sandstone	1,2,3	20.0	2.0	19.2	2.0
2	gk	till of Keene member	1	25.0	2.5	25.5	2.5
21	gk	till of Keene member in LPR headwaters	1	25.0	2.5	24.9	2.6
3	gd	till of Mapleview member	1	25.0	2.5	23.6	2.5
4	od	offshore sediment over till	1	1.0	0.1	1.0	0.1
5	ou, oc	meltwater stream and offshore sediment	1,2	33.0	33.0	21.0	21.0
6	sp	postglacial stream sediment	1	15.0	15.0	16.4	15.6
8	p	peat	1	1.0	1.0	1.0	1.0
81	p	peat in LPR headwaters	1	1.0	1.0	1.0	1.0
9	su	streams and offshore lakes (variable; uses pilot points)	1,2	220.0	7.0	190–350	6–8
13	ou, oc	meltwater stream and offshore sediment	1,2	200.0	10.0	158.0	10.0
14	ou, oc	meltwater stream and offshore sediment	1	35.0	3.5	47.8	3.5
15	ou, oc	meltwater stream and offshore sediment	2	35.0	3.5	48.7	3.7

Abbreviations: Kx = horizontal hydraulic conductivity; Kv = vertical hydraulic conductivity.

tions to inform both the degree and pattern of heterogeneity. Figure 43 shows the estimated fields for horizontal and vertical hydraulic conductivity for the three model layers. In the vicinity of the Little Plover River, a similar high hydraulic conductivity body as shown by Kraft and others (2012) was estimated. This area is associated with Cambrian sandstone subcrops, which likely influenced the depositional conditions of the sand. Figure 44 shows anisotropy calculated as Kx/Kv for each layer, respectively. In the area around the highest values for Kx, the anisotropy peaks near 50. This high local anisotropy is consistent with observations of intervals of silty or clay-rich material in some of the field cores collected during this project (see appendix 1). On average, however, anisotropy typically is around 30 for zone 9 and between 1 and 10 in the homogeneous zones.

For the transient-parameter estimation, the hydraulic conductivity field was not adjusted. The only estimated parameters were specific yield, specific storage, streambed hydraulic conductivity (iteratively with the steady-state model), and recharge multipliers assigned to each month (3–12) for which the SWB estimate of recharge was greater than zero. Specific yield and specific storage were each estimated at their lower bounds of 0.12 and 1.0×10^{-3} ft^{-1}, respectively. In both cases, these were the lower bounds based on previous field measurements. The estimated values being low suggest that the storage parameters are compensating for model error in decreasing the time for system response to stresses. The streambed hydraulic conductivity, as with steady state, was estimated as 2.5 feet per day.

The best-calibrated steady-state model uses an estimated recharge multiplier of 1.08. This multiplier indicates that an increase throughout the model domain of 8 percent in recharge over the value estimated by SWB was required to result in a reasonable fit to observations. The

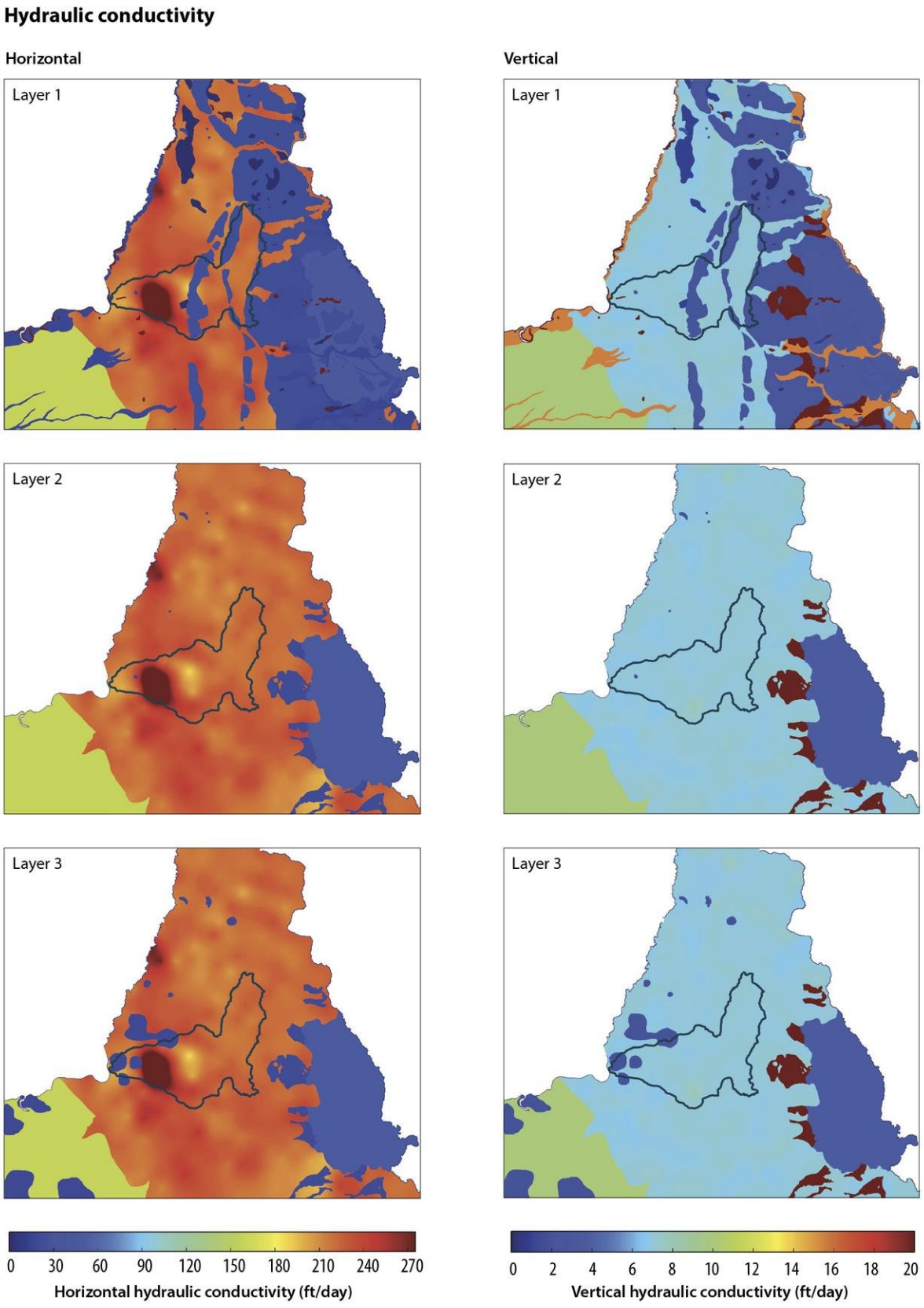

Figure 43. Estimated horizontal (left) and vertical (right) hydraulic conductivity fields for each layer.

Anisotropy

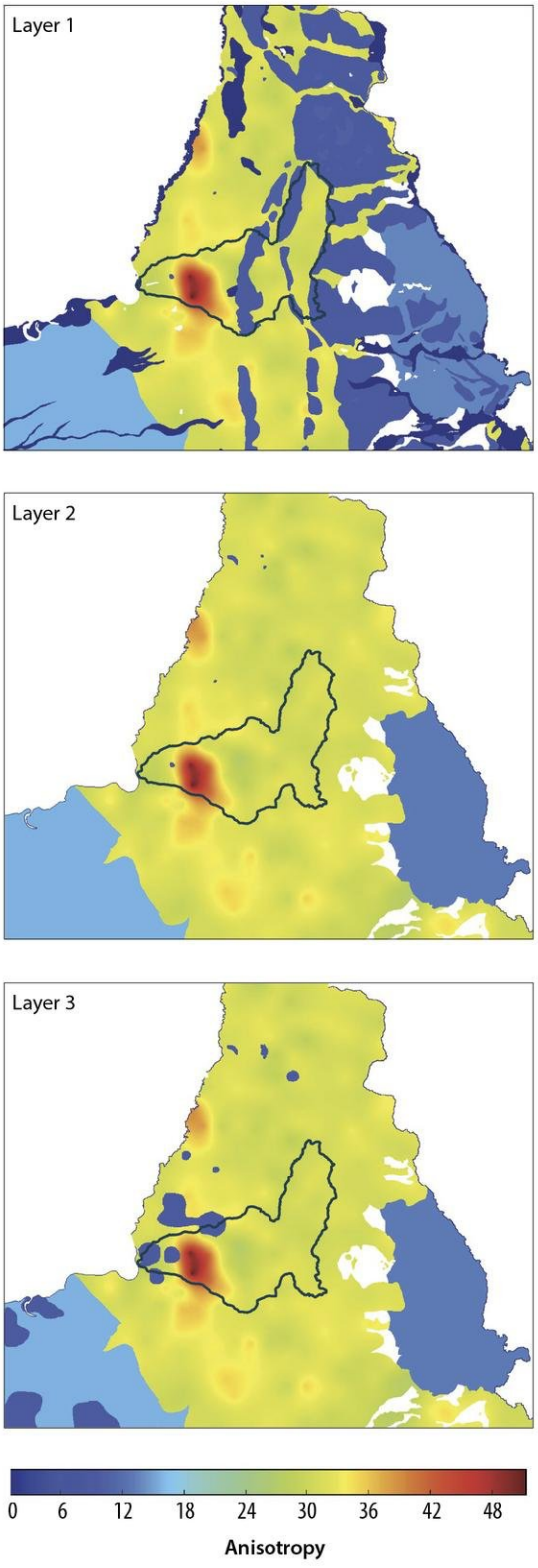

Figure 44. Estimated horizontal to vertical anisotropy (ratio, Kx/Kv).

base mean recharge (as estimated using SWB) over the model domain was 8.6 in/yr. After parameter estimation, the mean recharge applied in the MODFLOW model was 9.9 in/yr. For comparison, a previous model by Clancy and others (2009) calibrated with a recharge range of 10.5 to 13.7 in/yr. Weeks and others (1965) estimated recharge in the LPR basin at 8.9 to 9.5 in/yr for the climate in 1960 and 1961. Recent work by (Hart and others, 2016) determined annual recharge at a site in Adams County to be between 9.7 and 11.9 in/yr.

The recharge multipliers applied to each month of the year in the transient simulation are listed in table 12, along with the SWB-estimated recharge (in inches) for each non-zero month and the adjusted mean recharge. Figure 45 shows the 2014 monthly recharge graphically. The mean recharge for the year increased from 12.5 inches to 14.6 inches, representing an effective overall multiplier of 1.16—a similar value to the steady state. The major conclusions from the monthly adjustments are (1) the main spring recharge event due to snowmelt and associated runoff was estimated by SWB as occurring in April, but for MODFLOW it was better simulated in May, (2) recharge in winter was lower than simulated by SWB, and (3) an increase in autumn recharge was indicated by the parameter-estimation process that was not simulated by SWB.

Potential explanations for the first issue include flow through the vadose zone. SWB estimates deep drainage (water draining from the root zone) into the vadose zone, whereas MODFLOW simulates recharge occurring directly on the water table. The

Table 12. Monthly recharge multipliers for transient calibration.
Stress periods 1 and 2 have zero recharge due to frozen ground.

Stress period	SWB mean recharge (inches)	Estimated recharge multiplier (unitless)	Adjusted mean recharge (inches)
3	1.48	0.25	0.37
4	4.46	0.25	1.11
5	1.21	3.57	4.33
6	0.74	0.58	0.43
7	0.01	2.21	0.03
8	1.41	0.72	1.02
9	0.54	6.48	3.53
10	0.63	2.24	1.42
11	0.58	1.42	0.83
12	1.45	1.03	1.50
Annual total	**12.54**	**1.16**	**14.56**

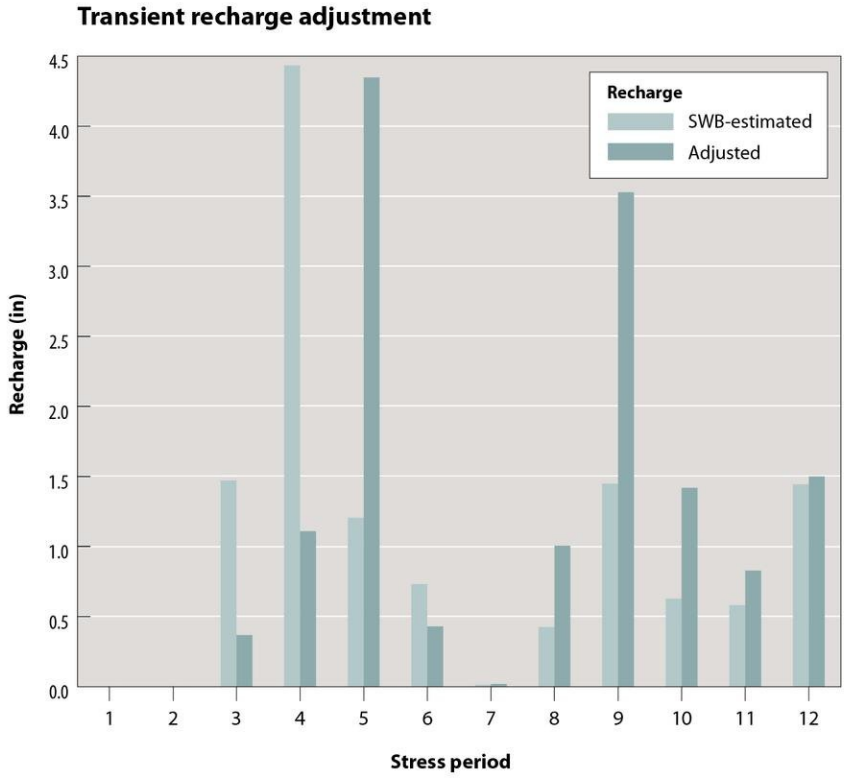

Figure 45. Transient recharge adjustment for each stress period.

timing of water movement through the vadose zone is not explicitly simulated, but in reality, there may be a delay from deep drainage to reaching the water table. As a result, better agreement between the model and observations are obtained in MODFLOW when the spring runoff is simulated as recharging the water table in May rather than in April. A second potential explanation is the relatively coarse resolution of monthly stress periods; precipitation occurring late in a month impacts groundwater levels and streamflow in the month after the precipitation occurs. The lower winter recharge following parameter estimation may result from temperature increases that SWB simulates as thawing the ground and allowing recharge to occur when, in fact, the ground remains frozen and no recharge can occur.

Sensitivity and identifiability

In modeling parlance, groundwater parameters with high identifiability are interpreted to be well informed by the observations, while parameters with low identifiability are interpreted to be ill informed by the observations and are generally held relatively constant in the history-matching process. The identifiability metric is calculated using both sensitivity and correlation, as discussed by Anderson and others (2015). In models with many parameters, identifiability is a more informative metric than sensitivity. Appendix 6 explores the identifiability of parameters for the steady-state model. Identifiability is a qualitative metric and should not be over-interpreted, but it can provide some insight into important model behavior. In a qualitative sense, parameters with high identifiability can be interpreted as important controls on model behavior.

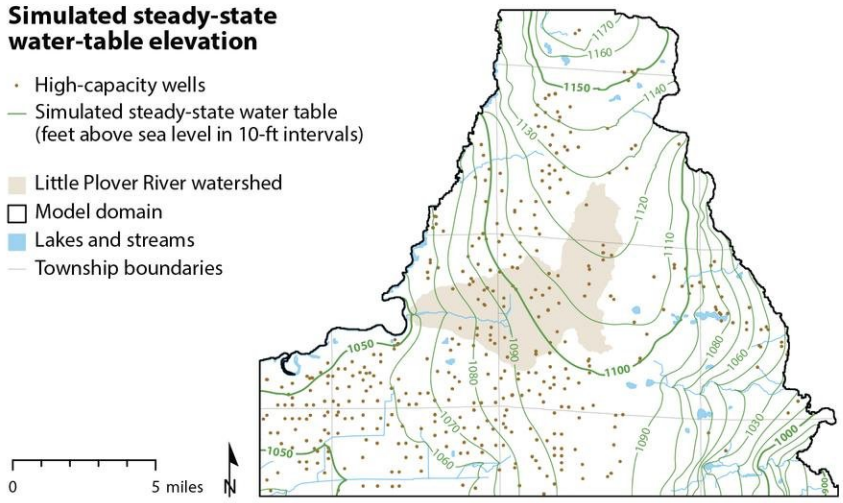

Figure 46. Simulated steady-state water-table elevation.

In the Little Plover River model, the two parameters with the highest identifiability are the recharge multiplier (rm1) and streambed hydraulic conductivity (sfrc). These two parameters are the main controls on overall water balance into the model and the connection to streams. The Little Plover River flow observations are the most important and highly weighted observations in the model, so it follows that the parameters controlling water exchange with the stream and overall water available in the model should be the most important. Other important parameters are horizontal hydraulic conductivity parameters: a mixture of homogeneous zones and pilot points. This highlights the importance of lateral groundwater flow to supply the streams and also to maintain a simulated head surface in good agreement with head observations. Vertical hydraulic-conductivity values are less identifiable, indicating that they control the solution less and are informed less by the observations. Overall, the identifiability analysis indicates that vertical hydraulic conductivity is less important to model results than is horizontal hydraulic conductivity.

Model results

Hydraulic head distribution

The overall steady-state hydraulic head distribution produced by the model is very similar to maps produced by previous investigations (Clancy and others, 2009; Weeks and others, 1965) and shows that the regional water table slopes gently from north to south across the model domain (fig. 46). Groundwater flow is perpendicular to these contour lines, and flow diverges to the east and west along a groundwater divide near the center of the model

domain. Figure 47 shows details of the simulated water table near the Little Plover River. Contours "v" upstream as they cross the river, indicating that groundwater discharges to the river. The presence of a dam on the west end of Springville Pond causes a steep hydraulic gradient just below the dam and results in bunched contours between the dam and the Wisconsin River.

Using the calibrated steady-state model for 2013 conditions, maps of the simulated groundwater inflow and baseflow distribution along the Little Plover indicate places where groundwater enters the river. Figure 48 plots the groundwater inflow at each model stream node along the Little Plover. Greatest simulated groundwater inflow, indicated by the darker blue nodes on the figure, occurs in the river reach between Eisenhower Avenue and Hoover Avenue. This finding is consistent with recent field observations and with the work of Weeks and others (1965), and coincides with an area where the aquifer thins. The river loses water to groundwater in some of the stretches upstream near Kennedy Avenue. Greater discharge from the river to the groundwater occurs along the upper part of Springville Pond, where the river has been artificially impounded. The dam for the pond raises the pond level above the local groundwater levels, creating a hydraulic gradient from the pond to the groundwater system.

The Streamflow Routing (SFR2) package used in the model adds the discharge of all the individual stream nodes together to produce the distribution of steady-state baseflow shown in figure 49. As expected, simulated baseflow increases downstream, and is a maximum of about 8 cfs at the river mouth. This simulated baseflow distribution can serve as a basis for comparison between alternative management scenarios for evaluating impacts on the groundwater component of streamflow. Plots similar to figure 49 could be constructed for transient conditions but are not shown in this report.

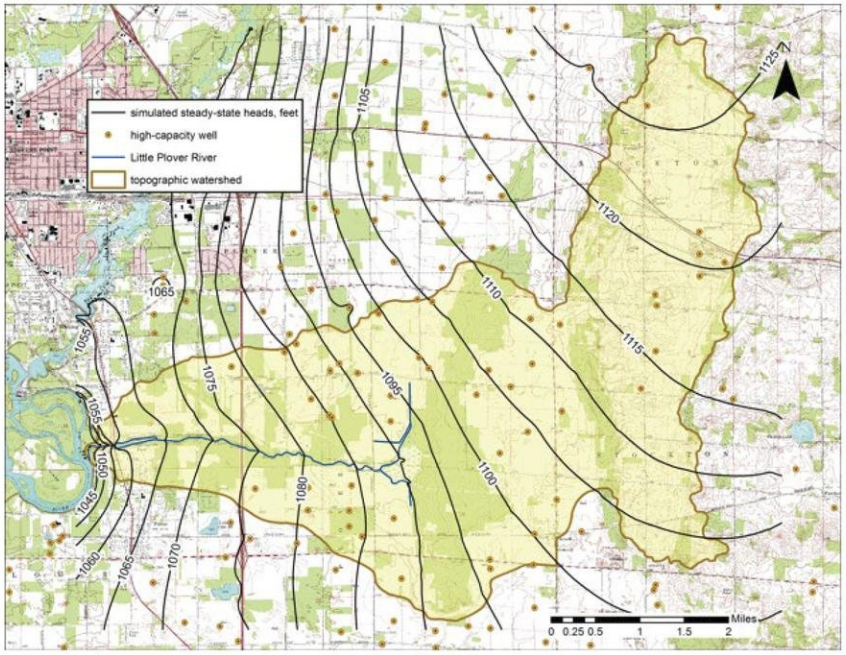

Figure 47. Hydraulic head distribution near the Little Plover River.

Figure 48. Simulated groundwater exchange with the Little Plover River

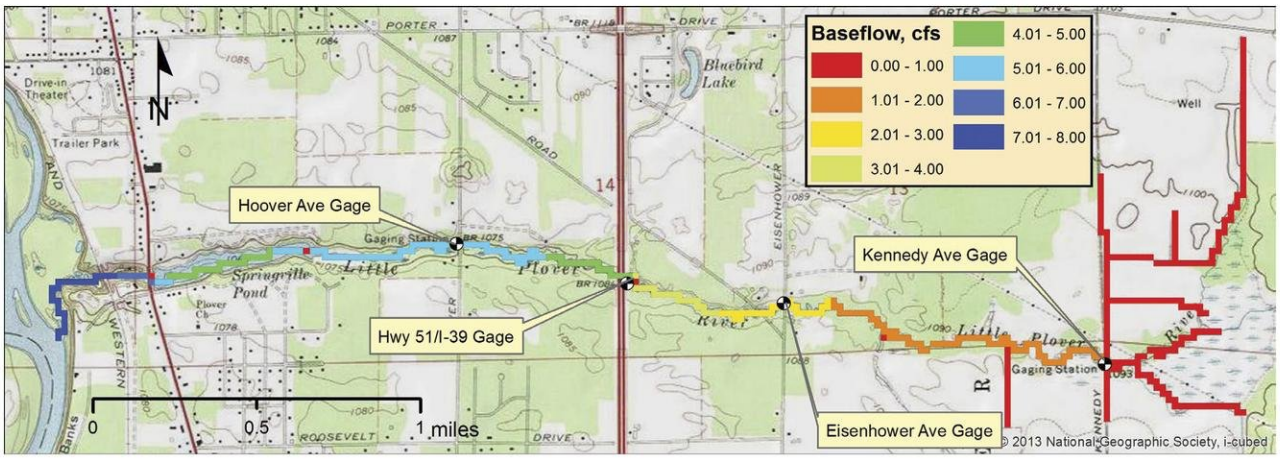

Figure 49. Simulated baseflow in the Little Plover River.

Table 13. Steady-state mass balance for the entire model domain and the Little Plover River watershed.

	cfd		cfs		in/yr	
Category	**Inflow**	**Outflow**	**Inflow**	**Outflow**	**Inflow**	**Outflow**
Entire model domain						
Recharge	1.31E+07	0.00E+00	151.9	0.0	9.9	0.0
Constant head	1.45E+06	6.17E+06	16.8	71.4	1.1	4.7
Drain (wetlands)	0.00E+00	2.08E+05	0.0	2.4	0.0	0.2
Well	0.00E+00	3.90E+06	0.0	45.1	0.0	2.9
Stream	4.22E+05	4.72E+06	4.9	54.7	0.3	3.6
Storage	0.00E+00	0.00E+00	0.0	0.0	0.0	0.0
TOTAL	1.50E+07	1.50E+07	173.6	173.6	11.3	11.3
Percent error	0.00		0.0		0.0	
LPR watershed						
Lateral groundwater flow	8.74E+05	1.16E+06	10.1	13.4	6.4	8.5
Recharge	1.40E+06	0.00E+00	16.3	0.0	10.4	0.0
Constant head	0.00E+00	0.00E+00	0.0	0.0	0.0	0.0
Well	0.00E+00	5.12E+05	0.0	5.9	0.0	3.8
Stream	1.44E+05	7.53E+05	1.7	8.7	1.1	5.6
Storage	0.00E+00	0.00E+00	0.0	0.0	0.0	0.0
TOTAL	2.42E+06	2.42E+06	28.0	28.0	17.9	17.9
Percent error	0.02		0.0		0.0	

Abbreviations: cfd = cubic feet per day; cfs = cubic feet per second.

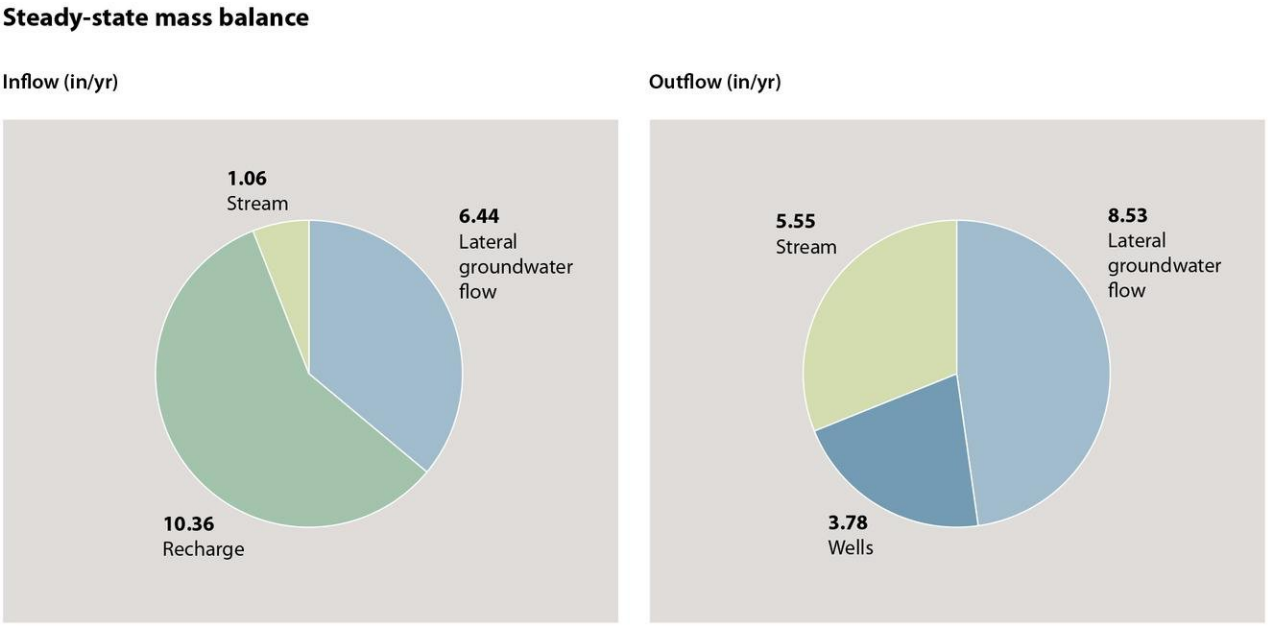

Figure 50. Steady-state mass balance for the Little Plover River basin.

Mass balance

The groundwater model yields excellent internal mass balance for both steady-state and transient simulations. Overall mass-balance error (the disagreement between volumes of water gained or lost in the model) is less than 0.01 percent, indicating that the model has reached a stable numerical solution. Table 13 summarizes the steady-state mass balance for both the entire active area of the model (209 square miles) and for the topographic basin of the Little Plover River (21.3 square miles). The table presents the results both as rates per time (cubic feet per day, cfd, and cubic feet per second, cfs) and as a depth of water over the model domain area (inches per year).

The largest single term in the overall steady-state model water balance is recharge (9.9 in/yr). The recharge term in the model budget is a lumped term that includes losses to evapotranspiration and gains from irrigation water. Most of this water eventually discharges to external boundaries (4.7 in/yr), internal streams (3.6 in/yr), wetlands (drain cells, 0.2 in/yr), or wells (2.9 in/yr). These numbers are slightly different if calculated only over the portion of the model that makes up the Little Plover River drainage basin. This basin is in the interior of the model and contains no constant-head cells, drains, or other features that serve as potential discharge points away from the river. Area-averaged recharge in the topographic basin (10.4 in/yr) is somewhat larger than in the overall model, and the Little Plover loses about 1.1 in/yr to the aquifer from the stream in losing reaches. The stream gains about 5.6 in/yr from the aquifer to the stream in gaining reaches. Wells simulated in the model use 3.8 in/yr, and the remainder of the water balance is made up of horizontal groundwater flow into and away from the basin, with net horizontal flow being 2.1 in/yr out of the basin. Figure 50 shows these water balances graphically.

Model simulation examples

The Little Plover River groundwater model is a tool to help illustrate the principles of groundwater flow and use in the region; to show the interrelationships of various sources and sinks, such as recharge, streamflow, and pumping; and to test different water-management scenarios. For the purposes of this report, a scenario is a model simulation in which certain model variables, such as well-pumping rates or recharge rates, have been changed from the calibrated base model in order to represent possible future (or past) conditions (Anderson and others, 2015). A simulation represents a single run of the model. The relevant information obtained from typical modeling scenarios includes distributions of hydraulic head (water levels), drawdown (change in water levels), mass balance (quantification of sources, sinks, and flows of water), and groundwater flow directions and velocities. The user's manual developed to accompany this report provides instructions on specific model applications (Bradbury and others, 2017).

This section of the report contains the following examples of model applications:

- Simulation of the addition of a new high-capacity well under both steady-state and transient conditions.
- Delineation of the area contributing groundwater to the Little Plover River under current-day conditions and predevelopment conditions.
- Groundwater management using depletion-potential mapping.

A fourth example, addressing groundwater management through constrained optimization, is included in appendix 7.

Example 1: Adding a high-capacity well

The Little Plover River model can be used to evaluate the potential effects of installing new high-capacity wells in and around the Little Plover River drainage basin. Impacts from pumping an individual well include drawdown at or immediately next to the well, development of a cone of depression around the well, and potential depletion of streamflow by capturing water that would have discharged to the stream as baseflow or by inducing flow from the stream to the aquifer. Simulation of a hypothetical new high-capacity well near the Little Plover River demonstrates the evaluation of these impacts.

The purpose of this example is to illustrate how the model can simulate a single new well under steady-state and transient conditions. The simulations were run under two different assumptions regarding recharge. Initial runs assumed no change in land use—other than the presence of the new well—and all discharge from the well was removed from the model. A second set of runs simulated additional recharge around the well that might occur as part of the irrigation process as a portion of the irrigated water infiltrates and replenishes the groundwater system.

Methodology

The example simulates the impact of a new high-capacity irrigation well along Porter Drive, about 1 mile north of the Little Plover River (fig. 51). The well is typical of many of the larger-capacity irrigation wells in the model domain. This hypothetical well pumps only during the growing season, with 28 percent of its annual use in June, 58 percent in July, and 14 percent in August. (These are percentages from an existing well elsewhere in the model.) Overall discharge from the well is 8.69 million cubic feet, or 65 million gallons (Mgal), per year. This translates to an average daily discharge of 23,800 cubic feet, or 0.18 Mgal, per day (124 gallons per minute, gpm).

We simulated the groundwater and surface-water responses to this pumping using both the steady-state and transient models with their calibrated recharge conditions (2013 conditions for steady state and 2014 conditions for transient; see calibration section of this report). Comparisons between baseline models and the new well simulation show the effects of the well on groundwater levels and on flow in the river. In addition, this example demonstrates the differences between steady-state and transient analyses. The example well was added at row 523, column 411 of the model, with the well open to layers 1, 2, and 3. The model com-

Simulated steady-state drawdown, with and without irrigation return

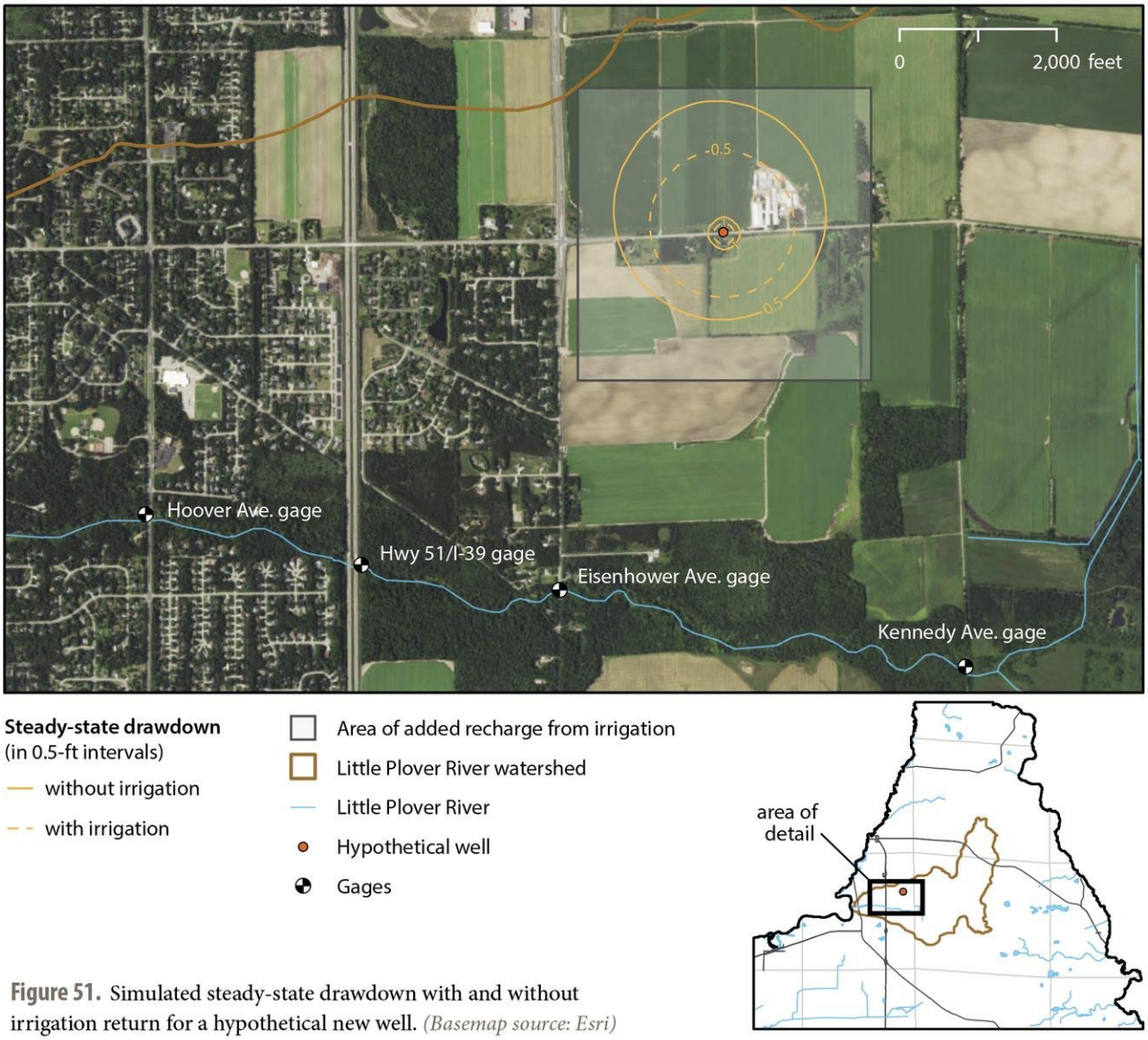

Figure 51. Simulated steady-state drawdown with and without irrigation return for a hypothetical new well. *(Basemap source: Esri)*

putes discharge to the well from each layer in proportion to the relative layer transmissivities at this model node. Initially, recharge rates were unchanged from the steady-state and transient calibrations. Transient runs were carried out in two stages for a 5-year simulation period, repeating a single pumping cycle five times. In the first stage, the example well was pumped only during the first year in order to examine the length of time needed for full recovery from the pumping stress. In the second stage, the well was pumped identically for each of the 5 years in order to examine the impact of a well being used in successive years. To simulate the recharge of irrigation water, we conducted a second set of runs in which additional recharge was applied over a rectangular area comprising 230 acres centered on the example well (fig. 51). An area of this size was chosen to be about equal to the area irrigated by the existing well on which this example is based. Additional recharge applied totaled 1.5 inches during the irrigation period (June, July, August); this value was taken from soil-water-balance calculations based on grower-reported irrigation for potatoes in 2014 (see recharge section of this report). The extra recharge was equally distributed over the irrigation season, with 0.5 inches added in each of the three simulated months. It is important to note that the irrigation return used in this example is intended for demonstration and is based on numerous assumptions about cropping, soils, and irrigation practice that might not be appropriate for other locations or time periods.

Steady-state results

Under steady-state assumptions, the well lowers the water table about 1 foot near the well and forms a cone of depression (as bounded by the 0.5 ft drawdown contour) about 1/2 mile across (solid lines, fig. 51). Simulated baseflow in the Little Plover River declines 0.1 cfs at Kennedy Avenue, 0.1 cfs at Eisenhower Avenue, and 0.2 cfs at Hoover Avenue (table 14). These values, divided by the steady-state well discharge, give depletion ratios of 18 to 69 percent, meaning 18 percent to 69 percent of the water produced by the well at steady state is water that otherwise would have discharged to the river. The remainder of the water produced by the well would have discharged elsewhere, primarily to the Wisconsin River.

Table 14. Baseflow changes at three locations with and without a new well—no change in recharge. See figure 9 for site locations. June, July, and August results refer to simulated flows at the end of these months.

Gage site	Baseline baseflow (cfs)	Baseflow with well (cfs)	Change (cfs)	Change (cfd)	Change (%)	Depletion ratio (%)
Steady state, 2013 (Q=23,800 cfd)						
Kennedy	1.0	0.9	0.1	4,320	5.1	18.2
Eisenhower	2.2	2.0	0.1	11,232	6.0	47.2
Hoover	5.4	5.2	0.2	16,416	3.5	69.0
Transient, 2014						
JUNE (Q=81,079 cfd)						
Kennedy	1.8	1.8	0.0	0	0.0	0.0
Eisenhower	3.8	3.8	0.0	1,728	0.5	2.1
Hoover	7.9	7.9	0.0	1,728	0.3	2.1
JULY (Q=162,531 cfd)						
Kennedy	1.2	1.1	0.0	2,592	2.6	1.6
Eisenhower	2.5	2.4	0.1	9,504	4.3	5.8
Hoover	6.2	6.1	0.1	11,491	2.1	7.1
AUGUST (Q=39,232 cfd)						
Kennedy	1.3	1.2	0.1	6,048	5.4	15.4
Eisenhower	2.9	2.7	0.2	16,416	6.6	41.8
Hoover	6.8	6.5	0.3	22,464	3.9	57.3

Abbreviations: cfd = cubic feet per day; cfs = cubic feet per second; Q = discharge of hypothetical well

Table 15. Baseflow changes at three locations with and without a new well—recharge increased in the vicinity of the well. See figure 9 for site locations. June, July, and August results refer to simulated flows at the end of these months.

Gage site	Baseline baseflow (cfs)	Baseflow with well (cfs)	Change (cfs)	Change (cfd)	Change (%)	Depletion ratio (%)
Steady state, 2013 (Q=23,800 cfd)						
Kennedy	1.0	0.9	0.1	4,320	5.1	18.2
Eisenhower	2.2	2.1	0.1	10,368	5.5	43.6
Hoover	5.4	5.2	0.2	15,552	3.3	65.3
Transient, 2014						
JUNE (Q=81,079 cfd)						
Kennedy	1.8	1.8	0.0	0	0.0	0.0
Eisenhower	3.8	3.8	0.0	1,728	0.5	2.1
Hoover	7.9	7.9	0.0	1,174	0.2	1.4
JULY (Q=162,531 cfd)						
Kennedy	1.2	1.1	0.0	2,592	2.6	1.6
Eisenhower	2.5	2.5	0.1	7,776	3.5	4.8
Hoover	6.2	6.1	0.1	9,438	1.8	5.8
AUGUST (Q=39,232 cfd)						
Kennedy	1.3	1.2	0.1	4,320	3.9	11.0
Eisenhower	2.9	2.7	0.2	13,824	5.5	35.2
Hoover	6.8	6.5	0.2	18,361	3.1	46.8

Abbreviations: cfd = cubic feet per day; cfs = cubic feet per second; Q = discharge of hypothetical well

Under steady-state conditions, simulating the return of irrigation water significantly reduces, but does not eliminate, the impacts of the well on the water table and on streamflows. Assuming irrigation return, the well lowers the water table about 1 foot near the well and the 0.5-foot drawdown contour is about 1/3 mile across (dashed lines, fig. 51). Simulated baseflow in the Little Plover River declines 0.1 cfs at Kennedy Avenue, 0.1 cfs at Eisenhower Avenue, and 0.2 cfs at Hoover Avenue (table 15). These values divided by the steady-state well discharge give depletion ratios of 18 to 65 percent.

Transient results

The transient simulation results show how the impacts of the well change through time, and are probably more representative of actual impacts than the steady-state results. However, because the transient simulation is based on precipitation and pumping during 2014, a year with higher-than-average precipitation, it may not be representative of impacts during drier years. Maximum drawdown occurs near the end of July, and the cone of depression developed then is similar in shape to—but larger than—the steady-state cone (fig. 52), with the 0.5 ft drawdown contour being about 1 mile across. The steady-state model underestimates maximum drawdown in this case (compare figs. 51 and 52) because the pumping rate is averaged over the entire year. Figure 53 shows how the drawdown cone changes through the year for the scenarios with and without irrigation return. It initially develops as pumping begins in June, continues to grow during July and August, and then diminishes during September. In both scenarios, the cone of depression remains through September, even though simulated pumping ceases at the end of August. Comparison of the scenarios with and without irrigation return (right and left parts of fig. 53) shows that

Simulated transient drawdown, with and without irrigation return

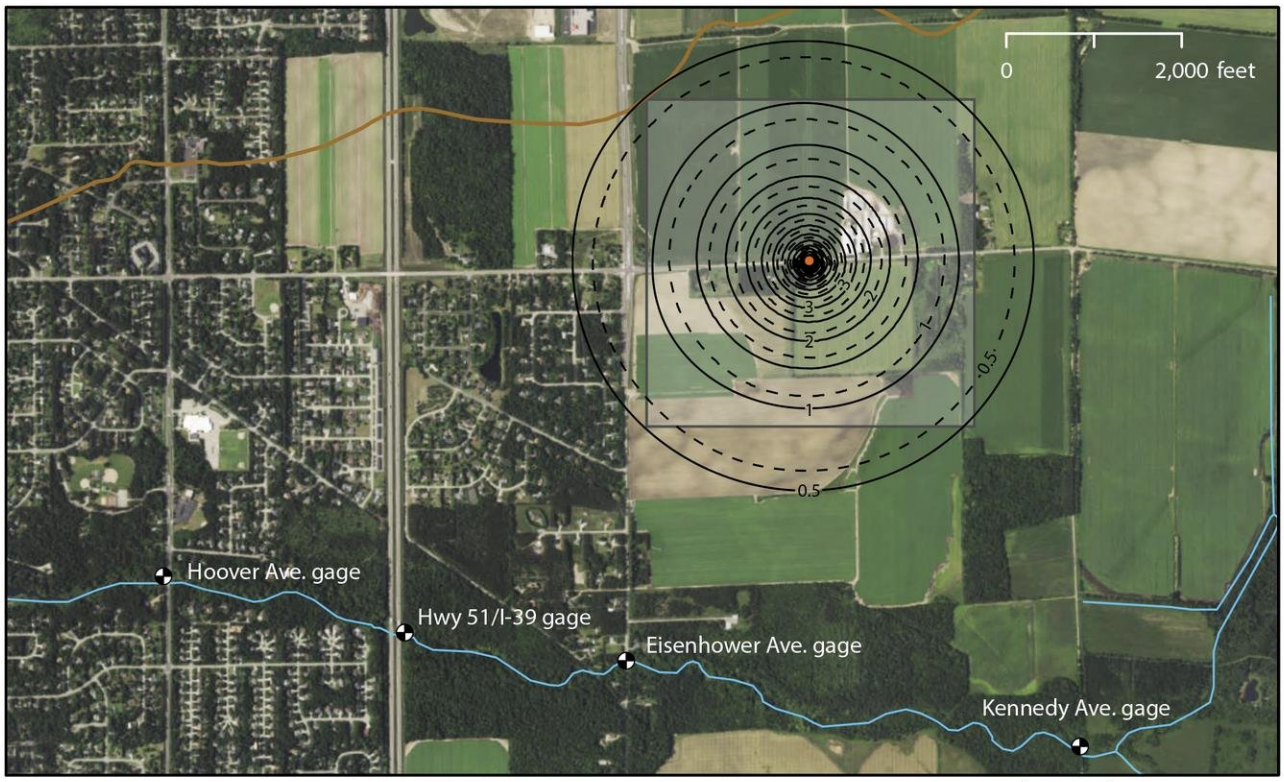

Transient drawdown in July
(in 0.5-ft intervals)

— without irrigation

– - with irrigation

Area of added recharge from irrigation

Little Plover River watershed

Little Plover River

Hypothetical well

Gages

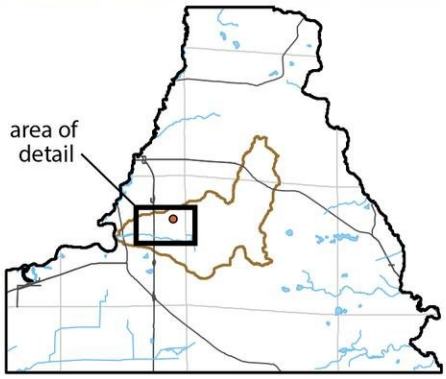

Figure 52. Simulated transient drawdown with and without irrigation return for a hypothetical new well. *(Basemap source: Esri)*

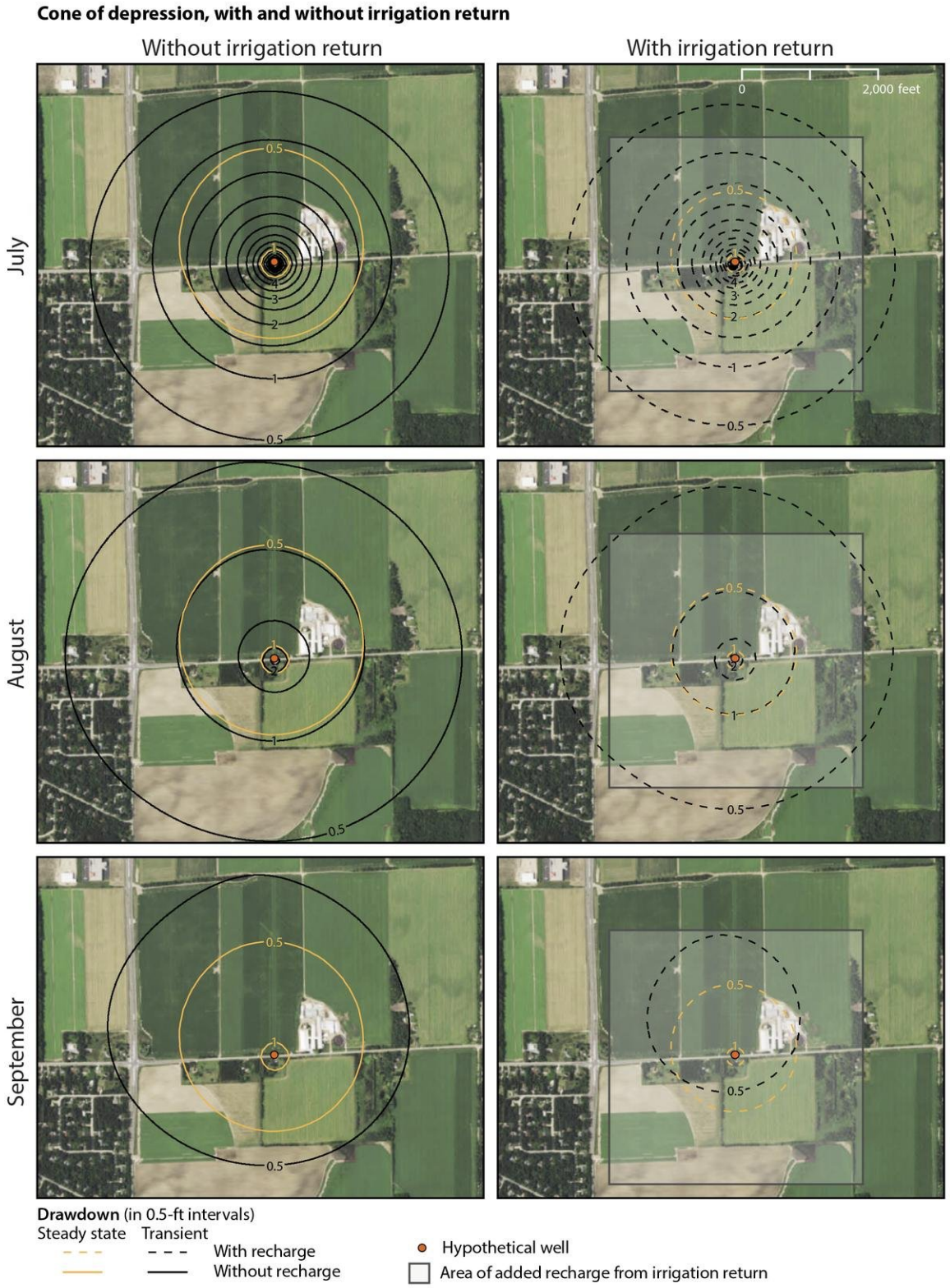

Figure 53. Expansion and contraction of cone of depression through time at the hypothetical new well, with (right) and without (left) irrigation return. *(Basemap source: Esri)*

less total drawdown occurs under the irrigation scenario and the cone of depression is slightly narrower.

In the transient simulation, drawdown at the well and impacts on streamflow vary with time and lag behind changes in pumping. This time lag is related to the concept of hydraulic diffusivity, defined as transmissivity divided by storativity, which governs the rate that a stress propagates through an aquifer (Anderson and others, 2015). The unconfined aquifer in the Little Plover River basin has a relatively high storativity (specific yield of 0.12), which means that the hydraulic diffusivity is small and the corresponding response time is long compared to confined aquifers composed of similar materials.

Plots of streamflow change and drawdown at the well versus simulation time (fig. 54) illustrate the effects of time lag. There is no drawdown at the pumped well until pumping begins in June, and maximum drawdown of about 10 feet occurs at the end of July. The well begins to recover as pumping decreases in August, but even though pumping ceases at the end of August, drawdown continues for several months. Simulated drawdown is 0.7 feet at the end of September, 0.4 feet at the end of October, and 0.3 feet at the end of November. The well does not fully recover until the following spring.

The time lag effect means that impacts at greater distances from the well are delayed more than impacts immediately adjacent to the well. The top three plots on figure 54 show hydrographs of the change in flow of the Little Plover River at the three gaging sites versus time. The plots show that even though pumping of the well begins in June, there is little impact on the streamflow until July, when streamflow at all three sites begins to decline relative to the baseline (no new well) condition. The streamflow begins to recover when pumping declines at the end of July, but the overall decline in streamflow continues for several months after pumping ceases, reaching a maximum decline in September before beginning to recover. When the well is operated only during first year of the simulation (top plots on fig. 54), the streamflow at all three sites is about 50 percent recovered at the end of year 1, but does not fully recover until midway through year 3. In contrast, when the well operates in successive years (bottom plots on fig. 54), the streamflow never fully recovers.

Accounting for re-infiltration of a proportion of irrigation water near the well reduces the impact on the stream only slightly. The dashed lines on figure 54 represent the simulated decline in streamflow that would occur with infiltrated irrigation added to the model. Under this scenario, maximum reductions in streamflow at the three gages during the first year of the 5-year simulation are about 0.1 cfs at the Kennedy gage, 0.2 cfs at the Eisenhower gage, and 0.2 cfs at the Hoover gage (table 15).

Comparison of simulated 2013 steady-state versus 2014 transient impacts on streamflow (table 14) shows that the transient impacts can be significantly different than the steady-state impacts, and that impacts differ by position along the stream. It is important to note that because 2014 was a wetter-than-average year, the simulated 2014 transient impacts might be somewhat less than for a dry or average year. The model is capable of simulating conditions in other years, but such simulations were beyond the scope of this report. The groundwater system in the Little Plover River area can take several months to reach steady state, and generally does not reach steady state during a typical growing season.

GROUNDWATER FUNDAMENTALS

Cumulative impact of pumping

DETAILS: Whenever a well is pumped, discharge is diverted from streams and water levels in an aquifer, lakes, and wetlands are lowered. Cumulative impacts refer to the additive effects as impacts from numerous wells in the same area overlap. When many wells in a region are being pumped, water level declines and streamflow diversions add to each other. So even though a single well may cause only a small decline or diversion, the additive effects of many wells can significantly impact lakes and streams.

WHY IT MATTERS: Unless located immediately adjacent to a surface water feature or another well, any single well typically has modest impacts on water levels or streamflow. However, when many wells are located in the same area the cumulative impacts of all these wells can become significant.

This example illustrates several important characteristics of steady-state versus transient flow simulations for this region. First, for typical irrigation wells that pump only during the growing season, the steady-state model might not represent a worst case (maximum impact) with respect to streamflow. Note that the steady-state 2013 results (tables 14 and 15) show a flow change of 3.3 to 3.5 percent at the Hoover gage, but the transient 2014 simulations show a change of 3.1 to 3.9 percent there at the end of August. Second, for typical irrigation wells, the transient simulation represents a worst case (maximum drawdown) at the well itself; the steady-state model underestimates maximum drawdown because the pumping rate is averaged over the entire model year. Third, the transient simulation provides useful information about the time lag between pumping periods and expected impacts on the stream. Depending on distance between the well and the stream, the effects of pumping on streamflow might not occur until several months have passed since pumping began—and typically continue—after pumping has ceased. This example shows that because of the time lag, the cumulative impacts of pumping might not be apparent for weeks or months after the onset of pumping.

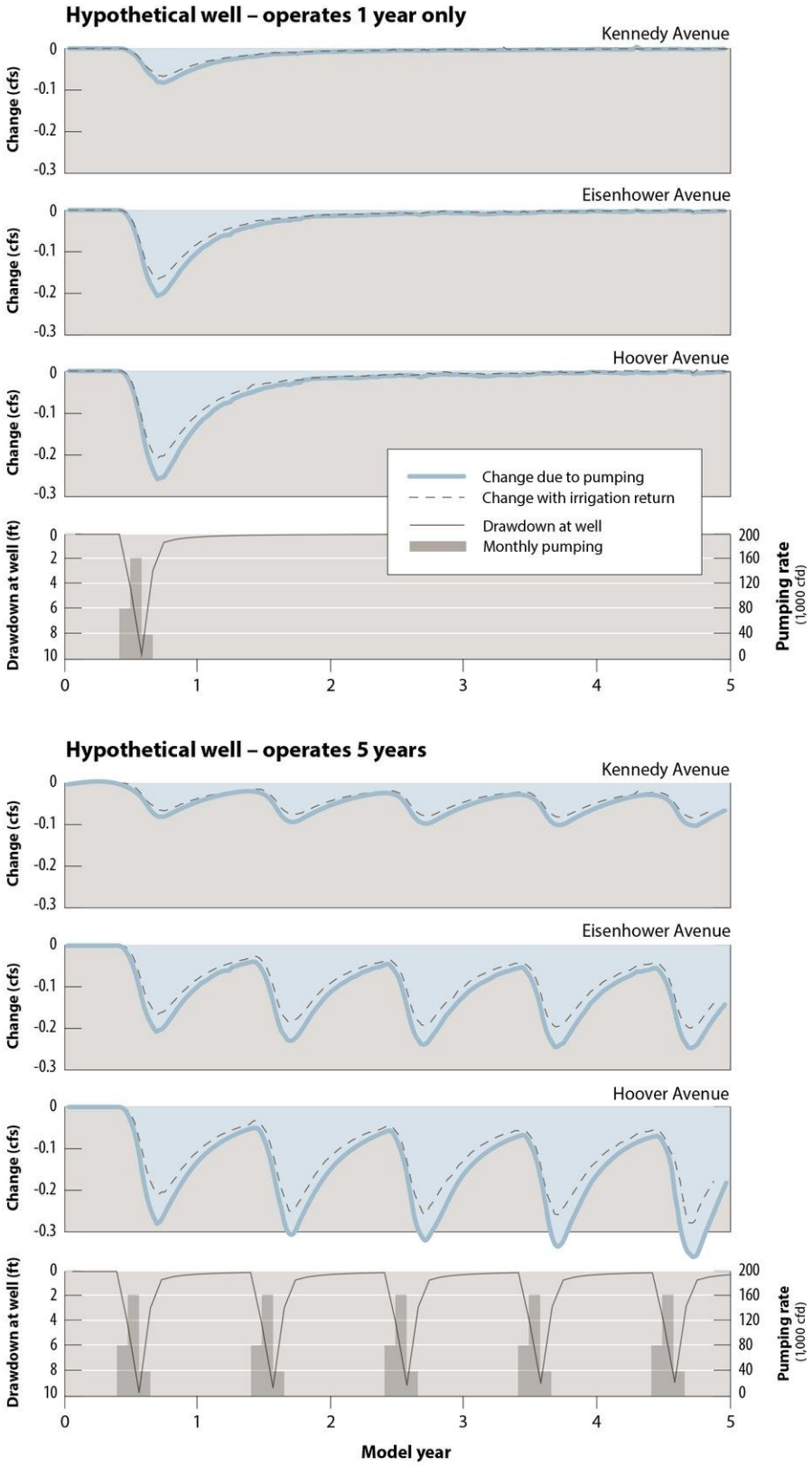

Figure 54. Simulated pumping schedule, drawdown, and streamflow change hydrographs for the hypothetical new well example. Top: Well operates for 1 year only. Bottom: Well operates for 5 successive years.

Simulated present-day contributing area

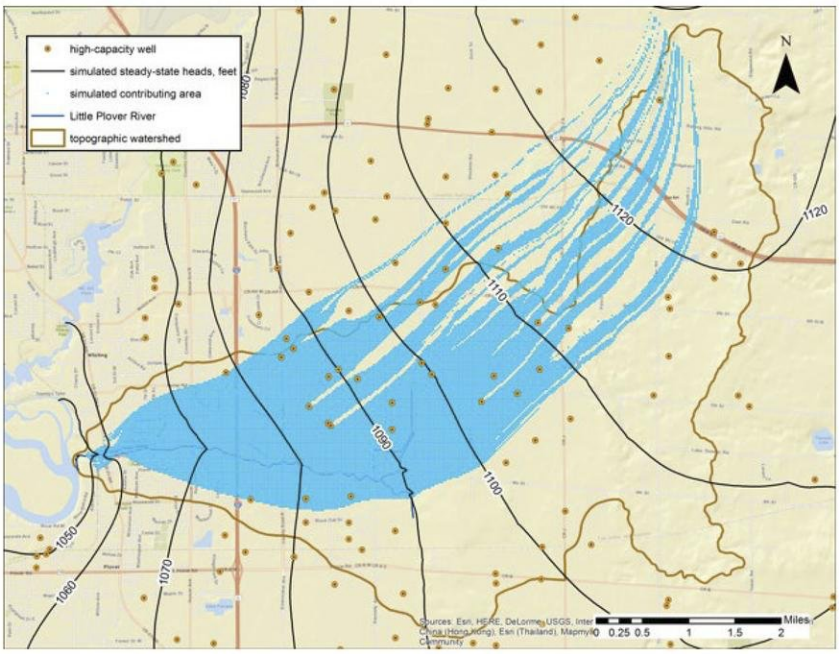

Figure 55. Simulated present-day contributing area for the Little Plover River.

Simulated predevelopment contributing area

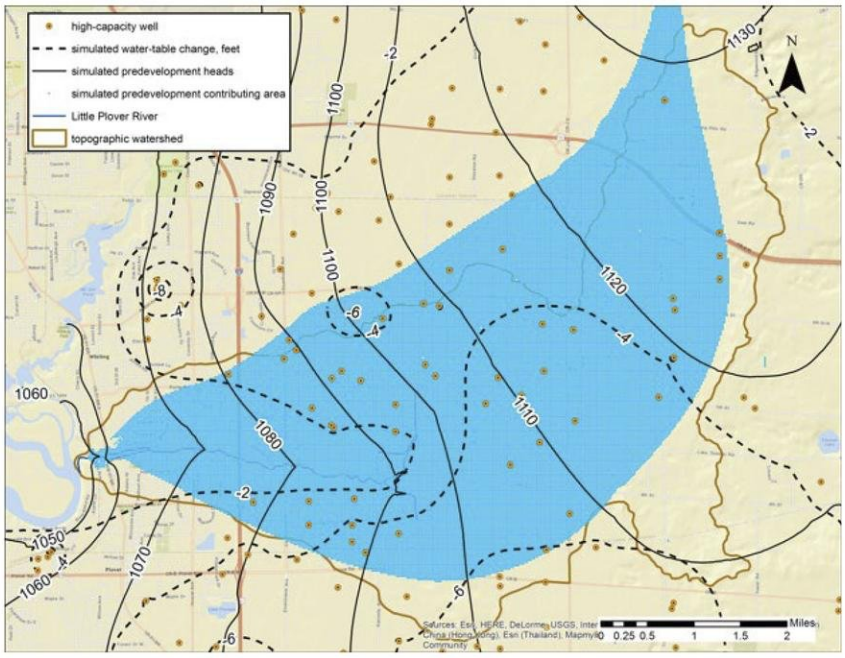

Figure 56. Simulated predevelopment contribution area for the Little Plover River. Dashed contour lines show simulated water-level change between predevelopment and current conditions.

Example 2: Simulating cumulative effect of existing pumping

Pumping within the model domain alters both the size of the area contributing groundwater to the river and average flow rates in the river. Simulated contributing areas, or capture zones, for the Little Plover River show the area of the landscape contributing groundwater to the river. Using the USGS MODPATH particle tracking code (Pollock, 2012), mathematical particles were placed at the water table and tracked forward in the steady-state model until they exited the model at a well or model boundary. The population of particles reaching the river makes up the contributing area for the river. The present-day (calibrated model) contributing area (fig. 55) forms an arc extending outside the topographic watershed boundaries and extending nearly 7 miles north of the river. The irregular shape of the contributing area arises from the presence of wells in the area, which capture flow at specific locations. The area of capture is 13.9 square miles. Groundwater inside this region eventually discharges to the Little Plover River and groundwater outside this region discharges elsewhere.

A steady-state simulation approximating predevelopment conditions (fig. 56) shows that the predevelopment contributing area was likely significantly larger than the present-day contributing area and streamflows were greater in the past. This simulation removes all wells from the model and replaces the calibrated recharge rates for irrigated land with calibrated values for the nearest nonirrigated

land, which is either broadleaf vegetation, grass/prairie, or evergreen trees. This change in land use results in a reduction in annual recharge of about 1.9 inches averaged over the Little Plover River basin (table 16). The resulting contributing area is similar in length to the one shown in figure 55, but is significantly broader, with an area of 19.1 square miles. River baseflow is directly proportional to the area of the capture zone. Although recharge is lower in the absence of pumping, the simulated predevelopment Little Plover River capture zone is larger in area, and consequently, baseflow in the river was greater than under current conditions. Figure 56 also shows the simulated change in the water table due to the combined presence of high-capacity wells in the area (dashed contours). Simulated steady-state drawdowns range from 0 to 6 feet, with about 2 feet in the vicinity of the main channel of the Little Plover River.

Comparing the simulated present-day streamflows to streamflows simulated in the absence of wells provides an estimate of the steady-state cumulative impacts of pumping on the Little Plover River at the three gaging sites (see fig. 9 for locations). Table 16 shows the results of this simulation. Under steady-state (2013) conditions, the simulated change in streamflow caused by land-use change (the combination of irrigation and crop introduction) is about 1.7 cfs at Kennedy Avenue, 3.3 cfs at Eisenhower Avenue, and 4.5 cfs at Hoover Avenue.

The model shows that even wells outside the contributing area (shaded regions on figs. 55 and 56) can impact the size and shape of the contributing area and affect groundwater discharge to the river. The model can be used to quantify the impacts of any particular well using the concept of depletion potential described in the next example.

Example 3: Mapping depletion potential

Background

"Depletion" is a term used to describe the interception or diversion of groundwater discharge that would go to a stream if no extraction wells were present. Extraction wells change the flow field and—in temperate regions such as central Wisconsin—derive the water they extract at the expense of surface-water bodies. This process, often called "capture," is independent of recharge (Bredehoeft, 2002). Other related terms include interception, diversion, and induced infiltration. Interception occurs when water that was previously flowing toward a stream is, instead, captured by a nearby well. Diversion occurs when water that was initially or historically flowing toward a stream instead discharges to another surface-water feature or another location on the stream, due to changes in the flow field caused by a well. Induced infiltration occurs when water flows out of the stream and into the groundwater system due to well pumping. Induced infiltration is the most extreme case of a well affecting a nearby stream and represents a change from gaining conditions to losing conditions. Increased pumping results in a decrease in stream flow, and the change in simulated baseflow when an additional well is added to the model shows the impact of that particular well. Depletion potential is the percentage of water pumped from the well that would have eventually reached the stream if the well was not pumping.

From first principles, depletion is controlled in large measure by the proximity of wells to surface-water features. For example, Jenkins (1968a, 1968b) presented a "streamflow depletion factor" (SDF) which indicates the timing of depletion:

(EQUATION 11)

$$SDF = \frac{d^2}{D}$$

where: SDF is the stream depletion factor, d is the distance from a well to a surface water body, and D is hydraulic diffusivity (defined as hydraulic conductivity (K) times aquifer thickness (b) divided by specific yield (S_y)). Large values of SDF indicate long times required for depletion to reach surface water, and small values

Table 16. Comparison of 2013 calibrated simulation, with predevelopment simulation. Recharge, pumping, and streamflow values are given for the Little Plover River topographic basin.

Simulation	Flow			Recharge (cfs)	Recharge (in/yr)	Pumping (cfs)	Pumping (in/yr)
	Kennedy (cfs)	Eisenhower (cfs)	Hoover (cfs)				
Present day	1.0	2.2	5.4	16.3	10.4	5.9	3.8
Predevelopment	2.7	5.5	9.9	13.3	8.5	0.0	0.0
Change	–1.7	–3.3	–4.5	3.0	1.9	5.9	3.8
Percent change	–63	–60	–45	23	22		

Abbreviations: cfd = cubic feet per day; cfs = cubic feet per second.

indicate depletion occurring in short times. Note that distance between the well and the surface-water body is squared, so its influence is very large. More recent work by Fienen and others (2016) shows that other surface-water characteristics, such as the spatial density of surface-water features near a well, can also be important, although it is not considered in the analytical solutions.

A groundwater model provides a test bed to evaluate how groundwater extraction impacts streamflow in the Little Plover River. In addition to determining the SDF, a model can be used to determine the source of water to wells. Various surface-water features compete to provide water to wells—once again, largely as a function of proximity. In this project, the main surface water feature of concern is the Little Plover River. The modeling code GWM-VI (Groundwater Management—Version Independent (Banta and Ahlfeld, 2013)), is integrated with MODFLOW, and performs systematic analyses of optimization scenarios. These optimization scenarios either maximize or minimize a managed quantity (for example, pumping rate in a well) subject to a constraint (for example, a public rights flow level in a stream). A necessary step in this process is to calculate a response matrix. This is made up of calculated changes in streamflow at constraint locations due to a change in pumping rate at a managed well;

(EQUATION 12)

$$R = \frac{\Delta Q_{stream}}{\Delta Q_{well}}$$

where *R* is the response, also called *"depletion potential,"* ΔQ_{stream} is the change in flow at a stream constraint location, and ΔQ_{well} is the change in well pumping simulated. To make these calculations, a base model run is followed by a run for each well in which the pumping in each well is increased. The model then calculates decreases in streamflow at each constraint location that can be attributed to pumping at each specific well. Due to the conservation of mass, changes in streamflow due to additional pumping represent depletion by the pumping. Such simulations require N+1 model runs where N is the number of decision variables. A decision variable refers to an adjustable quantity for optimization. In this case, it is the flow at either a single well or a group of wells managed together. The units of flow in both the stream and the well are consistent, so depletion potential (R) represents a ratio between 0 and 1.0 (or a percentage between 0 and 100) of the amount of water pumped at a well that is derived (either through interception, diversion, or reversed flow) from each stream. Example 1 also illustrates this concept.

The following section presents depletion-potential calculations for wells in the Little Plover River basin. We then explore several optimization and management options that make use of the depletion-potential values to focus management on wells that have the greatest impact on the Little Plover River. Finally, in appendix 7, we explore optimization options using GWM-VI to perform constrained optimization with various groupings of managed wells.

Using the calculations of depletion potential in equation 12, we can explore the relationship between each existing well from 2013 to 2014 DNR-reported water use and each of the four Little Plover River gage locations at which a public rights flow value exists. Figures 57, 58, and 59 show maps of the depletion potential calculated for each well that was actively pumping in 2013 relative to public rights flow gage locations at Kennedy Avenue, Eisenhower Avenue, and Hoover Avenue.

As expected from theory, wells that are closest to the Little Plover River generally show the highest values of depletion potential. The only exception to this finding is in cases where wells are close to the Little Plover River, but also close to the Wisconsin River—in such cases, more water may be diverted from the Wisconsin River (or other surface-water features) than from the Little Plover River. As illustrated in figures 57, 58, and 59, the simulations show that wells outside of the contributing area for the river can impact discharge to the river. These impacts happen because even drawdown from wells that are outside the contributing area can alter the water table enough to divert groundwater that otherwise would discharge to the river to discharge elsewhere. As discussed earlier, in this temperate climate, wells derive all the water they pump from surface-water features; the question is timing and the amount of water derived from each surface-water feature. As a result, wells with low depletion potential with respect to the Little Plover River must have high depletion potential with respect to another surface-water feature. Theoretically, the depletion potential for a well with respect to all surface-water features in the region adds up to 1.0.

One-by-one well removal

Using the depletion-potential calculations, it is possible to rank the depletion potential in each well relative to a specific gage. Appendix 8 reports the depletion-potential rank relative to the Hoover gage for the wells that were actively pumped in 2013 and 2014, are in the Little Plover River area, and have depletion potential greater than 0.25. The Hoover gage was selected for this analysis because it is the farthest downstream, and thus, most closely represents overall impact on the river. Depletion potential ranges from 0.857 near

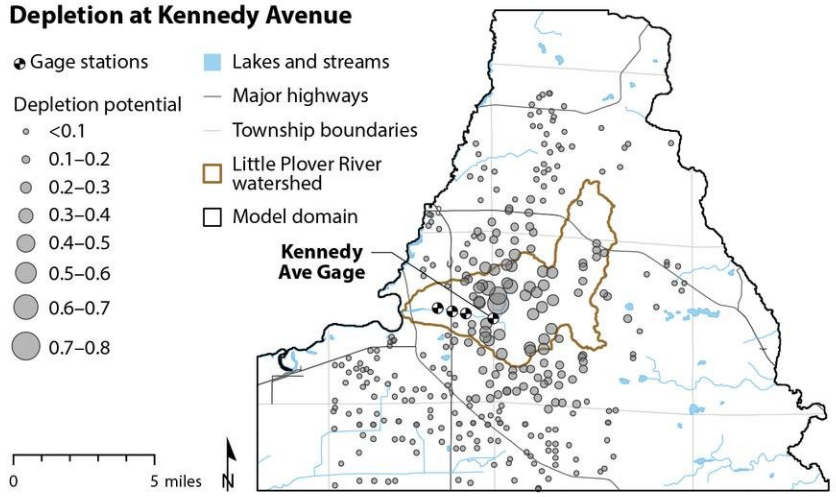

Figure 57. Depletion analysis at Kennedy Avenue.

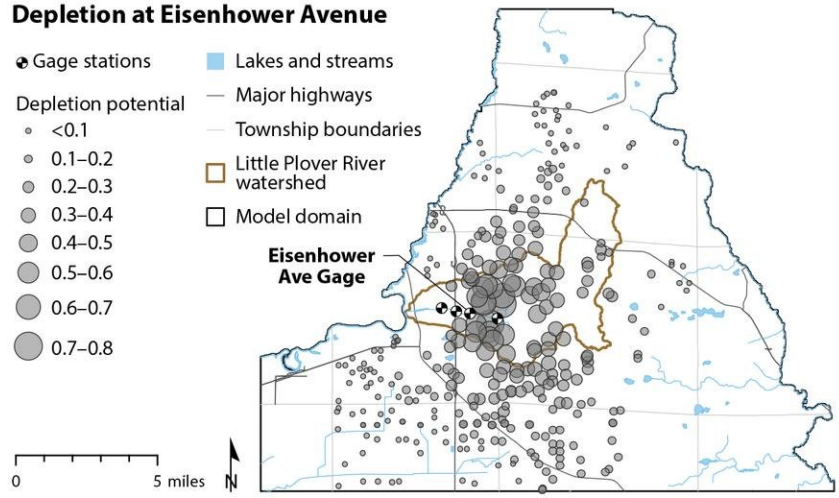

Figure 58. Depletion analysis at Eisenhower Avenue.

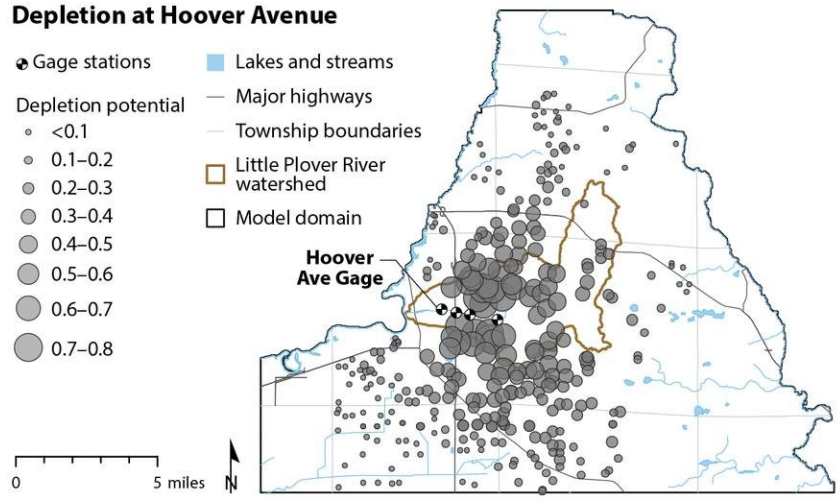

Figure 59. Depletion analysis at Hoover Avenue.

the river to nearly 0.0 distant from the river, consistent with the figures discussed above. Using this rank, however, it is possible to evaluate the increase in streamflow that would result from eliminating pumping in wells with high depletion potential. To evaluate this response, two evaluations were conducted: one for steady state (2013) and one for transient (2014). The public rights flow (PRF) is reported for all four gage locations, along with the baseflow portion of the PRF (calculated as 80 percent of the public rights flow, representative of the baseflow separation analysis for this project). The baseflow portion—referred to here as the public rights baseflow—is considered because changes in pumping only impact the baseflow part of total streamflow and have no impact on the stormflow component. The public rights baseflow and PRF are both depicted on graphs for the analysis of well removal in this section. The MODFLOW model only simulates baseflow, so comparing model results to the total PRF would not be accurate. In each case, wells were removed sequentially in order from highest to lowest depletion potential, the model was run with the selected wells removed, and streamflow was evaluated at all four gage locations. This result assumes that recharge and land use remain the same as the wells are removed. In reality, recharge would likely decrease due to the reduction in irrigation-return water, depending on land-use changes, and so the stream response might be less that predicted by this simulation.

Steady-state results

After the removal of 16 wells, the public rights baseflow is met or exceeded in the steady-state simulation at all four gages. Table 17 presents the results for the steady-state analysis for the 35 wells with highest depletion potential; figure 60 shows the same information graphically for all 317 wells evaluated.

Transient results

Transient well-removal analysis focused on July and August flow values for 2014. Simulated baseflow is low during this period, as well as in late winter. However, simulated baseflow was below the public rights flow values in February and March, even with no pumping simulated in the model. This is attributed to the lack of gage measurements during winter due to river ice, and model results for these months in 2014 are not reliable. The July/August period is most directly impacted by irrigation pumping that makes up a major component of the withdrawals in the area, so is also the most likely to respond to changes in water use. Appendix tables 8e, 8f, 8g, and 8h report the transient streamflow values per month for simulations sequentially and cumulatively, removing the wells with highest depletion potential. Results for removing wells are presented up to the point where public rights flow values are achieved. Figure 61 shows the hydrographs for the four gage locations, with the brown band

Table 17. Simulated baseflow under steady-state conditions for wells with highest depletion potential. Baseflow was calculated using the indicated number of wells set to zero pumping rate. Shading indicates flow values at or above the public rights baseflow (light blue) and flow (dark blue) rates.

	Gaging site			
	Kennedy	Eisenhower	Hwy 51/I-39	Hoover
Public rights baseflow, cfs	1.52	3.20	4.64	5.44
Public rights flow, cfs	1.90	4.00	5.80	6.80
Number of wells removed	**Simulated baseflow under steady-state conditions, cfs**			
1	0.97	2.13	3.72	5.26
2	0.99	2.17	3.76	5.31
3	1.00	2.19	3.78	5.33
4	1.02	2.26	3.87	5.43
5	1.06	2.36	3.99	5.56
6	1.11	2.44	4.07	5.64
7	1.13	2.51	4.16	5.75
8	1.14	2.52	4.18	5.77
9	1.15	2.55	4.22	5.81
10	1.24	2.79	4.49	6.11
11	1.33	2.95	4.68	6.31
12	1.33	2.96	4.69	6.33
13	1.44	3.22	5.00	6.66
14	1.48	3.32	5.10	6.77
15	1.49	3.34	5.13	6.80
16	1.62	3.59	5.41	7.10
17	1.63	3.61	5.44	7.15
18	1.63	3.62	5.44	7.14
19	1.64	3.63	5.47	7.17
20	1.71	3.87	5.81	7.60
21	1.74	3.94	5.90	7.70
22	1.74	3.94	5.91	7.71
23	1.78	4.03	6.03	7.85
24	1.80	4.08	6.08	7.91
25	1.83	4.12	6.13	7.97
26	1.83	4.14	6.16	8.01
27	1.84	4.15	6.18	8.03
28	1.83	4.14	6.16	8.01
29	1.85	4.18	6.21	8.06
30	1.86	4.19	6.22	8.08
31	1.96	4.33	6.38	8.24
32	2.09	4.55	6.63	8.53
33	2.12	4.60	6.69	8.59
34	2.18	4.70	6.79	8.70
35	2.19	4.70	6.79	8.70

representing the hydrograph for each simulation with (from bottom to top) progressively more wells removed. The blue line in figure 61 represents the annual hydrograph when 11 wells were removed. In this simulation, removing 11 wells with the greatest depletion potential kept the July streamflow above the public rights baseflow at each of the four gages. Note that the shaded area below the gray line represents 10 wells, while the area above the line represents an additional 359 wells, demonstrating the diminishing effect of removing many more wells.

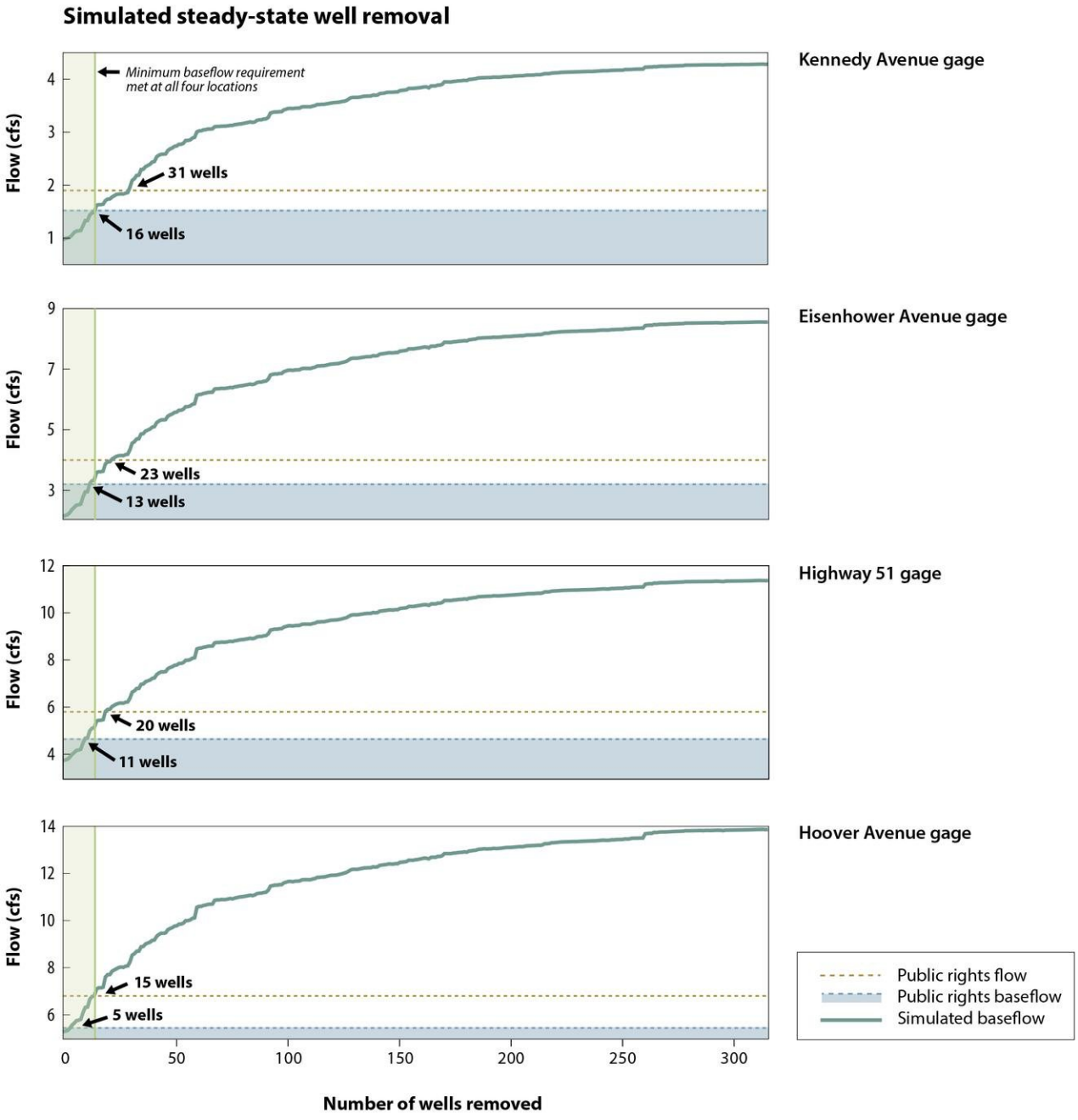

Figure 60. Steady-state flow results for one-by-one well removal. The vertical green bar (16 wells removed) marks the first time the river remains above public rights baseflow at all gage locations.

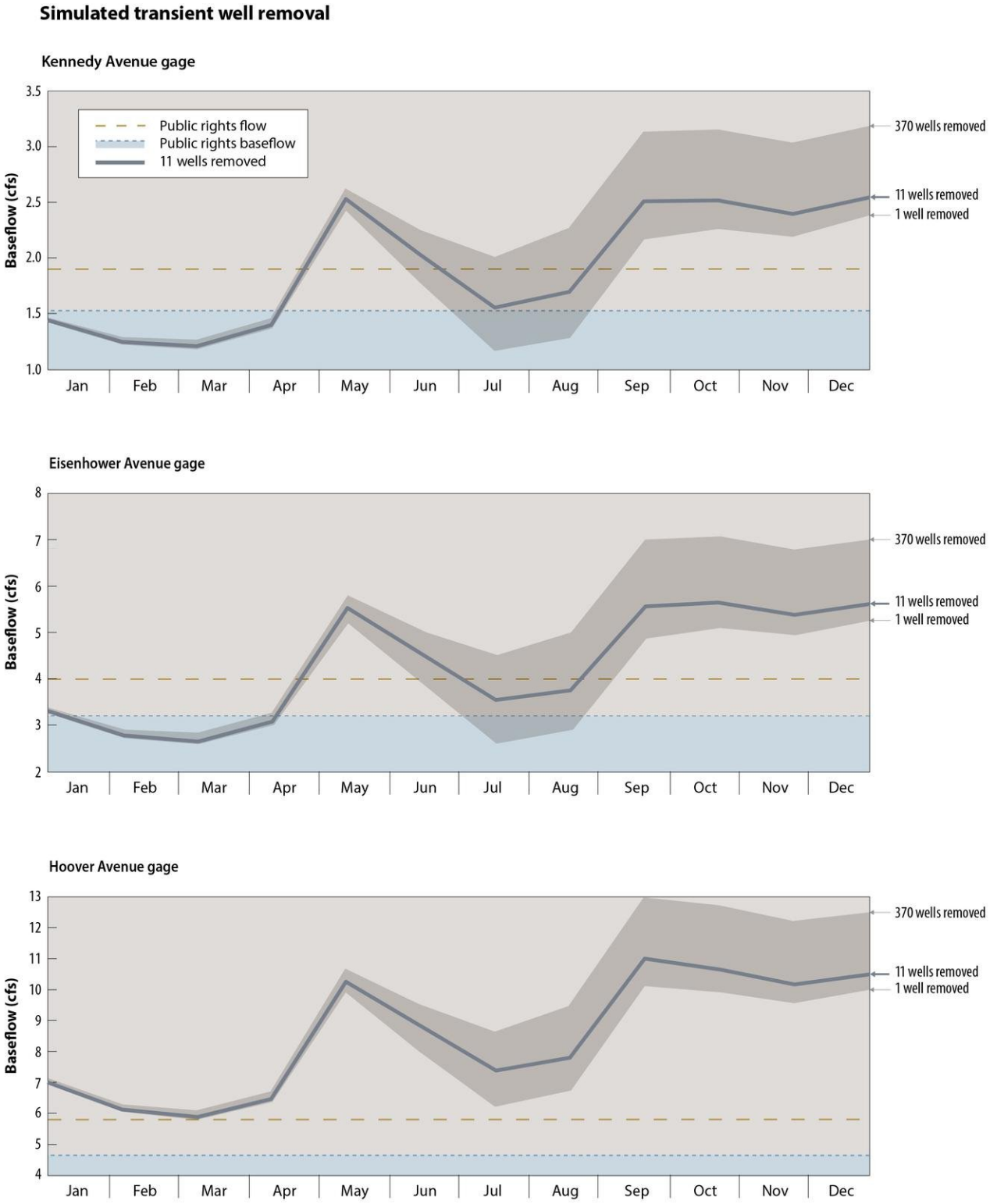

Figure 61. Transient simulation results for one-by-one well removal. The dark blue line (11 wells removed) marks the first time the river remains above public rights baseflow at all gage locations during July.

Summary and conclusions

Conclusions and significant findings

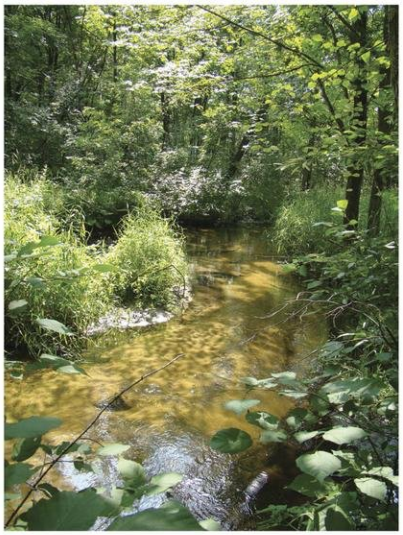

This project met the overall goals and objectives as stated in the purpose and scope of this report: developing a groundwater flow model for the Little Plover River basin in central Wisconsin. The Little Plover River model is an analytical tool that can be used for decision support for water management in the Little Plover River basin. The model can simulate a variety of water-use and land-use scenarios in both steady-state and transient conditions. The final model is publicly available for use in examining the interactions of groundwater and surface water in the model domain and for simulating various alternative land-use and climate scenarios. Analysis of specific future or historic issues is beyond the scope of this report, but the model is an appropriate tool for studying these issues.

Conclusions and significant findings from this work fall into two overlapping categories. Some conclusions are directly related to water-resource questions in the Little Plover River basin and surrounding model domain. Other conclusions are more general and relate to the application of these simulation approaches to other and larger parts of Wisconsin's Central Sands region.

Findings directly related to the Little Plover River and surrounding basin

1 Irrigation is the dominant water use in the model domain, with about 350 wells pumping 9,200 million gallons of water per year (mgy), or about 81 percent of the water used in the basin in 2013. During the three years simulated (2012, 2013, and 2014) using the SWB model, the estimated amount of irrigation that returned to recharge groundwater ranged from 10 to 21 percent. Almost all of this irrigation water use occurs during the summer growing season (June–August), and during this period, the total irrigation pumping in the model domain exceeds 100 million gallons per day (mgd).

2 Industrial water use in the model domain accounts for about 1,400 mgy, or about 12 percent of total water use. Municipal water supply (650 mgy) is the third largest water use, accounting for about 6 percent of total use. Water use by low-capacity domestic wells in the model domain is less than one percent of the use by high-capacity wells, and much of the domestic use returns to the system through septic tank return flow. The groundwater model does not include or simulate these low-capacity wells.

3 Reconstruction of streamflow records using a combination of measurements from the U.S. Geological Survey (USGS), Village of Plover, and UW-Stevens Point (UWSP) scientists has produced new hydrographs at stream gages at Kennedy Avenue and Eisenhower Avenue. For 2009 through 2014, streamflow at both these sites fell below long-term public rights flows established by the DNR during parts of five out of six years. Flow measurements by the USGS at the Eisenhower gage agree closely with measurements made at the same location by UW-Stevens Point personnel. This agreement during the period where the measurements overlap suggests that the longer-term UWSP measurements at this and other sites are a reliable representation of river flows during the UWSP gaging program, which started in 2005. Gaps in the data from all sources are related to the presence of ice and/or equipment malfunction.

4 Groundwater recharge varies with time and location over the model domain. During 2013, taken as a representative year, average steady-state recharge varied spatially from zero to 22 in/yr. Average soil-water-balance (SWB)-estimated recharge over the model domain varies from year to year, with estimates of 7.0 inches in a dry year (2012), 9.2 inches in a normal year (2013), and 12.5 inches in a wet year (2014). Calibration of the groundwater flow model to 2013 conditions required an upward adjustment of SWB-estimated recharge by about 8 percent; best-fit steady-state recharge in the groundwater flow model was 9.9 inches for 2013. Recharge varies significantly throughout the year, with little or no recharge in the winter months when the ground is frozen. Maximum recharge occurs during March and April following snow-

melt and prior to the major growing season, but the relative timing of recharge varies from year to year.

5 The calibrated groundwater flow model simulates hydraulic heads and stream discharges in the model domain similar to the observed values, and is a tool for understanding groundwater flow in and around the topographic basin of the Little Plover River and for simulating the impacts of changes in land use and pumping. The two model parameters with the highest identifiability—and therefore influence on the model—are the global recharge multiplier and the streambed hydraulic conductivity.

6 Model-simulated hydraulic head and water-table distributions in the Little Plover River basin are similar to maps produced by previous investigators, such as Clancy and others (2009) and Kraft and others (2012). Greatest groundwater inflow to the river occurs in the reach between Eisenhower and Hoover Avenues. The model-generated hydraulic heads and baseflow values serve as a basis of comparison to alternative management scenarios.

7 The Little Plover River is connected to the groundwater system, and as such, is vulnerable to impacts from nearby pumping. The impact of any particular well depends mainly on two factors: pumping rate of the well and distance from the river. Hydrogeologic conditions that control the impact are relatively constant in the area where wells are typically installed.

8 A typical high-capacity irrigation well in the Little Plover River basin creates a shallow (less than 5 feet of drawdown near the well) cone of depression, with a radius of approximately 1/2 mile under steady-state conditions. The transient simulations (using 2014 data) completed for this project show that for the same well, the cone of depression develops gradually during the pumping season, reaches a maximum comparable to or larger than the 2013 steady-state cone in late August, and diminishes in the fall as water levels recover. Due to variable pumping rates, transient simulations often produce more representative estimates of maximum drawdown than steady-state simulations for the recharge conditions simulated in the transient model.

9 Transient simulations show the effects of a time lag between changes in pumping rates at the well and pumping impacts to water levels and streamflows distant from the well. This time lag is predicted by theory and is related to aquifer hydraulic diffusivity. The lag is greater at greater distances from the well. The practical effect of this time lag is that maximum impacts to the groundwater-surface water system are not necessarily coincident with times of maximum pumping, and in fact, might lag by a month or more, depending on location. Likewise, the recovery of the streamflow after the cessation of pumping can require long times, often on the order of months.

10 Model simulations show that accounting for additional recharge due to the return of irrigation water (applied irrigation that does not evapotranspire or become incorporated in plant biomass) reduces, but does not eliminate, the effects of high-capacity wells on water levels and streamflows. Under steady-state (2013) conditions, a simulated hypothetical well 1 mile away from the river reduces river flows by 3.5 to 6.0 percent (depending on location), with no adjustment for irrigation return. When irrigation return is added to the model, the simulated river flows are reduced by 3.3 to 5.1 percent at the same locations. Under transient (2014) conditions, the flow reductions at the end of August are 3.9 to 6.6 percent with no recharge adjustment and 3.1 to 5.5 percent with adjustment for irrigation return.

11 The model, used in conjunction with a companion particle-tracking code, can delineate the land area contributing groundwater to the Little Plover River under different pumping and land-use scenarios. Comparison of simulations with and without pumping wells in the basin shows that the present-day contributing area is substantially smaller than the predevelopment contributing area. Groundwater discharge to the river is directly proportional to the area contributing groundwater, and this is consistent with the observations of diminished streamflow in recent years. A model simulation in which pumping is set to zero and recharge is adjusted to non-irrigated land use suggests that the cumulative effects of pumping and land-use change have reduced baseflow in the Little Plover River by up to 4.5 cfs at the Hoover Avenue gage.

12 Depletion-potential modeling shows that wells outside the footprint of the area contributing groundwater to the Little Plover River can impact streamflow. It is important to consider depletion potential—rather than area contributing groundwater (or "groundwatershed" or "capture area")—when determining which wells should be considered for changes in pumping to maintain specific streamflow goals.

13 Using depletion-potential mapping, the model suggests that removal of a minimum of 11 to 16 of the wells with the highest depletion potential (also nearest the river) would substantially increase baseflow in a typical year.

Findings relevant to simulation models and water management in the larger Central Sands region

1 The findings of this study are generally consistent with the findings of earlier researchers (Clancy and others, 2009; Kraft and others, 2012; Weeks and others, 1965; Weeks and Stangland, 1971) who documented or calculated the impacts of pumping on streamflow. The current study uses numerical simulation methods not available to all these previous investigators.

2 The soil-water-balance (SWB) recharge estimation method used in this report produces results that, when spatially averaged, are consistent with recharge estimates done by other methods. The SWB simulations appear to slightly underestimate steady and transient recharge needed to calibrate the groundwater flow model. The SWB approach provides insight into the range of variation of recharge across the landscape and through time. In particular, the SWB results demonstrate the seasonal nature of recharge and the value of transient simulations.

3 The concept of depletion potential, in which the model calculates the relative depletion of nearby surface-water features caused by each individual well, shows promise as a method for balancing water use with environmental needs. Using depletion potential as a guide, targeted reductions in pumping can achieve the desired stream flows with the fewest number of wells adjusted.

4 In addition to pumping rate and pumping schedule, in the Central Sands hydrogeologic setting, the most important control on impacts from an individual well, or group of wells, on surface-water features is the lateral distance between the well and the surface-water feature.

5 The water-management solutions demonstrated here provide a starting point for evaluation of specific scenarios informed by other conditions, such as land ownership or water transfer from one part of the basin to another.

6 The model calibration indicated that streambed conductance is an important calibration parameter for the Central Sands. This finding differs from the authors' experience in simulating groundwater flow in other regions of Wisconsin, where streambed conductance was not a sensitive parameter. The sensitivity in central Wisconsin likely occurs because the sandy aquifer and the sandy streambed have similar properties and the low-relief landscape causes hydraulic gradients near the stream to be small. Future simulations of other parts of central Wisconsin should treat streambed conductance as an important parameter, prioritizing field observations of streambed conductivity or simulating spatially variable streambed parameters.

7 Where model objectives include simulation of streamflow, obtaining field data on current and historical stream flows is essential. In addition, accurate field measurements of stream water-surface elevations, and streambed elevations taken in the stream channel are needed for proper model construction. We discovered that existing data sets, such as 7.5-minute topographic maps or available digital-elevation models, do not report stream elevations with enough precision for correct streamflow simulation, especially where the stream channel or drainage ditch is narrow and incised. This problem occurs because the low-relief topography in the Central Sands causes stream gradients to be small. Consequently, small errors in elevation can have large impacts on predicted streamflow and groundwater-surface water interaction.

8 The model grid spacing of 100 feet on a side is probably finer than needed for models of this region. The fine grid adds detail that is not needed for the model objectives, resulting in larger model files and longer run times than necessary for the numerical simulations. However, the fine grid allows very accurate location of individual wells and other model features, which may contribute to better acceptance of model results by stakeholders.

9 Stakeholder input, including crop data, pumping and irrigation information, water-level data, streamflow, and numerous personal insights about area geology and history, was critical to the success of this project.

Model uses and limitations

Every effort to make a model of a natural system is an approximation of that true system. In this section, we highlight the limitations of the modeling and analysis that we are aware of, and the uses of the model that are within these limitations.

1 The MODFLOW model and optimization work described in this report are specific to the Little Plover River watershed. The techniques established can be applied to other areas, but would require construction of models focused on these areas.

2 The model was designed to simulate the Little Plover River basin and is considered an accurate representation of that system. The remainder of the model domain serves as a buffer for the focused area of interest, and results there are approximate and not of sufficient accuracy for decision-making.

3 Determining input parameters for the soil-water-balance (SWB) model is challenging, given the large number of land-use/land-cover types and the parameters possible for each land-use type. Numerous parameters related to crop properties, soil properties, climate, and irrigation in SWB offset each other, and the SWB model can produce non-unique solutions. Accordingly, the water-budget components should be analyzed with discretion. Further analyses with specific focus on actual ET field investigations over different land-use types would improve this modeling technique. Investigating the sensitivity and uncertainty of SWB input parameters, as was conducted by Smith and Westenbroek (2015), may be a good first step in identifying where and how to focus future field investigations.

4 The groundwater-flow model calibration was limited to two years (2013 and 2014) based on the current availability of land-use and water-pumping data. Additional calibration, which was outside the scope of this project, would enhance the ability of the model to represent future unusually dry or wet years. However, the model framework can accommodate more detailed information on recharge (climate) and groundwater pumping, and land use to simulate particular years going forward.

5 The calibration process results in parameters estimated to be specific not only to the area of the Little Plover River basin, but also specific to the calibration process. Single values were used to represent storage parameters, and distributed fields of parameters represented the hydraulic conductivity parameters in the sands. Anderson and others (2015) point out the challenge of nonuniqueness when modeling physical systems. In other words, there are many combinations of parameter values that can provide the same level of agreement between the model and measured values. The calibration strategy adopted here is one that strives for the least complicated set of parameters that can adequately represent the system. Comparison with other models of the same area may identify minor differences among the estimated parameters, but in general, the model design, parameters, and outcomes are in line with other work.

6 The depletion-potential simulations were limited to removing wells from the model domain. Accompanying land-use changes—for example, the change of an irrigated field to grassland, forest, or a non-irrigated equivalent crop—would also influence the results. Both limitations in the method to calculate depletion and the lack of data associating specific wells with specific fields precluded including such land-use changes in the analyses presented here, but land-use change should be included more specifically in future simulations. This is an active area of research and software development going forward.

7 The MODFLOW model simulates stream baseflow. The public rights flow is a total streamflow value that includes both groundwater supplied baseflow and surface runoff (stormflow) not simulated by the model. As a result, the baseflow component of the public rights flow was used as the formal constraint for optimization and was presented in the well-removal scenarios. Other constraints could be used to prove the concept of using groundwater management to explore water-use scenarios that result in desirable streamflows.

Suggestions for future work

1 The simulation approaches described here, use of MODFLOW combined with the soil-water-balance (SWB) recharge code, are readily transferrable to model construction in the remainder of Wisconsin's Central Sands.

2 The recharge estimates arrived at with SWB and the MODFLOW model are reasonable, noting that the transient recharge was higher than previous studies because 2014 was a relatively wet year. However, there are few field measurements of recharge in the Central Sands. Research on field measurements of recharge of the type being undertaken by Hart and others (2016) and others should continue.

3 Future transient-model calibrations should address a variety of climatic conditions. The choice of a single year for transient calibration was largely governed by data availability at the time the calibration was being conducted. At that time, 2014 was the only year for which we had reliable transient-pumping data, transient-streamflow data, and transient-water-level data, and 2014 was a wetter-than-average year. Going forward, as more data become available, the model could be improved by additional transient calibration.

4 Measurements of groundwater discharge and water-level fluctuations are critical for successful and robust model calibration. Stakeholders should encourage additional collection of water levels in monitoring wells and baseflows in streams in the Central Sands region. Water-level measurement should include the development of nested piezometers, particularly in the southern Central Sands where the New Rome Formation potentially forms an aquitard (Hart and others, 2016). Water levels must be referenced to a common datum and collected throughout the year, preferably at least monthly.

5 If groundwater-model development moves to the southern Central Sands, there is a major data gap in western Waushara County, where no modern Quaternary maps currently exist. Wisconsin Geological and Natural History Survey geologists have begun mapping this area.

References

Ahlfeld, D.P., Barlow, P.M., Mulligan, A.E., 2005, GWM—A groundwater management process for the U.S. Geological Survey modular groundwater model (MODFLOW-2000): U.S. Geological Survey Open-File Report 2005-1072, 124 p.

Allen, R.G., Pereira, L.S., Raes, D., and Smith, M., 1998, Crop evapotranspiration guidelines for computing crop water requirements: Food and Agriculture Organization of the United Nations, Irrigation and Drainage Paper 56. 15 p.

Anderson, M.P., Woessner, W.W., and Hunt, R.J., 2015, Applied groundwater modeling, 2nd Edition: Amsterdam, Academic Press, 630 p.

Banta, E.R., and Ahlfeld, D.P., 2013, GWM-VI: Groundwater management with parallel processing for multiple MODFLOW versions: U.S. Geological Survey Techniques and Methods 6-A48, 33 p.

Bradbury, K.R., Faustini, J.M., and Stoertz, M.W., 1992, Groundwater flow systems and recharge in the Buena Vista basin, Portage and Wood Counties, Wisconsin: Wisconsin Geological and Natural History Survey Information Circular 72, 31 p.

Bradbury, K.R., Fehling, A.C., and Parsen, M.J., 2017, Groundwater flow model for the Little Plover River basin in Wisconsin's Central Sands—User's manual: Wisconsin Geological and Natural History Survey Bulletin 111-supplement, 30 p.

Bradbury, K.R., Kraft, G.J., Drought, J., Fienen, M.N., Hunt, R.J., and Hart, D.J., 2017, Groundwater quantity fundamentals in Wisconsin's Central Sands region: Prepared for the Wisconsin Food, Land, and Water Project Groundwater Quantity Work Group, 7 p.

Bradbury, K.R., and Muldoon, M.A., 1990, Hydraulic conductivity determinations in unlithified glacial and fluvial materials, in Nielsen, D.M., and Johnson, A.I., eds., Ground water and vadose zone monitoring: Philadelphia, American Society for Testing Materials, p. 138–151.

Bradbury, K.R., and Rothschild, E.R., 1985, A computerized technique for estimating the hydraulic conductivity of aquifers from specific capacity data: *Groundwater*, v. 23, no. 2, p. 240–246.

Bredehoeft, J.D., 2002, The water budget myth revisited: Why hydrogeologists model: *Groundwater*, v. 40, no. 4, p. 340–345.

Clancy, K., Kraft, G.J., and Mechenich, D.J., 2009, Knowledge development for groundwater withdrawal management around the Little Plover River, Portage County, Wisconsin: Center for Watershed Science and Education, College of Natural Resources, University of Wisconsin–Stevens Point/Extension, 47 p.

Clayton, L., 1986, Pleistocene geology of Portage County, Wisconsin: Wisconsin Geological and Natural History Survey Information Circular, 19 p.

Doherty, J., 2014, PEST, model-independent parameter estimation: User manual, 5th ed.: Brisbane, Australia, Watermark Numerical Computing.

Doherty, J.E., Fienen, M.N., and Hunt, R.J., 2010, Approaches to highly parameterized inversion: Pilot-point theory, guidelines, and research directions: U.S. Geological Survey Investigations Report 2010-5168, 36 p.

Dripps, W.R., and Bradbury, K.R., 2007, A simple daily soil-water-balance model for estimating the spatial and temporal distribution of groundwater recharge in temperate humid areas: *Hydrogeology Journal*, v. 15, no. 3, p. 433–444.

Enivironmental Simulations, Inc, 2011, Guide to using Groundwater Vistas: Leesport, Pa., ESI Inc., 213 p.

Faustini, J.M., 1985, Delineation of groundwater flow patterns in a portion of the central sand plain of Wisconsin: University of Wisconsin-Madison, M.S. thesis, 117 p.

Feinstein, D.T., Hunt, R.J., and Reeves, H.W., 2010, Regional groundwater-flow model of the Lake Michigan Basin in support of Great Lakes Basin water availability and use studies: U.S. Geological Survey Scientific Investigations Report 2010–5109, 379 p.

Fienen, M.N., Nolan, B.T., and Feinstein, D.T., 2016, Evaluating the sources of water to wells: Three techniques for metamodeling of a groundwater flow model: *Environmental Modelling and Software*, v. 77, p. 95–107.

Gebert, W.A., Walker, J.F., and Kennedy, J.L., 2011, Estimating 1970–99 average annual groundwater recharge in Wisconsin using streamflow data: U.S. Geological Survey Open-File Report 2009–1210, 118 p.

Harbaugh, A.W., 2005, MODFLOW-2005: The U.S. Geological Survey modular groundwater model—the groundwater flow process: U.S. Geological Survey Techniques and Methods 6-A16, variously p.

Hargreaves, G.H., and Samani, Z.A., 1985, Reference crop evapotranspiration from temperature: *Transaction of ASAE*, v. 1, no. 2, p. 96–99.

Hart, D.J., Streiff, C., and Kniffin, M., 2016, Estimating recharge in the Central Sands using water-table fluctuations [abs.]: Proceedings of the American Water Resources Association—Wisconsin Section, 40th Annual Meeting, Wisconsin Dells, Wis., p 49.

Henrich, E.W., and Daniel, D.N., 1983, Drainage-area data for Wisconsin streams: U.S. Geological Survey Open-File Report 83-933, 322 p.

Hill, M.C., and Tiedeman, C.R., 2007, Effective groundwater model calibration with analysis of data, sensitivities, predictions, and uncertainty: Hoboken, N.J., Wiley-Interscience, 455 p.

Holt, C.L.R., Jr., 1965, Geology and water resources of Portage County, Wisconsin: U.S. Geological Survey Water-Supply Paper 1796, 77 p.

Hsieh, P.A., and Winston, R.B., 2002, User's guide to Model Viewer, a program for three-dimensional visualization of groundwater model results: U.S. Geological Survey Open-File Report 02-106, 18 p.

Hunt, R.J., and Feinstein, D.T., 2012, MODFLOW-NWT: Robust handling of dry cells using a Newton Formulation of MODFLOW-2005: *Ground Water*, v. 50, no. 5, p. 659–663.

Illinois State Water Survey, 2015, 7-day, 10-year low flow maps: Illinois State Water Survey, www.isws.illinois.edu/docs/maps/lowflow/background.asp.

Jenkins, C.T., 1968a, Computation of rate and volume of stream depletion by wells: U.S. Geological Survey Techniques of Water-Resources Investigations 04-D1, 17 p.

Jenkins, C.T., 1968b, Techniques for computing rate and volume of stream depletion by wells: *Ground Water*, v. 6, no. 2, p. 37–46.

Karnauskas, R.J., 1977, The hydrogeology of the Nepco Lake watershed in central Wisconsin, with a discussion of management implications: University of Wisconsin-Madison, M.S. thesis, 249 p.

Kniffin, M., Potter, K.W., Bussan, A.J., Colquhoun, J., and Bradbury, K., 2014, Sustaining Central Sands water resources: State of the science 2014: University of Wisconsin–Extension, Cooperative Extension Publishing, G4058, 100 p.

Kraft, G.J., Clancy, K., Mechenich, D.J., and Haucke, J., 2012, Irrigation effects in the northern lake states: Wisconsin Central Sands revisited: *Ground Water*, v. 50, no. 2, p. 308–318.

Kraft, G.J., and Mechenich, D.J., 2010, Groundwater pumping effects on groundwater levels, lake levels, and streamflows in the Wisconsin Central Sands: Center for Watershed Science and Education, College of Natural Resources, University of Wisconsin–Stevens Point/Extension, 67 p.

Kraft, G.J., Mechenich, D.J., and Haucke, J., 2014, Information support for groundwater management in the Wisconsin Central Sands, 2011–2013: Center for Watershed Science and Education, College of Natural Resources, University of Wisconsin–Stevens Point/Extension, 60 p. plus appendices.

Kucharik, C.J., Serbin, S.P., Vavrus, S., Hopkins, E.J., and Motew, M.M., 2010, Patterns of climate change across Wisconsin from 1950 to 2006: Physical Geography, v. 31, no. 1, p. 1–28.

McKay, L., Bondelid, T., Dewald, T., Johnston, J., Moore, R., and Rea, A., 2012, NHDPlus version 2—User guide: U.S. Environmental Protection Agency, 181 p.

Motew, M.M., and Kucharik, C.J., 2013, Climate-induced changes in biome distribution, NPP, and hydrology in the Upper Midwest U.S.: A case study for potential vegetation: Journal of Geophysical Research: Biogeosciences, v. 118, no. 1, p. 248–264.

Mueller, D.S., Wagner, C., Rehmel, M.S., Oberg, K.A., and Rainville, F., 2013, Measuring discharge with acoustic Doppler current profilers from a moving boat: U.S. Geological Survey Techniques and Methods 3-A22, 72 p.

Naber, M.R., 2011, One-dimensional soil-plant-atmosphere modeling of the Wisconsin Central Sand Plain to estimate evapotranspiration and groundwater recharge under different vegetation types: University of Wisconsin-Madison, M.S. thesis, 58 p.

Niswonger, R.G., Panday, S., and Ibaraki, M., 2011, MODFLOW-NWT, a Newton formulation for MODFLOW-2005: US Geological Survey Techniques and Methods 6–A37, 44 p.

Niswonger, R.G., and Prudic, D.E., 2005, Documentation of the streamflow-routing (SFR2) package to include unsaturated flow beneath streams—a modification to SFR1: U.S. Geological Survey Techniques and Methods 6–A13, 50 p.

Pollock, D.W., 2012, User guide for MODPATH version 6—A particle-tracking model for MODFLOW, U.S. Geological Survey Techniques and Methods 6–A41, 58 p.

Prudic, D.E., Konikow, L.F., and Banta, E.R., 2004, A new streamflow-routing (SFR1) package to simulate stream-aquifer Interaction with MODFLOW-2000: U.S. Geological Survey Open-File Report 2004-1042, 95 p.

Smith, E.A., and Westenbroek, S.M., 2015, Potential groundwater recharge for the State of Minnesota using the Soil-Water-Balance model, 1996–2010: U.S. Geological Survey Scientific Investigations Report 2015–5038, 85 p.

Thornthwaite, C.W., and Mather, J.R., 1957, Instructions and table for computing potential evapotranspiration and the water balance: Centerton, N.J., Laboratory of Climatology, Publications in Climatology, v. 10, no. 3, p 185–311.

Turnipseed, D.P., and Sauer, V.B., 2010, Discharge measurements at gaging stations: U.S. Geological Survey Techniques and Methods book 3, chap. A8, 87 p.

Water Science and Technology Board, 2004, Assessing the national streamflow information program: Washington, D.C., National Academies Press, 160 p.

Weeks, E.P., 1969, Determining the ratio of horizontal to vertical permeability by aquifer-test analysis: Water Resources Research, v. 5, no. 1, p. 196–214.

Weeks, E.P., Ericson, D.W., and Holt, C.L.R., Jr., 1965, Hydrology of the Little Plover River basin Portage County, Wisconsin, and the effects of water resource development: U.S. Geological Survey Water-Supply Paper 1811, 76 p.

Weeks, E.P., and Stangland, H.G., 1971, Effects of irrigation on streamflow in the central sand plain of Wisconsin: U.S. Geological Survey Open-File Report 70-362, 113 p.

Westenbroek, S.M., Doherty, J., Walker, J.F., Kelson, V. A., Hunt, R., and Cera, T.B., 2012, Approaches in highly parameterized inversion: TSPROC, a general time-series processor to assist in model calibration and result summarization: U.S. Geological Survey Techniques and Methods 7-C7, 101 p.

Westenbroek, S.M., Kelson, V.A., Dripps, W.R., Hunt, R.J., and Bradbury, K.R., 2010, SWB—A modified Thornthwaite-Mather soil-water-balance code for estimating groundwater recharge: U.S. Geological Survey Techniques and Methods 6-A31, 60 p.

Published by and available from:

Wisconsin Geological and Natural History Survey

3817 Mineral Point Road ▪ Madison, Wisconsin 53705-5100
608.263.7389 ▪ www.WisconsinGeologicalSurvey.org
Kenneth R. Bradbury, Director and State Geologist

ISSN: 0375-8265
ISBN: 978-0-88169-986-9

UW Extension
University of Wisconsin-Extension

Our Mission

The Survey conducts earth-science surveys, field studies, and research. We provide objective scientific information about the geology, mineral resources, water resources, soil, and biology of Wisconsin. We collect, interpret, disseminate, and archive natural resource information. We communicate the results of our activities through publications, technical talks, and responses to inquiries from the public. These activities support informed decision making by government, industry, business, and individual citizens of Wisconsin.

Appendix 1. Geographic Data for Download

This appendix can be downloaded at https://wgnhs.uwex.edu/pubs/b111/.

Appendix 2. Supplemental recharge data

This appendix contains supplemental data and results from the Soil Water Balance (SWB) model.

A. Land use inputs
B. Irrigation inputs
C. Parameter references
D. SWB results (2012–2014)—*annual precipitation, recharge, actual evapotranspiration, and irrigation spatially averaged over the model domain*
E. SWB results (2012–2014)—*annual recharge, actual evapotranspiration, and irrigation, spatially averaged over irrigated and nonirrigated areas*
F. SWB results, no irrigation (2012–2014)—*annual recharge and actual evapotranspiration spatially averaged over areas originally designated as irrigated and nonirrigated in the model domain*
G. SWB results—annual land use (2012–2014)
H. SWB results—monthly recharge (2012, 2014)
I. SWB results—monthly outputs (2012–2014)
References

Appendix 2A. Supplemental recharge data: LAND-USE INPUTS

			National Resource Conservation							Maximum infiltration rates (in/day)							Interception storage		Depth of root zone (ft)						
Land use code	Description	Assumed impervious area	Soil A	Soil B	Soil C	Soil D	Soil A/D	Soil B/D	Null	Soil A	Soil B	Soil C	Soil D	Soil A/D	Soil B/D	Null	Growing Season	Not growing season	Soil A	Soil B	Soil C	Soil D	Soil A/D	Soil B/D	Null
141	Deciduous Forest	0	30	55	70	77	30	77	100	4	0.6	0.2	0.1	4	0.1	0.1	0.05	0	3.12	2.50	2.50	2.00	3.12	2.00	0
1	Field corn	0	65	75	82	86	65	86	100	4	0.6	0.2	0.1	4	0.1	0.1	0	0	2.00	2.00	2.00	2.00	2.00	2.00	0
36	Alfalfa	0	30	58	71	78	30	78	100	4	0.6	0.2	0.1	4	0.1	0.1	0	0	2.25	2.25	2.25	2.25	2.25	2.25	0
121	Developed / Open	0	49	69	79	84	49	84	100	4	0.6	0.2	0.1	4	0.1	0.1	0	0	2.50	2.50	2.50	2.50	2.50	2.50	0
176	Grass / Pasture	0	39	61	74	80	39	80	100	4	0.6	0.2	0.1	4	0.1	0.1	0	0	2.50	2.50	3.13	2.50	2.50	2.50	0
12	Sweet corn	0	65	75	82	86	65	86	100	4	0.6	0.2	0.1	4	0.1	0.1	0	0	1.88	1.88	1.88	1.88	1.88	1.88	0
43	Potatoes	0	67	78	85	89	67	89	100	4	0.6	0.2	0.1	4	0.1	0.1	0	0	1.00	1.00	1.00	1.00	1.00	1.00	0
122	Developed/Low	0.65	67	78	85	89	67	89	100	4	0.6	0.2	0.1	4	0.1	0.1	0	0	1.50	1.50	1.50	1.50	1.50	1.50	0
42	Snap beans	0	67	78	85	89	67	89	100	4	0.6	0.2	0.1	4	0.1	0.1	0	0	1.50	1.50	1.50	1.50	1.50	1.50	0
190	Woody wetlands	0	30	48	65	73	30	73	100	4	0.6	0.2	0.1	4	0.1	0.1	0	0	3.38	3.38	3.38	3.38	3.38	3.38	0
142	Evergeen	0	30	55	70	77	30	77	100	4	0.6	0.2	0.1	4	0.1	0.1	0.1	0.1	1.56	1.25	1.25	1.00	1.56	1.00	0
5	Soybeans	0	67	78	85	89	67	89	100	4	0.6	0.2	0.1	4	0.1	0.1	0	0	1.88	1.88	1.88	1.88	1.88	1.88	0
37	Non-alfalfa hay	0	30	58	71	78	30	78	100	4	0.6	0.2	0.1	4	0.1	0.1	0	0	2.50	2.50	3.13	2.50	2.50	2.50	0
53	Peas	0	67	78	85	89	67	89	100	4	0.6	0.2	0.1	4	0.1	0.1	0	0	1.50	1.50	1.50	1.50	1.50	1.50	0
111	Open water	not applicable	100	100	100	100	100	100	100	4	0.6	0.2	0.1	4	0.1	0.1	0	0	0.00	0.00	0.00	0.00	0.00	0.00	0
123	Development -	0.75	77	85	90	92	77	92	100	4	0.6	0.2	0.1	4	0.1	0.1	0	0	1.50	1.50	1.50	1.50	1.50	1.50	0
143	Mixed forest	0	30	55	70	77	30	77	100	4	0.6	0.2	0.1	4	0.1	0.1	0.06	0.03	3.12	2.50	2.50	2.00	3.12	2.00	0
195	Herbaceous wetlands	0	30	58	71	78	30	78	100	4	0.6	0.2	0.1	4	0.1	0.1	0	0	3.38	3.38	3.38	3.38	3.38	3.38	0

Appendix 2B. Supplemental recharge data: IRRIGATION INPUTS

			Crop Coefficients (Kcb) per crop development stage					Length of growth stages				Measures of growth	Readily available water (inches)						
Land use code	Description	Maximum crop height (ft)	initial	mid	late	min	Planting date	Initial (days)	Development (days)	Mid (days)	Late (days)	('Day of Year' - DOY - or 'Growing Degree Days' -	Soil A	Soil B	Soil C	Soil D	Soil A/D	Soil B/D	Null
141	Deciduous Forest	32.8	0.45	1.15	0.9	0.45	30-Mar	20	70	90	30	DOY	0.196	0.295	0.393	0.472	0.196	0.472	0.472
1	Field corn	8	0.2	0.96	0.6	0.2	1-May	20	50	40	30	DOY	0.196	0.295	0.393	0.472	0.196	0.472	0.472
36	Alfalfa	2.296	0.4	0.95	0.9	0.4	15-Apr	10	30	90	30	DOY	0.196	0.295	0.393	0.472	0.196	0.472	0.472
121	Developed / Open Space	5	0.3	1	0.8	0.15	30-Mar	20	70	90	30	DOY	0.196	0.295	0.393	0.472	0.196	0.472	0.472
176	Grass / Pasture	0.492	0.4	0.85	0.85	0.3	15-Apr	10	30	35	35	DOY	0.196	0.295	0.393	0.472	0.196	0.472	0.472
12	Sweet corn	6	0.2	0.96	0.6	0.2	5-May	20	50	40	20	DOY	0.196	0.295	0.393	0.472	0.196	0.472	0.472
43	Potatoes	1.968	0.2	0.9	1.05	0.2	10-May	20	70	30	10	DOY	0.196	0.295	0.393	0.472	0.196	0.472	0.472
122	Developed/Low Intensity	5	0.3	1	0.8	0.15	30-Mar	20	70	90	30	DOY	0.196	0.295	0.393	0.472	0.196	0.472	0.472
42	Snap beans	1.312	0.5	1.05	0.95	0.5	20-May	20	30	40	20	DOY	0.196	0.295	0.393	0.472	0.196	0.472	0.472
190	Woody wetlands	3.28	0.3	1.2	0.3	0.3	1-May	10	30	80	20	DOY	0.196	0.295	0.393	0.472	0.196	0.472	0.472
142	Evergeen	32.8	0.45	1.15	0.9	0.45	30-Mar	20	70	90	30	DOY	0.196	0.295	0.393	0.472	0.196	0.472	0.472
5	Soybeans	2.75	0.2	1.05	0.3	0.2	20-May	20	30	60	25	DOY	0.196	0.295	0.393	0.472	0.196	0.472	0.472
37	Non-alfalfa hay	1.968	0.4	0.9	0.85	0.4	1-May	10	30	25	10	DOY	0.196	0.295	0.393	0.472	0.196	0.472	0.472
53	Peas	1.64	0.5	1.15	0.3	0.15	15-Apr	35	25	30	20	DOY	0.196	0.295	0.393	0.472	0.196	0.472	0.472
111	Open water	1	0.15	1.05	1.05	0.15	30-Mar	20	70	90	30	DOY	0.196	0.295	0.393	0.472	0.196	0.472	0.472
123	Development - medium intensity	5	0.3	1	0.8	0.15	30-Mar	20	70	90	30	DOY	0.196	0.295	0.393	0.472	0.196	0.472	0.472
143	Mixed forest	26.24	0.6	1	0.9	0.6	30-Mar	20	70	90	30	DOY	0.196	0.295	0.393	0.472	0.196	0.472	0.472
195	Herbaceous wetlands	3.28	0.3	1.2	0.3	0.3	1-May	10	30	80	20	DOY	0.196	0.295	0.393	0.472	0.196	0.472	0.472

				Total evaporable water (inches)												
Soil A	Soil B	Soil C	Soil D	Soil A/D	Soil B/D	Null	Plant Stress Depletion Fraction	Growing degree day temperature (F) - base	Growing degree day temperature (F) - max	Maximum allowable depletion	Irrigation start date	Irrigation end date	Irrigation amount per application (inches)	Fraction of irrigation from groundwater	Fractional irrigation efficiency (GW)	Fractional irrigation efficiency (SW)
0.354	0.669	0.906	1.063	0.354	1.063	1.063	0.5	50	130	1	15-Jun	1-Sep	0	1	1	1
0.354	0.669	0.906	1.063	0.354	1.063	1.063	0.55	50	130	0.5	15-Jun	10-Sep	0.5	1	1	1
0.354	0.669	0.906	1.063	0.354	1.063	1.063	0.6	50	130	0.6	1-Apr	1-Sep	0.2	1	1	1
0.354	0.669	0.906	1.063	0.354	1.063	1.063	0.1	50	130	1	15-Jun	1-Sep	0	1	1	1
0.354	0.669	0.906	1.063	0.354	1.063	1.063	0.55	50	130	1	15-Jun	1-Sep	0	1	1	1
0.354	0.669	0.906	1.063	0.354	1.063	1.063	0.55	50	130	0.5	15-Jun	1-Sep	0.5	1	1	1
0.354	0.669	0.906	1.063	0.354	1.063	1.063	0.45	50	130	0.55	15-Jun	1-Sep	0.5	1	1	1
0.354	0.669	0.906	1.063	0.354	1.063	1.063	0.5	50	130	1	15-Jun	1-Sep	0	1	1	1
0.354	0.669	0.906	1.063	0.354	1.063	1.063	0.45	50	130	0.55	15-Jun	1-Sep	0.5	1	1	1
0.354	0.669	0.906	1.063	0.354	1.063	1.063	0.6	50	130	1	15-Jun	1-Sep	0	1	1	1
0.354	0.669	0.906	1.063	0.354	1.063	1.063	0.7	50	130	1	15-Jun	1-Sep	0	1	1	1
0.354	0.669	0.906	1.063	0.354	1.063	1.063	0.5	50	130	0.5	1-Aug	10-Sep	0.5	1	1	1
0.354	0.669	0.906	1.063	0.354	1.063	1.063	0.55	50	130	0.55	15-Jun	1-Sep	0.5	1	1	1
0.354	0.669	0.906	1.063	0.354	1.063	1.063	0.35	50	130	0.35	15-Jun	1-Sep	0.5	1	1	1
0.354	0.669	0.906	1.063	0.354	1.063	1.063	0.99	50	130	1	15-Jun	1-Sep	0	1	1	1
0.354	0.669	0.906	1.063	0.354	1.063	1.063	0.5	50	130	1	15-Jun	1-Sep	0	1	1	1
0.354	0.669	0.906	1.063	0.354	1.063	1.063	0.6	50	130	1	15-Jun	1-Sep	0	1	1	1
0.354	0.669	0.906	1.063	0.354	1.063	1.063	0.5	50	130	1	15-Jun	1-Sep	0	1	1	1

Appendix 2C. Supplemental recharge data: PARAMETER REFERENCES

Soil, land use and irrigation parameters	References
Curve numbers, maximum infiltration rates	USDA, NRCS, 2004, 1986; Thornthwaite and Mather, 1957; Hart and others, 2016
Interception storage	Thornthwaite and Mather, 1957
Depth of root zone	Bussan, 2015; DeByle, 1957; Thornthwaite and Mather, 1957; Allen and others, 1998; Jackson and others, 1996; Crow, 2005
Maximum crop height	Allen and others, 1998; Bussan, 2015; Wullschleger and others, 1998
Crop coefficient (Kcb)	Allen and others, 1998; USDA SCS, 1955
Planting dates, crop growth stages	Allen and others, 1998; Bussan, 2015; Wisconsin Potato and Vegetable Grower Association - Water Task Force, 2014-2015, personal communication
Readily evaporable water (REW), total evaporable water (TEW)	Allen and others, 1998; USDA SCS, 1955
Maximum allowable depletion, irrigation start/end dates, amount per application, fractional efficiency	Allen and others, 1998; USDA SCS, 1955, Wisconsin Potato and Vegetable Grower Association - Water Task Force, 2014-2015, personal communication

Appendix 2D. Supplemental recharge data: ANNUAL RESULTS (2012-2014)— precipitation, recharge, actual ET, irrigation

Results spatially averaged over the model domain

		Uncalibrated SWB Results					Calibrated SWB Results
Var	Year	Min (inches / year)	Mean (inches / year)	Median (inches/ year)	Max (inches/ year)	Standard Deviation (inches/ year)	Mean (inches/year)
Precipitation	2012	27.92	27.92	27.92	27.92	0.0	
Recharge	2012	0.0	7.0	6.5	44.1	3.2	-
Actual ET	2012	0.0	21.8	21.3	33.2	4.4	-
Irrigation	2012	0.0	2.8	0.0	40.0	5.0	-
Precipitation	2013	31.5	31.5	31.5	31.5	0.0	
Recharge	2013	0.0	9.2	9.5	44.4	3.3	9.9
Actual ET	2013	0.0	23.7	24.0	34.1	3.7	-
Irrigation	2013	0.0	2.2	0.0	36.3	4.0	-
Precipitation	2014	36.5	36.5	36.5	36.5	0.0	
Recharge	2014	0.0	12.5	12.6	49.7	4.5	14.8
Actual ET	2014	0.0	25.2	25.7	34.1	3.8	-
Irrigation	2014	0.0	1.8	0.0	30.0	3.3	-

Appendix 2E. Supplemental recharge data: SWB RESULTS FOR IRRIGATED AND NONIRRIGATED AREAS (2012–2014)

Results spatially averaged over the model domain

Var	Year	Uncalibrated SWB Results	
		Irrigated areas (in/yr)	Nonirrigated areas (in/yr)
Recharge	2012	9.6	6.1
Actual ET	2012	27.3	19.9
Irrigation	2012	10.8	0.0
Recharge	2013	12.5	8.1
Actual ET	2013	26.8	22.6
Irrigation	2013	8.5	0.0
Recharge	2014	16.4	11.2
Actual ET	2014	26.7	24.6
Irrigation	2014	7.0	0.0

Appendix 2F. Supplemental recharge data: SWB RESULTS FOR NONIRRIGATED AREAS (2012–2014)—annual recharge and actual evapotranspiration for comparison

Results spatially averaged over areas originally designated as irrigated and nonirrigated in the model domain

This table shows the results from running SWB without irrigation and all other parameters held constant. Comparing this simulation to the original simulation gives the amount of recharge due to irrigation alone (compare to Appendix 2e). No irrigation was applied for the model simulation with summarized results below.

Var	Year	Irrigated area*	Nonirrigated area*
		inches/year	inches/year
Recharge	2012	8.5	6.1
Actual ET	2012	17.7	19.9
Recharge	2013	11.3	8.0
Actual ET	2013	19.7	22.6
Recharge	2014	15.2	11.2
Actual ET	2014	21.1	24.6

*As delineated in the original model run. See figure 20 for "irrigated" and "nonirrigated" areas within the model doma

Appendix 2G. Supplemental recharge data: SWB ANNUAL RESULTS, UNCALIBRATED (2012–2014)—recharge, irrigation, actual evapotranspiration by top vegetation types in model domain

		Annual Recharge - 2012					Annual Irrigation - 2012				
Code	Type	Min (in/yr)	Mean (in/yr)	Median (in/yr)	Max (in/yr)	std (in/yr)	Min (in/yr)	Mean (in/yr)	Median (in/yr)	Max (in/yr)	std (in/yr)
141	Deciduous forest	0.0	4.8	4.6	25.2	2.0	0.0	0.0	0.0	15.5	0.7
1	Corn	0.0	7.1	6.3	25.2	2.2	0.0	0.7	0.0	15.5	2.6
36	Alfalfa	0.0	6.6	6.2	25.2	1.7	0.0	0.2	0.0	15.5	1.7
176	Grass/pasture	0.0	7.4	6.5	25.2	2.3	0.0	0.1	0.0	15.5	1.3
991	Irrigated corn	0.0	8.6	7.3	25.2	2.5	0.0	10.0	10.5	15.5	1.8
9943	Irrigated potatoes	1.3	10.7	11.5	25.2	3.1	0.0	12.0	13.0	15.5	2.7
121	Developed open space	0.0	7.4	8.2	25.2	2.2	0.0	0.3	0.0	15.0	1.7
9912	Irrigated sweet corn	1.7	9.7	10.4	25.2	2.4	0.0	9.9	10.0	15.5	1.5
190	Woody wetlands	0.0	4.6	4.3	25.2	2.6	0.0	0.0	0.0	12.8	0.3
122	Developed - low intensity	0.0	8.4	8.9	25.2	1.9	0.0	0.2	0.0	15.5	1.4
9942	Irrigated snap beans	2.6	9.8	10.0	25.2	2.3	0.0	10.7	10.5	15.5	1.7
142	Evergreen forest	0.0	4.8	4.7	25.2	1.9	0.0	0.0	0.0	15.0	0.7
9936	Irrigated alfalfa	1.8	7.6	6.7	24.4	2.0	0.0	11.7	12.2	15.5	2.4
37	Non-alfalfa hay	0.0	7.2	6.7	25.2	2.2	0.0	0.1	0.0	15.0	1.2
195	Herbaceous wetlands	0.0	5.5	5.3	25.2	3.4	0.0	0.1	0.0	15.0	1.0
5	Soybeans	0.0	7.3	6.3	25.2	2.2	0.0	0.6	0.0	15.5	2.2
42	Snap beans	1.3	8.7	9.1	25.2	2.5	0.0	2.0	0.0	15.0	4.3
12	Sweet corn	1.7	8.7	8.4	24.6	2.4	0.0	2.4	0.0	15.0	4.4
995	Irrigated soybeans	2.0	8.4	7.6	25.2	2.5	0.0	5.9	5.0	15.5	2.3
111	Open water	0.0	0.8	0.0	25.2	3.1	0.0	0.0	0.0	12.0	0.4
123	Developed medium intensity	0.0	8.5	8.8	25.2	2.2	0.0	0.0	0.0	11.5	0.5
9953	Irrigated peas	1.6	8.3	6.7	25.2	2.8	0.0	11.8	13.0	15.5	2.6
143	Mixed forest	0.0	5.1	4.9	25.2	2.1	0.0	0.0	0.0	13.0	0.6

Annual Actual Evapotranspiration - 2012					Annual Recharge - 2013				
Min (in/yr)	Mean (in/yr)	Median (in/yr)	Max (in/yr)	std (in/yr)	Min (in/yr)	Mean (in/yr)	Median (in/yr)	Max (in/yr)	std (in/yr)
0.0	21.6	21.6	33.2	2.0	0.0	6.7	7.0	23.5	1.8
0.0	19.2	18.7	33.2	2.5	0.0	10.1	10.1	23.5	1.6
0.0	19.8	19.7	33.2	1.8	0.0	8.5	8.3	23.5	1.2
0.0	18.9	18.3	33.2	2.2	0.0	9.3	9.6	23.5	1.8
0.0	27.2	27.9	33.2	1.7	0.0	11.4	11.4	23.5	1.5
15.7	27.4	26.4	33.2	2.8	2.6	14.4	14.2	23.5	2.1
0.0	19.4	18.9	33.2	2.3	0.0	9.2	9.6	23.5	1.9
16.5	26.4	25.5	33.2	1.6	2.9	12.3	12.2	23.5	1.5
0.0	21.8	21.9	33.2	3.9	0.0	6.3	6.6	23.5	2.6
0.0	18.5	18.2	32.8	1.8	0.0	9.7	10.2	23.5	1.5
16.5	27.2	26.9	33.2	1.6	2.8	12.7	12.7	22.4	1.5
0.0	22.0	22.3	33.2	2.2	0.0	4.7	3.7	23.5	2.4
16.9	30.4	31.4	33.2	2.4	2.9	9.2	8.8	22.4	1.7
0.0	18.9	18.3	32.9	2.1	0.0	9.4	9.8	23.5	1.8
0.0	19.6	20.6	33.2	6.1	0.0	7.2	7.3	23.5	3.4
0.0	19.0	18.9	33.2	2.3	0.0	10.2	10.0	23.5	1.6
14.8	19.5	18.4	31.8	3.9	2.5	11.3	11.6	23.5	1.8
15.5	19.8	18.3	33.0	4.1	2.7	11.4	11.6	18.1	1.6
16.7	23.6	23.3	33.2	2.2	3.5	11.1	11.0	22.8	1.7
0.0	2.5	0.0	33.2	7.3	0.0	1.0	0.0	23.5	3.6
0.0	18.3	18.1	29.2	1.3	0.0	9.7	9.7	23.5	1.8
17.0	29.2	31.3	33.2	3.0	2.8	11.6	11.0	23.5	1.9
0.0	21.3	21.4	29.9	2.5	0.0	6.5	7.0	23.5	2.2

Annual Irrigation - 2013					Annual Actual Evapotranspiration - 2013				
Min (in/yr)	Mean (in/yr)	Median (in/yr)	Max (in/yr)	std (in/yr)	Min (in/yr)	Mean (in/yr)	Median (in/yr)	Max (in/yr)	std (in/yr)
0.0	0.0	0.0	14.0	0.5	0.0	24.3	24.1	33.3	2.0
0.0	0.5	0.0	14.0	2.0	0.0	21.2	20.8	33.3	2.0
0.0	0.1	0.0	14.0	1.0	0.0	22.6	22.7	33.3	1.3
0.0	0.1	0.0	14.0	1.0	0.0	21.7	21.2	33.3	2.1
0.0	7.5	7.5	14.0	1.9	0.0	27.1	27.7	33.3	1.8
0.0	10.3	11.0	14.0	2.8	17.5	26.8	25.7	33.3	2.7
0.0	0.2	0.0	14.0	1.4	0.0	22.0	21.5	33.3	2.2
0.0	7.2	7.5	14.0	1.9	18.6	25.9	25.2	33.3	1.7
0.0	0.0	0.0	10.5	0.2	0.0	24.3	24.3	33.3	4.0
0.0	0.1	0.0	14.0	1.1	0.0	21.4	21.2	33.3	1.6
0.0	8.5	9.0	14.0	1.6	18.7	26.8	26.3	33.3	1.5
0.0	0.0	0.0	14.0	0.6	0.0	26.8	28.1	33.3	3.1
0.0	5.9	5.6	14.0	1.8	20.1	27.7	28.2	33.3	1.4
0.0	0.1	0.0	14.0	0.9	0.0	21.6	21.1	33.3	2.0
0.0	0.1	0.0	14.0	0.8	0.0	22.0	23.7	33.3	6.6
0.0	0.5	0.0	14.0	1.8	0.0	21.1	21.0	33.2	2.0
0.0	1.6	0.0	14.0	3.4	15.7	21.3	20.6	31.5	3.0
0.0	1.8	0.0	14.0	3.4	17.4	21.3	20.5	32.7	3.1
0.0	5.9	5.5	13.0	1.5	19.0	25.7	26.1	33.2	1.5
0.0	0.0	0.0	10.5	0.3	0.0	2.8	0.0	33.3	8.0
0.0	0.0	0.0	9.5	0.4	0.0	21.3	21.3	33.0	1.4
0.0	10.2	11.5	14.0	2.7	20.2	29.4	31.5	33.3	2.9
0.0	0.0	0.0	11.5	0.5	0.0	24.4	24.1	33.3	2.9

Annual Recharge - 2014					Annual Irrigation - 2014				
Min (in/yr)	Mean (in/yr)	Median (in/yr)	Max (in/yr)	std (in/yr)	Min (in/yr)	Mean (in/yr)	Median (in/yr)	Max (in/yr)	std (in/yr)
0.0	8.9	9.0	39.3	3.0	0.0	0.0	0.0	12.0	0.5
0.0	13.5	12.7	39.3	2.8	0.0	0.4	0.0	12.0	1.6
0.0	12.2	11.6	39.3	2.2	0.0	0.1	0.0	12.0	1.0
0.0	13.4	12.9	39.3	3.3	0.0	0.1	0.0	12.0	0.8
0.0	15.3	13.8	39.3	3.0	0.0	5.8	6.0	12.0	1.4
3.4	17.8	18.5	39.3	3.6	0.0	8.7	9.0	12.0	2.7
0.0	13.4	14.7	39.3	3.2	0.0	0.2	0.0	12.0	1.1
4.1	16.6	17.6	39.3	2.9	0.0	6.0	5.5	12.0	1.5
0.0	8.6	8.4	39.3	4.1	0.0	0.0	0.0	9.0	0.2
0.0	14.6	15.5	39.3	2.5	0.0	0.1	0.0	12.0	1.0
4.2	16.4	17.3	39.3	2.8	0.0	7.1	7.0	12.0	1.4
0.0	7.5	7.1	39.3	3.3	0.0	0.0	0.0	12.0	0.5
3.1	14.0	13.0	37.6	2.5	0.0	6.3	6.8	12.0	1.6
0.0	13.3	12.7	39.3	3.1	0.0	0.1	0.0	12.0	0.7
0.0	10.1	10.4	39.3	5.4	0.0	0.1	0.0	12.0	0.6
0.0	13.6	12.6	39.3	2.9	0.0	0.3	0.0	12.0	1.4
3.0	15.3	16.0	39.3	3.0	0.0	1.3	0.0	12.0	2.8
3.8	15.4	15.5	39.3	2.8	0.0	1.5	0.0	12.0	2.8
4.3	15.0	14.0	39.3	3.2	0.0	3.4	3.0	12.0	1.6
0.0	1.4	0.0	39.3	5.2	0.0	0.0	0.0	8.0	0.2
0.0	14.7	15.0	39.3	2.9	0.0	0.0	0.0	8.0	0.3
3.9	14.8	13.1	39.3	3.2	0.0	9.3	10.5	12.0	2.3
0.0	9.1	9.1	39.3	3.3	0.0	0.0	0.0	10.0	0.4

Annual Actual Evapotranspiration - 2014				
Min (in/yr)	Mean (in/yr)	Median (in/yr)	Max (in/yr)	std (in/yr)
0.0	27.4	27.6	34.1	2.3
0.0	22.6	22.4	34.1	1.9
0.0	24.2	24.4	34.1	1.6
0.0	23.0	22.2	34.1	2.8
0.0	26.4	27.2	34.1	1.4
19.2	27.2	26.2	33.8	2.4
0.0	23.4	22.9	34.1	2.7
19.6	25.8	25.1	32.9	1.5
0.0	26.5	26.8	34.1	4.3
0.0	22.6	22.3	34.1	1.9
19.6	26.9	26.8	34.1	1.2
0.0	28.6	29.2	34.1	3.3
20.0	28.7	29.5	33.5	1.4
0.0	22.9	22.1	34.1	2.6
0.0	24.0	26.4	34.1	7.3
0.0	22.5	22.5	32.6	1.9
17.6	22.3	21.8	32.7	2.6
18.8	22.4	21.8	32.7	2.6
19.6	24.6	24.6	32.4	1.6
0.0	3.0	0.0	34.1	8.6
0.0	22.4	22.3	33.1	1.5
20.7	30.0	31.8	34.1	2.5
0.0	27.0	27.6	34.1	3.2

Appendix 2H: Soil Water Balance Results – Annual Recharge, Irrigation, Actual Evapotranspiration for Most Prevalent Vegetation Types in Model Domain (2012-2014)

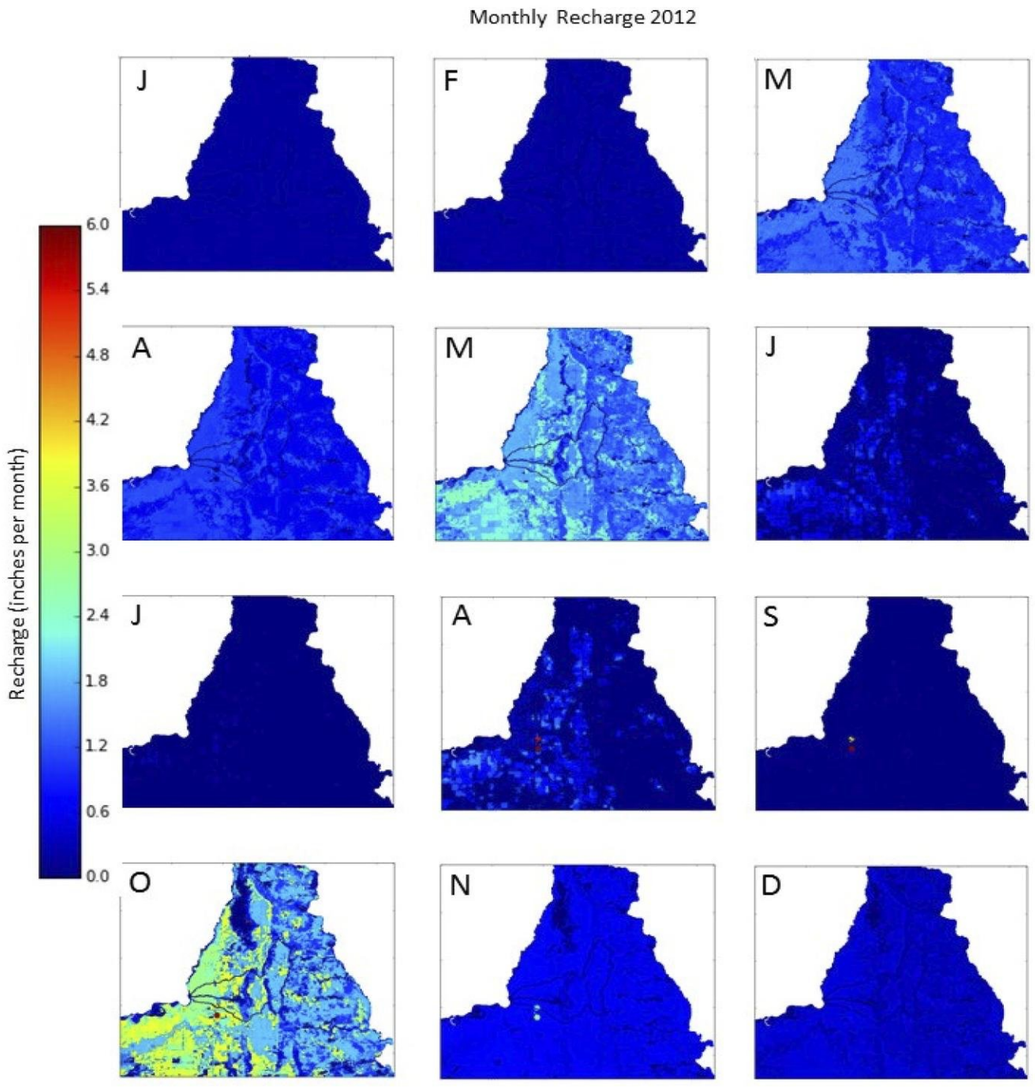

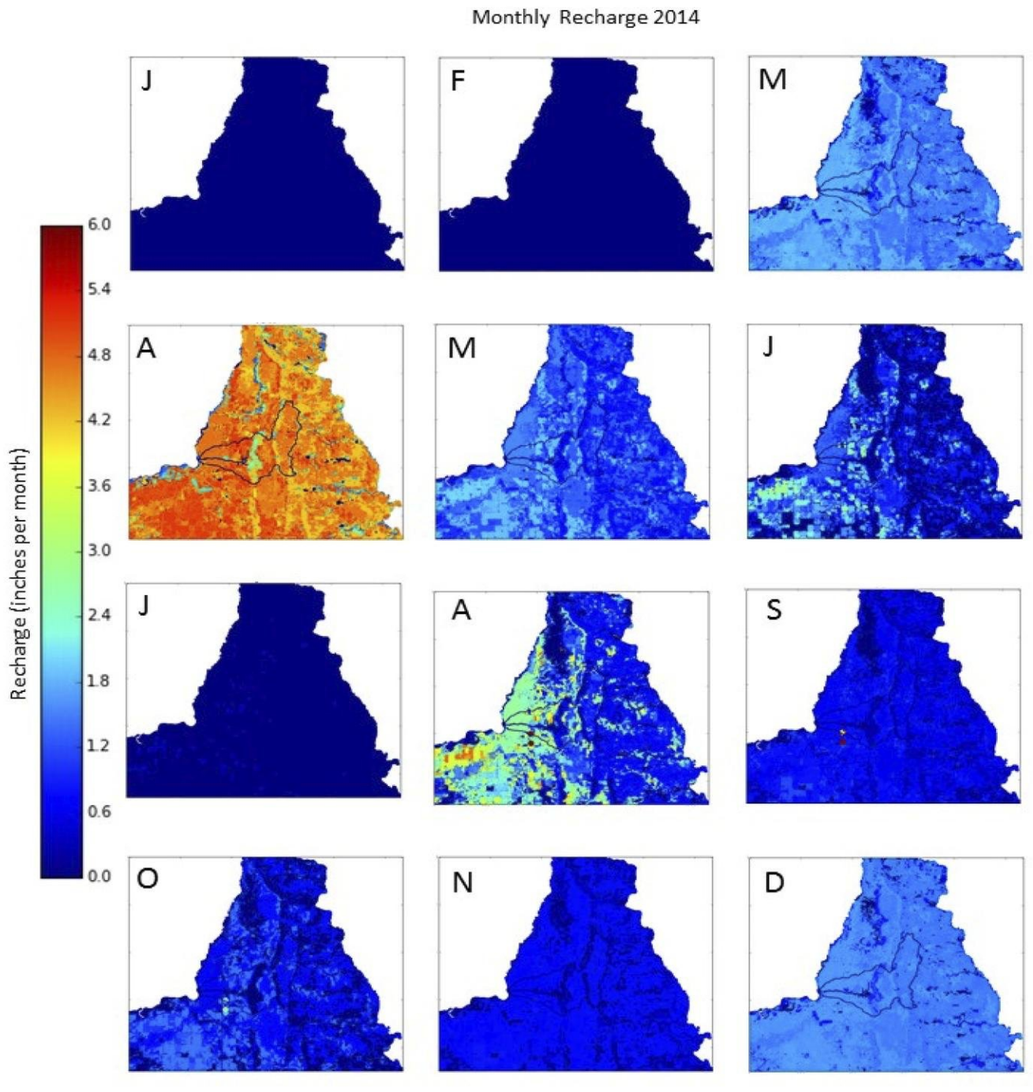

Appendix 2I. Supplemental recharge data: SWB MONTHLY RESULTS, UNCALIBRATED (2012–2014)—precipitation, recharge, irrigation, actual evapotranspiration

		January					February				
YEAR	VAR	Min (in/ month)	Mean (in/ month)	Median (in/ month)	Max (in/ month)	Standard deviation (in/ month)	Min (in/ month)	Mean (in/ month)	Median (in/ month)	Max (in/ month)	Standard deviation (in/ month)
2012	Precipitatio	1.0	1.0	1.0	1.0	0.0	1.2	1.2	1.2	1.2	0.0
2013	Precipitatio	1.6	1.6	1.6	1.6	0.0	1.6	1.6	1.6	1.6	0.0
2014	Precipitatio	1.3	1.3	1.3	1.3	0.0	1.2	1.2	1.2	1.2	0.0
2012	Recharge	0.0	0.1	0.1	0.3	0.0	0.0	0.2	0.2	0.6	0.1
2013	Recharge	0.0	0.2	0.2	0.6	0.1	0.0	0.0	0.0	0.0	0.0
2014	Recharge	0.0	0.0	0.0	0.1	0.0	0.0	0.0	0.0	0.0	0.0
2012	Irrigation	0.0	0.0	0.0	0.0	0.0	0.0	0.0	0.0	0.0	0.0
2013	Irrigation	0.0	0.0	0.0	0.0	0.0	0.0	0.0	0.0	0.0	0.0
2014	Irrigation	0.0	0.0	0.0	0.0	0.0	0.0	0.0	0.0	0.0	0.0
2012	Actual_ET	0.0	0.5	0.5	1.2	0.2	0.0	0.6	0.6	1.3	0.2
2013	Actual_ET	0.0	0.4	0.4	1.2	0.2	0.0	0.4	0.4	1.3	0.2
2014	Actual_ET	0.0	0.2	0.2	0.9	0.1	0.0	0.2	0.1	0.7	0.1

March					April				
Min (in/ month)	Mean (in/ month)	Median (in /month)	Max (in/month)	Standard deviation (in/ month)	Min (in/ month)	Mean (in/ month)	Median (in/ month)	Max (in/ month)	Standard deviation (in/ month)
1.8	1.8	1.8	1.8	0.0	2.7	2.7	2.7	2.7	0.0
1.7	1.7	1.7	1.7	0.0	4.2	4.2	4.2	4.2	0.0
1.1	1.1	1.1	1.1	0.0	5.7	5.7	5.7	5.7	0.0
0.0	1.0	1.0	4.4	0.4	0.0	0.8	0.6	4.1	0.4
0.0	0.8	0.8	2.1	0.2	0.0	5.2	5.3	12.3	1.0
0.0	1.5	1.5	5.0	0.4	0.0	4.5	4.7	11.9	0.9
0.0	0.0	0.0	0.0	0.0	0.0	0.0	0.0	1.2	0.1
0.0	0.0	0.0	0.0	0.0	0.0	0.0	0.0	0.2	0.0
0.0	0.0	0.0	0.0	0.0	0.0	0.0	0.0	0.4	0.0
0.0	1.4	1.4	2.8	0.3	0.0	2.0	2.0	3.7	0.5
0.0	0.8	0.8	1.7	0.2	0.0	2.2	2.1	4.1	0.5
0.0	1.0	1.0	1.8	0.3	0.0	2.6	2.5	4.6	0.6

May					June				
Min (in/ month)	Mean (in/ month)	Median (in/ month)	Max (in/ month)	Standard deviation (in/ month)	Min (in/ month)	Mean (in/ month)	Median (in/ month)	Max (in/ month)	Standard deviation (in/ month)
4.5	4.5	4.5	4.5	0.0	2.2	2.2	2.2	2.2	0.0
4.5	4.5	4.5	4.5	0.0	4.4	4.4	4.4	4.4	0.0
4.2	4.2	4.2	4.2	0.0	4.7	4.7	4.7	4.7	0.0
0.0	1.6	1.6	5.5	0.6	0.0	0.1	0.0	1.9	0.3
0.0	0.5	0.4	1.7	0.6	0.0	0.4	0.2	3.0	0.6
0.0	1.2	1.2	4.5	0.5	0.0	0.7	0.7	4.6	0.8
0.0	0.0	0.0	1.6	0.1	0.0	0.5	0.0	4.0	1.0
0.0	0.0	0.0	0.6	0.0	0.0	0.3	0.0	3.0	0.7
0.0	0.0	0.0	0.2	0.0	0.0	0.4	0.0	3.5	0.7
0.0	3.4	3.4	6.2	0.9	0.0	3.6	3.2	7.8	1.1
0.0	3.5	3.4	5.9	0.8	0.0	5.3	5.1	8.5	1.1
0.0	3.9	3.9	6.6	1.0	0.0	4.4	4.2	7.5	1.1

July					August				
Min (in/ month)	Mean (in/ month)	Median (in/ month)	Max (in/ month)	Standard deviation (in/ month)	Min (in/ month)	Mean (in/ month)	Median (in/ month)	Max (in/ month)	Standard deviation (in/ month)
0.7	0.7	0.7	0.7	0.0	3.4	3.4	3.4	3.4	0.0
2.4	2.4	2.4	2.4	0.0	2.5	2.5	2.5	2.5	0.0
1.5	1.5	1.5	1.5	0.0	7.4	7.4	7.4	7.4	0.0
0.0	0.0	0.0	0.5	0.0	0.0	0.2	0.0	2.4	0.4
0.0	0.1	0.0	1.3	0.2	0.0	0.1	0.0	1.5	0.3
0.0	0.0	0.0	1.0	0.1	0.0	1.4	0.9	6.3	1.2
0.0	1.4	0.0	7.5	2.4	0.0	0.8	0.0	6.0	1.5
0.0	0.8	0.0	6.0	1.6	0.0	0.9	0.0	5.5	1.6
0.0	0.9	0.0	6.0	1.6	0.0	0.5	0.0	5.0	0.9
0.0	2.5	1.1	8.6	2.5	0.0	3.5	2.8	8.0	1.7
0.0	4.0	3.2	8.3	1.7	0.0	3.0	2.2	7.3	1.7
0.0	3.3	2.5	8.2	1.8	0.0	4.0	3.4	8.2	1.5

September					October				
Min (in/ month)	Mean (in/ month)	Median (in/ month)	Max (in/ month)	Standard deviation (in/ month)	Min (in/ month)	Mean (in /month)	Median (in/ month)	Max (in/ month)	Standard deviation (in/ month)
2.1	2.1	2.1	2.1	0.0	5.1	5.1	5.1	5.1	0.0
1.8	1.8	1.8	1.8	0.0	3.2	3.2	3.2	3.2	0.0
2.8	2.8	2.8	2.8	0.0	3.1	3.1	3.1	3.1	0.0
0.0	0.0	0.0	0.2	0.0	0.0	2.0	1.9	8.8	1.2
0.0	0.0	0.0	0.2	0.0	0.0	0.8	0.7	1.9	0.7
0.0	0.5	0.6	2.1	0.3	0.0	0.6	0.7	3.3	0.5
0.0	0.0	0.0	1.0	0.2	0.0	0.0	0.0	0.0	0.0
0.0	0.1	0.0	2.0	0.3	0.0	0.0	0.0	0.0	0.0
0.0	0.0	0.0	0.0	0.0	0.0	0.0	0.0	0.0	0.0
0.0	1.9	1.6	4.1	0.6	0.0	1.2	1.1	2.4	0.4
0.0	1.7	1.5	4.2	0.6	0.0	1.6	1.6	3.3	0.5
0.0	3.2	2.9	5.4	1.0	0.0	1.5	1.5	3.0	0.4

November					December				
Min (in/ month)	Mean (in/ month)	Median (in/ month)	Max (in/ month)	Standard deviation (in/ month)	Min (in/ month)	Mean (in/ month)	Median (in/ month)	Max (in/ month)	Standard deviation (in/ month)
1.3	1.3	1.3	1.3	0.0	1.8	1.8	1.8	1.8	0.0
2.3	2.3	2.3	2.3	0.0	1.4	1.4	1.4	1.4	0.0
2.1	2.1	2.1	2.1	0.0	1.4	1.4	1.4	1.4	0.0
0.0	0.6	0.6	1.3	0.2	0.0	0.4	0.4	0.6	0.1
0.0	1.0	1.2	3.5	0.4	0.0	0.0	0.0	0.0	0.0
0.0	0.6	0.7	1.3	0.3	0.0	1.5	1.5	4.9	0.4
0.0	0.0	0.0	0.0	0.0	0.0	0.0	0.0	0.0	0.0
0.0	0.0	0.0	0.0	0.0	0.0	0.0	0.0	0.0	0.0
0.0	0.0	0.0	0.0	0.0	0.0	0.0	0.0	0.0	0.0
0.0	0.8	0.9	1.3	0.2	0.0	0.4	0.4	1.2	0.2
0.0	0.7	0.7	1.6	0.2	0.0	0.3	0.2	1.3	0.2
0.0	0.5	0.6	1.6	0.2	0.0	0.4	0.4	1.2	0.2

Appendix 2. Supplemental recharge data: REFERENCES

The following references are cited in this appendix:

Allen, R.G., Pereira, L.S., Raes, D., and Smith, M., 1998, Crop evapotranspiration guidelines for computing crop water requirements: Food and Agriculture Organization of the United Nations, Irrigation and Drainage Paper 56.

Bussan, A.J., 2015, Presentation at Wisconsin Potato and Vegetation Grower Association Meeting.

Crow, P., 2005, The influence of soils and species on tree root depth: Edinburgh, *Forestry Commission Information Note 078*, 8 p.

De Byle, N., 1957, Oak and jack pine rooting habits on plainfield sand in Central Wisconsin: University of Wisconsin-Madison, M.S. thesis.

Hart, D.J., Streiff, C., and Kniffin, M., 2016, Estimating recharge in the Central Sands using water-table fluctuations [abs.]: Proceedings of the American Water Resources Association—Wisconsin Section, 40th Annual Meeting, Wisconsin Dells, Wis., p 49.

Jackson, R., Canadell, J., Ehleringer, J., Mooney, H., Sala, O., and Schulze, E., 1996, A global analysis of root distributions for terrestrial biomes: *Oecologia*, v. 108, no. 3, p. 389–411.

Kucharik, C.J., Serbin, S.P., Vavrus, S., Hopkins, E.J., and Motew, M.M., 2010, Patterns of climate change across Wisconsin from 1950 to 2006: *Physical Geography*, v. 31, no. 1, p. 1–28.

Smith, E.A., and Westenbroek, S.M., 2015, Potential groundwater recharge for the state of Minnesota using the soil-water-balance model, 1996–2010: USGS Scientific Investigations Report 2015–5038, 85 p.

Thornthwaite, C.W., and Mather, J.R., 1957, Instructions and tables for computing potential evapotranspiration and the water balance: Centerton, N.J., Laboratory of Climatology, Publications in Climatology, v. 10, no. 3, p. 185–311.

USDA, Soil Conservation Service, 1955, Irrigation - water management guide for Wisconsin - tentative, for the design of sprinkler irrigation systems. 57.2: 7.1, Madison, WI.

USDA, Natural Resources Conservation Service, 1986, Urban hydrology for small watersheds: *Soil Conservation*, Technical Release 55, 164 p.

USDA, Natural Resources Conservation Service, 2004, Part 630 Hydrology—National Engineering Handbook, Chapter 11: Snowmelt: United States Department of Agriculture, 21 p.

Wisconsin Potato and Vegetable Grower Association - Water Task Force Meetings, personal communication, 2014-2015.

Appendix 3. Parameter-estimation algorithm

The parameter-estimation process was achieved through history matching, using observations of both steady-state and transient conditions, as described in the Parameter Estimation and Model Calibration section of the report, and using the Gauss-Levenberg-Marquardt algorithm implemented in the PEST software suite (Doherty, 2014) and SVD-assist (Tonkin and Doherty, 2005). In this section we briefly summarize the technique which is described in greater detail in Doherty (2014), Doherty and Hunt (2010), and references therein.

The Gauss-Levenberg-Marquardt method is a gradient-based search algorithm that adjusts parameters in pursuit of the minimum value of an objective function. The objective function is the weighted sum of squared errors comparing field observations with forecasts at the same time and place made by the model. The objective function is referred to as

$$\mathbf{\Phi}=(\mathbf{y}\text{-}g(\mathbf{p}))^T\,\mathbf{Q^{-1}}\,(\mathbf{y}\text{-}g(\mathbf{p}))$$

where:

Φ is the objective function;

y is a vector of observations;

$g(\mathbf{p})$ is a vector of modeled values collocated in time and space with the observations, evaluated at parameter values **p**;

Q is a matrix of observation weights (in this work, **Q** is a diagonal matrix indicating no correlation among observation errors is assumed). The units of **Q** are 1/(units of **y**);

$(\cdot)^T$ indicates a vector transpose; and

$(\cdot)^{-1}$ indicates a matrix inversion.

The term **(y-*g*(p))** is the vector of residuals, also called errors, comparing measured and modeled results. The observation weights play important roles both in enforcing an appropriate level of fit (correspondence between observed and modeled results) and in balancing Φ such that observations of various types all contribute to the objective function. Assignment and adjustment of weights are discussed in more detail in the Parameter Estimation and Model Calibration section of the report.

The use of variable observation weights acknowledges that a perfect match between modeled and observed values is unattainable and, in fact, undesirable. Among the many reasons for this are error in the observations, the necessary fact that the model is a simplification of the true physical system, the smoothing of time signals by the model, and a host of others. The flexibility that this imparts, however, means that many (in fact, infinite) arrangements of parameters can result in the same value of Φ. This non-uniqueness motivates the need to incorporate expert ("soft") knowledge to arrive at a set of parameters that satisfies both the desired level of fit and conforms to expert understanding of reasonable values for the parameters.

The introduction of qualitative expert prior information is made through several avenues, including (1) enforcing the level of fit desired through the assignment of weights, (2) normalizing observation group weight contributions through weight adjustment as discussed in the Parameter Estimation and Model Calibration section, (3) addition of a penalty to the objective function for parameters deviating from a preferred condition through regularization, and (4) the singular value decomposition algorithm. Decisions made regarding all these aspects of prior information are inherently subjective. However, it is an important way for an understanding of the groundwater-flow system to play a role in the process beyond blind trust in the algorithm, leading to more meaningful results (Fienen, 2013, for example).

The penalty to the objective function is assigned as a form of Tikhonov regularization (Tikhonov 1963a, b) through an additional term in the objective function that penalizes deviation from a preferred condition—in this case, preferred homogeneity of spatially distributed parameters.

$$\mathbf{\Phi} = \left(\mathbf{y} - g(\mathbf{p})\right)^T \mathbf{Q^{-1}} \left(\mathbf{y} - g(\mathbf{p})\right) + \boldsymbol{\beta}\mathbf{p}^T\mathbf{Z}\mathbf{p}$$

where:

β is a weight-balancing regularization with fit as a function of Φ_{MLIM};

Φ_{MLIM} is the user-adjusted variable that controls the strength of regularization by calculating **β** (Doherty 2003, Fienen and others, 2009); and

Z is a matrix of kriging weights relating parameters to one another based on an exponential variogram and the distances between them. The kriging weights are set at the beginning of the process and remain constant. However, the strength with which the regularization is enforced changes throughout the iterations of PEST.

The variable Φ_{MLIM} was set to a value the same order of magnitude as the number of observations, as suggested by Fienen and others (2009) to balance the level of fit with the importance of the prior information.

Singular value decomposition (SVD) was also used to enhance solution stability and provide a secondary level of regularization. In SVD, the sensitivity of observations to parameters is transformed to align with

principal orientations of maximum information. This transformed space can then be divided into the calibration space and the null space. The calibration space is the region in which information from observations is meaningfully projected onto parameters while the null space represents a space where variability in parameters has little or no impact on model outputs of interest. This division between solution and null space is controlled by the stability of the sensitivity matrix and the settings recommended by Doherty and Hunt (2010) was adopted. Finally, to make the history-matching process more computationally tractable, SVD-assist (Tonkin and Doherty, 2005) was used with 80 super parameters compared with 686 base parameters. Details of the method are in Tonkin and Doherty (2005) and Doherty (2014).

References

Doherty, J., 2003, Ground water model calibration using pilot points and regularization: *Ground Water*, v. 41, p. 170–177, doi:10.1111/j.1745-6584.2003.tb02580.x.

Doherty, J., 2014, PEST, model-independent parameter estimation: User manual, 5th ed.: Brisbane, Australia, Watermark Numerical Computing, [variously paged].

Doherty, J.E., and Hunt, R.J., 2010, Approaches to highly parameterized inversion: A guide to using PEST for groundwater-model calibration: U.S. Geological Survey Scientific Investigations Report 2010-5169, 59 p.

Fienen, M.N., 2013, We speak for the data: *Ground Water*, v. 51, p. 157, doi:10.1111/gwat.12018.

Fienen, M.N., Muffels, C.T., and Hunt, R.J., 2009, On constraining pilot point calibration with regularization in PEST: *Ground Water*, v. 47, p. 835–844, doi:10.1111/j.1745-6584.2009.00579.x.

Tikhonov, A.N., 1963a, Solution of incorrectly formulated problems and the regularization method: *Soviet Math. Dokl.,* v. 4, p. 1035–1038.

Tikhonov, A.N., 1963b, Regularization of incorrectly posed problems: *Soviet Math. Dokl.*, v. 4, p. 1624–1627.

Tonkin, M.J., and Doherty, J., 2005, A hybrid regularized inversion methodology for highly parameterized models: *Water Resources Research*, v. 41, no. 10, 16 p.

Appendix 4. Calibration targets

A. Heads
B. Head groups
C. Flow
D. Transient heads
E. Transient flows

Appendix 4A. Calibration targets: HEADS

Name	Head Value (feet MSL)	Group
WISA_1	1090.59	WISA_H
WISA_2	1087.51	WISA_H
WISA_3	1088.16	WISA_H
WISA_4	1089.32	WISA_H
WISA_5	1090.30	WISA_H
WISA_6	1089.11	WISA_H
DM_7	1077.68	DM_H
DM_8	1077.24	DM_H
DM_9	1077.00	DM_H
DM_10	1079.80	DM_H
DM_11	1079.59	DM_H
DM_12	1079.40	DM_H
DM_13	1080.95	DM_H
DM_14	1076.48	DM_H
DM_15	1080.99	DM_H
DM_16	1077.74	DM_H
DM_17	1077.56	DM_H
DM_18	1077.47	DM_H
PRF_19	1129.37	PRF_H
PRF_20	1128.13	PRF_H
PRF_21	1128.13	PRF_H
PRF_22	1138.51	PRF_H
PRF_23	1140.49	PRF_H
PRF_24	1143.61	PRF_H
PRF_25	1137.35	PRF_H
PRF_26	1084.91	PRF_H
PRF_27	1084.93	PRF_H
PRF_28	1125.82	PRF_H
PRF_29	1122.67	PRF_H
PRF_30	1124.66	PRF_H
PRF_31	1120.04	PRF_H
PRF_32	1120.35	PRF_H
PRF_33	1115.91	PRF_H
PRF_34	1126.38	PRF_H
PRF_35	1137.86	PRF_H
RI_36	1015.09	RI_H
RI_37	1133.68	RI_H
RI_38	1134.83	RI_H
RI_39	1048.70	RI_H
RI_40	1165.42	RI_H
RI_41	1118.02	RI_H
RI_42	1057.01	RI_H
RI_43	1092.00	RI_H
RI_44	1117.97	RI_H
RI_45	1080.44	RI_H
RI_46	1103.51	RI_H
RI_47	1054.97	RI_H
RI_48	1066.96	RI_H
RI_49	1056.46	RI_H
RI_50	1104.27	RI_H
RI_51	1127.26	RI_H
RI_52	1097.21	RI_H
RI_53	1156.02	RI_H
RI_54	1042.56	RI_H
RI_55	1142.32	RI_H
RI_56	1119.35	RI_H
RI_57	1053.93	RI_H
RI_58	1105.05	RI_H
RI_59	1081.15	RI_H
RI_60	1086.92	RI_H
USGS_61	1087.79	USGS_H
USGS_62	1081.27	USGS_H
USGS_63	1094.80	USGS_H
VP_64	1076.14	VP_H
VP_65	1076.79	VP_H
VP_66	1089.80	VP_H
VP_67	1089.37	VP_H
VP_68	1070.93	VP_H
VP_69	1073.03	VP_H
WGNHS_70	1073.73	WGNHS_H
WGNHS_71	1085.18	WGNHS_H
WGNHS_72	1085.07	WGNHS_H
WGNHS_73	1090.55	WGNHS_H
WGNHS_74	1090.70	WGNHS_H
WGNHS_75	1102.65	WGNHS_H
WGNHS_76	1103.24	WGNHS_H
WGNHS_77	1097.92	WGNHS_H
WGNHS_78	1097.92	WGNHS_H
WGNHS_79	1082.37	WGNHS_H
WGNHS_80	1068.20	WGNHS_H
WGNHS_81	1107.95	WGNHS_H
LAKE_82	1106.75	LAKE_H
LAKE_83	1088.70	LAKE_H
LAKE_84	1025.20	LAKE_H
LAKE_85	1074.20	LAKE_H
LAKE_86	1072.50	LAKE_H
LAKE_87	1066.60	LAKE_H
LAKE_88	1076.10	LAKE_H
LAKE_89	1114.60	LAKE_H

Appendix 4B. Calibration targets: HEAD GROUPS

Head Group	Initial standard deviation	Initial Weight	Adjusted Weight	Adjusted Standard Deviation	Target PHI - Steady State	Target PHI - Transient
WISA_H	1.00	1.00	0	0	0.0%	0.0%
DM_H	0.50	2.00	0.65	1.55	4.0%	12.3%
PRF_H	2.00	0.50	0.30	3.32	2.0%	7.7%
RI_H	3.00	0.33	0.25	4.04	2.0%	-na-
USGS_H	0.25	4.00	1.37	0.73	2.0%	7.7%
VP_H	1.00	1.00	0.72	1.39	4.0%	12.3%
WGNHS_H	0.25	4.00	0.65	1.54	4.0%	6.2%
LAKE_H	2.00	0.50	0.35	2.88	2.0%	-na-

Appendix 4C. Calibration targets: FLOWS

Name	Decription	Flow (cubic feet per day)	Flow (cubic feet per second)	Group	Initial Weight	Adjusted Weight
lprken	LPR at Kenedy	78519.13	0.91	flux_lpr	11.00	27.74
lpri39	LPR at I-39	345770.06	4.00	flux_lpr	2.50	6.30
lprhoov	LPR at Hoover	450914.10	5.22	flux_lpr	1.92	4.83
lpreis	LPR at Eisenhower	168245.23	1.95	flux_lpr	5.14	12.95
bearq	Bear Creek at Q	738365.37	8.55	flux	1.17	1.66
springq	Spring Creek	316717.77	3.67	flux	2.73	3.88
ditch2	Isherwood Ditch	417935.93	4.84	flux	2.07	2.94
noname	No name	105001.14	1.22	flux	8.23	11.69
swcan3	Southwest Canal 3	1375512.43	15.92	flux	0.63	0.89
swcan2	Southwest Canal 2	1059151.72	12.26	flux	0.82	1.16
swcan1	Southwest Canal 1	649281.48	7.51	flux	1.33	1.89

Appendix 4D. Calibration targets: TRANSIENT HEADS

Name	Head Value (feet MSL)	Group
dm_10_4	1078.85	dm_h
dm_10_6	1080.25	dm_h
dm_11_4	1078.2	dm_h
dm_11_6	1080.2	dm_h
dm_12_4	1077.93	dm_h
dm_12_6	1080.03	dm_h
dm_13_4	1079.34	dm_h
dm_13_6	1081.54	dm_h
dm_14_4	1074.56	dm_h
dm_14_6	1076.76	dm_h
dm_15_4	1078.94	dm_h
dm_15_6	1081.24	dm_h
dm_16_4	1075.61	dm_h
dm_16_6	1077.91	dm_h
dm_17_4	1075.32	dm_h
dm_17_6	1077.72	dm_h
dm_18_4	1075.22	dm_h
dm_18_6	1077.62	dm_h
dm_7_4	1075.78	dm_h
dm_7_6	1077.98	dm_h
dm_8_4	1076.27	dm_h
dm_8_6	1077.47	dm_h
dm_9_4	1075.92	dm_h
dm_9_6	1077.62	dm_h
prf_19_4	1129.92	prf_h
prf_20_4	1128.49	prf_h
prf_21_4	1128.49	prf_h
prf_22_4	1137.92	prf_h
prf_23_4	1139.94	prf_h
prf_24_4	1142.85	prf_h
prf_25_4	1138.47	prf_h
prf_26_4	1084.1	prf_h
prf_27_4	1083.43	prf_h
prf_28_4	1126.16	prf_h
prf_29_4	1123.32	prf_h
prf_30_4	1125.01	prf_h
prf_31_4	1119.72	prf_h
prf_32_4	1120.35	prf_h
prf_33_4	1115.91	prf_h
prf_34_4	1126.17	prf_h
prf_35_4	1139.46	prf_h
usgs_61_1	1086.6	usgs_h
usgs_61_4	1088.38	usgs_h
usgs_61_7	1089.38	usgs_h
usgs_61_9	1089.49	usgs_h
usgs_61_10	1089.59	usgs_h
usgs_62_2	1079.01	usgs_h
usgs_62_4	1079.72	usgs_h
usgs_62_5	1080.8	usgs_h
usgs_62_7	1081.93	usgs_h
usgs_62_9	1081.77	usgs_h
usgs_63_7	1094.99	usgs_h
vp_64_1	1073.54	vp_h
vp_64_4	1074.66	vp_h
vp_64_5	1075.49	vp_h
vp_64_6	1075.91	vp_h
vp_65_1	1074.56	vp_h
vp_65_4	1075.43	vp_h
vp_65_5	1076.11	vp_h
vp_65_6	1076.81	vp_h
vp_66_1	1088.42	vp_h
vp_66_3	1088.38	vp_h
vp_66_4	1089.4	vp_h
vp_66_5	1090.15	vp_h
vp_66_6	1090.27	vp_h

Name	Head Value (feet MSL)	Group
vp_67_1	1088.07	vp_h
vp_67_3	1087.97	vp_h
vp_67_4	1089.17	vp_h
vp_67_5	1089.85	vp_h
vp_67_6	1089.8	vp_h
vp_68_1	1070.58	vp_h
vp_68_3	1070.43	vp_h
vp_68_4	1071.15	vp_h
vp_68_5	1071.96	vp_h
vp_68_6	1072.53	vp_h
vp_69_1	1072.35	vp_h
vp_69_3	1072.53	vp_h
vp_69_4	1073.45	vp_h
vp_69_5	1072.97	vp_h
vp_69_6	1072.9	vp_h
wgnhs_72_8	1085.81	wgnhs_h
wgnhs_72_9	1085.46	wgnhs_h
wgnhs_72_10	1084.85	wgnhs_h
wgnhs_72_11	1084.62	wgnhs_h
wgnhs_72_12	1084.99	wgnhs_h
wgnhs_73_8	1090.8	wgnhs_h
wgnhs_73_9	1090.7	wgnhs_h
wgnhs_73_10	1090.52	wgnhs_h
wgnhs_73_11	1090.43	wgnhs_h
wgnhs_73_12	1090.63	wgnhs_h
wgnhs_74_8	1090.94	wgnhs_h
wgnhs_74_9	1090.91	wgnhs_h
wgnhs_74_10	1090.72	wgnhs_h
wgnhs_74_11	1090.56	wgnhs_h
wgnhs_74_12	1090.77	wgnhs_h
wgnhs_75_8	1102.7	wgnhs_h
wgnhs_75_9	1104.15	wgnhs_h
wgnhs_75_10	1103.93	wgnhs_h
wgnhs_75_11	1103.83	wgnhs_h
wgnhs_75_12	1104	wgnhs_h
wgnhs_76_8	1102.65	wgnhs_h
wgnhs_76_9	1103.75	wgnhs_h
wgnhs_76_10	1104.25	wgnhs_h
wgnhs_76_11	1103.92	wgnhs_h
wgnhs_76_12	1103.97	wgnhs_h
wgnhs_77_8	1098.27	wgnhs_h
wgnhs_77_9	1099.08	wgnhs_h
wgnhs_77_10	1098.88	wgnhs_h
wgnhs_77_11	1098.66	wgnhs_h
wgnhs_77_12	1098.85	wgnhs_h
wgnhs_78_8	1098.17	wgnhs_h
wgnhs_78_9	1098.98	wgnhs_h
wgnhs_78_10	1098.78	wgnhs_h
wgnhs_78_11	1098.55	wgnhs_h
wgnhs_78_12	1098.8	wgnhs_h
wgnhs_81_8	1107.5	wgnhs_h
wgnhs_81_9	1108.32	wgnhs_h
wgnhs_81_10	1109.01	wgnhs_h
wgnhs_81_11	1107.85	wgnhs_h
wgnhs_81_12	1108.67	wgnhs_h
wisa_2_1	1087.6	wisa_h
wisa_2_2	1087.45	wisa_h
wisa_2_3	1087.38	wisa_h
wisa_2_5	1088.02	wisa_h
wisa_2_6	1087.99	wisa_h
wisa_2_7	1087.53	wisa_h
wisa_2_8	1087.55	wisa_h
wisa_2_9	1088.04	wisa_h
wisa_2_10	1088.02	wisa_h
wisa_2_11	1087.97	wisa_h
wisa_3_1	1088.47	wisa_h
wisa_3_2	1088.19	wisa_h

4d. heads_transient

Name	Head Value (feet MSL)	Group
wisa_3_3	1088.09	wisa_h
wisa_3_4	1088.62	wisa_h
wisa_3_5	1088.54	wisa_h
wisa_3_6	1088.46	wisa_h
wisa_3_7	1088.15	wisa_h
wisa_3_8	1088.18	wisa_h
wisa_3_9	1088.4	wisa_h
wisa_3_10	1088.57	wisa_h
wisa_3_11	1088.51	wisa_h
wisa_4_1	1089.22	wisa_h
wisa_4_4	1090.46	wisa_h
wisa_4_5	1090.85	wisa_h
wisa_4_6	1090.81	wisa_h
wisa_4_7	1090.07	wisa_h
wisa_4_8	1089.71	wisa_h
wisa_4_9	1091.14	wisa_h
wisa_4_10	1090.87	wisa_h
wisa_4_11	1090.84	wisa_h
wisa_5_1	1090.19	wisa_h
wisa_5_2	1090.07	wisa_h
wisa_5_3	1090.45	wisa_h
wisa_5_4	1090.89	wisa_h
wisa_5_5	1091.03	wisa_h
wisa_5_6	1090.93	wisa_h
wisa_5_7	1090.45	wisa_h
wisa_5_8	1090.56	wisa_h
wisa_5_9	1091.02	wisa_h
wisa_5_10	1091.12	wisa_h
wisa_5_11	1091.13	wisa_h
wisa_6_1	1089.06	wisa_h
wisa_6_5	1089.52	wisa_h
wisa_6_6	1089.47	wisa_h
wisa_6_7	1089.16	wisa_h
wisa_6_8	1089.1	wisa_h
wisa_6_9	1089.55	wisa_h
wisa_6_10	1089.65	wisa_h
wisa_6_11	1089.66	wisa_h

4E. Calibration targets: TRANSIENT FLOWS

Name	Decription	Flow (cubic feet per second)	Group	Initial Weight	Adjusted Weight
bearq_10	Bear Creek: October	12.70	q_other	0.79	0.00
ditch2_1	Isherwood Ditch 2: January	6.28	q_other	1.59	0.00
ditch2_2	Isherwood Ditch 2: February	5.86	q_other	1.71	0.00
ditch2_3	Isherwood Ditch 2: March	6.49	q_other	1.54	0.00
ditch2_4	Isherwood Ditch 2: April	6.91	q_other	1.45	0.00
ditch2_5	Isherwood Ditch 2: May	8.40	q_other	1.19	0.00
ditch2_6	Isherwood Ditch 2: June	8.16	q_other	1.23	0.00
ditch2_7	Isherwood Ditch 2: July	5.82	q_other	1.72	0.00
ditch2_8	Isherwood Ditch 2: August	5.28	q_other	1.89	0.00
ditch2_9	Isherwood Ditch 2: September	6.53	q_other	1.53	0.00
ditch2_10	Isherwood Ditch 2: October	6.81	q_other	1.47	0.00
ditch2_11	Isherwood Ditch 2: November	6.51	q_other	1.54	0.00
ditch2_12	Isherwood Ditch 2: December	6.48	q_other	1.54	0.00
lpreis_4	Little Plover at Eisenhower: April	5.16	q_lpr	1.94	2.81
lpreis_5	Little Plover at Eisenhower: May	5.35	q_lpr	1.87	2.71
lpreis_6	Little Plover at Eisenhower: June	3.94	q_lpr	2.54	3.68
lpreis_7	Little Plover at Eisenhower: July	2.23	q_lpr	4.48	6.50
lpreis_8	Little Plover at Eisenhower: August	2.70	q_lpr	3.70	5.36
lpreis_9	Little Plover at Eisenhower: September	4.33	q_lpr	2.31	3.35
lpreis_10	Little Plover at Eisenhower: October	4.44	q_lpr	2.25	3.27
lpreis_11	Little Plover at Eisenhower: November	4.61	q_lpr	2.17	3.15
lpreis_12	Little Plover at Eisenhower: December	4.61	q_lpr	2.17	3.15
lprhoov_1	Little Plover at Hoover: January	5.01	q_lpr	2.00	2.89
lprhoov_2	Little Plover at Hoover: February	4.36	q_lpr	2.29	3.33
lprhoov_3	Little Plover at Hoover: March	4.17	q_lpr	2.40	3.48
lprhoov_4	Little Plover at Hoover: April	8.69	q_lpr	1.15	1.67
lprhoov_5	Little Plover at Hoover: May	10.30	q_lpr	0.97	1.41
lprhoov_6	Little Plover at Hoover: June	7.59	q_lpr	1.32	1.91
lprhoov_7	Little Plover at Hoover: July	6.41	q_lpr	1.56	2.26
lprhoov_8	Little Plover at Hoover: August	6.16	q_lpr	1.62	2.35
lprhoov_9	Little Plover at Hoover: September	9.76	q_lpr	1.02	1.49
lprhoov_10	Little Plover at Hoover: October	9.34	q_lpr	1.07	1.55
lprhoov_11	Little Plover at Hoover: November	9.02	q_lpr	1.11	1.61
lprhoov_12	Little Plover at Hoover: December	8.58	q_lpr	1.17	1.69
lprken_1	Little Plover at Kennedy: January	1.64	q_lpr	6.10	8.85
lprken_2	Little Plover at Kennedy: February	1.61	q_lpr	6.21	8.99
lprken_3	Little Plover at Kennedy: March	1.55	q_lpr	6.45	9.38
lprken_4	Little Plover at Kennedy: April	3.21	q_lpr	3.12	4.52
lprken_5	Little Plover at Kennedy: May	3.32	q_lpr	3.01	4.37
lprken_6	Little Plover at Kennedy: June	2.45	q_lpr	4.08	5.93
lprken_7	Little Plover at Kennedy: July	1.50	q_lpr	6.67	9.68
lprken_8	Little Plover at Kennedy: August	1.54	q_lpr	6.49	9.43
lprken_9	Little Plover at Kennedy: September	2.80	q_lpr	3.57	5.18
lprken_10	Little Plover at Kennedy: October	3.07	q_lpr	3.26	4.72
lprken_11	Little Plover at Kennedy: November	3.21	q_lpr	3.12	4.52
lprken_12	Little Plover at Kennedy: December	3.71	q_lpr	2.70	3.91
springq_1	Spring Creek: January	20.00	q_other	0.50	0.00
springq_3	Spring Creek: March	18.00	q_other	0.56	0.00
springq_4	Spring Creek: April	15.10	q_other	0.66	0.00
springq_5	Spring Creek: May	13.50	q_other	0.74	0.00
springq_6	Spring Creek: June	9.94	q_other	1.01	0.00
springq_7	Spring Creek: July	12.70	q_other	0.79	0.00
springq_8	Spring Creek: August	12.10	q_other	0.83	0.00
springq_9	Spring Creek: September	15.80	q_other	0.63	0.00
springq_10	Spring Creek: October	13.60	q_other	0.74	0.00
springq_11	Spring Creek: November	13.50	q_other	0.74	0.00
springq_12	Spring Creek: December	14.90	q_other	0.67	0.00

Appendix 5. Calibration tables

A. Steady-state heads
B. Steady-state flows
C. Transient heads
D. Transient flows
E. Transient recharge multipliers
F. Steady-state statistics
G. Transient statistics
H. K zones

Appendix 5A. Calibration tables: STEADY-STATE HEADS

Name	Observed Head Value (feet MSL)	Modeled Head Value from Calibration (feet MSL)	Difference (feet)	Relative percent difference (%)	Modeled Head Value Following Minor Model Revisions After Review (feet MSL)
wisa_1	1090.59	1086.00	4.589	0.4%	1086.01
wisa_2	1087.51	1088.21	-0.699	0.1%	1088.23
wisa_3	1088.163	1088.22	-0.057	0.0%	1088.24
wisa_4	1089.317	1086.00	3.317	0.3%	1086.01
wisa_5	1090.299	1090.14	0.156	0.0%	1090.16
wisa_6	1089.105	1090.15	-1.045	0.1%	1090.17
dm_7	1077.68	1075.62	2.065	0.2%	1075.65
dm_8	1077.243	1075.37	1.878	0.2%	1075.41
dm_9	1076.995	1075.32	1.671	0.2%	1075.37
dm_10	1079.795	1079.02	0.78	0.1%	1079.05
dm_11	1079.592	1077.04	2.551	0.2%	1077.08
dm_12	1079.397	1077.05	2.35	0.2%	1077.08
dm_13	1080.948	1079.10	1.847	0.2%	1079.13
dm_14	1076.477	1075.62	0.853	0.1%	1075.66
dm_15	1080.99	1079.14	1.846	0.2%	1079.17
dm_16	1077.735	1075.42	2.311	0.2%	1075.46
dm_17	1077.562	1075.16	2.398	0.2%	1075.19
dm_18	1077.47	1075.11	2.364	0.2%	1075.13
prf_19	1129.37	1129.33	0.042	0.0%	1129.20
prf_20	1128.128	1127.20	0.927	0.1%	1127.10
prf_21	1128.128	1131.16	-3.029	0.3%	1131.04
prf_22	1138.507	1138.44	0.071	0.0%	1138.28
prf_23	1140.487	1141.55	-1.058	0.1%	1141.41
prf_24	1143.613	1145.11	-1.493	0.1%	1144.94
prf_25	1137.345	1137.46	-0.114	0.0%	1137.37
prf_26	1084.912	1094.78	-9.872	0.9%	1094.77
prf_27	1084.93	1095.46	-10.528	1.0%	1095.44
prf_28	1125.823	1124.09	1.737	0.2%	1124.00
prf_29	1122.67	1123.06	-0.388	0.0%	1122.98
prf_30	1124.656	1123.19	1.468	0.1%	1123.10
prf_31	1120.036	1121.26	-1.228	0.1%	1121.19
prf_32	1120.35	1120.11	0.241	0.0%	1120.04
prf_33	1115.914	1114.48	1.434	0.1%	1114.46
prf_34	1126.384	1125.71	0.679	0.1%	1125.61
prf_35	1137.864	1140.13	-2.265	0.2%	1140.03

Explanation:
Name = target name assigned by PEST
Observed head value = measured value at target
Modeled head value = simulated value at target
Difference = observed value – calibration value
Relative percent difference = (difference/observed value) *100

Name	Observed Head Value (feet MSL)	Modeled Head Value from Calibration (feet MSL)	Difference (feet)	Relative percent difference (%)	Modeled Head Value Following Minor Model Revisions After Review (feet MSL)
ri_36	1015.09	1014.73	0.358	0.0%	1013.82
ri_37	1133.68	1133.42	0.258	0.0%	1133.28
ri_38	1134.83	1130.62	4.213	0.4%	1130.37
ri_39	1048.7	1047.49	1.21	0.1%	1046.73
ri_40	1165.42	1176.41	-10.986	0.9%	1176.33
ri_41	1118.02	1120.34	-2.317	0.2%	1120.16
ri_42	1057.01	1059.48	-2.471	0.2%	1059.51
ri_43	1092	1092.45	-0.452	0.0%	1092.42
ri_44	1117.97	1112.98	4.995	0.4%	1112.60
ri_45	1080.44	1078.76	1.677	0.2%	1077.92
ri_46	1103.51	1106.93	-3.423	0.3%	1106.93
ri_47	1054.97	1047.44	7.534	0.7%	1047.45
ri_48	1066.96	1057.26	9.699	0.9%	1057.31
ri_49	1056.46	1054.15	2.31	0.2%	1054.16
ri_50	1104.27	1098.74	5.53	0.5%	1098.98
ri_51	1127.26	1127.02	0.244	0.0%	1126.90
ri_52	1097.21	1099.91	-2.698	0.2%	1099.83
ri_53	1156.02	1149.93	6.095	0.5%	1149.47
ri_54	1042.56	1047.45	-4.888	0.5%	1047.45
ri_55	1142.32	1148.40	-6.083	0.5%	1148.29
ri_56	1119.35	1114.83	4.522	0.4%	1114.47
ri_57	1053.93	1051.13	2.8	0.3%	1051.25
ri_58	1105.05	1106.23	-1.179	0.1%	1105.86
ri_59	1081.15	1086.68	-5.527	0.5%	1086.66
ri_60	1086.92	1088.22	-1.3	0.1%	1088.21
usgs_61	1087.79	1085.98	1.806	0.2%	1085.45
usgs_62	1081.27	1078.91	2.358	0.2%	1078.93
usgs_63	1094.8	1094.74	0.06	0.0%	1094.66
vp_64	1076.14	1070.79	5.352	0.5%	1070.81
vp_65	1076.787	1074.67	2.116	0.2%	1074.70
vp_66	1089.803	1085.84	3.963	0.4%	1085.85
vp_67	1089.368	1085.14	4.227	0.4%	1085.16
vp_68	1070.934	1071.45	-0.515	0.0%	1072.45
vp_69	1073.028	1073.87	-0.842	0.1%	1073.94

Name	Observed Head Value (feet MSL)	Modeled Head Value from Calibration (feet MSL)	Difference (feet)	Relative percent difference (%)	Modeled Head Value Following Minor Model Revisions After Review (feet MSL)
wgnhs_70	1073.73	1072.54	1.19	0.1%	1072.60
wgnhs_71	1085.18	1082.56	2.624	0.2%	1082.58
wgnhs_72	1085.07	1082.56	2.51	0.2%	1082.59
wgnhs_73	1090.55	1086.19	4.356	0.4%	1086.21
wgnhs_74	1090.7	1086.20	4.503	0.4%	1086.21
wgnhs_75	1102.65	1101.22	1.43	0.1%	1101.26
wgnhs_76	1103.24	1101.25	1.993	0.2%	1101.29
wgnhs_77	1097.92	1093.44	4.478	0.4%	1093.53
wgnhs_78	1097.92	1093.44	4.484	0.4%	1093.53
wgnhs_79	1082.37	1083.61	-1.242	0.1%	1083.93
wgnhs_80	1068.2	1066.73	1.474	0.1%	1067.13
wgnhs_81	1107.95	1110.01	-2.056	0.2%	1109.97
lake_82	1106.75	1114.40	-7.649	0.7%	1114.26
lake_83	1088.7	1093.99	-5.288	0.5%	1093.94
lake_84	1025.2	1024.71	0.489	0.0%	1024.71
lake_85	1074.2	1074.49	-0.287	0.0%	1074.52
lake_86	1072.5	1072.76	-0.263	0.0%	1072.81
lake_87	1066.6	1060.24	6.358	0.6%	1060.46
lake_88	1076.1	1079.87	-3.773	0.4%	1080.27
lake_89	1114.6	1115.98	-1.381	0.1%	1115.99

Appendix 5B. Calibration tables: STEADY-STATE FLOWS

Name	Observed Baseflow Value (CFS)	Modeled Baseflow Value (CFS)	Difference (CFS)	Relative percent difference (%)	Modeled Baseflow Value Following Minor Model Revisions After Review (feet MSL)
lpri39	4.00	3.69	0.31	8.0%	3.96
lprhoov	5.22	5.24	-0.02	0.4%	5.42
lpreis	1.95	2.11	-0.16	7.9%	2.19
bearq	8.55	7.70	0.84	10.4%	n/a
springq	3.67	5.29	-1.62	36.2%	n/a
ditch2	4.84	4.74	0.10	2.0%	n/a
noname	1.22	1.38	-0.17	12.7%	n/a
swcan3	15.92	18.40	-2.48	14.4%	n/a
swcan2	12.26	13.62	-1.36	10.5%	n/a
swcan1	7.51	3.18	4.34	81.1%	n/a
lprken	0.91	0.96	-0.05	5.9%	0.99

Explanation:

Name = target name assigned by PEST

Observed base flow value = measured value at target

Modeled base flow value = simulated value at target

Difference = observed value – calibration value

Relative percent difference = (difference/observed value) *100

Appendix 5C. Calibration tables: TRANSIENT HEADS

Name	Observed Head Value (feet MSL)	Modeled Head Value (feet MSL)	Difference (feet)	Relative percent difference (%)	Modeled Head Value Following Minor Model Revisions After Review (feet MSL)
dm_10_4	1078.85	1080.02	-1.173	0.1%	1080.02
dm_10_6	1080.25	1080.78	-0.533	0.0%	1080.78
dm_11_4	1078.2	1078.74	-0.536	0.0%	1078.74
dm_11_6	1080.2	1079.63	0.57	0.1%	1079.63
dm_12_4	1077.93	1078.74	-0.811	0.1%	1078.74
dm_12_6	1080.03	1079.64	0.395	0.0%	1079.64
dm_13_4	1079.34	1080.48	-1.141	0.1%	1080.48
dm_13_6	1081.54	1081.48	0.059	0.0%	1081.48
dm_14_4	1074.56	1077.02	-2.462	0.2%	1077.02
dm_14_6	1076.76	1078.06	-1.297	0.1%	1078.06
dm_15_4	1078.94	1080.56	-1.62	0.2%	1080.56
dm_15_6	1081.24	1081.67	-0.431	0.0%	1081.67
dm_16_4	1075.61	1076.82	-1.207	0.1%	1076.82
dm_16_6	1077.91	1077.86	0.053	0.0%	1077.86
dm_17_4	1075.32	1076.58	-1.26	0.1%	1076.58
dm_17_6	1077.72	1077.56	0.157	0.0%	1077.56
dm_18_4	1075.22	1076.53	-1.305	0.1%	1076.53
dm_18_6	1077.62	1077.50	0.122	0.0%	1077.50
dm_7_4	1075.78	1077.01	-1.231	0.1%	1077.01
dm_7_6	1077.98	1078.05	-0.068	0.0%	1078.05
dm_8_4	1076.27	1076.43	-0.156	0.0%	1076.43
dm_8_6	1077.47	1077.19	0.284	0.0%	1077.19
dm_9_4	1075.92	1076.78	-0.864	0.1%	1076.78
dm_9_6	1077.62	1077.59	0.028	0.0%	1077.59
prf_19_4	1129.92	1129.78	0.142	0.0%	1129.90
prf_20_4	1128.49	1127.58	0.914	0.1%	1127.62
prf_21_4	1128.49	1131.51	-3.015	0.3%	1131.58
prf_22_4	1137.92	1138.66	-0.738	0.1%	1138.79
prf_23_4	1139.94	1141.50	-1.555	0.1%	1141.54
prf_24_4	1142.85	1145.23	-2.383	0.2%	1145.29
prf_25_4	1138.47	1137.40	1.074	0.1%	1137.40
prf_26_4	1084.1	1094.73	-10.625	1.0%	1094.72
prf_27_4	1083.43	1095.01	-11.581	1.1%	1095.01
prf_28_4	1126.16	1124.46	1.702	0.2%	1124.48
prf_29_4	1123.32	1123.30	0.025	0.0%	1123.31

Explanation:
Name = target name assigned by PEST
Observed head value = measured value at target
Modeled head value = simulated value at target
Difference = observed value – calibration value
Relative percent difference = (difference/observed value) *100

Name	Observed Head Value (feet MSL)	Modeled Head Value (feet MSL)	Difference (feet)	Relative percent difference (%)	Modeled Head Value Following Minor Model Revisions After Review (feet MSL)
prf_30_4	1125.01	1123.82	1.194	0.1%	1123.84
prf_31_4	1119.72	1121.55	-1.83	0.2%	1121.57
prf_32_4	1120.35	1120.16	0.189	0.0%	1120.17
prf_33_4	1115.91	1114.45	1.464	0.1%	1114.45
prf_34_4	1126.17	1125.98	0.19	0.0%	1126.02
prf_35_4	1139.46	1140.28	-0.816	0.1%	1140.29
usgs_61_1	1086.6	1086.59	0.015	0.0%	1086.58
usgs_61_4	1088.38	1086.30	2.084	0.2%	1086.30
usgs_61_7	1089.38	1086.98	2.397	0.2%	1086.98
usgs_61_9	1089.49	1087.19	2.296	0.2%	1087.12
usgs_61_10	1089.59	1087.38	2.209	0.2%	1087.35
usgs_62_2	1079.01	1080.05	-1.035	0.1%	1080.05
usgs_62_4	1079.72	1080.31	-0.585	0.1%	1080.31
usgs_62_5	1080.8	1081.83	-1.027	0.1%	1081.83
usgs_62_7	1081.93	1080.94	0.992	0.1%	1080.94
usgs_62_9	1081.77	1082.53	-0.763	0.1%	1082.23
usgs_63_7	1094.99	1096.01	-1.023	0.1%	1096.04
vp_64_1	1073.54	1072.71	0.828	0.1%	1072.72
vp_64_4	1074.66	1072.11	2.554	0.2%	1072.11
vp_64_5	1075.49	1072.90	2.594	0.2%	1072.90
vp_64_6	1075.91	1072.33	3.582	0.3%	1072.33
vp_65_1	1074.56	1076.07	-1.507	0.1%	1076.07
vp_65_4	1075.43	1076.08	-0.646	0.1%	1076.08
vp_65_5	1076.11	1077.40	-1.292	0.1%	1077.40
vp_65_6	1076.81	1077.02	-0.211	0.0%	1077.02
vp_66_1	1088.42	1087.08	1.342	0.1%	1087.08
vp_66_3	1088.38	1086.92	1.461	0.1%	1086.92
vp_66_4	1089.4	1087.18	2.219	0.2%	1087.18
vp_66_5	1090.15	1088.61	1.541	0.1%	1088.61
vp_66_6	1090.27	1086.81	3.457	0.3%	1086.81
vp_67_1	1088.07	1086.28	1.786	0.2%	1086.28
vp_67_3	1087.97	1086.08	1.889	0.2%	1086.08
vp_67_4	1089.17	1086.38	2.795	0.3%	1086.38
vp_67_5	1089.85	1087.83	2.023	0.2%	1087.83
vp_67_6	1089.8	1086.28	3.525	0.3%	1086.28
vp_68_1	1070.58	1071.91	-1.325	0.1%	1071.91
vp_68_3	1070.43	1071.22	-0.79	0.1%	1071.28

Name	Observed Head Value (feet MSL)	Modeled Head Value (feet MSL)	Difference (feet)	Relative percent difference (%)	Modeled Head Value Following Minor Model Revisions After Review (feet MSL)
vp_68_4	1071.15	1071.40	-0.251	0.0%	1071.52
vp_68_5	1071.96	1073.70	-1.737	0.2%	1073.87
vp_68_6	1072.53	1073.32	-0.787	0.1%	1073.55
vp_69_1	1072.35	1074.62	-2.273	0.2%	1074.62
vp_69_3	1072.53	1074.08	-1.552	0.1%	1074.08
vp_69_4	1073.45	1074.29	-0.844	0.1%	1074.30
vp_69_5	1072.97	1075.61	-2.642	0.2%	1075.62
vp_69_6	1072.9	1075.06	-2.162	0.2%	1075.07
wgnhs_72_8	1085.81	1082.97	2.841	0.3%	1082.97
wgnhs_72_9	1085.46	1083.96	1.497	0.1%	1083.81
wgnhs_72_1(	1084.85	1084.10	0.747	0.1%	1084.04
wgnhs_72_1:	1084.62	1084.00	0.623	0.1%	1084.00
wgnhs_72_1:	1084.99	1084.11	0.883	0.1%	1084.11
wgnhs_73_8	1090.8	1086.57	4.233	0.4%	1086.57
wgnhs_73_9	1090.7	1087.63	3.066	0.3%	1087.49
wgnhs_73_1(	1090.52	1087.87	2.649	0.2%	1087.80
wgnhs_73_1:	1090.43	1087.82	2.606	0.2%	1087.83
wgnhs_73_1:	1090.63	1087.99	2.639	0.2%	1087.99
wgnhs_74_8	1090.94	1086.58	4.365	0.4%	1086.58
wgnhs_74_9	1090.91	1087.64	3.273	0.3%	1087.49
wgnhs_74_1(	1090.72	1087.88	2.836	0.3%	1087.82
wgnhs_74_1:	1090.56	1087.84	2.719	0.2%	1087.84
wgnhs_74_1:	1090.77	1088.01	2.763	0.3%	1088.01
wgnhs_75_8	1102.7	1102.09	0.611	0.1%	1102.09
wgnhs_75_9	1104.15	1103.34	0.806	0.1%	1103.20
wgnhs_75_1(	1103.93	1103.85	0.076	0.0%	1103.76
wgnhs_75_1:	1103.83	1103.97	-0.136	0.0%	1103.97
wgnhs_75_1:	1104	1104.29	-0.294	0.0%	1104.30
wgnhs_76_8	1102.65	1102.11	0.545	0.0%	1102.11
wgnhs_76_9	1103.75	1103.36	0.395	0.0%	1103.21
wgnhs_76_1(	1104.25	1103.86	0.387	0.0%	1103.78
wgnhs_76_1:	1103.92	1103.98	-0.061	0.0%	1103.99
wgnhs_76_1:	1103.97	1104.31	-0.341	0.0%	1104.32
wgnhs_77_8	1098.27	1094.42	3.851	0.4%	1094.42
wgnhs_77_9	1099.08	1096.51	2.575	0.2%	1096.20
wgnhs_77_1(	1098.88	1096.94	1.938	0.2%	1096.79
wgnhs_77_1:	1098.66	1096.80	1.86	0.2%	1096.81

Name	Observed Head Value (feet MSL)	Modeled Head Value (feet MSL)	Difference (feet)	Relative percent difference (%)	Modeled Head Value Following Minor Model Revisions After Review (feet MSL)
wgnhs_77_1	1098.85	1096.97	1.877	0.2%	1096.99
wgnhs_78_8	1098.17	1094.40	3.769	0.3%	1094.40
wgnhs_78_9	1098.98	1096.48	2.501	0.2%	1096.18
wgnhs_78_1(	1098.78	1096.93	1.852	0.2%	1096.78
wgnhs_78_1	1098.55	1096.79	1.757	0.2%	1096.80
wgnhs_78_1	1098.8	1096.97	1.834	0.2%	1096.98
wgnhs_81_8	1107.5	1110.04	-2.538	0.2%	1110.04
wgnhs_81_9	1108.32	1111.22	-2.896	0.3%	1111.12
wgnhs_81_1(	1109.01	1111.78	-2.765	0.2%	1111.68
wgnhs_81_1	1107.85	1111.98	-4.134	0.4%	1111.99
wgnhs_81_1	1108.67	1112.43	-3.761	0.3%	1112.44
wisa_2_1	1087.6	1088.57	-0.973	0.1%	1088.57
wisa_2_2	1087.45	1088.40	-0.945	0.1%	1088.40
wisa_2_3	1087.38	1088.36	-0.982	0.1%	1088.36
wisa_2_5	1088.02	1089.36	-1.335	0.1%	1089.36
wisa_2_6	1087.99	1088.81	-0.817	0.1%	1088.81
wisa_2_7	1087.53	1088.33	-0.802	0.1%	1088.33
wisa_2_8	1087.55	1088.50	-0.951	0.1%	1088.50
wisa_2_9	1088.04	1089.35	-1.308	0.1%	1089.20
wisa_2_10	1088.02	1089.34	-1.32	0.1%	1089.29
wisa_2_11	1087.97	1089.23	-1.262	0.1%	1089.24
wisa_3_1	1088.47	1088.58	-0.114	0.0%	1088.58
wisa_3_2	1088.19	1088.41	-0.216	0.0%	1088.41
wisa_3_3	1088.09	1088.37	-0.284	0.0%	1088.37
wisa_3_4	1088.62	1088.53	0.093	0.0%	1088.53
wisa_3_5	1088.54	1089.37	-0.827	0.1%	1089.37
wisa_3_6	1088.46	1088.82	-0.359	0.0%	1088.82
wisa_3_7	1088.15	1088.34	-0.193	0.0%	1088.34
wisa_3_8	1088.18	1088.51	-0.332	0.0%	1088.51
wisa_3_9	1088.4	1089.36	-0.959	0.1%	1089.21
wisa_3_10	1088.57	1089.35	-0.781	0.1%	1089.30
wisa_3_11	1088.51	1089.24	-0.733	0.1%	1089.25
wisa_4_1	1089.22	1087.00	2.22	0.2%	1087.00
wisa_4_4	1090.46	1087.05	3.411	0.3%	1087.05
wisa_4_5	1090.85	1088.46	2.387	0.2%	1088.46
wisa_4_6	1090.81	1087.09	3.724	0.3%	1087.09
wisa_4_7	1090.07	1085.62	4.452	0.4%	1085.62

Name	Observed Head Value (feet MSL)	Modeled Head Value (feet MSL)	Difference (feet)	Relative percent difference (%)	Modeled Head Value Following Minor Model Revisions After Review (feet MSL)
wisa_4_8	1089.71	1086.63	3.079	0.3%	1086.63
wisa_4_9	1091.14	1088.24	2.905	0.3%	1088.00
wisa_4_10	1090.87	1088.51	2.362	0.2%	1088.42
wisa_4_11	1090.84	1088.46	2.38	0.2%	1088.46
wisa_5_1	1090.19	1090.62	-0.431	0.0%	1090.62
wisa_5_2	1090.07	1090.42	-0.351	0.0%	1090.42
wisa_5_3	1090.45	1090.37	0.079	0.0%	1090.37
wisa_5_4	1090.89	1090.56	0.333	0.0%	1090.56
wisa_5_5	1091.03	1091.56	-0.526	0.0%	1091.56
wisa_5_6	1090.93	1090.98	-0.048	0.0%	1090.98
wisa_5_7	1090.45	1090.48	-0.026	0.0%	1090.48
wisa_5_8	1090.56	1090.45	0.112	0.0%	1090.45
wisa_5_9	1091.02	1091.12	-0.099	0.0%	1091.01
wisa_5_10	1091.12	1091.22	-0.101	0.0%	1091.19
wisa_5_11	1091.13	1091.20	-0.069	0.0%	1091.20
wisa_6_1	1089.06	1090.63	-1.568	0.1%	1090.63
wisa_6_5	1089.52	1091.56	-2.043	0.2%	1091.56
wisa_6_6	1089.47	1090.99	-1.516	0.1%	1090.99
wisa_6_7	1089.16	1090.48	-1.324	0.1%	1090.49
wisa_6_8	1089.1	1090.46	-1.356	0.1%	1090.46
wisa_6_9	1089.55	1091.13	-1.577	0.1%	1091.02
wisa_6_10	1089.65	1091.23	-1.579	0.1%	1091.20
wisa_6_11	1089.66	1091.21	-1.547	0.1%	1091.21

Appendix 5D. Calibration tables: TRANSIENT FLOWS

Name	Observed Baseflow Value (CFS)	Modeled Baseflow Value (CFS)	Difference (CFS)	Relative percent difference (%)	Modeled Baseflow Value Following Minor Model Revisions After Review (CFS)
lpreis_4	5.16	3.01	2.15	52.7%	3.03
lpreis_5	5.35	5.24	0.11	2.0%	5.27
lpreis_6	3.94	3.76	0.18	4.7%	3.78
lpreis_7	2.23	2.52	-0.29	12.3%	2.54
lpreis_8	2.7	2.87	-0.17	5.9%	2.89
lpreis_9	4.33	4.86	-0.53	11.6%	4.87
lpreis_10	4.44	5.10	-0.66	13.8%	5.13
lpreis_11	4.61	4.94	-0.33	6.9%	4.97
lpreis_12	4.61	5.25	-0.64	13.1%	5.28
lprhoov_1	5.01	7.03	-2.02	33.6%	5.37
lprhoov_2	4.36	6.09	-1.73	33.1%	4.62
lprhoov_3	4.17	5.83	-1.66	33.2%	4.43
lprhoov_4	8.69	6.41	2.28	30.2%	4.94
lprhoov_5	10.3	9.96	0.34	3.4%	7.82
lprhoov_6	7.59	7.92	-0.33	4.3%	6.05
lprhoov_7	6.41	6.19	0.22	3.6%	4.56
lprhoov_8	6.16	6.72	-0.56	8.6%	4.99
lprhoov_9	9.76	10.10	-0.34	3.4%	7.68
lprhoov_10	9.34	9.95	-0.61	6.3%	7.78
lprhoov_11	9.02	9.59	-0.57	6.1%	7.55
lprhoov_12	8.58	10.01	-1.43	15.4%	7.92
lprken_1	1.64	1.43	0.21	13.6%	1.45
lprken_2	1.61	1.23	0.38	26.7%	1.25
lprken_3	1.55	1.19	0.36	26.4%	1.20
lprken_4	3.21	1.37	1.84	80.2%	1.39
lprken_5	3.32	2.44	0.88	30.6%	2.48
lprken_6	2.45	1.77	0.68	32.2%	1.79
lprken_7	1.5	1.15	0.35	26.6%	1.16
lprken_8	1.54	1.28	0.27	18.8%	1.29
lprken_9	2.8	2.17	0.63	25.4%	2.20
lprken_10	3.07	2.27	0.80	30.2%	2.30
lprken_11	3.21	2.20	1.01	37.5%	2.23
lprken_12	3.71	2.38	1.33	43.7%	2.42
springq_1	20	6.92	13.08	97.2%	n/a
springq_3	18	5.99	12.01	100.1%	n/a

Explanation:
Name = target name assigned by PEST
Observed base flow value = measured value at target
Modeled base flow value = simulated value at target
Difference = observed value – calibration value
Relative percent difference = (difference/observed value) *100

Name	Observed Baseflow Value (CFS)	Modeled Baseflow Value (CFS)	Difference (CFS)	Relative percent difference (%)	Modeled Baseflow Value Following Minor Model Revisions After Review (CFS)
springq_4	15.1	5.99	9.11	86.4%	n/a
springq_5	13.5	6.90	6.60	64.7%	n/a
springq_6	9.94	6.43	3.51	43.0%	n/a
springq_7	12.7	6.03	6.67	71.2%	n/a
springq_8	12.1	5.82	6.28	70.1%	n/a
springq_9	15.8	6.43	9.37	84.3%	n/a
springq_10	13.6	6.39	7.21	72.1%	n/a
springq_11	13.5	6.30	7.20	72.8%	n/a
springq_12	14.9	6.40	8.50	79.8%	n/a
bearq_10	12.7	9.55	3.151968	28.3%	n/a
ditch2_1	6.28	6.65	-0.371968	5.8%	n/a
ditch2_2	5.86	5.95	-0.092778	1.6%	n/a
ditch2_3	6.49	5.67	0.817778	13.4%	n/a
ditch2_4	6.91	5.75	1.162894	18.4%	n/a
ditch2_5	8.4	6.96	1.436343	18.7%	n/a
ditch2_6	8.16	6.33	1.832454	25.3%	n/a
ditch2_7	5.82	5.76	0.058889	1.0%	n/a
ditch2_8	5.28	5.60	-0.320231	5.9%	n/a
ditch2_9	6.53	6.43	0.104074	1.6%	n/a
ditch2_10	6.81	6.54	0.265324	4.0%	n/a
ditch2_11	6.51	6.40	0.105486	1.6%	n/a
ditch2_12	6.48	6.60	-0.122662	1.9%	n/a

Appendix 5E. Calibration tables: TRANSIENT RECHARGE MULTIPLIERS

Stress Period	SWB Mean Recharge (inches)	Estimated Recharge Multiplier (unitless)	Adjusted Mean Recharge (inches)
3	1.47	0.25	0.37
4	4.43	0.25	1.11
5	1.21	3.61	4.35
6	0.73	0.59	0.43
7	0.01	1.45	0.02
8	0.43	2.36	1.01
9	1.45	2.44	3.53
10	0.63	2.26	1.42
11	0.58	1.43	0.83
12	1.44	1.04	1.50
Annual Total	**12.38**	**1.18**	**14.55**

Explanation:

Stress period = model stress period (no recharge in stress periods 1 and 2)

SWB mean recharge = mean recharge over model domain predicted by SWB model for indicated stress period

Estimated recharge multiplier = model-wide multiplier for stress period

Adjusted mean recharge = final mean recharge over model domain for indicated stress period

Appendix 6. Parameter sensitivity and identifiability

In the history-matching process, the change of observation values in response to changes in parameters, known as the sensitivity of observations to parameters, is used to define the magnitude and directions of changes in candidate parameter values from iteration to iteration. The Jacobian matrix is a matrix of these sensitivity values relating each observation to each parameter. The Jacobian matrix is defined as:

$$\frac{\partial \mathbf{y}_i}{\partial \boldsymbol{p}_j} \cong \frac{g(\mathbf{p}_j + \boldsymbol{\Delta p}) - g(\mathbf{p}_j)}{\boldsymbol{\Delta p}}$$

where

y is an observation

p is a parameter value

*g(**x**)* is the model outcome corresponding to observation time and location **y**

i is a dummy variable in [1,…,NOBS];

j is a dummy variable in [1,…,NPAR];

NOBS is the number of observations;

NPAR is the number of parameters; and

Δ**p** is a small (10%) increment in parameter value.

The result of evaluating this equation for all combinations of parameters and observations is the NOBS * NPAR Jacobian matrix **X**. Beyond its use in the history-matching algorithm, sensitivity can provide insight into which parameters have the greatest impact on forecasts made by the model. In fact, sensitivity can be considered as one metric of parameter importance. A challenge is encountered in that parameters are often correlated with one another, so sensitivity can be misleading if thought of as the only measure of parameter importance. Correlation is evaluated in pairs of parameters so with hundreds or thousands of parameters it is impractical to deconvolve sensitivity from correlation. Identifiability addresses this issue because it is based on singular value decomposition (SVD) (described in appendix 3), which splits information content among correlated parameters. For this reason, we focus on identifiability here.

By virtue of using SVD for parameter estimation, it is also possible to calculate identifiability (Doherty and Hunt, 2009). This is a qualitative metric that indicates how much information from the observations (taken as a whole set) is projected onto the parameters in the history-matching process. Based on a singular value cutoff, the identifiability value calculates the projection of information from observations onto the calibration space. The remaining information is projected onto the null space, meaning parameter values can change, potentially by large amounts, without impacting the model outputs of interest.

Parameters with high identifiability are interpreted to be well-informed by the observations, while parameters with low identifiability are interpreted to be ill-informed by the observations and are generally held relatively constant in the history-matching process. Identifiability values are normalized to a maximum value of 1.0. In this report, we explore the identifiability of parameters for the steady-state model. The reason for this is that the transient model has few parameters whereas the steady state represents the tradeoffs among hydraulic conductivity, recharge, and stream parameters. The lower number of parameters in the transient model is due to holding hydraulic conductivity and stream parameters constant in the transient calibration. Figure 1 presents the identifiability of all parameters with values greater than 0.5. In the figure, the overall height of each bar indicates its identifiability on a normalized scale of 0.0, where the parameter is not informed by the observations, to 1.0, where the parameter is fully informed by the observations.

By definition, if all singular values are considered, all identifiability values will be equal to 1.0. The identifiability value quantifies the projection of observation information onto the solution space of the parameters as defined by an SVD cutoff. As more singular values are considered to be part of the solution space, fewer are in the null space, and the amount of projection onto solution space increases. The SVD cutoff for the parameters shown in figure 1 is 80, which is the number of SVD-Assist (SVDA) super parameters used in this model. In addition to the 80 singular-value cutoff, a stability criterion was used to enforce a threshold on how many of those super parameters were considered part of the solution space. For each parameter, higher bars on figure 1 indicate the most identifiable parameters. On each bar, however, the contribution to identifiability due to each singular value is displayed which helps to distinguish parameters with similar total identifiability. Hotter colors (reds, oranges, and yellows) indicate identifiability attributable to most-informative singular values (1, 2, and so on), whereas cooler colors (greens and blues) indicate identifiability attributable to the least-informative singular values (78, 79, 80). This spectrum is displayed to highlight that no particular singular-value cutoff is the perfect definition of separating the solution

space from the null space, but bars that are made up almost entirely of hot colors can be qualitatively interpreted to have overall higher identifiability than those containing cooler colors. To avoid plotting bars for all parameters, only those with identifiability (at 80 singular values) greater than 0.5 are displayed on figure 1.

Identifiability is a qualitative metric and should not be over-interpreted; it can, however, provide insight into important model behavior. In a qualitative sense, parameters with high identifiability can be interpreted as important controls on model behavior. The two parameters with the highest identifiability are rm1 and sfrc, which are the recharge multiplier and streambed hydraulic conductivity, respectively. These two parameters are the main controls on overall water balance into the model and the connection to streams. The Little Plover River flow observations are the most important and highly weighted observations in the model, so it follows that the parameters controlling water exchange with the stream and overall water available in the model should be the most important. The remaining parameters with identifiability > 0.5 are horizontal hydraulic conductivity parameters—a mixture of homogeneous zones and pilot points. This highlights the importance of lateral distribution of groundwater to supply the streams and also to maintain a head surface honoring head observations. Vertical hydraulic conductivity values are less identifi-

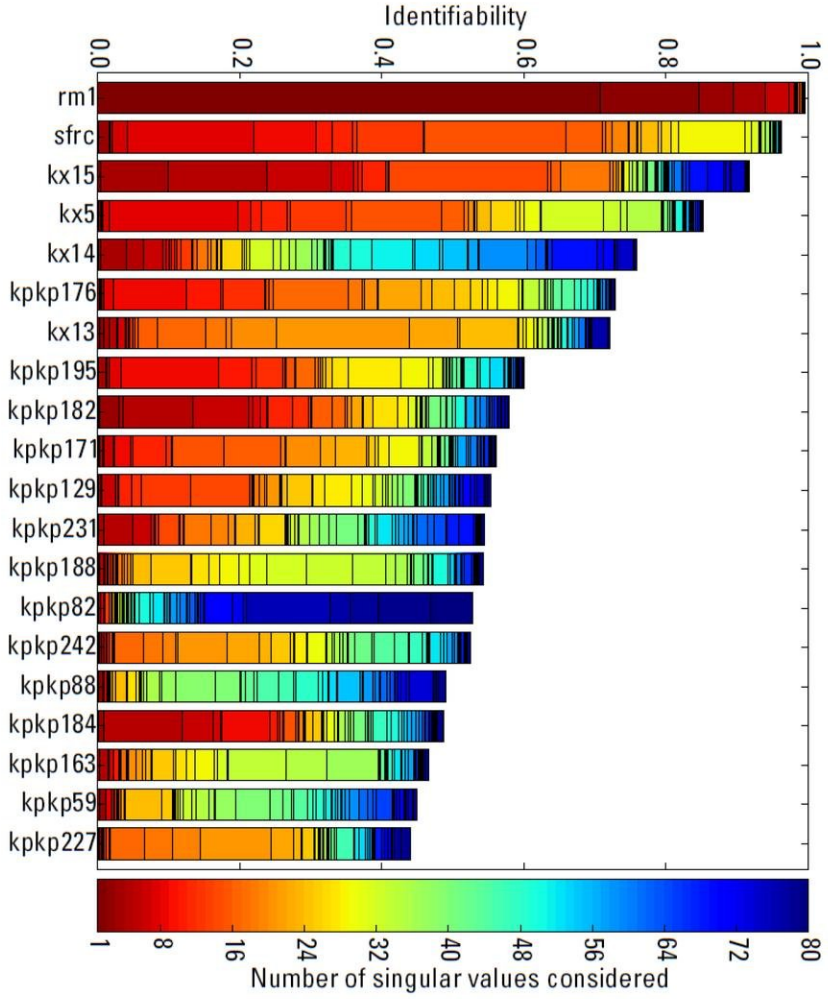

Figure 1. Identifiability of parameters. Set includes only those with identifiability (at 80 singular values) greater than 0.5. The color scale indicates identifiability for each singular value.

Appendix 7. Constrained-optimization example

Constrained optimization is an approach to management of water use by using a groundwater flow model. In this context, groundwater pumping rates are adjusted to meet an optimal condition, subject to a set of constraints. For example, the optimal condition may be to maximize pumping subject to the constraint of maintaining a specified flow rate in a stream. Or, if streamflow is already lower than a constraint value, we can minimize the reduction in pumping necessary to achieve streamflow at or above the constraint value.

This approach uses the mathematical technique of linear programming to solve the constrained minimization/maximization problem. Details of the implementation in MODFLOW and of the algorithm are available in Ahlfeld and others (2005) and references within.

Setting a constraint

A potential management scenario was set up to evaluate potential uses of MODFLOW-GWM in the Little Plover River area. This scenario is based on using the steady state model for 2013 and the public rights baseflow value at the Eisenhower gage as a constraint. The steady-state model is conservative with respect to streamflow and is more efficient to use for optimization. A similar approach can be extended to the transient model explicitly, but at a higher computational cost beyond the scope of this proof-of-concept. While multiple constraints can be evaluated at once, Eisenhower was chosen for evaluation both to simplify interpretation to a single constraint and because the Eisenhower gage is the only location on the Little Plover River with continuous streamflow measurements. The public rights flow value is 4.0 cubic feet per second (cfs) with a corresponding baseflow value of 80 percent or 3.2 cfs. In 2013, the measured baseflow at Eisenhower was 1.95 cfs and the optimal modeled value was 2.09 cfs, below the public rights baseflow value. To achieve flow at or above the public rights baseflow value, one management option to explore is to minimize the reduction of existing pumping required to achieve the public rights baseflow. The deficit in flow is 1.11 cfs or 498 gpm. Based on the depletion-potential calculations described in the Example 3: Depletion-Potential Mapping section of the main report, only wells with depletion potential (relative to the Eisenhower gage) greater than 0.25 were included as managed wells. Wells with depletion potential less than 0.25 obtain 75 percent of the water they extract from surface water features other than the Eisenhower gage on the Little Plover River. As a result, they are not considered in the management with respect to the Little Plover.

Decision variables

To meet the constraint, pumping in wells is adjusted to minimize the reduction in pumping. Managing each well individually is computationally expensive and also results in numerical instability as the response due to a single well may be small. As a result, most optimization efforts group wells into "decision variables," or groups of wells to manage as a unit. Several approaches to grouping the pumping wells into decision variables were explored, including:

- Using a single decision variable with all wells in it. This applies the same reduction to each well in the area equally, regardless of depletion potential.
- Create groups based on clustering analysis (discussed below) and apply the same reduction to each well within a group.
- For each clustering scenario, we can either limit the reduction in pumping (for example, no single group or well can reduce its pumping rate more than 35 percent) or we can allow groups to be reduced by 100 percent (in other words, be completely shut off).

Table 1 outlines the names of the scenarios evaluated and shows the total amount of pumping reported for the managed wells in each scenario and the amount of reduction required to meet the public rights baseflow constraint. The following sections further define and present the results of each of these approaches.

Single-decision variable

Applying the same reduction to all wells in the management group is one concept of an equitable solution, spreading the change to water consumption equally among all wells in the area. However, this does not account for the fact that not all wells impact the stream equally. As a result, it is expected that more reduction will be required in aggregate than more flexible approaches. The total pumping without optimization for the 75 managed wells was 4,527 gpm. At this level of pumping, the flow rate at Eisenhower is 1.11 cfs lower than the constraint value of 3.2 cfs. This is a deficit in flow of 498 gpm. The reduction in pumping required (if applied evenly across all wells) to maintain streamflow at the constraint value of 3.2 cfs, however, is 1,356 gpm. Spread evenly across all managed wells, this represents a reduction of 30 percent applied to each well. When apportioning the same reduction among

Table 1. Percent reduction targets

Scenario	Number of clusters	Max. reduction permitted per group (%)	Baseline base pumping (gpm)	Reduction in pumping (gpm)	Percent reduction (%)
Single-decision variable	1	100	4,527	1,356	30
35% max reduction	20	35	4,527	1,155	26
100% max reduction	20	100	4,527	908	20
35% max reduction, non-irrigation separate	20	35	4,477	1,192	27
100% max reduction, non-irrigation separate	20	100	4,477	883	20

all wells, some wells that are far from the gage with relatively low depletion potential must reduce by the same amount as wells that are much closer with higher depletion potential. Clearly, while the burden of pumping reduction throughout the basin is borne equally in a sense, the overall reduction of pumping in the basin is high. By managing smaller groups and focusing on wells with higher depletion potential, the deficit in flow can be made up with an overall lower reduction in pumping from the whole basin. Both the overall reduction in pumping throughout the basin is expected to be lower, and the burden is focused on fewer wells that have the most impact rather than requiring all wells in the area to have reduced flow. Both approaches can be interpreted as fair by different criteria.

Cluster analysis

Dividing the entire set of wells into management groups can be done in many ways. Of course, issues such as property ownership and crop value should be taken into consideration when creating groups as decision variables. To illustrate the general characteristics of the methods available, however, we looked for a systematic way to make groups and settled on cluster analysis.

K-means clustering (Ahlfeld and others, 2005; Hastie and others, 2009) is a cluster-analysis technique where wells are grouped into k groups (determined by the user) such that the sum of their numerical attributes is minimized. If those numerical attributes are x-coordinate, y-coordinate, and depletion potential, the result is groups of wells that are located near each other and have similar depletion potential values.

Using the depletion potential values calculated for wells that were actively pumped in 2013 and with depletion potential greater than 0.25, a set of clusters was generated with 20 clusters. The number of clusters was chosen as illustrative and other numbers could be implemented easily. Additionally, two variants of this group were generated—one with all wells grouped into clusters, and another with non-irrigation wells managed as individual decision variables and groups made up only of irrigation wells. Figure 1 shows the 20-cluster arrangement created with k-means clustering. Figure 2 shows the 20-cluster arrangements with non-irrigation wells managed individually (the non-irrigation wells are assigned values 20 and greater). For non-irrigation wells, if the reported pumping rate was less than 75 gpm in the steady-state model for 2013, the well was left out of the management scenario to limit the number of decision variables. Such a limitation was not used for the other scenarios as the wells with lower pumping rates were incorporated into groups.

In addition to grouping wells into decision variables, a decision must be made regarding how much pumping can be reduced in each decision variable to meet the constraint. We evaluated two cases: one where the maximum reduction was 35 percent, and another where the maximum reduction was 100 percent.

Table 1 outlines the scenarios showing the various combinations of the number of groups (including cases where non-irrigation wells were managed separately) and the maximum pumping reduction allowed. In the following sections, the results of these scenarios are presented and discussed.

20 clusters

In these two scenarios, k-means clustering was used to define 20 groups for management and the maximum pumping reduction allowed in each group was set at either 35 percent and 100 percent. In other words, in the 35% Max Reduction scenario, no pumping reduction for a group was allowed to drop by more than 35

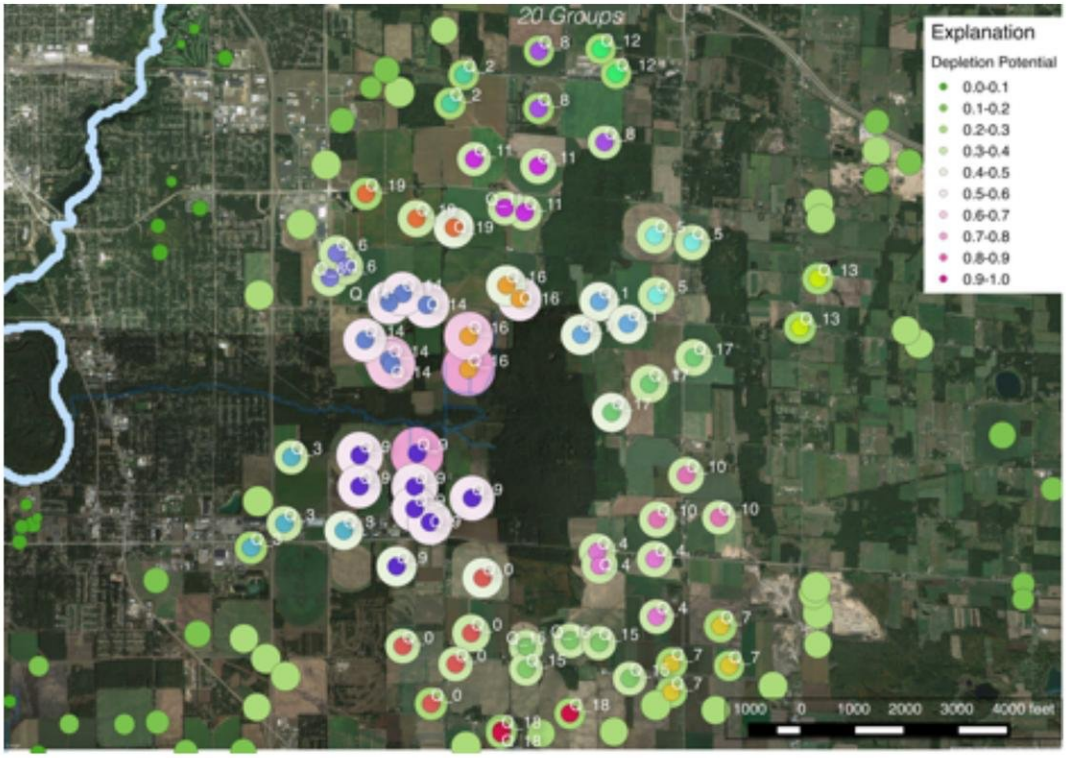

Figure 1. Arrangement of wells into 20 clusters.

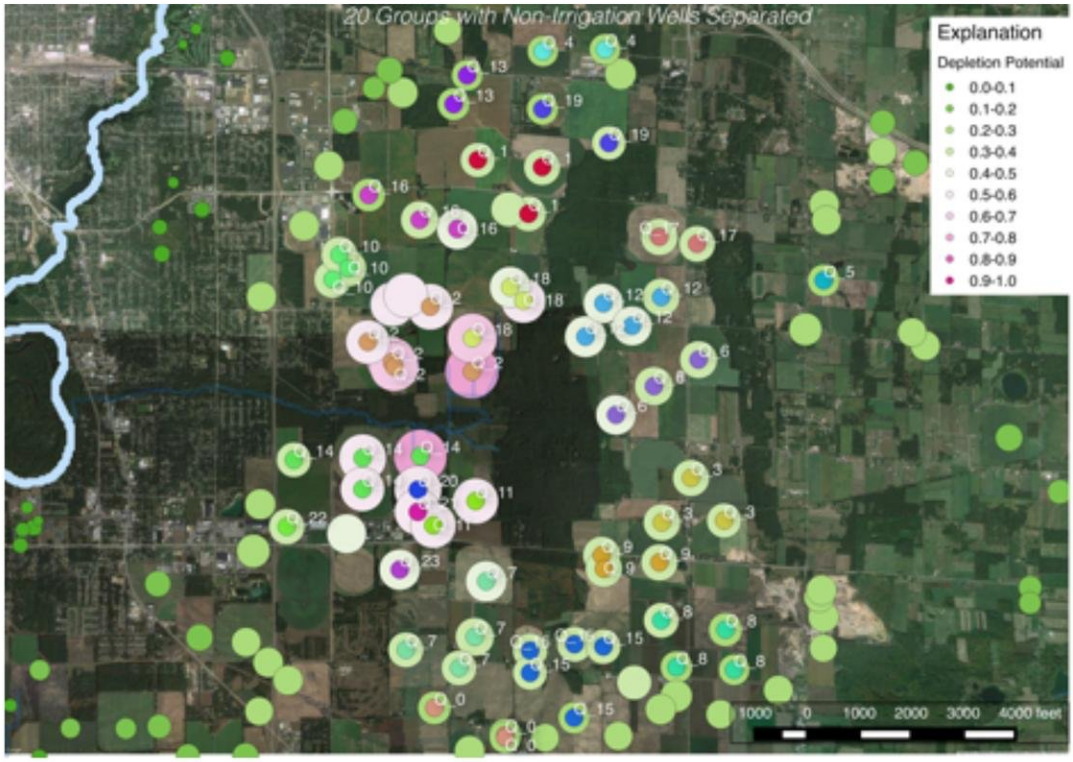

Figure 2. Arrangement of wells into 20 clusters with non-irrigation wells kept separate.

percent. In the 100% Max Reduction scenario, groups were allowed to be completely turned off, thus simulating a more binary response with wells either on or off. Figures 3 and 4 show the amount and locations of pumping that must be reduced to maintain the constraint of the public rights baseflow at the Eisenhower gage. Table 1 highlights the overall percent reduction in pumping required over the entire set of managed wells. Relative to the first scenario with all wells subject to the same level of reduction (single-decision variable), the subdivided (grouped) scenarios are more efficient, requiring about 5–10 percent less reduction to meet the constraint. The 35% Max Reduction scenario requires an overall reduction in pumping of 1,155 gpm while the 100% Max Reduction scenario required an overall reduction of 908 gpm. This efficiency is realized by focusing the reduction on wells with the highest depletion potential. Wells with lower depletion potential are obtaining water from sources other than the Eisenhower gage, so reducing their pumping is a less-efficient way to increase flow at the gage. Indeed, a similar difference is related to the maximum amount of reduced pumping allowed. For the 100% Max Reduction scenario, the constraint can be met by turning off wells that are closest to the gage (highest depletion potential). However, if the reduction is limited to 35 percent, the constraint can only be met by also reducing pumping in wells with lower depletion potential in addition to wells with highest depletion potential, thus the overall reduction in pumping is higher (25.5 percent vs. 20.1 percent).

20 clusters, nonirrigation wells separate

These two scenarios are the same as the previous two with the exception that non-irrigation wells were not considered as part of the k-means clustering process and individual non-irrigation wells with a pumping rate less than 75 gpm were not managed. Table 1 shows that overall reduction in pumping required is similar to the 20 cluster scenarios. Figures 5 and 6 graphically show the amount and locations of pumping that must be reduced to maintain the constraint at the Eisenhower gage with maximum allowable reduction at a single well of 35 percent and 100 percent, respectively. The results with non-irrigation wells managed separately are similar to the previous cases—particularly for the maximum reduction of 35 percent. The 35% Max Reduction Non-Irrigation

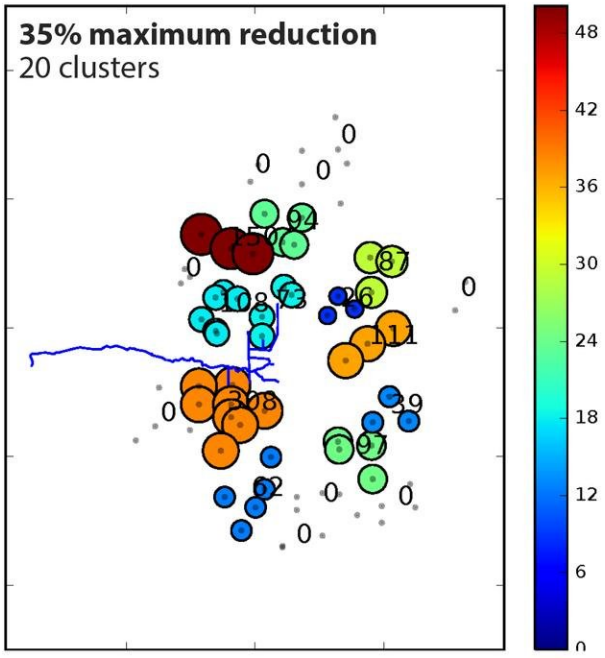

Figure 3. Optimal rates of pumping reduction for 20 clusters, constrained to meeting the public rights baseflow at Eisenhower, when maximum allowable flow reduction is 35 percent.

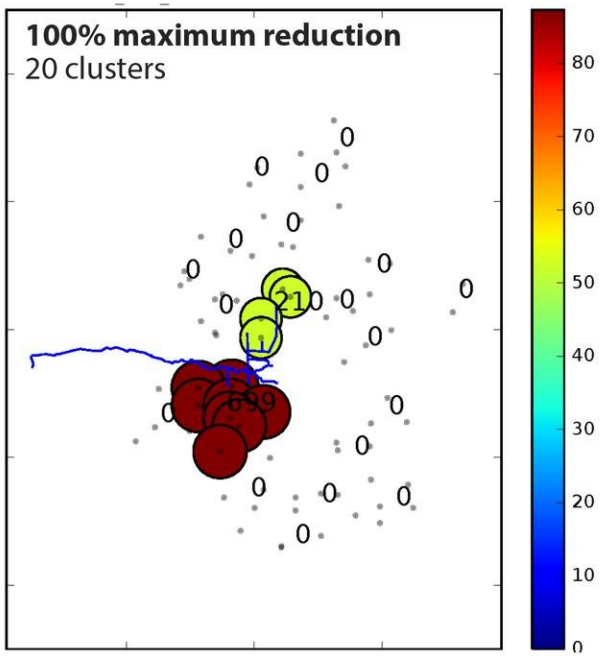

Figure 4. Optimal rates of pumping reduction for 20 clusters, constrained to meeting the public rights baseflow at Eisenhower, when maximum allowable flow reduction is 100 percent.

Separate scenario and the 100% Max Reduction variant require total reduction in pumping of 1,192 gpm and 883 gpm, respectively. The patterns observed in figures 3 and 5 and are similar, although in figure 5, where non-irrigation wells are separated out, greater reduction is achieved in some individual wells, which shifts the pattern of pumping reduction around. In the 100% Max Reduction case, the patterns are more distinct because the flexibility of more management groups (because some non-irrigation wells are pulled out from groups south of the river) allows for focused reductions. The main difference here is that urban or industrial wells are not expected to be managed by the same entities as irrigation wells. Separating out the groups allows decisions variables to be composed of wells that are more likely managed similarly with one another and by consistent managers.

Conclusions

Constrained optimization is a powerful tool to objectively adjust well pumping to meet a constraint of streamflow. Wells are managed such that the most impactful wells—those with the highest depletion potential—are targeted for reduction so the streamflow constraint is maintained with the least amount of reduction possible. The arrangement of decision variables, either grouping all wells into one or splitting into smaller groups using cluster analysis or other techniques, has profound ramifications both on how much each well is affected, and how much total reduction in pumping is required.

In managing a basin, stakeholders and decision makers must determine a concept of fairness to apply. Requiring each well to reduce by the same percent spreads the burden throughout the managed wells, but results in many more wells being reduced and a less efficient allocation of that reduction than when smaller groups are managed. However, at the other extreme, if individual wells or small groups of them are allowed to reduce by 100 percent, some wells will shoulder all of the burden while others will not be affected at all. As a basin, mechanisms to compensate the most impacted users would need to be developed which is beyond the scope of this work.

References

Ahlfeld, D. P., Barlow, P. M., and Mulligan, A.E., 2005, GWM—A groundwater management process for the U.S. Geological Survey modular groundwater model (MODFLOW–2000): U.S. Geological Survey Open-File Report 2005-1072, 124 p.

Hastie, T., Tibshirani, R., and Friedman, J.H., 2009, The elements of statistical learning: Data mining, inference, and prediction: New York, Springer, Springer Series in Statistics, 745 p.

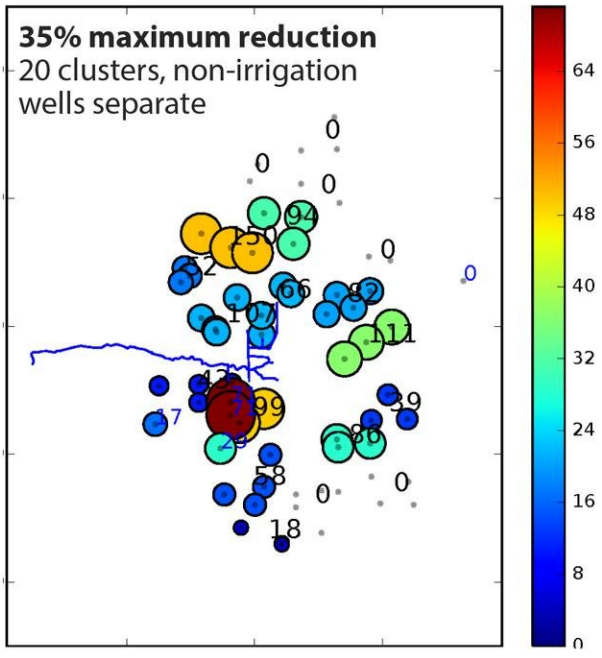

Figure 5. Optimal rates of pumping reduction for 20 clusters, constrained to meeting the public rights baseflow at Eisenhower, when maximum allowable flow reduction is 35 percent. Non-irrigation wells managed individually.

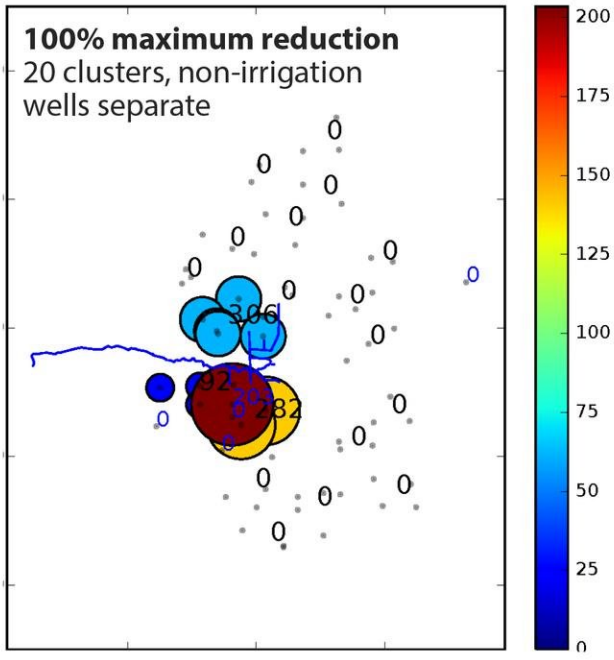

Figure 6. Optimal rates of pumping reduction for 20 clusters, constrained to meeting the public rights baseflow at Eisenhower, when maximum allowable flow reduction is 100 percent. Non-irrigation wells managed individually.

Appendix 8. Depletion-potential mapping

This appendix presents detailed results of depletion potential mapping, as discussed in the main report. Below, each sheet is listed with a brief description of its contents.

	Sheet Name	Description
A	PercentReduction	Summary of required pumping reduction to restore flow in the Little Plover at Eisenhower to the public rights baseflow, as determined by the steady state model and optimzition using MODFLOW-GWMVI
B	ReductionRankHoover	Well locations ranked by depletion potential from highest to lowest, as calculated with respect to the Hoover gage using both the steady-state and transient models. Note that only wells with depletion potential greater than 0.25 are listed
C	ReductionRankHoover2014	Well locations ranked by depletion potential from highest to lowest, as calculated with respect to the Hoover gage using only the transient model.
D	SS_OneOut	Modeled recovery of baseflow in the Little Plover River as pumping wells are succesively set to a pumping rate of 0, using the steady state model, starting with the highest depletion potential and moving down the ranks of depletion potential
E	Trans_OneOut_Kennedy	Modeled recovery of baseflow in the Little Plover River at the Kennedy gage as pumping wells are succesively set to a pumping rate of 0, using the transient model, starting with the highest depletion potential and moving down the ranks of depletion potential
F	Trans_OneOut_Eisenhower	Modeled recovery of baseflow in the Little Plover River at the Eisenhower gage as pumping wells are succesively set to a pumping rate of 0, using the transient model, starting with the highest depletion potential and moving down the ranks of depletion potential
G	Trans_OneOut_I39	Modeled recovery of baseflow in the Little Plover River at the I39 gage as pumping wells are succesively set to a pumping rate of 0, using the transient model, starting with the highest depletion potential and moving down the ranks of depletion potential

H	Trans_OneOut_Hoover	Modeled recovery of baseflow in the Little Plover River at the Hoover gage as pumping wells are succesively set to a pumping rate of 0, using the transient model, starting with the highest depletion potential and moving down the ranks of depletion potential

Appendix 8a. Depletion-potential mapping: PERCENT REDUCTION

Summary of required pumping reduction to restore flow in the Little Plover at Eisenhower to the public rights baseflow, as determined by the steady state model and optimzition using MODFLOW-GWMVI

Scenario	Number of Clusters	Maximum Reduction Permitted per Group (%)	Baseline Base Pumping (gpm)	Reduction in Pumping (gpm)	Percent Reduction
LPR_Eisenhower1_100_bnd.reduce	1	100	4,527	1,356	30%
LPR_Eisenhower20_35_bnd.reduce	20	35	4,527	1,155	26%
LPR_Eisenhower20_100_bnd.reduce	20	100	4,527	908	20%
LPR_Eisenhower20_35_irr.reduce	20	35	4,477	1,192	27%
LPR_Eisenhower20_100_irr.reduce	20	100	4,477	883	20%
LPR_Eisenhower50_35_bnd.reduce	50	35	4,527	1,216	27%
LPR_Eisenhower50_100_bnd.reduce	50	100	4,527	884	20%
LPR_Eisenhower50_35_irr.reduce	50	35	4,477	1,209	27%
LPR_Eisenhower50_100_irr.reduce	50	100	4,477	915	20%

Appendix 8b. Depletion-potential mapping: REDUCTION RANK HOOVER

Well locations ranked by depletion potential from highest to lowest, as calculated with respect to the Hoover gage using both the steady-state and transient models. Note that only wells with depletion potential greater than 0.25 are listed

	2013 Steady State			2014 Transient		
Rank	Row	Column	Depletion Potential	Row	Column	Depletion Potential
1	588	429	0.857	588	429	0.857
2	550	452	0.846	550	452	0.846
3	546	416	0.839	546	416	0.839
4	589	403	0.813	589	403	0.813
5	548	417	0.796	548	417	0.796
6	535	452	0.762	535	452	0.762
7	537	405	0.761	537	405	0.761
8	520	416	0.731	520	416	0.731
9	603	403	0.728	603	403	0.728
10	613	428	0.725	613	428	0.725
11	521	433	0.718	521	433	0.718
12	590	372	0.715	590	372	0.715
13	603	428	0.710	603	428	0.710
14	619	435	0.694	619	435	0.694
15	516	422	0.692	516	422	0.692
16	608	454	0.639	521	419	0.677
17	509	389	0.629	608	454	0.639
18	518	475	0.625	509	389	0.629
19	623	396	0.617	518	475	0.625
20	620	369	0.607	623	396	0.617
21	639	420	0.598	620	369	0.607
22	498	392	0.582	639	420	0.598
23	504	396	0.581	498	392	0.582
24	486	445	0.578	504	396	0.581
25	644	459	0.567	486	445	0.578
26	610	357	0.545	644	459	0.567
27	517	357	0.542	642	403	0.554
28	631	354	0.530	610	357	0.545
29	669	454	0.522	517	357	0.542
30	534	503	0.520	662	436	0.535
31	512	469	0.514	649	396	0.532
32	482	428	0.510	631	354	0.530
33	519	511	0.497	631	354	0.530
34	569	517	0.494	669	454	0.522
35	529	524	0.488	534	503	0.520
36	556	534	0.468	512	469	0.514
37	675	423	0.455	482	428	0.510
38	632	511	0.450	519	511	0.497
39	544	554	0.445	569	517	0.494
40	489	536	0.444	529	524	0.488
41	458	483	0.443	484	402	0.486
42	635	537	0.441	556	534	0.468
43	516	537	0.440	675	423	0.455
44	471	405	0.437	632	511	0.450
45	683	447	0.436	544	554	0.445
46	617	538	0.435	489	536	0.444
47	485	376	0.428	458	483	0.443
48	638	512	0.428	635	537	0.441
49	492	553	0.424	516	537	0.440
50	672	499	0.422	471	405	0.437
51	597	551	0.413	683	447	0.436
52	661	538	0.410	617	538	0.435
53	675	479	0.409	485	376	0.428
54	689	526	0.406	638	512	0.428
55	673	512	0.406	492	553	0.424
56	455	454	0.402	672	499	0.422
57	701	436	0.399	597	551	0.413
58	685	479	0.396	661	538	0.410
59	479	477	0.389	675	479	0.409
60	447	513	0.384	689	526	0.406
61	681	361	0.384	673	512	0.406
62	665	567	0.384	523	557	0.406
63	477	468	0.381	455	454	0.402

8b. ReductionRankHoover

	2013 Steady State			2014 Transient		
Rank	Row	Column	Depletion Potential	Row	Column	Depletion Potential
64	616	566	0.379	701	436	0.399
65	672	351	0.377	685	479	0.396
66	713	468	0.376	479	477	0.389
67	458	387	0.371	447	513	0.384
68	430	443	0.369	681	361	0.384
69	689	370	0.366	665	567	0.384
70	728	410	0.359	477	468	0.381
71	425	420	0.345	616	566	0.379
72	703	357	0.344	519	605	0.378
73	695	545	0.341	672	351	0.377
74	714	468	0.341	713	468	0.376
75	705	499	0.338	458	387	0.371
76	530	602	0.337	430	443	0.369
77	417	449	0.336	689	370	0.366
78	682	545	0.335	728	410	0.359
79	670	330	0.333	425	420	0.345
80	727	437	0.332	703	357	0.344
81	405	511	0.331	695	545	0.341
82	508	610	0.331	714	468	0.341
83	380	509	0.328	705	499	0.338
84	432	483	0.328	530	602	0.337
85	646	311	0.328	417	449	0.336
86	416	518	0.323	682	545	0.335
87	720	452	0.323	670	330	0.333
88	406	483	0.322	727	437	0.332
89	683	571	0.318	405	511	0.331
90	659	611	0.314	508	610	0.331
91	701	538	0.308	380	509	0.328
92	650	609	0.306	432	483	0.328
93	728	397	0.302	646	311	0.328
94	647	610	0.299	416	518	0.323
95	692	591	0.290	720	452	0.323
96	752	454	0.285	406	483	0.322
97	474	610	0.284	683	571	0.318
98	723	351	0.283	741	424	0.318
99	537	656	0.281	659	611	0.314
100	703	565	0.273	701	538	0.308
101	735	559	0.271	650	609	0.306
102	736	572	0.268	698	598	0.305
103	481	611	0.266	728	397	0.302
104	397	440	0.265	647	610	0.299
105	741	458	0.264	506	605	0.299
106	741	398	0.262	692	591	0.290
107	738	599	0.261	752	454	0.285
108	713	519	0.261	474	610	0.284
109	438	394	0.260	723	351	0.283
110	531	650	0.260	537	656	0.281
111	450	636	0.260	703	565	0.273
112	415	414	0.258	735	559	0.271
113	747	546	0.258	736	572	0.268
114	714	486	0.256	481	611	0.266
115	776	502	0.256	397	440	0.265
116	776	502	0.256	741	458	0.264
117	774	456	0.256	741	398	0.262
118	774	456	0.256	738	599	0.261
119	767	452	0.255	713	519	0.261
120	786	546	0.255	744	504	0.261
121	783	467	0.254	438	394	0.260
122	798	532	0.253	531	650	0.260
123	760	438	0.253	450	636	0.260
124	376	472	0.253	415	414	0.258
125				747	546	0.258
126				714	486	0.256
127				776	502	0.256
128				776	502	0.256
129				774	456	0.256
130				774	456	0.256
131				767	452	0.255
132				786	546	0.255

8b. ReductionRankHoover

	2013 Steady State			2014 Transient		
Rank	Row	Column	Depletion Potential	Row	Column	Depletion Potential
133				748	559	0.255
134				783	467	0.254
135				798	532	0.253
136				760	438	0.253
137				376	472	0.253

Appendix 8c. Depletion-potential mapping:
REDUCTION RANK HOOVER 2014

All well locations ranked by depletion potential from highest to lowest, as calculated with respect to the Hoover gage using only the transient model.

Rank	Row	Column	Depletion Potential 2014
1	588	429	0.856962
2	550	452	0.846206
3	546	416	0.83895
4	589	403	0.813303
5	548	417	0.796153
6	535	452	0.761944
7	537	405	0.761178
8	520	416	0.730675
9	603	403	0.727866
10	613	428	0.724566
11	521	433	0.717947
12	590	372	0.714972
13	603	428	0.709666
14	619	435	0.693541
15	516	422	0.691794
16	521	419	0.676631
17	608	454	0.639119
18	509	389	0.629181
19	518	475	0.625253
20	623	396	0.617272
21	620	369	0.606938
22	639	420	0.597759
23	498	392	0.582053
24	504	396	0.581269
25	486	445	0.578403
26	644	459	0.566709
27	642	403	0.554069
28	610	357	0.545325
29	517	357	0.541619
30	662	436	0.5352
31	649	396	0.531644
32	631	354	0.529625
33	631	354	0.529625
34	669	454	0.522006
35	534	503	0.520084
36	512	469	0.513631
37	482	428	0.510122
38	519	511	0.496513
39	569	517	0.493928
40	529	524	0.488438
41	484	402	0.485797
42	556	534	0.46795
43	675	423	0.455178
44	632	511	0.450159
45	544	554	0.444769
46	489	536	0.444481
47	458	483	0.443069
48	635	537	0.440566
49	516	537	0.439994
50	471	405	0.436953
51	683	447	0.436225
52	617	538	0.434656
53	485	376	0.428494
54	638	512	0.427953
55	492	553	0.424356
56	672	499	0.422494
57	597	551	0.413031
58	661	538	0.410366
59	675	479	0.408506
60	689	526	0.406253
61	673	512	0.405703

8c. ReductionRankHoover2014

Rank	Row	Column	Depletion Potential 2014
62	523	557	0.405531
63	455	454	0.402366
64	701	436	0.398697
65	685	479	0.396041
66	479	477	0.389481
67	447	513	0.384491
68	681	361	0.384328
69	665	567	0.383816
70	477	468	0.38105
71	616	566	0.378934
72	519	605	0.378359
73	672	351	0.376944
74	713	468	0.376384
75	458	387	0.37115
76	430	443	0.3694
77	689	370	0.366428
78	728	410	0.3592
79	425	420	0.344706
80	703	357	0.343616
81	695	545	0.341334
82	714	468	0.341209
83	705	499	0.338294
84	530	602	0.337334
85	417	449	0.335637
86	682	545	0.335181
87	670	330	0.333044
88	727	437	0.332081
89	405	511	0.331003
90	508	610	0.330594
91	380	509	0.328197
92	432	483	0.327738
93	646	311	0.327663
94	416	518	0.322822
95	720	452	0.322809
96	406	483	0.322156
97	683	571	0.31765
98	741	424	0.317634
99	659	611	0.313831
100	701	538	0.308188
101	650	609	0.306381
102	698	598	0.305337
103	728	397	0.3023
104	647	610	0.299178
105	506	605	0.299059
106	692	591	0.29
107	752	454	0.28515
108	474	610	0.283737
109	723	351	0.283459
110	537	656	0.280788
111	703	565	0.273275
112	735	559	0.271331
113	736	572	0.267669
114	481	611	0.265916
115	397	440	0.265431
116	741	458	0.264025
117	741	398	0.261809
118	738	599	0.261163
119	713	519	0.2608
120	744	504	0.260625
121	438	394	0.260266
122	531	650	0.259781
123	450	636	0.259578
124	415	414	0.2582
125	747	546	0.257991
126	714	486	0.256353
127	776	502	0.256225
128	776	502	0.256225

8c. ReductionRankHoover2014

Rank	Row	Column	Depletion Potential 2014
129	774	456	0.255531
130	774	456	0.255531
131	767	452	0.255291
132	786	546	0.254919
133	748	559	0.254656
134	783	467	0.254088
135	798	532	0.253425
136	760	438	0.252819
137	376	472	0.252625
138	578	694	0.248844
139	755	371	0.247175
140	710	312	0.246894
141	797	513	0.246787
142	733	618	0.245625
143	673	611	0.244016
144	775	379	0.242719
145	775	379	0.242719
146	723	325	0.238591
147	757	520	0.237444
148	756	592	0.234884
149	813	559	0.232444
150	355	512	0.229769
151	839	559	0.228022
152	777	432	0.227881
153	777	432	0.227881
154	704	677	0.227803
155	806	656	0.226603
156	762	421	0.221191
157	750	672	0.220234
158	726	526	0.219688
159	372	473	0.219372
160	463	636	0.211556
161	330	537	0.211194
162	651	703	0.211006
163	774	405	0.207784
164	774	405	0.207784
165	812	546	0.206225
166	713	664	0.205644
167	455	651	0.204569
168	437	636	0.200784
169	786	559	0.199887
170	355	484	0.199591
171	826	559	0.198109
172	842	598	0.197781
173	773	658	0.197341
174	773	658	0.197341
175	602	717	0.195378
176	711	297	0.194513
177	878	546	0.19395
178	685	258	0.191866
179	852	559	0.190697
180	815	585	0.184413
181	828	505	0.183497
182	828	505	0.183497
183	807	452	0.182306
184	357	536	0.182016
185	423	407	0.181725
186	836	512	0.181478
187	850	519	0.180169
188	645	704	0.1799
189	859	651	0.179431
190	339	571	0.179303
191	495	730	0.1783
192	336	449	0.175922
193	751	659	0.175731
194	801	379	0.173806
195	794	399	0.173691

8c. ReductionRankHoover2014

Rank	Row	Column	Depletion Potential 2014
196	864	533	0.172909
197	896	526	0.17195
198	711	272	0.171288
199	825	546	0.170756
200	837	668	0.170166
201	498	312	0.169741
202	896	527	0.167697
203	731	277	0.166722
204	868	599	0.164809
205	652	704	0.164134
206	652	704	0.164134
207	865	644	0.163794
208	841	474	0.162944
209	806	438	0.155963
210	897	526	0.155672
211	897	526	0.155672
212	777	299	0.152475
213	777	299	0.152475
214	783	345	0.149812
215	317	523	0.14965
216	746	979	0.147291
217	877	533	0.146497
218	362	605	0.146481
219	252	696	0.140959
220	315	557	0.140209
221	315	557	0.140209
222	478	330	0.137372
223	859	452	0.136466
224	881	482	0.136444
225	304	537	0.134488
226	486	311	0.134341
227	621	255	0.130137
228	674	198	0.127881
229	289	537	0.124463
230	299	546	0.124156
231	299	523	0.117731
232	731	290	0.115297
233	629	249	0.113956
234	254	565	0.113309
235	652	225	0.112078
236	809	346	0.111772
237	177	515	0.111753
238	849	472	0.110947
239	260	570	0.110816
240	691	225	0.109472
241	474	763	0.109437
242	638	212	0.109009
243	556	748	0.106909
244	750	325	0.106297
245	638	225	0.105234
246	662	194	0.104963
247	410	341	0.104663
248	266	549	0.104547
249	724	258	0.104469
250	807	412	0.103519
251	258	689	0.103487
252	852	444	0.102516
253	673	205	0.102222
254	217	517	0.102119
255	796	278	0.101306
256	158	535	0.101247
257	207	554	0.100822
258	622	250	0.0992219
259	757	172	0.0987906
260	526	795	0.0979125
261	180	575	0.0978906
262	251	538	0.0968281

8c. ReductionRankHoover2014

Rank	Row	Column	Depletion Potential 2014
263	251	695	0.0956313
264	251	695	0.0956313
265	672	186	0.0945
266	189	552	0.0938313
267	303	445	0.0928875
268	472	768	0.0926687
269	821	373	0.0914875
270	293	563	0.0904219
271	789	441	0.0902906
272	679	172	0.0902312
273	156	548	0.0890375
274	316	419	0.0886375
275	796	345	0.0886344
276	478	768	0.0882813
277	232	543	0.0868969
278	763	325	0.0867219
279	803	272	0.0864
280	771	265	0.0853719
281	771	265	0.0853719
282	701	245	0.0844844
283	474	835	0.0836
284	652	172	0.0830594
285	420	736	0.081925
286	255	590	0.08135
287	200	556	0.0805594
288	296	425	0.0785656
289	612	252	0.0777375
290	221	645	0.0763937
291	706	198	0.0735969
292	828	350	0.0732031
293	882	259	0.0720594
294	512	782	0.0718031
295	745	146	0.0711531
296	117	676	0.0703844
297	466	317	0.0685969
298	666	127	0.0682875
299	164	529	0.0681563
300	686	192	0.0659656
301	314	557	0.0643844
302	665	146	0.06335
303	618	257	0.0626156
304	504	289	0.0617438
305	829	299	0.061625
306	692	8	0.0616125
307	835	792	0.061475
308	851	87	0.0609813
309	820	412	0.0600781
310	218	530	0.0580281
311	384	327	0.058025
312	196	512	0.05635
313	512	801	0.0558813
314	789	325	0.0553469
315	665	159	0.0551688
316	397	327	0.054575
317	480	789	0.05385
318	698	166	0.0531
319	679	101	0.0505969
320	383	323	0.0504531
321	886	400	0.05025
322	303	647	0.0486062
323	678	212	0.0468969
324	532	856	0.0448406
325	731	238	0.0446563
326	882	219	0.0440344
327	250	410	0.0437188
328	678	127	0.0436438
329	829	191	0.0417469

8c. ReductionRankHoover2014

Rank	Row	Column	Depletion Potential 2014
330	752	143	0.0407844
331	228	576	0.0397187
332	758	61	0.0385375
333	850	158	0.0370344
334	758	8	0.0370062
335	769	238	0.0363406
336	809	292	0.0348437
337	533	857	0.0344469
338	785	145	0.033525
339	404	321	0.0325594
340	757	225	0.0322281
341	751	192	0.0313906
342	750	245	0.0310188
343	777	192	0.0309656
344	777	192	0.0309656
345	890	146	0.0299563
346	724	219	0.0292281
347	191	529	0.0273063
348	764	1	0.0267781
349	804	258	0.0261375
350	880	377	0.0248969
351	883	246	0.0229094
352	732	146	0.0227875
353	882	192	0.0227844
354	270	415	0.0221156
355	777	218	0.0219594
356	777	218	0.0219594
357	39	592	0.0218813
358	796	198	0.0208469
359	294	680	0.0192281
360	698	206	0.0174531
361	311	399	0.0167781
362	821	386	0.0130594
363	803	218	0.0128594
364	249	776	0.0119344
365	747	978	0.00723125
366	758	159	0.00443437
367	851	88	0.00349375
368	856	245	0.00335937
369	829	272	0.00200937
370	471	830	0.00143438

Appendix 8d. Depletion-potential mapping: STEADY STATE, ONE OUT—FOUR GAGES

Modeled baseflow in the Little Plover River using the steady-state model at the four gages as an increasing number of wells are set to zero pumping, as ranked by depletion potential. The **bold** number indicates modeled flow recovering to above the public rights baseflow values, and the ***bold italic*** number indicates modeled flow recovering to above the public rights flow.

	Kennedy	Eisenhower	I-39	Hoover
Public Rights Flow (cfs)	1.90	4.00	5.80	6.80
Public Rights Baseflow (cfs)	1.52	3.20	4.64	5.44
Number of wells set to 0 pumping				
1	0.9675	2.1332	3.7181	5.264
2	0.9949	2.1725	3.7604	5.3089
3	1.0023	2.1924	3.7833	5.3332
4	1.0165	2.2591	3.8681	5.4265
5	1.0565	2.3623	3.9904	**5.561**
6	1.1081	2.4356	4.0674	5.64
7	1.1331	2.5075	4.1616	5.7493
8	1.1396	2.5216	4.1792	5.7696
9	1.1467	2.55	4.2159	5.8106
10	1.2409	2.7852	4.4889	6.1071
11	1.3322	2.9493	**4.6782**	6.3149
12	1.3328	2.9554	4.6914	6.3321
13	1.4374	**3.2229**	4.9954	6.6579
14	1.4775	3.3152	5.1016	6.7729
15	1.4882	3.3362	5.1271	***6.8019***
16	**1.6223**	3.5883	5.405	7.0968
17	1.6321	3.6146	5.4427	7.145
18	1.6334	3.6152	5.4428	7.1448
19	1.64	3.6328	5.4655	7.1707
20	1.7078	3.866	***5.8128***	7.6028
21	1.7374	3.9399	5.903	7.7037
22	1.7396	3.9428	5.9061	7.7068
23	1.7765	***4.0318***	6.0263	7.8539
24	1.8035	4.0755	6.0758	7.908
25	1.8267	4.1226	6.1302	7.9675
26	1.8324	4.1419	6.1605	8.0076
27	1.8367	4.1519	6.1755	8.0284
28	1.8328	4.1432	6.1642	8.0149
29	1.8487	4.1765	6.205	8.0612

	30	1.859	4.1905	6.219	8.0752
	31	***1.9589***	4.3341	6.3753	8.2417
	32	2.0899	4.5543	6.6339	8.5321
	33	2.1221	4.6032	6.689	8.5924
	34	2.1834	4.695	6.7888	8.6983
	35	2.1887	4.7007	6.7941	8.7032

Appendix 8e. Depletion-potential mapping: TRANSIENT, ONE OUT—KENNEDY GAGE

Modeled baseflow in the Little Plover River using the transient model at the Kennedy gage as an increasing number of wells are set to zero pumping, as ranked by depletion potential. The **bold** number indicates modeled flow recovering to above the public rights baseflow values, and the ***bold italic*** number indicates modeled flow recovering to above the public rights flow.

Kennedy Gage												
Public Rights Flow (cfs)	1.90											
Public Rights Baseflow (cfs)	1.52											
Modeled flow in the Little Plover River at Kennedy (cfs)												
Number of wells set to 0 pumping	January	February	March	April	May	June	July	August	September	October	November	December
1	1.431	1.231	1.189	1.372	2.439	1.786	1.175	1.289	2.177	2.271	2.200	2.381
2	1.431	1.231	1.189	1.372	2.439	1.807	1.245	1.345	2.206	2.287	2.211	2.389
3	1.431	1.231	1.189	1.372	2.446	1.827	1.264	1.360	2.219	2.295	2.217	2.394
4	1.431	1.231	1.189	1.372	2.446	1.830	1.273	1.371	2.228	2.302	2.222	2.398
5	1.431	1.231	1.189	1.372	2.485	1.933	1.368	1.443	2.284	2.341	2.252	2.421
6	1.431	1.231	1.189	1.372	2.485	1.951	1.440	1.544	2.359	2.387	2.284	2.444
7	1.431	1.231	1.189	1.372	2.494	1.977	1.476	1.585	2.393	2.413	2.304	2.461
8	1.431	1.231	1.191	1.375	2.498	1.980	1.479	1.589	2.398	2.419	2.310	2.467
9	1.431	1.231	1.191	1.375	2.498	1.980	1.484	1.598	2.405	2.425	2.315	2.471
10	1.439	1.244	1.206	1.396	2.527	2.013	1.517	1.632	2.441	2.462	2.353	2.511
11	1.439	1.244	1.206	1.396	2.530	2.028	**1.553**	1.694	2.509	2.517	2.395	2.544
12	1.439	1.244	1.206	1.396	2.530	2.029	1.555	1.697	2.511	2.519	2.397	2.546
13	1.453	1.276	1.252	1.446	2.582	2.087	1.617	1.757	2.571	2.580	2.458	2.605
14	1.453	1.276	1.252	1.446	2.588	2.117	1.686	1.839	2.642	2.635	2.502	2.641
15	1.453	1.277	1.253	1.446	2.588	2.118	1.686	1.839	2.642	2.635	2.502	2.641
16	1.453	1.277	1.253	1.446	2.588	2.119	1.692	1.849	2.654	2.646	2.511	2.649
17	1.453	1.277	1.253	1.446	2.605	2.209	1.889	2.033	2.791	2.746	2.587	2.710
18	1.453	1.277	1.253	1.446	2.605	2.209	1.891	2.038	2.798	2.753	2.594	2.716
19	1.453	1.277	1.253	1.446	2.605	2.211	1.895	2.044	2.805	2.758	2.598	2.720
20	1.453	1.277	1.253	1.446	2.605	2.211	1.896	2.046	2.807	2.761	2.601	2.723
21	1.453	1.278	1.254	1.447	2.607	2.213	1.899	2.055	2.826	2.789	2.635	2.760
22	1.453	1.278	1.254	1.447	2.607	2.214	***1.904***	2.065	2.839	2.803	2.647	2.770

Appendix 8f. Depletion-potential mapping: TRANSIENT, ONE OUT—EISENHOWER GAGE

Modeled baseflow in the Little Plover River using the transient model at the Eisenhower gage as an increasing number of wells are set to zero pumping, as ranked by depletion potential. The **bold** number indicates modeled flow recovering to above the public rights baseflow values, and the ***bold italic*** number indicates modeled flow recovering to above the public rights flow.

Eisenhower Gage												
Public Rights Flow (cfs)	4.00											
Public Rights Baseflow (cfs)	3.20											
	Modeled flow in the Little Plover River at Eisenhower (cfs)											
Number of wells set to 0 pumping	January	February	March	April	May	June	July	August	September	October	November	December
1	3.269	2.746	2.608	3.009	5.242	3.817	2.614	2.903	4.884	5.111	4.947	5.249
2	3.269	2.746	2.608	3.009	5.242	3.838	2.686	2.971	4.928	5.138	4.965	5.261
3	3.269	2.746	2.608	3.009	5.268	3.902	2.740	3.010	4.955	5.156	4.979	5.272
4	3.269	2.746	2.608	3.009	5.268	3.949	2.856	3.077	4.992	5.179	4.991	5.284
5	3.269	2.746	2.608	3.009	5.406	4.283	3.124	3.265	5.122	5.267	5.060	5.339
6	3.269	2.746	2.608	3.009	5.406	4.299	3.199	3.383	5.258	5.341	5.112	5.372
7	3.269	2.746	2.608	3.009	5.455	4.406	**3.342**	3.506	5.316	5.405	5.161	5.409
8	3.268	2.746	2.612	3.015	5.462	4.414	3.350	3.516	5.329	5.417	5.174	5.424
9	3.268	2.746	2.612	3.015	5.462	4.421	3.395	3.561	5.359	5.439	5.190	5.435
10	3.294	2.783	2.656	3.077	5.548	4.512	3.489	3.654	5.457	5.539	5.293	5.543
11	3.294	2.783	2.656	3.077	5.548	4.531	3.546	3.752	5.571	5.637	5.370	5.603
12	3.294	2.783	2.656	3.077	5.556	4.555	3.567	3.769	5.583	5.648	5.379	5.610
13	3.338	2.883	2.796	3.221	5.704	4.724	3.745	3.936	5.751	5.815	5.544	5.771
14	3.338	2.883	2.796	3.221	5.720	4.801	3.921	4.141	5.925	5.949	5.649	5.856
15	3.339	2.886	2.798	3.222	5.718	4.801	3.921	4.141	5.925	5.950	5.650	5.856
16	3.339	2.886	2.798	3.222	5.718	4.805	3.934	4.163	5.949	5.973	5.669	5.872
17	3.339	2.886	2.798	3.222	5.745	4.947	***4.259***	4.499	6.215	6.171	5.823	5.996

Appendix 8g. Depletion-potential mapping: TRANSIENT, ONE OUT—HWY 51/I-39 GAGE

Modeled baseflow in the Little Plover River using the transient model at the Hwy 51/I-39 gage as an increasing number of wells are set to zero pumping, as ranked by depletion potential. The **bold** number indicates modeled flow recovering to above the public rights baseflow values, and the ***bold italic*** number indicates modeled flow recovering to above the public rights flow.

Hwy 51/I-39 Gage	
Public Rights Flow (cfs)	5.80
Public Rights Baseflow (cfs)	4.64

	Modeled flow in the Little Plover River at Hwy 51/I-39 (cfs)											
Number of wells set to 0 pumping	January	February	March	April	May	June	July	August	September	October	November	December
1	5.196	4.470	4.272	4.768	7.594	5.901	4.463	4.828	7.461	7.542	7.310	7.673
2	5.196	4.470	4.272	4.768	7.594	5.921	4.532	4.895	7.507	7.571	7.329	7.686
3	5.196	4.470	4.272	4.768	7.623	5.993	4.595	4.943	7.541	7.594	7.347	7.700
4	5.196	4.470	4.272	4.768	7.623	6.049	**4.736**	5.030	7.589	7.625	7.366	7.716
5	5.196	4.470	4.272	4.768	7.772	6.417	5.047	5.255	7.749	7.734	7.450	7.783
6	5.196	4.470	4.272	4.768	7.772	6.433	5.119	5.371	7.886	7.813	7.508	7.821
7	5.196	4.470	4.272	4.768	7.834	6.573	5.307	5.533	7.974	7.896	7.571	7.869
8	5.195	4.470	4.278	4.776	7.844	6.583	5.317	5.546	7.991	7.912	7.587	7.888
9	5.195	4.470	4.278	4.776	7.844	6.591	5.374	5.603	8.031	7.941	7.608	7.902
10	5.222	4.509	4.325	4.843	7.941	6.693	5.478	5.710	8.142	8.055	7.725	8.025
11	5.222	4.509	4.325	4.843	7.937	6.712	5.538	5.814	8.269	8.165	7.814	8.096
12	5.222	4.509	4.325	4.843	7.962	6.778	5.584	5.844	8.289	8.181	7.827	8.106
13	5.267	4.612	4.473	5.001	8.125	6.963	5.781	6.032	8.477	8.370	8.013	8.287
14	5.267	4.612	4.473	5.001	8.142	7.042	***5.964***	6.254	8.673	8.525	8.136	8.389

Appendix 8h. Depletion-potential mapping: TRANSIENT, ONE OUT—HOOVER GAGE

Modeled baseflow in the Little Plover River using the transient model at the Hoover gage as an increasing number of wells are set to zero pumping, as ranked by depletion potential. The ***bold italic*** number indicates modeled flow recovering to above the public rights flow.

Hoover Gage												
Public Rights Flow (cfs)	6.80											
Public Rights Baseflow (cfs)	5.44											
	Modeled flow in the Little Plover River at Hoover (cfs)											
Number of wells set to 0 pumpir	January	February	March	April	May	June	July	August	September	October	November	December
1	7.031	6.093	5.834	6.410	9.959	7.979	6.277	6.760	10.124	9.968	9.603	10.005
2	7.031	6.093	5.834	6.410	9.959	7.998	6.346	6.827	10.171	9.998	9.624	10.020
3	7.031	6.093	5.834	6.410	9.988	8.071	6.412	6.878	10.209	10.024	9.645	10.036
4	7.031	6.093	5.834	6.410	9.988	8.128	6.555	6.972	10.264	10.060	9.668	10.055
5	7.031	6.093	5.834	6.410	10.137	8.502	***6.883***	7.216	10.442	10.185	9.763	10.131